Université du Québec
Institut National de la Recherche Scientifique
Centre Énergie Matériaux Télécommunications

ÉTUDE DE PERFORMANCE ET CO-SIMULATION D'INFRASTRUCTURES DE COMMUNICATIONS INTÉGRÉES OPTIQUES ET SANS FIL POUR LES RÉSEAUX ÉLECTRIQUES INTELLIGENTS

Par

Martin Lévesque

Thèse présentée pour l'obtention du grade de
Philosophiae Doctor, Ph.D.
en Télécommunications

Jury d'évaluation

Examinateurs externes	Prof. Fabrice Labeau McGill University
	Prof. Christine Tremblay ÉTS
Examinateur interne	Prof. Long Le INRS-ÉMT
Directeur de recherche	Prof. Martin Maier INRS-ÉMT
Co-directeur de recherche	Prof. Géza Joós McGill University

Remerciements

J'aimerais tout d'abord remercier spécialement mon superviseur de thèse, Prof. Martin Maier, pour ses nombreux conseils et son support tout au long de cette thèse.

J'aimerais également remercier Prof. Géza Joós pour cette collaboration multidisciplinaire ainsi que ses nombreuses critiques et suggestions ayant permis de significativement améliorer le contexte en ce qui attrait le système électrique, notamment. Je remercie également ses étudiants de maîtrise, Da Qian Xu et Samah Mansour, pour cette collaboration fructueuse.

Je remercie les évaluateurs internes et externes pour leurs commentaires fructueux.

Je suis également très reconnaissant envers Prof. Frank Aurzada (Technische Universität Darmstadt, Allemagne) et Prof. Martin Reisslein (Arizona State University, USA) pour leurs nombreux conseils techniques et critiques, m'ayant ainsi permis d'améliorer la qualité et la précision dans mon travail.

J'aimerais remercier Eric Schultz et Eric Suignard de EDF R&D ayant rendu possible ce stage de recherche sur la multi-simulation smart grid avancée. Ce stage m'a permis de comprendre concrètement plusieurs concepts smart grids. Je remercie également toute l'équipe du département MIRE, notamment Christophe Béchet, Anne Picault et Ricardo Jover, pour les nombreux échanges durant ce stage mémorable.

Je remercie également Bishnu Prasad Bhattarai, Aalborg University (Danemark), pour ce travail collaboratif titanesque de banc d'essai smart grid. Les échanges durant ces 4 mois m'ont fait prendre conscience de plusieurs notions fondamentales des systèmes électriques.

Je suis reconnaissant à Louis Lamarche (Hydro-Québec) pour ses nombreux commentaires sur mes travaux et sur sa vision des smart grids.

Je remercie Liviu Ivănescu pour son aide dans le laboratoire et pour ces discussions nombreuses.

J'aimerais également remercier les stagiaires Yash Desai, Harmeet Singh, Taycir Louati et le chercheur visiteur Dr. Tomaz Beriza ayant contribué avec effort dans le cadre de cette thèse.

Je remercie également tous les membres du laboratoire Optical Zeitgeist, notamment Dr. Wansu Lim, Bhaskar Prasad Rimal, Hamzeh Beyranvand, Intissar Harrabi, Ahmed Belgana et Abdelhakim Cherif.

Finalement, mais surtout, je remercie ma famille et mes amis pour leur amour et support à travers les années, pour croire en moi et m'encourager dans mes activités.

Résumé

Le réseau intelligent est une amélioration significative du système électrique du XX^{e} siècle caractérisée essentiellement par une amélioration de l'efficacité énergénique par l'entremise de flux bidirectionnels d'information et d'énergie. Cette thèse porte sur l'étude multidisciplinaire des réseaux intelligents et des réseaux d'accès optiques-sans fil de prochaines générations, où la forte capacité des réseaux d'accès ne profite pas seulement au secteur des télécommunications, mais à l'ensemble des systèmes de la société, incluant les secteurs de l'énergie et du transport.

En premier lieu, le premier modèle analytique des réseaux optiques-sans-fil émergents basés sur les technologies de réseaux optiques passifs et réseaux maillés IEEE 802.11n/e/ac est proposé, permettant de (i) évaluer/comparer des algorithmes de routage FiWi et (ii) trouver la borne théorique supérieure de débit de données maximal des capteurs smart grids sans affecter négativement les performances délai-débit de traffic régulier. Utilisant un modèle analytique FiWi des performances de la couche MAC et combinant des échecs probabilistes des fibres optiques et des stations de base, la disponibilité du réseau est modélisée et quantifiée, permettant ainsi de la comparer aux exigences d'applications smart grids.

En second lieu, les applications de véhicules électriques et sources d'énergie renouvelables sont étudiées de façon multidisciplinaire en tenant compte à la fois des perspectives de technologies de l'information, de communications et du système électrique. Considérant la complexité de l'élaboration d'un banc d'essai smart grid, la co- et multi-simulation est une approche prometteuse permettant d'étudier l'ensemble des perspectives smart grids en intégrant plusieurs simulateurs. Plusieurs approches de multi-simulation sont possibles, avec ou sans mécanisme de synchronisation pour coupler les simulateurs. Pour montrer l'utilité de telles multi-simulations, les perspectives de communications et du système électrique sont couplées pour modéliser les performances d'un algo-

rithme proposé (nommé IntVGR) intégrant la coordination de véhicules électriques et les sources d'énergie renouvelables en échangeant des paquets via un réseau d'accès optique-sans fil. La perspective de technologies de l'information est ensuite ajoutée pour étudier une application de télécontrôle smart grid basée sur des configurations réelles d'un système de distribution en France, où la finalité de la multi-simulation est de permettre de tester et valider de bout-en-bout de nouveaux mécanismes smart grids. Par l'entremise d'un banc d'essai d'un système de distribution réel miniaturisé, un modèle de programmation dynamique de coordination de véhicule électrique permet de significativement améliorer les performances du réseau électrique tout en tenant compte des exigences des clients. Le modèle est démontré expérimentalement via un réseau hétérogène Ethernet couplé au réseau de distribution, où un modèle proposé de synchronisation de capteurs coordonnés permet d'améliorer la synchronisation d'arrivée des mesures comparativement à une approche utilisant des capteurs périodiques.

Abstract

The smart grid is an improved power system of the 20th century characterized essentially by a two-way flow of energy and information. In that sense, the smart grid is sometimes called Energy Internet, where actors and components exchange energy and data with each other, similarly to the Internet where components and actors exchange data over a shared infrastructure. Many wired and wireless communications technologies could be used for smart grid communications. According to IEEE P2030, the three main quality attributes for robust smart grid communications are latency, reliability, and quality of service. Communications latency between a given pair of source and destination nodes is expressed as the time when the message is generated and the time when it is received at the reception side. Reliability is formally defined as the ability to perform a certain task for given conditions during a certain period of time.

According to Telecom Italia, the current trend in the access networks is the convergence of fiber-to-the-home (FTTH) for their durability, reliability, and energy efficiency. China Telecom deployed over 70 millions FTTH ports between 2004 and 2012. Furthermore, China Telecom predicts that the major upcoming trends are: (*i*) increase of fiber penetration (*ii*) more capacity and speed, from 1 Gbps passive optical networks (PONs) towards 40 Gbps in a single PON system and (*iii*) increase of the coverage by integrating wired, wireless, and mobile nodes. According to China Telecom, PONs will converge into fiber-wireless (FiWi) networks to combine their respective advantages. Optical networks offer huge capacity, immunity against electromagnetic interference, and wireless networks can be deployed quickly at a low cost and offer mobility.

FiWi networks can also be enriched by integrating optical and wireless sensors. Such networks can use fiber Bragg grating optical-based sensors and wireless sensors compliant with IEEE 802.15.4

ZigBee. Integrating sensors allow to interact with real-world systems to monitor different parameters, including temperature, pressure, sound, etc. This is a great opportunity for the telecommunications and many economic sectors, that is, sharing low-cost access networks for improved efficiency and sustainability.

In the following, we quantify the performance of emerging FiWi access networks and propose new mechanisms by means of probabilistic analyses. Such probabilistic analyses allow to quickly quantify the communications performance for large topologies. In smart grid solutions, innovative partnerships hold great promise to enable utilities and other players to share smart grid communications infrastructures investments by transitioning from the traditional vertical network integration model towards splitting the value chain into multi-tier business models. Current Gigabit-class PONs evolve into next-generation PONs, whereby high-speed 10+ Gb/s time division multiplexing (TDM) and long-reach wavelength-broadcasting/routing wavelength division multiplexing (WDM) PONs are a promising solution near-term candidates. On the other hand, next-generation wireless local area networks (WLANs) based on frame aggregation techniques will leverage physical layer enhancements, giving rise to Gigabit-class very high throughput (VHT) WLANs. We develop an analytical framework for evaluating the capacity and delay performance of a wide range of routing algorithms in converged FiWi broadband access networks based on different next-generation PONs and a Gigabit-class multi-radio multi-channel WLAN-mesh front-end. Our framework is very flexible and incorporates arbitrary frame size distributions, traffic matrices, optical/wireless propagation delays, data rates, and fiber faults. We verify the accuracy of our probabilistic analysis by means of simulation for the wireless and wireless-optical-wireless operation modes of various FiWi network architectures under peer-to-peer, upstream, uniform, and nonuniform traffic scenarios. The results indicate that our proposed optimized FiWi routing algorithm (OFRA) outperforms minimum (wireless) hop and delay routing in terms of throughput for balanced and unbalanced traffic loads, at the expense of a slightly increased mean delay at small to medium traffic loads. This first analytical framework for FiWi networks does not take into account quality-of-service (QoS), which is quite important for smart grids. We next study the performance of multi-tier integrated FiWi smart grid communications infrastructures based on low-cost, simple, and reliable next-generation Ethernet passive optical network (EPON), emerging high-speed TDM and multi-channel WDM

PONs of extended fiber reach and QoS enabled VHT WLANs in terms of capacity, latency, and reliability. By means of probabilistic analysis and verifying simulations we study the coexistence of human-to-human (H2H), e.g., triple-play voice, video, data, traffic and machine-to-machine (M2M) traffic originating from wireless sensors operating on a wide range of possible data rates, time scales, and duty cycles. Our analysis enables the quantification of the maximum achievable data rates of both event- and time-driven wireless sensors without violating given upper delay limits of H2H traffic. The obtained results can be used as a theoretical upper bound of coexisting M2M traffic for the design and realization of future yet unforeseen smart grid applications. We next study in more detail the availability, which is an important metric of the reliability quality attribute. Availability is qualitatively defined in the IEEE P2030 standard. However, the availability metric must be quantified in order to validate given smart grid application requirements. In recent related work, availability has been quantified for wireless and optical backhaul networks in terms of communications reachability, while in some other work availability was not formally defined in a fine-grained manner and was assumed to be known. We develop a novel probabilistic availability model for integrated PON and WiMAX networks in order to quantify this metric according to medium access control (MAC) protocol limits as well as fiber and base station failures. The obtained numeric results show interesting availability behaviors, including the impact on availability depending on the number of base stations. We also investigate optical traffic re-routing through WiMAX when fiber faults occur and show that there exists a maximum amount of re-routed traffic for maximizing availability. Furthermore, we investigate a scenario of real-world smart grid traffic configurations shared with regular traffic and find the maximum sensor data rate to meet the availability requirements. We next study the opportunity to efficiently use the WiMAX channel dedicated to the utility in Canada. By using experimental measurements of smart grid applications compliant with IEC 61850 in trace-driven WiMAX simulations, we show that the WiMAX MAC protocol efficiency decreases for an increasing number of stations. To avoid this shortcoming, a novel WiMAX MAC protocol is proposed and analyzed for smart grid applications, which uses lattice correlators to improve the throughput-delay performance significantly. For the considered configurations, the obtained maximum throughput of the proposed MAC protocol outperforms the current WiMAX MAC protocol by up to 41%.

Next, to provide insights into smart grid applications, we study the coordination of electric vehicles and renewable energy sources in a multidisciplinary manner by means of experimental demonstrations and co-simulation studies. To evaluate large-scale smart grid systems, co- and multi-simulation experiments can be modeled. Multiple simulation tools have been built and studied independently in the communications and power system perspectives of IEEE P2030 to study new smart grid applications. However, very few studies have been done on co-simulation by combining both perspectives in a multidiciplinary manner. The implementation details of a novel communications and power distribution network co-simulator based on OMNeT++ and OpenDSS are discussed. The novelty of the co-simulator is demonstrated by showing the impact of data rate-based and event-based sensors on reactive/uncoordinated control algorithms of plug-in electric vehicles (PEVs) to reduce critical voltage durations. PEVs have great potential of being the alternative for the next-generation of transportation. Uncoordinated PEV charging, however, may put a significant pressure on the distribution grid. Using a modified IEEE-13 Node distribution network of 342 residential customers, a converged fiber-wireless infrastructure based on EPON, WiMAX, wireless mesh network and sensor technologies to support coordinated charging of PEVs is proposed. To measure the performance of both the communications and power system perspectives of proactive scheduling algorithms and proposed reactive control protocols, our developed hybrid co-simulator based on OMNeT++ and OpenDSS is used. Co-simulation results show that the proposed low-cost communications infrastructure enables to efficiently schedule the charging of PEVs and quickly stabilize the voltage in a stress scenario. To extend this co-simulation study, a novel integrated vehicle-to-grid, grid-to-vehicle, and renewable energy sources (IntVGR) coordination algorithm is then proposed. Its focus is on providing a multidisciplinary study on implementing the proposed IntVGR scheme over a broadband fiber-wireless communications infrastructure by co-simulating both power and communications perspectives. For the power systems perspective, results show that the scheme is able to achieve a 21% reduction in peak demand compared to uncontrolled charging, and a better performance in flattening the overall demand profile and maintaining network constraints in comparison to a benchmark scenario. The scheme also demonstrates to successfully coordinate PEVs to take maximum utilization of local renewable energy. For the communications perspective, the measured upstream traffic for executing the proposed IntVGR scheme on a residential area is found to be 1-2 Mbps with an end-to-end latency level of 1 ms. The scheme has also been validated from both perspectives in a sensitivity analysis with a higher PEV adoption rate. Note that this work focus on the communications and power system perspectives. A multi-simulation model is then proposed to measure the performance of all smart grid perspectives as defined in the IEEE P2030 standard. As a preliminary implementation, a novel information technology (IT) and communication multi-simulator is developed following a High Level Architecture (HLA). To illustrate the usefulness of such a multi-simulator, a case study of a distribution network operation application is presented using real-world topology configurations in France with realistic communication traffic based on IEC 61850. The multi-simulator allows to quantify, in terms of communication delay and system reliability, the impact of aggregating all traffic on a low-capacity wireless link based on Digital Mobile Radio (DMR) when a Long Term Evolution (LTE) network failure occurs. The case study illustrates that such a multi-simulator can be used to experiment new smart grid mechanisms and verify their impact on all smart grid perspectives in an automated manner. More importantly, multi-simulation can prevent problems before modifying/upgrading a smart grid and thus potentially reduce costs to the utility. High penetration of renewable energy sources and electric vehicles (EVs) creates power imbalance and congestion in the existing power network and hence causes significant problems in the control and operation. Despite huge efforts from the electric utilities, governments, and researchers, smart grid is still at the developmental stage to address those issues. In this regard, a smart grid testbed (SGT) is desirable to develop, analyze, and demonstrate various novel smart grid solutions, namely demand response, real-time pricing, and congestion management. We first present a novel SGT developed in our laboratory by scaling a 250 kVA, 0.4 kV real low voltage distribution feeder down to 1 kVA, 0.22 kV. Information and communication technology (ICT) is integrated in the scaled-down network to establish real-time monitoring and control. The novelty of the developed testbed is demonstrated by optimizing coordinated EV charging realized through the synchronized exchange of monitoring and control packets via a heterogeneous Ethernet-based mesh network. The developed SGT is a step forward to (*i*) find practical problems and (*ii*) validate and experiment new smart grid mechanisms in realistic physical conditions.

Table des matières

Remerciements iii

Résumé v

Abstract vii

Table des matières xiii

Liste des figures xvii

Liste des tableaux xxi

Liste des acronymes xxiii

I Synthèse 1

1 Introduction 3
- 1.1 Contributions . . . 4
- 1.2 Structure de la thèse . . . 7

2 État de l'art 9
- 2.1 Introduction . . . 9
- 2.2 Applications primaires attendues des réseaux intelligents . . . 11
  - 2.2.1 Véhicule électrique . . . 12
  - 2.2.2 Micro-réseau . . . 13
  - 2.2.3 Compteur intelligent . . . 13
  - 2.2.4 Surveillance et contrôle en temps réel des systèmes de distribution . . . 13
- 2.3 Technologies de communications pour les réseaux intelligents . . . 14
  - 2.3.1 Sans fil . . . 14
  - 2.3.2 Filaire . . . 17
- 2.4 Les réseaux FiWi . . . 19
  - 2.4.1 Radio-via-fibre . . . 19
  - 2.4.2 Radio-et-fibre . . . 20
  - 2.4.3 Fiber-wireless sensor networks (Fi-WSNs) . . . 20
- 2.5 Résumé . . . 21

3 Analyse de coexistence de trafic H2H et M2M via une infrastructure FiWi 23
- 3.1 Introduction . . . 23

3.2 Infrastructure de communications FiWi pour les réseaux intelligents 25
3.3 Analyse de coexistence 26
3.3.1 Modèle réseau 27
3.3.2 Modèle de trafic 28
3.3.3 Analyse de capacité et de stabilité 28
3.3.4 Analyse de délai 30
3.3.5 Calcul de la borne théorique supérieure du trafic M2M 39
3.3.6 Résultats 39
3.4 Résumé 44

4 Co-simulation Dynamique Smart Grid **47**
4.1 Introduction 47
4.2 Modèle de multi-simulation smart grid 49
4.3 Design et implémentation 49
4.3.1 Perspectives de technologies de l'information et de communications 50
4.3.2 Perspectives de communications et du système électrique 51
4.4 Etude de cas 52
4.4.1 Télécontrôle du réseau de distribution 52
4.4.2 Véhicules électriques 55
4.5 Résultats 55
4.5.1 Télécontrôle du réseau de distribution 55
4.5.2 Véhicules électriques 57
4.6 Résumé 58

5 Banc d'essai expérimental de véhicules électriques coordonnés **59**
5.1 Introduction 59
5.2 Banc d'essai expérimental 60
5.2.1 Réseau de distribution miniaturisé 60
5.2.2 Perspective de communications 63
5.2.3 Perspective de technologies de l'information 63
5.2.4 Synchronisation 65
5.3 Modèle de coordination optimisé de véhicules électriques 65
5.3.1 Algorithme centralisé d'ordonnancement inter-slot 66
5.3.2 Algorithme décentralisé intra-slot 67
5.4 Résultats expérimentaux 67
5.4.1 Algorithmes proposés 67
5.4.2 Complexité et synchronisation 69
5.5 Résumé 70

6 Conclusions et travaux futurs **73**
6.1 Conclusions 73
6.2 Suggestions pour les travaux futurs 75

7 Publications réalisées **77**

Bibliographie **81**

II Articles 89

8 Probabilistic Availability Quantification of PON and WiMAX Based FiWi Access Networks for Future Smart Grid Applications 91
8.1 Abstract . . . 93
8.2 Introduction . . . 93
8.3 Integrated TDM/WDM PON and WiMAX Network Architectures . . . 97
8.4 Network Availability Analysis . . . 99
8.4.1 Network Model . . . 101
8.4.2 Traffic Matrix . . . 104
8.4.3 Traffic Intensity . . . 104
8.4.4 Probabilistic Availability . . . 109
8.4.5 Adaptation of Framework to Mesh-based Topologies . . . 112
8.4.6 Solving the Analytical Framework . . . 113
8.5 Numerical Results . . . 114
8.5.1 Configurations . . . 114
8.5.2 WB TDM/WDM PONs . . . 115
8.5.3 Next-Generation FiWi Settings with Integrated WR WDM PONs . . . 116
8.5.4 Impact of Fiber and BS Failures . . . 119
8.5.5 Coexistence of Human-to-Human (H2H) and Smart Grid Traffic . . . 120
8.6 Conclusions . . . 122

9 Integrated V2G, G2V, and Renewable Energy Sources Coordination over a Converged Fiber-Wireless Broadband Access Network 127
9.1 Abstract . . . 129
9.2 Introduction . . . 129
9.3 Power Distribution and Communications Interactions . . . 132
9.3.1 Workplace/public parking garage . . . 132
9.3.2 Home . . . 133
9.4 Integrated V2G, G2V, and RES Scheduling Algorithm . . . 133
9.4.1 IntVGR main parameters . . . 134
9.4.2 Objective function . . . 135
9.4.3 Constraints . . . 138
9.4.4 Electricity market concerns . . . 139
9.5 Co-simulation Results . . . 141
9.5.1 Co-simulation configurations . . . 141
9.5.2 Results for the performance of distribution grid . . . 145
9.5.3 Interoperability with the supporting communications infrastructure . . . 149
9.6 Conclusions . . . 152

III Appendices 157

10 FiWi Access Networks Based on Next-Generation PON and Gigabit-Class WLAN Technologies: A Capacity and Delay Analysis 159
10.1 Abstract . . . 161
10.2 Introduction . . . 161
10.3 Related Work . . . 164

10.4 FiWi Access Networks 166
10.4.1 Next-Generation PONs 168
10.4.2 Gigabit-Class WLAN 169
10.5 Network Model 171
10.5.1 Network Architecture 171
10.5.2 Traffic Model and Routing 172
10.6 Fiber Backhaul Network 173
10.6.1 Capacity Analysis 173
10.6.2 Delay Analysis 174
10.7 Wireless Front-End Network 176
10.7.1 Frame Traffic Modeling 177
10.7.2 Frame Aggregate Error Probability 178
10.7.3 Probabilities for Frame Aggregate Collision and Successful Frame Aggregate Transmission 179
10.7.4 Duration of Single Frame Aggregate Transmission 179
10.7.5 Service Time for Frame Aggregate 181
10.7.6 Delay at WMN Node 182
10.7.7 Delay on WMN Path 184
10.8 FiWi Network Stability and Delay 184
10.9 Numerical and Simulation Results 185
10.9.1 Model Verification 185
10.9.2 FiWi Routing Algorithms 189
10.9.3 Fiber Failures 193
10.9.4 Very High Throughput WLAN 195
10.10 Conclusions 196

11 Dependable Fiber-Wireless (FiWi) Access Networks and Their Role in a Sustainable Third Industrial Revolution Economy 203
11.1 Abstract 205
11.2 Introduction 210
11.3 FiWi Access Networks 212
11.4 FiWi Network Dependability Techniques 219
11.4.1 Reliability 219
11.4.2 Availability 219
11.4.3 Survivability 221
11.4.4 Security and Safety 227
11.5 FiWi Smart Grid Communications Networks Based on Multi-Tier Business Models . 228
11.5.1 The Über-FiWi Network 229
11.5.2 Coexistence of H2H and M2M Traffic 231
11.5.3 Co-Simulation 233
11.5.4 Experimental Smart Grid System 236
11.6 Conclusions 237

Liste des figures

2.1 Interactions entre les perspectives smart grids telles que définies dans IEEE P2030. . 10
2.2 Modèle conceptuel des domaines d'un réseau intelligent [1]. 11
2.3 Impact sur la charge globale du système électrique des approches coordonnées/non coordonnées de véhicules électriques [2]. 12
2.4 Topologie d'un réseau d'accès PON conventionnel [3]. 17
2.5 Banc d'essai R&F d'un réseau EPON et wireless mesh network (WMN) [4]. 20
2.6 Le réseau Fi-WSN, permettant l'intéraction avec des systèmes complexes hétérogènes. 21

3.1 Architecture générique de communications Smart Grid FiWi. 25
3.2 Cycle de l'accès au canal pour modéliser les noeuds événements et par le temps. . . . 31
3.3 Probabilités d'état d'équilibre des valeurs du compteur de backoff du modèle EDCA avec des conditions non-saturées. 34
3.4 Délai de bout-en-bout moyen vs. débit de données des capteurs. 40
3.5 Fiabilité des capteurs en fonction de la charge du trafic H2H. 41
3.6 Impact de différentes charges réseau de trafic H2H sur le délai des capteurs. 43

4.1 Modèle de multi-simulation couvrant toutes les perspectives smart grids. 49
4.2 Modèle de multi-simulation pour valider de bout-en-bout une smart grid. 50
4.3 Design de la co-simulation des perspectives de technologies de l'information et de communications. 51
4.4 Design de la co-simulation des perspectives de communications et du système électrique. 52
4.5 Structure du réseau de distribution interconnecté via des liens sans fil LTE et DMR. 53
4.6 Topologie du réseau de distribution basée sur de réelles configurations en France pour un poste électrique donné. Dimension : 15x15 kilomètres, nombre de clients en basse tension : 3139, nombre de noeuds haute tension/basse tension : 332 (noeuds pleins), nombre de noeuds de coupure : 26 (noeuds avec croix). 54
4.7 Fiabilité du système sans utilisation de mécanisme de QdS. Le lien LTE devient indisponible au temps 500. 56
4.8 Délai du système avec utilisation de mécanisme de QdS (WFQ: weighted fair queuing, RA: Rate adaptive). 56
4.9 Résultats selon les perspectives de communications et du système électrique avec différents algorithmes d'allocation de charge de véhicules électriques (niveau de pénétration : 66 %). 57

5.1 Schéma du banc d'essai du réseau ingelligent miniaturisé de 13 noeuds. 61
5.2 Réseau de distribution miniaturisé composé d'un serveur DMS (1), d'une interface graphique (2), d'un EPON (3) et du réseau de distribution (nodes 1-13). 62

5.3 Noeud intelligent (correspond au noeud 10) composé des configurations de résistance et d'inductance (1), appareil pour déchargement (2), capteurs (3), batterie (4), contrôleur local (5), charge dynamique (6), interrupteur électrique contrôlable (7) et chargeur (8). 63
5.4 Infrastructure de communications composée de nano-ordinateurs utilisés comme contrôleurs, de routeurs Ethernet et d'un EPON (NC : nano-computer). 64
5.5 Modèle de programmation dynamique pour coordination optimisée de chargement des véhicules électriques. 65
5.6 Configurations concernant les arrivées-départs des véhicules et profil de coût. 68
5.7 Optimisation centralisée des véhicules électriques. 68
5.8 Profil de tension de l'algorithme décentralisé. 69
5.9 Durée de calcul du processus d'optimisation centralisée. 69
5.10 Performance de synchronisation avec capteurs périodiques et coordonnés. 70
5.11 Trafic capturé au port de sortie entre DMS et OLT. 71

8.1 Conventional cascaded PON and WiMAX architecture. 98
8.2 Pyramid-based FiWi topology with WR WDM PON consisting of 76 ONUs, whereby ONUs have WiMAX interfaces and can act as SS or BS (splitting ratio: 6). 99
8.3 Probabilistic model for a single-stage WB TDM/WDM PON. $B(\rho_w^{wi})$, $B(\rho^{op,u})$, and $B(\rho^{op,d})$ correspond to the blocking probabilities at the output ports of the SSs, ONUs, and OLT, respectively; $p_{0/1}^{op}$ denotes the fiber failure probability at stage 0 or 1, and p_z^{wi} denotes the BS failure probability. 102
8.4 Probabilistic model for a WR WDM PON ($\Xi = 3$). 112
8.5 Two-stage fixed-point iterations technique to solve the nonlinear equation system. . . 113
8.6 Computation duration (complexity) versus topology size (number of nodes). 114
8.7 WiMAX, WB TDM, and WDM PON availability performance vs. the offered load ($p^{wi} = p^{op} = 10^{-5}$). 116
8.8 Integrated WB TDM/WDM PON availability performance vs. the offered load ($p^{wi} = p^{op} = 10^{-5}$, $|\mathcal{W}| = 16 \cdot 3$). 116
8.9 Impact of WiMAX BS failure probability on overall network availability for different network offered loads ($p^{wi} = p_z^{wi}, \forall z \in \mathcal{B}$). 117
8.10 Impact of fiber failure probability on overall network availability for different offered loads ($p^{op} = p_s^{op}, \forall s \in \{0, ..., \Xi - 1\}$). 117
8.11 Availability performance vs. the offered load for a pyramid-based WR WDM PON consisting of 106 ONUs with a splitting ratio of 16. 118
8.12 Impact of the number of BSs per S (β) on availability. 118
8.13 Impact of the ratio of the traffic destined towards faulty fibers permitted be re-routed in the wireless domain (OL = 20.5 Gbps, $\delta^{wi} = \delta_{i,j}^{wi}, \forall i, j \in \mathcal{N}$). 119
8.14 Availability as a function of fiber and BS failures (OL = 686 Mbps). 120
8.15 Availability as a funciton of fiber and BS failures (OL = 20.5 Gbps). 120
8.16 Unavailability as a function of sensor data rate ($p^{op} = p^{wi} = 10^{-5}$). Regular traffic has an availability requirement of 99.99 % and 99.9999 % for SG traffic. 121

9.1 Interactions between the FiWi network nodes and the DMS to implement the proposed PEV coordination algorithm. 133
9.2 Schematic of the proposed scheduling algorithm. 137
9.3 Single line diagram of the 342-node distribution network topology. 143

9.4 Hourly distribution of the generation capacity from the local RES unit at the public parking garage (workplace). 145
9.5 The overall demand profile in different simulation scenarios based on a PEV penetration level of 42% and a summer base load profile. 148
9.6 Operation of G2V and V2G modes in the *IntVGR(0.90, w/o RES)* scenario based on a PEV penetration level of 42% and a summer base load profile. 148
9.7 Worst nodal voltage profile based on a PEV penetration level of 42% and a summer base load profile. 149
9.8 Operation of G2V and V2G modes in the *IntVGR(0.80, w/o RES)* scenario based on a PEV penetration level of 42% and a summer base load profile. 149
9.9 Workplace scheduling with RESs in the *IntVGR(0.90, w/o RES)* scenario based on a PEV penetration level of 42% and a summer base load profile. 150
9.10 Workplace scheduling with RESs based on a PEV penetration level of 84% and a summer base load profile, $\eta = 0.90$. 151
9.11 Upstream throughput measured at the DMS for different PLs. 151
9.12 Upstream end-to-end delay measured at the DMS for different PLs. 151

10.1 FiWi network architecture based on single- or multi-stage TDM or WDM PON and multihop WMN. 165
10.2 Next-generation PONs: (a) High-speed TDM PON, (b) wavelength-broadcasting WDM PON, and (c) wavelength-routing multi-stage WDM PON. 167
10.3 A-MSDU frame aggregation scheme. 170
10.4 A-MPDU frame aggregation scheme. 170
10.5 FiWi network configuration for verifying simulations: 4 ONU/MPPs, 4 MPs, and 16 STAs distributed over 11 wireless zones (dashed circles). 186
10.6 Mean delay vs. mean aggregate throughput performance of WMN and TDM PON based FiWi networks for peer-to-peer (P2P) and upstream traffic. 188
10.7 Mean delay vs. mean aggregate throughput performance of different FiWi network architectures for uniform and nonuniform traffic. 188
10.8 Mean delay vs. mean aggregate throughput performance of different FiWi routing algorithms for a conventional wavelength-routing (WR) WDM PON of 20 km range and $B = 1$. 191
10.9 Mean delay vs. mean aggregate throughput performance of different FiWi routing algorithms for (*i*) a conventional 20 km range and (*ii*) a 100 km long-reach wavelength-routing (WR) WDM PON and $B = 100$. 193
10.10 Impact of distribution fiber failures on throughput-delay performance of a 20 km range wavelength-routing WDM PON using OFRA with $B = 1$. 194
10.11 Throughput-delay performance of next-generation FiWi access networks based on high-speed wavelength-routing WDM PON and VHT WLAN technologies using minimum hop routing with $B = 1$ (optical and wireless data rates , $c^{(\lambda)}$ and r, are given in Gb/s and Mb/s, respectively). 195

11.1 Broadband subscribers across OECD countries by technology: fixed wired access technologies used in 2013 [13]. 214
11.2 FiWi access network architecture based on single- or multi-stage TDM or WDM PON and multihop WMN using legacy or VHT WLAN technologies. 218
11.3 Optical coding based PON monitoring: (a) architecture, (b) encoder, and (c) monitoring receiver. 220

11.4 Generic multi-stage NG-PON topology with historical or estimated fiber failure probability p_i assigned to each stage i. 222
11.5 Average number D of failure-free connections vs. number M of wirelessly upgraded ONUs for a five-stage NG-PON topology ($N = 465$) with and without partial optical protection. 223
11.6 Mean delay vs. mean aggregate throughput performance of different FiWi routing algorithms for (i) a conventional 20 km range, and (ii) a 100 km long-reach wavelength-routing WDM PON. 225
11.7 Mean delay vs. mean aggregate throughput performance of next-generation FiWi access networks based on high-speed wavelength-routing WDM PON and VHT WLAN technologies ($c^{(\lambda)}$, and r are given in Gb/s, and Mb/s, respectively). 227
11.8 Fiber-wireless sensor networks (Fi-WSNs) enable the monitoring of and interaction with the electrical power grid. 228
11.9 The Über-FiWi network architecture. 230
11.10 Average end-to-end delay performance vs. data rate per sensor. 232
11.11 IEEE 13-node distribution power network with grid-connected PEVs. 233
11.12 Daily voltage deviations for uniform, and non-uniform PEV distributions at different PEV penetration levels. 234
11.13 PEV coordination performance of underlying IEEE 13-node distribution power network (in terms of voltage profile and power consumption), and overlaid Über-FiWi network (in terms of delay and throughput). 235
11.14 The Über-FiWi network testbed. 237
11.15 Throughput measurements for MAP_9 experiencing a power blackout with malicious MAPs generating a DDoS attack. 238

Liste des tableaux

2.1 Comparatif des technologies sans fil considérées. 16
2.2 Comparatif des technologies filaires considérées. 18

3.1 Paramètres du modèle réseau FiWi. 27
3.2 Paramètres du modèle de trafic FiWi. 28
3.3 Mesures expérimentales d'applications smart grids de surveillance suivant le standard IEC 61850 [5]. 41
3.4 Bornes théoriques supérieures (en Mbps) du trafic M2M avec un seuil de délai H2H de 2.5 ms. 43

4.1 Mesures expérimentales, moyennes de la taille des corps des messages suivant la norme IEC 61850. 54

5.1 Configurations avant et après miniaturisation des principaux paramètres du réseau de distribution. 61

8.1 Configurations 115
8.2 Experimental measurements of smart grid applications based on the IEC 61850 standard. 119

9.1 PEV Model Configuration 143
9.2 Co-simulation results for a PL of 42% and a summer base load profile. 146
9.3 Co-simulation results for a PL of 84% and a summer base load profile. 149

10.1 FiWi Network Parameters 185

Liste des acronymes

AIFS	Arbitration inter-frame space
A-MSDU	Aggregate MAC service data unit
A-MPDU	Aggregate MAC protocol data unit
AP	Access point
AWG	Arrayed-waveguide grating
CAPEX	Capital expenditures
CSMA/CA	Carrier sense multiple access with collision avoidance
DCF	Distributed coordination function
DSM	Demand side management
DMR	Digital Mobile Radio
DMS	Distribution management system
EDCA	Enhanced distributed channel access
EPON/GPON	Ethernet/Gigabit passive optical network
FiWi	Fiber-wireless
Fi-WSN	Fiber-wireless sensor network
FMI	Functional Mockup Interface
FTTH	Fiber-to-the-home
G2V	Grid-to-vehicle

GPRS	General Packet Radio Service
H2H	Human-to-human
HLA	High Level Architecture
IoT	Internet of Things
IPS	Intelligent power switch
LR-PON	Long-reach PON
LTE	Long Term Evolution
M2M	machine-to-machine
MAC	Medium access control
MAP	Mesh access point
MP	Mesh point
MPP	Mesh portal point
NAN	Neighborhood area network
OLT	Optical line terminal
ONU	Optical network unit
OXC	Optical cross-connect
V2G	Vehicle-to-grid
PEV	Plug-in electric vehicle
PLC	Power Line Communication
PON	Passive optical network
PU	Per unit
QdS	Qualité-de-service
RAU	Remote antenna unit
R&F	Radio-and-fiber

RN	Remote node
RoF	Radio-over-fiber
RSOA	Reflective semiconductor optical amplifier
STA	Station
TCP	Transmission Control Protocol
TDM	Time division multiplexing
VHT	Very high throughput
WASA	Wide-area situational awareness
WLAN	Wireless local area network
WDM	Wavelength division multiplexing
WiMAX	Worldwide Interoperability for Microwave Access
WR-PON	Wavelength-routing PON
WB-PON	Wavelength-broadcasting PON

Première partie

Synthèse

Chapitre 1

Introduction

L'augmentation de la demande de consommation d'énergie et l'augmentation d'émissions de gaz carbonique révèlent que des améliorations significatives de l'efficacité énergétique sont nécessaires au niveau des réseaux électriques existants. Ces améliorations doivent notamment permettre de réduire la demande durant les périodes de pointe et exploiter la génération distribuée d'électricité par des sources d'énergie renouvelables [6, 7]. Selon les estimations faites par la *U.S. Energy Information Administration*, la génération d'énergie à base de sources d'énergie renouvelables dans les pays OECD Europe dépassera celle provenant des sources non-renouvelables dans les années à venir [8]. De par la nature intermittente des sources d'énergie renouvelables telles que les panneaux solaires et les éoliennes, des communications de bout-en-bout sont nécessaires pour assurer que la quantité d'énergie générée équivaut à la quantité d'énergie consommée, auquel cas des problèmes significatifs de tension et de fréquence peuvent survenir.

Étant donné que les maisons jouent un rôle central dans les smart grids, de nouveaux liens de communications devront apparaître des postes électriques aux maisons, liens qui sont présentement indisponibles [9]. Effectivement, 50 % de l'énergie consommée provient des maisons, les véhicules électriques y seront chargées et les maisons pourront devenir des acteurs primaires de génération d'électricité verte en installant des panneaux solaires et des éoliennes [9].

Étant donné la pluralité des domaines techniques contenus dans une smart grid, soit les technologies de l'information, les communications et le système électrique, et le fait que ce soit un domaine de recherche relativement récent, très peu de modèles formels smart grid existent. IEEE P2030 [10] est un important modèle tentant de définir formellement les composantes d'une smart grid et ses interactions. Cependant, ce modèle est générique et ne considère aucune technologie spécifique, notamment au niveau des technologies de communications.

Une panoplie de technologies de communications sans fil et filaires peuvent être utilisées pour interconnecter les postes électriques aux maisons. Les réseaux optiques sont particulièrement intéressants dans le cadre des smart grids puisqu'ils sont immunisés contre les interférences électromagnétiques, offrent une grande capacité avec faible latence, sont durables et peuvent évoluer de 1 à plus de 100 Gbps. C'est ce qu'ont choisi 22 compagnies d'électricité Suisse, en s'unissant pour former le réseau multi-niveau Swiss Fibre Net, offrant de façon ouverte des communications optiques efficientes en termes de coût pour les compagnies d'électricité et pour les fournisseurs de service (vidéo, voix, données, etc.). D'un autre côté, les réseaux sans fil offrent les propriétés de mobilité, de flexibilité et d'adaptation. Il est donc considéré que les réseaux d'accès convergeront sous la forme de réseaux optiques et sans fil [4].

La première partie de cette thèse consiste à étudier en détail les réseaux FiWi, plus particulièrement les réseaux *passive optical networks* (PONs), IEEE 802.11 et WiMAX dans un contexte smart grid. Effectivement, les performances des réseaux FiWi n'ont pas été quantifiés en termes de délai, capacité et fiabilité.

Il n'existe pas ou très peu d'études multidisciplinaires smart grids sur les perspectives de communications et du système électrique tenant compte de technologies convergentes. Ainsi, dans cette thèse, on s'intéresse en premier lieu à étudier de façon multidisciplinaire les réseaux FiWi appliqués aux smart grids par l'entremise d'élaboration de banc d'essai et par l'étude de modèles de co-simulations. Cette partie est utile pour (*i*) étudier en détail ces deux perspectives et (*ii*) mesurer des configurations réalistes d'applications smart grids, pouvant ensuite les utiliser pour étudier les performances des réseaux FiWi dans un cadre smart grid.

1.1 Contributions

Les contributions de cette thèse sont résumées comme suit. Les réseaux optiques passifs de prochaines générations sont premièrement passés en revue, permettant l'évolution à court terme et la révolution à long terme [11, 12, 13] où les réseaux optiques et sans fil (FiWi) intégrés représentent la finalité des réseaux d'accès. Nous soulignons l'opportunité d'intégrer des capteurs optiques et sans fil avec les réseaux d'accès FiWi et proposons Über-FiWi dont le potentiel permet de bénéficier non pas seulement au secteur des télécommunications, mais dans une multitude de secteurs économiques tels que l'énergie (smart grid) et le transport.

On note ensuite que les deux attributs de qualité de communications sont la fiabilité et la latence, tels que définis dans IEEE P2030. On propose d'agréger le trafic smart grid et *triple-play* (vidéo, voix et données) à un réseau d'accès convergent EPON et réseau maillé sans fil (IEEE 802.11) [14, 15]. On montre en premier lieu que lorsque la charge réseau augmente dans le réseau FiWi, une dégradation des performances en termes de délai et de perte sont notés puisque le réseau EPON n'offre pas de qualité de service. Pour contrer ce problème, on propose un processus d'admission *token bucket* multidimensionel permettant ainsi d'assurer une qualité de service par classe et par hôte (host).

Le premier modèle analytique FiWi est proposé dans [16, 17], permettant ainsi d'évaluer la performance de différents algorithmes de routage FiWi. Le modèle est très flexible et incorpore différentes distributions de taille de trame, de débit de données et d'échec de fibre optique. Le modèle analytique est vérifié au moyen de simulations FiWi avec différentes architectures suivant des scénarios de trafic *peer-to-peer*, en amont, uniforme et non-uniforme. Un nouvel algorithme de routage, *optimized FiWi routing algorithm* (OFRA), est proposé et surpasse les approches de minimisation par nombre de sauts ou par délai en termes de débit maximal au détriment d'une augmentation mineure du délai pour des charges de trafic faibles à moyennes.

Ensuite, les performances de réseaux multi-niveau FiWi intégrés avec trafic *human-to-human* (H2H) et *machine-to-machine* (M2M) sont étudiées en terme de délai, capacité et fiabilité [18]. Considérant le protocole EDCA de IEEE 802.11e avec qualité de service, le modèle existant considérant un trafic saturé [19] est adapté et vérifié avec un trafic non-saturé. De plus, des capteurs événementiels (*event-driven*) et périodiques (*time-driven*) sont considérés. L'analyse permet de quantifier la borne théorique du débit de données maximal du trafic M2M sans violer un seuil de délai du trafic H2H.

Tel que défini qualitativement dans IEEE P2030, la disponibilité est un des plus importants attributs de qualité pour les communications smart grids. Cependant, cette métrique doit être quantifiée pour permettre de valider les exigences smart grids. Dans les travaux reliés, la disponibilité a été quantifiée pour les réseaux sans fil et optiques en termes d'accessibilité. Bien qu'il soit utile de connaître l'accessibilité lors de l'installation, il faut également connaître la disponibilité probabiliste lorsque l'installation est terminée et que le réseau est fonctionnel. On propose alors un modèle probabiliste multi-classe original pour les réseaux PONs et WiMAX intégrés [5]. Comparativement aux autres travaux, le modèle prend en compte (i) les limites des protocoles MACs et (ii) les échecs probabilistes de fibres optiques et des stations de base. En utilisant les configurations réalistes mesurées d'applications smart grids dans [20], on quantifie le débit de données maximal des capteurs pouvant être généré permettant de respecter les exigences de disponibilité des capteurs et du trafic régulier.

De plus, la coordination et l'optimisation de véhicules électriques et source d'énergie renouvelables sont étudiées de façon multidisciplinaire. En premier temps, un co-simulateur sans synchronisation est proposé dans [21], combinant les simulateurs OMNeT++ et OpenDSS existants, permettant ainsi de montrer l'impact de capteurs périodiques vs. événementiels sur un algorithme de contrôle de tension. Ensuite, un multi-simulateur suivant une architecture High Level Architecture est proposé [20], permettant de synchroniser un ensemble de simulateurs pour modéliser toutes les perspectives smart grids. Dans le cadre de ce travail, un cas d'usage basé sur des configurations réelles en France a été développé, et notamment les caractérisques d'applications smart grids ont été mesurées et injectées dans le modèle de multi-simulation. Utilisant l'original co-simulateur développé en [21], un algorithme de coordination intégré pour véhicule et sources d'énergie renouvelables est proposé et interagit via une infrastructure de communications convergente FiWi [22, 23]. L'algorithme est évalué par co-simulation où la perspective du système de distribution électrique interagit dynamiquement avec le modèle d'infrastructure FiWi, où moins de 2 Mbps est nécessaire pour diminuer de 21 % la puissance durant la période de pointe.

Finalement, les configurations d'un système de distribution réel du Danemark sont miniaturisées et un banc d'essai expérimental est développé suivant ces configurations réalistes [24]. Dans le cadre de ce travail, une méthode de coordination des capteurs est proposée pour améliorer la synchronisation de mesures échangées via une architecture de communications multi-saut. De plus, un mécanisme original de programmation dynamique est proposé pour tenir compte de façon jointe des performances du réseau de distribution et de la minimisation du coût client.

1.2 Structure de la thèse

Cette thèse est structurée en deux parties. Dans la partie I, une synthèse est premièrement effectuée. Au chapitre 2, le contexte et l'état de l'art sur les réseaux intelligents, ses principales applications et les technologies de communications potentielles sont résumées.

Le chapitre 3 porte sur la quantification de la borne théorique supérieure de trafic machine-to-machine (M2M) sans violer un seuil maximal de délai de trafic *human-to-human* (H2H). Ensuite, au chapitre 4, des cas d'usage multidisciplinaires sur la coordination de véhicules électriques et de sources d'énergie renouvelables sont présentés de façon multidisciplinaire via co-simulation. Au chapitre 5, la faisabilité pratique d'un nouvel algorithme de coordination de véhicules électriques est démontrée expérimentalement sur un banc d'essai d'un système de distribution réel du Danemark miniaturisé. Finalement, les conclusions et les publications réalisées sont présentées aux chapitres 6 et 7, respectivement.

Dans la seconde et troisième parties, les articles des journaux acceptés sont présentés. Le chapitre 8 présente un modèle de quantification probabiliste de la disponibilité de réseaux intégrés PON et WiMAX. Au chapitre 9, une étude multidisciplinaire de co-simulation d'un algorithme de coordination optimisée de véhicules électriques et de sources d'énergie renouvelables opéré via une infrastructure de communications FiWi est présentée. Au chapitre 10, une analyse est proposée sur des réseaux PONs intégrés avec des réseaux multi-sauts WiFi de prochaines générations. Finalement, le chapitre 11 porte sur les réseaux FiWi dans le cadre de la troisième révolution industrielle où ils ne sont pas seulement utilisés par le secteur des télécommunications, mais également exploités par l'ensemble des secteurs économiques, incluant l'énergie et le transport pour augmenter leur efficacité et durabilité.

Chapitre 2

État de l'art

Dans ce chapitre, les notions générales en rapport avec les problèmes considérés dans cette thèse sont présentées. En premier lieu, la notion de réseau intelligent est définie selon une norme récemment proposée. Ensuite, les applications primaires attendues des réseaux intelligents sont résumées. En troisième lieu, les technologies de communications smart grids potentielles sont brièvement définies. Finalement, les réseaux *fiber-wireless* (FiWi), qui est la technologie de communications étudiée en détail dans le cadre de cette thèse pour les smart grids, sont introduits.

2.1 Introduction

Le réseau électrique intelligent, aussi appelé *Smart Grid* ou réseau intelligent, est une amélioration significative du réseau électrique du 20ème siècle caractérisée essentiellement par des flux bidirectionnels d'information et d'énergie [1, 6, 25]. En ce sens, les réseaux intelligents sont parfois appelés *Energy Internet*, où les acteurs et les composantes échangent de l'énergie et des données entre eux, similairement au réseau Internet où ses composantes et acteurs partagent des données sur une infrastructure partagée [26, 27]. Selon le rapport du National Institute of Standards and Technology (NIST) [28], les principaux avantages attendus sont l'amélioration de la fiabilité et de la qualité de la puissance, amélioration de la capacité et de l'efficacité des réseaux électriques existants, faciliter la maintenance prédictive et l'auto-correction des problèmes du système et faciliter le déploiement des sources d'énergie renouvelables. De plus, le rapport NIST souligne également

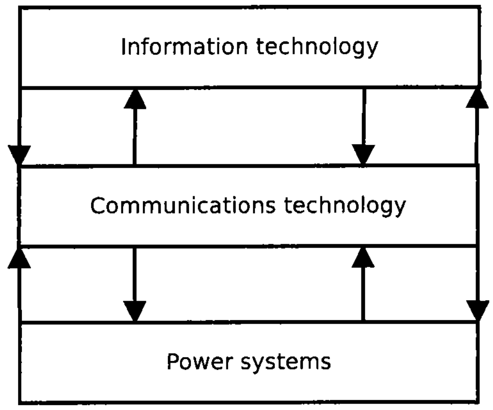

Figure 2.1 – Interactions entre les perspectives smart grids telles que définies dans IEEE P2030.

qu'un réseau intelligent doit idéalement diminuer les émissions de gaz carbonique en permettant le déploiement des véhicules électriques couplés à de nouvelles sources d'énergie renouveables, réduire la consommation de pétrole en réduisant la génération inefficace lors des périodes de pointe.

Récemment, la norme IEEE P2030 a été publié et représente une des premières tentatives pour normaliser les réseaux intelligents et rendre ainsi ses composantes et acteurs interopérables [10]. La norme offre un modèle de référence d'interopérabilité smart grid, qui définit des interfaces génériques entre les domaines fonctionnels pour trois perspectives, comme représentées à la Figure 2.1 et listées comme suit :

— *Perspective d'interopérabilité architecturale des systèmes électriques :* Cette perspective gère la génération, le transport et la consommation de l'énergie électrique.
— *Perspective d'interopérabilité architecturale de technologies de communications :* Cette perspective comporte les composantes réseautiques et les protocoles de communications.
— *Perspective d'interopérabilité architecturale des technologies de l'information :* Cette perspective comporte les processus et le contrôle des flux de données en relation avec les applications qui opèrent et gèrent le réseau intelligent.

Les éléments primaires d'un réseau intelligent sont définis en 7 domaines (Figure 2.2) : (*i*) production et stockage, (*ii*) transmission, (*iii*) distribution, (*iv*) client (résidentiel, commercial et industriel), (*v*) contrôle et opérations, (*vi*) les marchés et (*vii*) les fournisseurs de services.

Dans le cadre de cette thèse, l'accent est mis plus particulièrement au niveau du contrôle et des opérations associées au domaine de la distribution. L'étude porte essentiellement sur la perspective

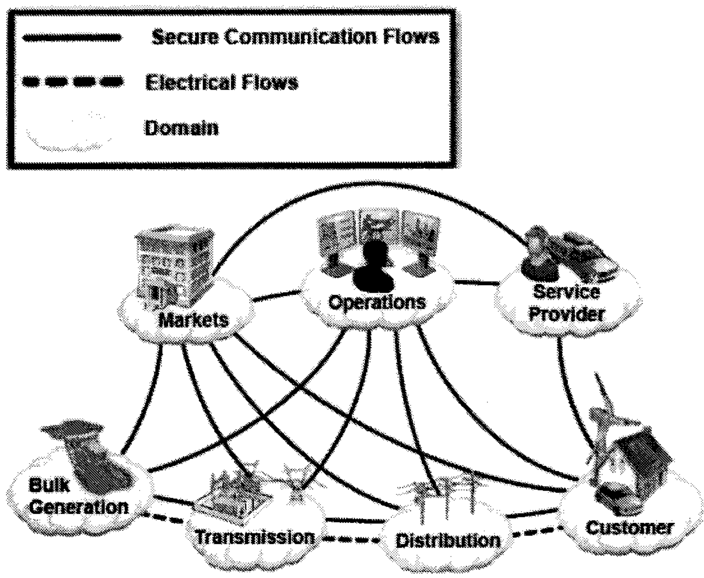

Figure 2.2 – Modèle conceptuel des domaines d'un réseau intelligent [1].

des techniques de communications, mais tient également compte des deux autres perspectives en effectuant des études multidisciplinaires. Le domaine de la distribution dans le contexte des réseaux intelligents comporte le contrôle et la surveillance au-delà des postes électriques vers les clients. Effectivement, présentement il n'y a peu ou pas d'échange de données entre les postes électriques et les clients [29], et il y a donc un besoin nouveau de communiquer efficacement, de façon fiable et à faible coût entre ces acteurs. Ces nouveaux liens de communications entre les postes électriques et les clients rendent possibles de nouvelles applications smart grids qui sont décrites dans la section suivante.

2.2 Applications primaires attendues des réseaux intelligents

Tel que mentionné dans [1], les applications smart grids de véhicules électriques, microréseaux et de compteurs intelligents nécessitent des liens de communications de bout-en-bout, qui sont décrits dans cette section.

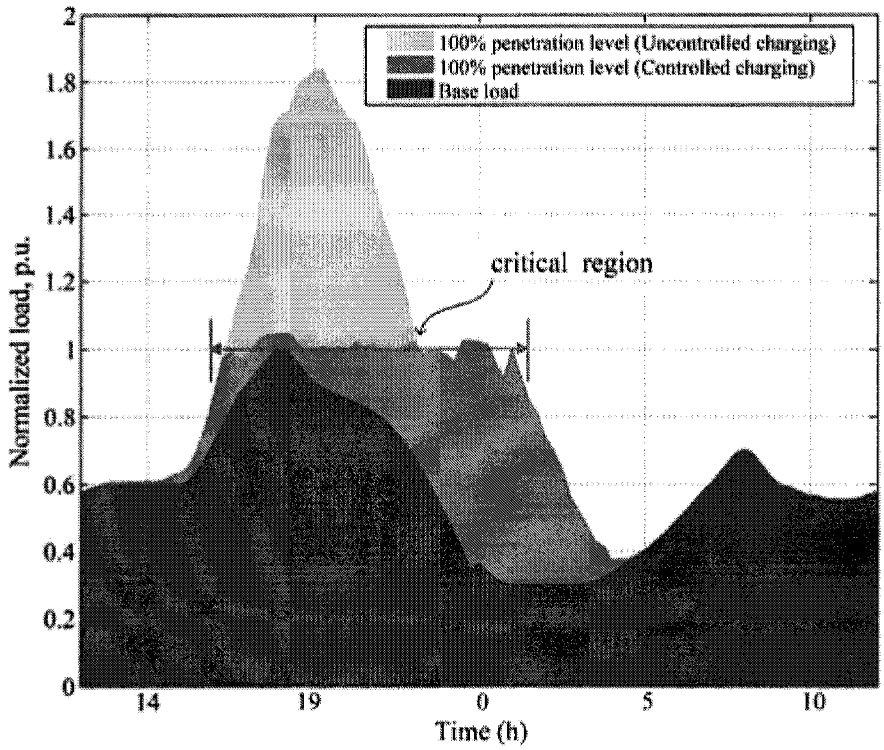

Figure 2.3 – Impact sur la charge globale du système électrique des approches coordonnées/non coordonnées de véhicules électriques [2].

2.2.1 Véhicule électrique

Les véhicules électriques (ou *plug-in electric vehicles* (PEV)s) sont intéressants pour pallier à la dépendance au pétrole et pour diminuer la génération de gaz carbonique. Les véhicules conventionnels peuvent causer des smogs dans les villes fortement peuplées, notamment récemment observés à Paris (France) [1] où la ville a dû significativement limiter le nombre de véhicules conventionnels et a priorisé notamment les PEVs et le transport collectif.

Les PEVs ont 2 modes possibles dans le cadre des réseaux intelligents : (*i*) *grid-to-vehicle* (G2V) et (*ii*) *vehicle-to-grid* (V2G) [30, 31]. Le mode G2V consiste à stocker la puissance dans les batteries de PEVs à partir d'une source d'énergie externe. La Figure 2.3 illustre l'impact sur la charge globale du système électrique d'une pénétration de 100 % de véhicules électriques en utilisant des approches coordonnées et non-coordonnées. On dénote que l'approche coordonnée permet de significativement diminuer la charge maximale durant la période de pointe.

1. http://www.tf1.fr/auto-moto/actualite/circulation-alternee-a-paris-fonctionnement-exceptions-et-8384177.html

De plus, l'électrification des transports permet potentiellement d'augmenter la génération d'énergie à partir des sources d'énergie renouvelables. Couplés à un système de communications de bout-en-bout, les PEVs peuvent être coordonnés pour diminuer les pertes de puissance et améliorer le profil de la tension [32]. Les PEVs peuvent également être chargés de façon décentralisée pour diminuer la quantité de données transférées, mais des échanges de données sont également nécessaires [2].

2.2.2 Micro-réseau

Bien que les sources d'énergie renouvelables peuvent générer de l'énergie de façon distribuée et durable, ils génèrent de l'énergie de façon intermittente et aléatoire. Si une telle production intermittente est injectée sans contrôle, cela va augmenter significativement la différence entre la puissance générée et celle utilisée, ce qui cause des problèmes de tension et de fréquence [33, 34]. Ces problèmes peuvent être évités en isolant et contrôlant certaines régions du réseau intelligent pour ainsi former des micro-réseaux (*microgrids*) ou nanoréseaux [35].

2.2.3 Compteur intelligent

Une importante capacité des réseaux intelligents est d'offrir de nouveaux services permettant aux clients de réagir en utilisant des appareils intelligents à domicile, qui est une technique mieux connue sous le nom de *demand side management* DSM [36, 37]. Une utilité significative potentielle de déployer de tels compteurs intelligents est d'offrir des prix d'électricité variables en fonction du temps, ce qui peut permettre notamment d'offrir de plus faibles prix lorsque le réseau intelligent est faiblement chargé et inversement lorsque le réseau est fortement chargé [38], ce qui a pour conséquence de diminuer la charge de pointe. De plus, un tel compteur intelligent permet également de connaître en temps réel la charge à chaque noeud du réseau avec une granularité fine.

2.2.4 Surveillance et contrôle en temps réel des systèmes de distribution

Une application smart grid significative nécessitant des communications de bout-en-bout est la surveillance et le contrôle des réseaux de distribution en temps réel, mieux connu sous le nom de *wide-*

area situational awareness (WASA) [25]. L'application WASA permet d'avoir une vue d'ensemble dynamique des réseaux de distribution de façon synchronisée.

2.3 Technologies de communications pour les réseaux intelligents

Il existe une panoplie de technologies sans fil et filaires pouvant servir de communications pour les réseaux intelligents. Selon la norme IEEE P2030, les trois attributs de qualité les plus importants de la perspective de communications des domaines *client* et *distribution* sont la latence, la fiabilité et la qualité de service. La *latence* de communications entre une entité source donnée vers une destination donnée est exprimée par le temps que met un certain message à parcourir un ou plusieurs noeuds intermédiaires jusqu'à sa réception. La *fiabilité* est formellement définie comme étant l'habileté d'effectuer une certaine tâche selon des conditions et un temps déterminés. Selon la technologie de communications, la latence et la fiabilité varient. Le but de cette thèse n'est pas de quantifier le choix technologique de communications, qui peut varier en fonction du pays et de facteurs politiques et commerciaux, mais plutôt d'étudier les attributs de qualité de communications d'une technologie sélectionnée à fort potentiel. Plus spécifiquement, on s'intéresse aux communications entre les postes électriques jusqu'aux clients, nommé *neighborhood area network* (NAN) dans la norme IEEE P2030. Il est à noter que plusieurs protocoles ZigBee (IEEE 802.15.4) ont été développés chez les clients [39]. Dans cette section, les principales technologies de communications considérées dans la littérature sont résumées [1, 39].

2.3.1 Sans fil

IEEE 802.11 (WiFi)

WiFi est une technologie sans fil mondialement éprouvée et utilisée. Pour gérer l'accès multiple, IEEE 802.11 utilise le protocole *distributed coordination function* (DCF) sans qualité de service (QdS). Chaque noeud WiFi implémentant la fonction DCF attend à chaque début de transmission une période fixe *DCF interframe space* (DIFS) pour écouter le canal. Lorsqu'aucune autre station n'a transmis durant cette période, la station attend une période aléatoire de *backoff* (augmentant exponentiellement à chaque collision) et transmet ensuite. IEEE 802.11s permet également de former des réseaux WiFi maillés multi-sauts [40]. IEEE 802.11n offre deux techniques d'aggrégation de trames *Medium Access Control* (MAC), soit *aggregate MAC service data unit* (A-MSDU) et *aggregate MAC protocol data unit* (A-MPDU) qui permettent de concaténer plusieurs trames lors d'une certaine transmission pour améliorer l'efficacité [41, 42]. De plus, la norme de très haut débit IEEE 802.11ac offre un débit de données de 6.9 Gbps. Également, IEEE 802.11e offre une fonction d'accès multiple avec QdS, nommée *enhanced distributed channel access* (EDCA) [43] permettant de prioriser les trames par classe.

IEEE 802.16 (WiMAX)

Worldwide Interoperability for Microwave Access (WiMAX) est une technologie point-à-multipoint très intéressante au Canada pour les réseaux intelligents puisqu'une bande séparée est dédiée aux systèmes électriques et cette technologie offre une connectivité à longue distance et plusieurs mécanismes de QdS. Pour transmettre, les stations doivent rivaliser en utilisant une méthode à accès multiple *carrier sense multiple access with collision avoidance* (CSMA/CA) avec *backoff* binaire exponentiel similaire aux protocoles MAC WiFi DCF et EDCA [44, 45].

ZigBee

ZigBee (IEEE 802.15.4) est une technologie initialement conçue pour déployer largement des capteurs sans fil à faible débit. En ce sens, il est très bien adapté pour l'intérieur des bâtiments. Il est à noter que ZigBee partage les mêmes fréquences que IEEE 802.11 (2.4 GHz). ZigBee peut également être utilisé pour des transmissions de longue distance au delà de plusieurs kilomètres [46] et peut donc être considéré pour les réseaux NANs considérés dans cette thèse.

LTE

Dans des travaux récents, la faisabilité d'utiliser Long Term Evolution (LTE) pour les réseaux intelligents a été démontrée pour les applications de *distribution automation* en utilisant de très faibles débits (1-480 bps) supposant des exigences de latence de l'ordre de 1-4 secondes [45]. Un avantage significatif d'utiliser les réseaux cellulaires LTE pour les réseaux intelligents est qu'aucune nouvelle infrastructure de communications ne doit être ajoutée. Un inconvénient majeur est cependant la latence puisque certaines applications smart grids nécessitent une latence de moins de 20 ms [25] et un délai d'ordonnancement LTE minimal de 65 ms a été mesuré dans [45]. De plus, le débit offert aux clients des réseaux cellulaires est limité [39], ce qui peut restreindre les possibilités de nouvelles applications smart grids.

Comparatif

Tableau 2.1 – Comparatif des technologies sans fil considérées.

	Partagé ?	Capacité (Mbps)	Couverture (kilomètres)	Avantages	Inconvénients
802.11n/ac	Oui	600/6900	1-32	Capacité élevée.	Partagé par plusieurs applications.
WiMAX	Oui/Non	75	1-50	Longue portée et canal dédié au Canada.	Non utilisé à grande échelle.
ZigBee	Oui	0.25-2	1-45	Dépense peu d'énergie.	Faible capacité.
LTE	Oui	N/D	1-10	Infrastructure existante.	Débit coûteux et limité.

Le tableau 2.1 compare les technologies sans fil considérées. Globalement, toutes les technologies sont partagées par plusieurs applications, outre WiMAX qui peut être dédié pour les réseaux intelligents. En terme de capacité, WiFi offre de loin le débit de données le plus élevé. Il est à noter que des équipements WiFi à longue portée existent déjà [2]. Bien que le débit sortant ne peut jamais égaler la capacité, une plus grande capacité est en général préférable pour (*i*) obtenir de plus faible délai et (*ii*) permettre de supporter de potentielles applications futures nécessitant des débits de données qui peuvent croître. Étant donné la forte capacité qu'offre WiFi et l'aspect dédié de WiMAX, ces deux technologies sans fil sont considérées dans la présente thèse pour le réseau NAN.

2. Voir `http://www.cisco.com/c/en/us/products/wireless/aironet-1300-series/index.html`.

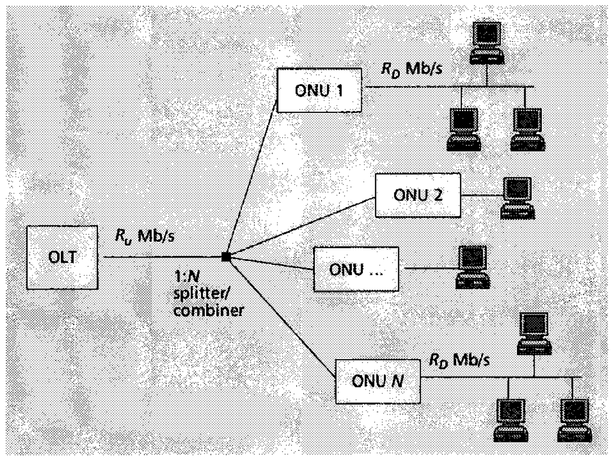

Figure 2.4 – Topologie d'un réseau d'accès PON conventionnel [3].

2.3.2 Filaire

Optique

Selon Telecom Italia [47], il ne fait aucun doute que les réseaux d'accès tendront vers des réseaux optiques *fiber-to-the-home* (FTTH) pour des raisons de durabilité, évolutivité et d'efficacité énergétique. China Telecom a déployé plus de 70 millions de ports FTTHs de 2004 à 2012 [48]. Selon China Telecom, les tendances majeures sont : (*i*) augmentation de la pénétration de la fibre, où les noeuds optiques deviennent de plus en plus près des clients pour améliorer le débit et la qualité des services réseaux, (*ii*) plus de volume et de rapidité, de *Ethernet/Gigabit passive optical network* (EPONs/GPONs) vers 10G-EPON à 40 Gbps en un seul système PON et (*iii*) augmentation de la couverture en combinant les communications filaires, sans fil et mobiles.

Il est à noter qu'un réseau PON est complètement passif (sans consommation d'électricité) entre le noeud central *optical line terminal* (OLT) et les noeuds clients *optical network units* (ONUs), illustré à la Figure 2.4. Comparativement aux réseaux WLANs qui utilisent un mécanisme décentralisé de gestion d'allocation de la bande passante, le noeud central OLT dans les réseaux EPONs s'occupe d'allouer dynamiquement la bande passante en fonction de messages *REPORT* des ONUs qui spécifient la quantité de trafic en attente de transmission.

Les réseaux EPONs (IEEE 802.11ah) couvrent 20 kilomètres et le *long-reach PON* (LR-PON) a été proposé pour étendre significativement cette distance vers 100 kilomètres [49]. Les réseaux *wavelength division multiplexing* PONs (WDM PONs) fonctionnent sur plusieurs longueurs d'onde ce qui permet d'avoir divers clients partageant le même réseau de façon indépendante. En utilisant la technique de *reflective semiconductor optical amplifier* (RSOA), les ONUs peuvent réfléchir et remoduler les signaux optiques générés par l'OLT, ce qui permet de simplifier les noeuds clients et diminuer les coûts. Les réseaux *wavelength-routing PONs* (WR-PONs) utilisent des *arrayed-waveguide grating* (AWGs) comme noeuds intermédiaires passifs pour démultiplexer et multiplexer en aval et en amont, respectivement, pour former des liens point-à-points (contrairement aux EPONs et WDM PONs qui sont point-à-multipoints) et qui améliorent ainsi la sécurité et la confidentialité.

Power Line Communication

Power Line Communication (PLC) est une technique qui utilise les lignes électriques existantes pour transmettre des données [39]. En France, cette technologie est en cours d'investigation pour le projet de compteurs intelligents Linky, où PLC est utilisé pour transmettre les mesures à des concentrateurs de données où ensuite le réseau *General Packet Radio Service* (GPRS) est utilisé pour lier les concentrateurs au centre de traitement de données. Bien que PLC peut être une solution efficiente en termes de coût pour des applications simples telles que Linky, cette technologie a cependant l'inconvénient d'utiliser le même média qui est en fait mesuré. Ainsi, si un lien est brisé et qu'une panne survient, le lien de communications devient indisponible, soit le moment exact où on en aurait besoin.

Comparatif

Tableau 2.2 – Comparatif des technologies filaires considérées.

	Partagé ?	Capacité	Couverture (kilomètres)	Avantages	Inconvénients
Optique/PON	Oui	1-100 Gbps	20-100	Evolutivité, fiabilité et grande capacité.	Partagé par plusieurs applications.
PLC	Non	20 Kbps-3 Mbps	2-3	Réseau déjà en place.	Non fiable et capacité limitée.

Le tableau 2.2 contient un comparatif des technologies filaires considérées. Etant donné la grande capacité, fiabilité et des multiples possibilités d'évolution des réseaux PONs, cette technologie est considérée dans cette présente thèse dans un cas de figure où le réseau PON est partagé efficacement pour plusieurs applications : smart grid, voix, vidéo, données, etc.

2.4 Les réseaux FiWi

Tel qu'estimé par China Telecom, les réseaux PONs vont converger en réseaux *fiber-wireless* (FiWi) pour combiner les avantages de ces deux médiums [4, 50]. En effet, les réseaux optiques offrent une grande capacité, une immunisation contre les interférences électromagnétiques et les réseaux sans fil se déploient rapidement, à faible coût et offrent la mobilité. Il existe deux variantes de réseau FiWi : radio-via-fibre (ou radio-over-fiber (RoF)) et radio-et-fibre (ou radio-and-fiber (R&F)). Un mécanisme FiWi intéressant est l'aggrégation de trame hiérarchique [42]. Tel que noté dans la Section 2.3.1, le protocole IEEE 802.11n offre l'aggrégation de trames pour transmettre plusieurs trames par transmission. D'un autre côté, les réseaux PONs n'offrent pas l'aggrégation puisque le réseau fonctionne en transmettant des rafales périodiquement. Il est donc possible d'optimiser le réseau FiWi en intégrant efficacement les 2 médiums [42].

2.4.1 Radio-via-fibre

Les réseaux RoF utilisent la fibre optique pour transmettre des signaux analogiques des fréquences radio dans le but diminuer la complexité (et ainsi le coût) des *remote antenna units* (RAUs) situés à l'interface optique-sans fil. La faisabilité d'une telle architecture a été démontrée au niveau de la couche physique. Cependant, les mécanismes de la couche MAC rendent cette approche inefficace pour certaines technologies, par exemple le WiFi. Effectivement, les valeurs de temps mort sont de 9 μs et 20 μs pour IEEE 802.11a/g et IEEE 802.11b, respectivement, ce qui est strictement inférieur au délai de propagation optique pour 20 kilomètres de fibre.

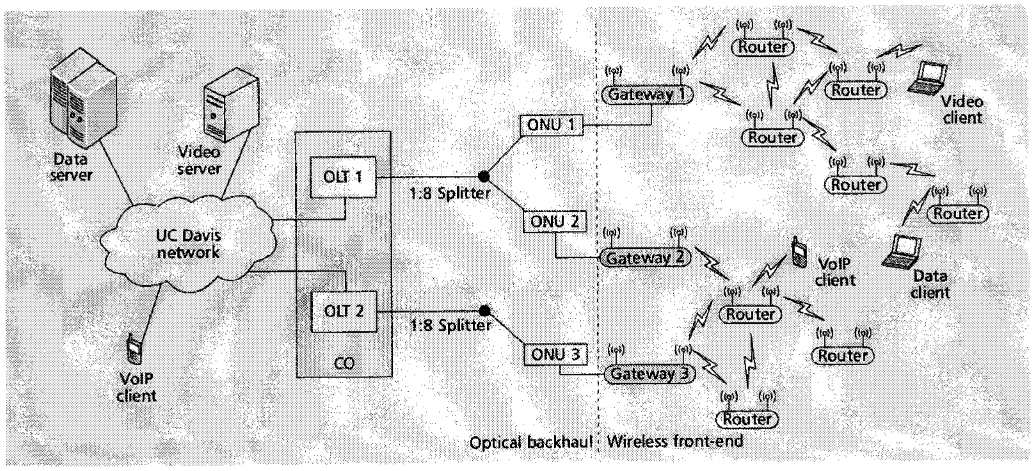

Figure 2.5 – Banc d'essai R&F d'un réseau EPON et wireless mesh network (WMN) [4].

2.4.2 Radio-et-fibre

Ces problèmes au niveau de la couche MAC peuvent être évités avec R&F, en utilisant deux protocoles MAC (un pour l'optique et un second pour le sans fil) séparément avec un mécanisme de conversion entre les 2 réseaux. Ceci crée cependant un certain nombre de problématiques à résoudre, incluant l'assemblage des trames et le contrôle de la congestion, qui sont décrits plus en détail dans [4]. La Figure 2.5 illustre un banc d'essai R&F récemment réalisé à University of California intégrant deux réseaux EPONs et un WLAN wireless mesh network (WMN) IEEE 802.11g permettant de transférer du trafic de données, de voix et de vidéo entre des noeuds Linux.

2.4.3 Fiber-wireless sensor networks (Fi-WSNs)

Les réseaux FiWi peuvent être enrichis en intégrant des capteurs sans fil et optiques, tel qu'illustré à la Fig. 2.6 (MP : *mesh point*, MPP : *mesh portal point*, MAP : *mesh access point*), proposés pour la première fois dans [51]. Un réseau Fi-WSN peut utiliser des capteurs optiques à base de réseaux de Bragg et IEEE 802.15.4 ZigBee pour les capteurs sans fil ou via un réseau maillé IEEE 802.11. Intégrer ces capteurs permet d'interagir avec des systèmes du monde réel pour surveiller divers paramètres, par exemple la température, la pression, le son, etc. Récemment, plusieurs travaux ont porté sur l'optimisation de la génération de CO_2 causée par les technologies de l'information. Ce n'est que récemment que le milieu de la recherche a commencé à explorer les nouveaux rôles des réseaux d'accès dans divers secteurs économiques pour améliorer son efficacité énergétique, où

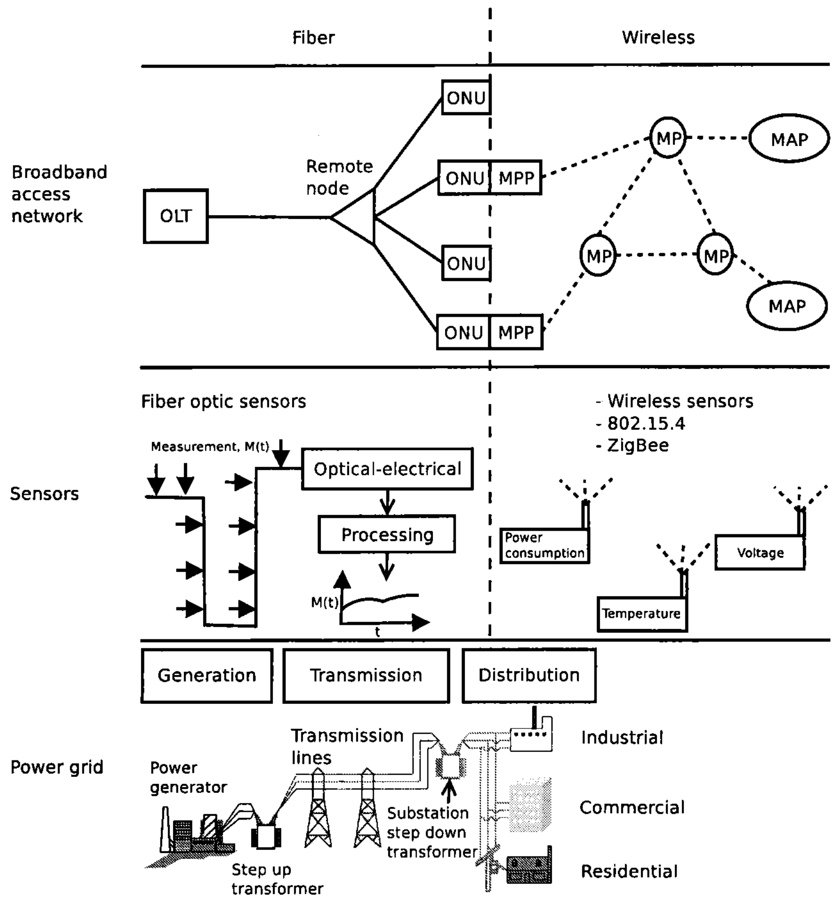

Figure 2.6 – Le réseau Fi-WSN, permettant l'intéraction avec des systèmes complexes hétérogènes.

les télécommunications ne deviennent plus un problème, mais une solution [52]. Les Fi-WSNs sont utilisés pour convertir les systèmes électriques traditionnels en réseaux intelligents.

2.5 Résumé

Dans ce chapitre, les notions générales en rapport avec les problèmes investigués sont définies. Selon la norme IEEE P2030, un réseau intelligent (smart grid) est composé de la perspective de technologies d'informations, de communications et du système électrique, où chaque perspective comporte un ensemble de domaines. Dans le cadre de cette thèse, l'accent est mis au niveau du contrôle et des opérations associées au domaine de la distribution pour les perspectives de communications, mais en tenant compte des deux autres perspectives. Les applications principales attendues d'un smart grid, incluant les véhicules électriques et les micro-réseaux, nécessitent des communications de bout-en-bout fiables, où de nouveaux réseaux NANs sont nécessaires entre les postes électriques et les clients. Il existe une panoplie de technologies de communications filaires et sans fil pour les réseaux NANs. Dans le cadre de cette thèse, étant donnée la convergence des réseaux intégrées optiques et sans fil tel qu'estimé par China Telecom, les technologies de communications WiFi, WiMAX et PONs sont considérées comme des réseaux d'accès fiables, adaptatifs, évolutifs et à faible coût. Les réseaux FiWi peuvent également être enrichis de capteurs pour surveiller des systèmes réels tels que les smart grids.

Cependant, pour intégrer efficacement les réseaux optiques, les réseaux sans fil et les capteurs, il est important de comprendre en détail l'influence que chacune des composantes peut avoir sur les autres composantes. Plus spécifiquement, dans le chapitre suivant, on s'intéresse à étudier la coexistence du trafic des capteurs, soit de *machine-to-machine* (M2M) et du trafic *human-to-human* (H2H).

Chapitre 3

Analyse de coexistence de trafic H2H et M2M via une infrastructure FiWi

Dans ce chapitre, l'accent est mis sur l'étude de la coexistence de trafic *triple-play human-to-human* (H2H) et de trafic *machine-to-machine* (M2M) via une infrastructure de communications partagée *fiber-wireless* (FiWi). L'originalité de ce chapitre se démarque selon les points suivants : (*i*) analyse probabiliste de délai-capacité de réseaux FiWi avec applications hétérogènes (*ii*) intégration de capteurs événementiels et périodiques (*iii*) les noeuds ne sont pas saturés, où chaque noeud n'a pas nécessairement de trames à transmettre et (*iv*) cas d'usage en tenant compte de mesures d'applications réelles smart grids. L'analyse permet de quantifier la borne théorique supérieure du trafic M2M sans violer un seuil maximal de délai du trafic H2H.

3.1 Introduction

Les exigences de communications des principales applications smart grids ont été quantifiées en termes de latence, bande passante, fiabilité et sécurité [25]. Les auteurs ont conclu que des communications rapides et fiables sont nécessaires pour permettre l'échange en temps réel entre des éléments distribués. Puisque la norme IEEE P2030 propose un cadre générique uniquement, il est préférable de s'appuyer sur de faibles latences des fibres optiques et sans fil, où la fibre couvre une certaine partie du territoire et où le sans fil complémente les régions sans fibre [53].

Dans cette section, l'accent est mis sur une infrastructure FiWi pour les réseaux intelligents basée sur les réseaux EPONs et *wireless local area network* (WLANs). Les EPONs combinent le faible coût et la simplicité des équipements Ethernet où une partie de l'infrastructure demeure passive (sans consommation d'électricité), ce qui les rend très fiables. Outre les réseaux EPONs existants, les bénéfices des réseaux ultra-rapides *time division multiplexing* (TDM) et WDM *passive optical networks* (PONs) représentent les candidats les plus prometteurs pour les réseaux d'accès optiques des prochaines générations [54]. Du côté du sans fil, des réseaux WLANs avec QdS avec plusieurs classes de trafic différenciées sont considérés, ainsi que les améliorations de la nouvelle norme *very high throughput* (VHT) IEEE 802.11ac.

Il a été démontré dans [55] que la coopération entre plusieurs compagnies d'électricité dans la phase de déploiement permet de sauver 17 % de *capital expenditures* (CAPEX) lors du déploiement de FTTH. Un exemple pratique de modèle d'affaire multi-niveau est le Swiss Fibre Net de OPENAXS qui regroupe 22 compagnies d'électricité en Suisse. Les compagnies sont responsables d'installer le réseau, mais permettent également l'accès au réseau avec d'autres fournisseurs de services (voix, vidéo, données, etc.).

L'objectif de cette section est d'étudier les performances des réseaux FiWi multi-niveaux permettant d'offrir des services triple-play *human-to-human* (H2H) et aussi en considérant des capteurs sans fil pour des applications *machine-to-machine* (M2M) telles que les réseaux intelligents, donnant ainsi un modèle de type *Internet of Things* (IoT). Des lignes directrices pratiques en termes de distance entre noeuds et fréquence de la coexistence de réseaux ZigBee et WLANs pour les réseaux intelligents ont été développées dans [56]. L'originalité dans cette section vient de l'investigation de la coexistence de trafic H2H et M2M en utilisant un réseau FiWi intégré basé sur des technologies de prochaines générations EPON et WLAN en termes d'analyse probabiliste de la capacité, de latence et de fiabilité. De façon pratique, ceci permet de quantifier le débit maximal dont les capteurs (noeuds M2M) sans fil peuvent être configurés sans altérer de façon négative le délai du trafic H2H, ayant pour finalité de connaître la borne supérieure théorique du trafic M2M pour supporter des applications smart grids futures.

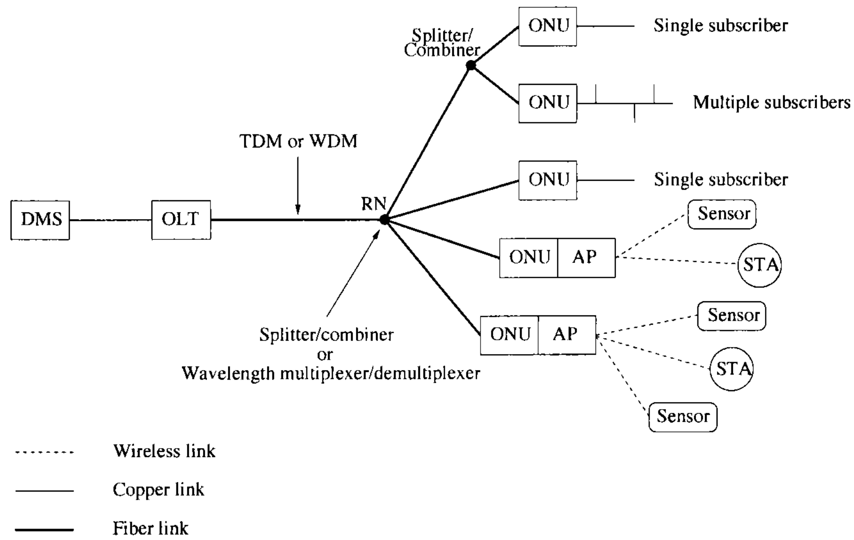

Figure 3.1 – Architecture générique de communications Smart Grid FiWi.

3.2 Infrastructure de communications FiWi pour les réseaux intelligents

L'architecture de communications FiWi considérée est illustrée à la Figure 3.1. Le réseau d'accès optique consiste en un EPON avec une topologie en forme d'arbre (*tree-and-branch*). Le noeud central OLT connecte le DMS du réseau intelligent. Les noeuds ONUs, soit les noeuds clients, sont attachés au niveau des feuilles. Un ONU peut servir pour un ou plusieurs abonnés et avoir un *access point* (AP) WLAN connectant des capteurs sans fil et des *stations* (STAs).

Plus spécifiquement, le réseau d'accès optique peut suivre la norme existante IEEE 802.3ah EPON qui utilise une longueur d'onde en aval et une autre en amont, chacune opérant à un débit de données de 1 Gbps. Le remote node (RN) consiste en un combineur/diviseur de puissance optique. En amont, la bande passante est dynamiquement alouée à chaque ONU par l'OLT selon le mécanisme *report-grant*. Alternativement, les réseaux ultra-rapide 10+ Gbps TDM PONs ou WR-PONs/*wavelength-broadcasting PONs* (WB-PONs) peuvent être utilisés. IEEE 802.3av 10G-EPON offrent de meilleurs débits de données symétriques et asymétriques, utilisant tout de même des mécanismes similaires. Dans le cas des WB-PONs, les diviseurs/combineurs au RNs peuvent être utilisés sans être changés et permettent d'avoir de multiples longueurs d'onde sur une seule fibre. Chacune de ces longueurs d'onde diffusent aux WDM ONUs et peuvent être utilisées bidirectionnellement.

Chaque WDM ONU peut sélectionner une longueur d'onde en utilisant un filtre passe-bande et réutilise le signal en aval en utilisant des techniques de remodulation. Dans le cas des WR-PONs, les diviseurs/combineurs aux RNs doivent être remplacés par des multiplexeurs/démultiplexeurs de longueur d'onde (par exemple, AWGs). Il est à noter qu'une longueur d'onde peut être dédiée à un seul ONU (par exemple, un abonné d'entreprise) ou peut être partagée dans le temps par plusieurs ONUs (par exemple, des abonnés résidentiels). Finalement, les réseaux WDM PONs *long-reach* avec une distance ONUs-OLT de maximalement 100 kilomètres peuvent être utilisés pour diminuer significativement les coûts en combinant les réseaux d'accès et d'agrégation.

Chaque AP forme une zone WLAN associant des STAs et des capteurs. Dans cette section, le protocole EDCA de IEEE 802.11e est utilisé. EDCA supporte la QdS aux STAs avec différenciation de service en utilisant quatre différentes *access categories* (ACs), chacune avec de différentes valeurs de *arbitration inter-frame space* (AIFS) et de *contention window* minimum et maximum CW_{min} et CW_{max}, respectivement. Outre des WLANs conventionnels IEEE 802.11 a/b/g/n (capacité : 54-600 Mbps), les réseaux émergents IEEE 802.11ac VHT (capacité : 6.9 Gbps) sont également considérés.

Pour les capteurs sans fil, outre des paramètres de base (tension et courant) de 12 kbps, les quantités calculées (amplitude de phase, angle de phase, etc.) vont augmenter les exigences de bande passante à 200-500 kbps, ou jusqu'à 2-5 Mbps pour un échantillonage plus rapide dans les systèmes de détection rapide de faute [53]. Ils peuvent opérer à différents cycles tels que 10-100 ms pour estimer des paramètres systèmes critiques [57]. Les capteurs sans fil peuvent être des périphériques ZigBee offrant 250 kbps de capacité, ou peuvent également utiliser des mécanismes de signalisation avancés disponibles dans IEEE 802.15.4 pour augmenter la capacité à 2 Mbps [58]. Alternativement, pour réutiliser les infrastructures WLANs et diminuer les coûts, les capteurs énergétiquement efficients basés sur IEEE 802.11 peuvent être utilisés pour des transmissions périodiques ou événementielles [59].

3.3 Analyse de coexistence

Dans [17] (et inclut dans le chapitre II.10), une première analyse FiWi de réseaux intégrés PONs et WLAN IEEE 802.11n/ac a été proposée, permettant d'évaluer les performances d'algorithmes de routage FiWi. Toutefois, ce travail ne tient pas compte de la QdS, puisque IEEE 802.11n/ac ne contient pas de mécasnime de QdS.

Cette analyse étend le travail récent d'analyse de WLAN EDCA dans des conditions de trafic saturé (les STAs ont toujours des trames à transmettre) [19]. Pour ce qui est de la partie PON, la même analyse de [17] est utilisée. L'originalité de l'analyse présentée ici se distingue comme suit :

- L'analyse de [19] est étendue en incluant les cas de trafic non-saturé et inhomogène, où les noeuds WLANs peuvent être des capteurs sans fil ou STAs.
- Chaque noeud a une ou plusieurs files d'attente, chacune ayant une classe EDCA.
- L'analyse tient compte de capteurs événementiels et périodiques. Dans le cas basé par l'événement, les capteurs rivalisent pour accéder au canal suivant le mécanisme EDCA, tandis que les capteurs périoques utilisent une allocation temporelle dédiée.

3.3.1 Modèle réseau

Les paramètres du modèle réseau sont définis comme suit :

Tableau 3.1 – Paramètres du modèle réseau FiWi.

Symbole	**Description**
O	Nombre d'ONUs attachés au OLT.
$\lambda = 1, ..., \Lambda$	Longueur d'onde λ, où Λ représente le nombre de longueurs d'onde.
O_λ	ONUs supportant la longueur d'onde λ.
$\tau^{(\lambda)}$	Délai de propagation via la longueur d'onde λ. Dans le cas d'un TDM PON avec une seule longueur d'onde, on a τ.
ς	Capacité en bps d'une longueur d'onde donnée.
r	Capacité en bps d'un canal WLAN dans une zone donnée.
$\mathcal{S}_\lambda$	ONUs dans secteur λ.

3.3.2 Modèle de trafic

Les principaux paramètres de trafic sont définis comme suit, où la génération de trafic est ergodique et stationnaire :

Tableau 3.2 – Paramètres du modèle de trafic FiWi.

Symbole	Description
O	Nombre d'ONUs attachés au OLT.
$\tilde{N}$	Nombre de capteurs sans fil et STAs.
$\mathcal{N}$	Ensemble de noeuds FiWi. $\lvert\mathcal{N}\rvert = 1 + O + \tilde{N}$.
$\mathbf{S} = (S_{ij})$	$i, j \in \mathcal{N}$, où S_{ij} représente le nombre de trames générées du noeud source i au noeud destination j. Pour $i = j, S_{ij} = 0$
$\bar{L}$	Moyenne de la taille des trames.
ψ_L^2	Variance de la taille des trames.
Γ_{ij}	Nombre de trames transmises entre les ONUs et l'OLT (i : noeud source, j : noeud destination), tenant compte le trafic provenant des noeuds sans fil.
$\lambda_{i,c}^{wi}$	Nombre de trames générées du noeud i de classe c destinées au DMS.

3.3.3 Analyse de capacité et de stabilité

Réseau d'accès optique Pour les réseaux WR-PONs, on définit le taux de trafic (trames/seconde) en aval selon un secteur donné λ :

$$R^{d,\lambda} := \sum_{k \in S_\lambda} \Gamma_{0k} + \sum_{k=1}^{O} \sum_{l \in S_\lambda} \Gamma_{kl}, \tag{3.1}$$

où le premier terme représente le trafic généré par l'OLT pour un secteur λ et le second terme représente le trafic de tous les ONUs envoyé au secteur λ par l'OLT. On définit le taux de trafic en amont de ONU k comme suit :

$$R_k^u := \Gamma_{k0} + \sum_{l=1}^{O} \Gamma_{kl}, \tag{3.2}$$

où le premier terme dénote le trafic destiné à l'OLT et le second terme représente le trafic envoyé aux autres ONUs par l'OLT. Le taux de trafic du secteur λ est défini par :

$$R^{u,\lambda} := \sum_{k \in S_\lambda} R_k^u. \tag{3.3}$$

Pour que le système soit stable, les taux de trafic en aval et en amont doivent satisfaire :

$$\bar{L} \cdot R^{d,\lambda} < \varsigma^{(\lambda)} \tag{3.4}$$

et

$$\bar{L} \cdot R^{u,\lambda} < \varsigma^{(\lambda)} \tag{3.5}$$

dans chaque secteur λ du réseau WR-PON. Ainsi, les intensités de trafic en aval et en amont sont définies par $\rho^{d,\lambda} = \frac{\bar{L} \cdot R^{d,\lambda}}{\varsigma^{(\lambda)}}$ et $\rho^{u,\lambda} = \frac{\bar{L} \cdot R^{u,\lambda}}{\varsigma^{(\lambda)}}$, respectivement.

Dans le cas des réseaux TDM/WDM PONs, on définit l'intensité de trafic en amont et en aval comme suit :

$$\rho^u := \frac{\bar{L}}{\Lambda \cdot \varsigma} \sum_{k=1}^{O} \sum_{l=0}^{O} \Gamma_{kl} \tag{3.6}$$

$$\rho^d := \frac{\bar{L}}{\Lambda \cdot \varsigma} \sum_{k=0}^{O} \sum_{l=1}^{O} \Gamma_{kl}, \tag{3.7}$$

où le système est stable si $\rho^u < 1$ et $\rho^d < 1$.

Réseau sans fil Au niveau du réseau sans fil, le système est stable si l'intensité de trafic de toute file d'attente c au noeud i satisfait :

$$\rho_{i,c} = D_{i,c}^{wi,a} \cdot \lambda_{i,c}^{wi} < 1, \tag{3.8}$$

où $D_{i,c}^{wi,a}$ dénote le délai d'accès moyen à la file d'attente c du noeud i, calculé sous peu.

3.3.4 Analyse de délai

Réseau d'accès optique Dans le WR-PON, l'OLT envoie une trame en aval à un ONU donné dans le secteur λ en transmettant la trame sur la longueur d'onde λ, qui est reçue par tous les ONUs dans ce secteur. On modélise toutes les transmissions en aval par une seule file d'attente. Pour une distribution Poisson, le délai de file d'attente est modélisé par une file d'attente M/G/1 caractérisée par la formule Pollaczek-Khintchine [60]

$$\Phi(\rho) := \frac{\rho}{2c^{(\lambda)}(1-\rho)} \left(\frac{\psi_L^2}{\bar{L}} + \bar{L} \right) \tag{3.9}$$

permettant de calculer le délai total en aval :

$$D^{d,\lambda} = \Phi\left(\rho^{d,\lambda}\right) + \frac{\bar{L}}{\varsigma^{(\lambda)}} + \tau^{(\lambda)}. \tag{3.10}$$

En faisant la moyenne des délais en fonction des intensités de trafic, on trouve le délai moyen en aval dans un cas de figure de WR-PON :

$$D^{d} = \frac{1}{\sum_{\lambda=1}^{\Lambda} \rho^{d,\lambda}} \sum_{\lambda=1}^{\Lambda} \rho^{d,\lambda} \cdot D^{d,\lambda}. \tag{3.11}$$

Pour le trafic en amont, on modélise le trafic via chaque longueur d'onde selon les un réseau conventionnel EPON. On obtient donc le délai moyen du secteur λ :

$$D^{u,\lambda} = 2\tau^{(\lambda)} \cdot \frac{2-\rho^{u,\lambda}}{1-\rho^{u,\lambda}} + \Phi\left(\rho^{u,\lambda}\right) + \frac{\bar{L}}{\varsigma^{(\lambda)}} \tag{3.12}$$

et le délai moyen en amont du WR-PON égale

$$D^{u} = \frac{1}{\sum_{\lambda=1}^{\Lambda} \rho^{u,\lambda}} \sum_{\lambda=1}^{\Lambda} \rho^{u,\lambda} \cdot D^{u,\lambda}. \tag{3.13}$$

De façon similaire, on peut calculer également les délais en amont et en aval des réseaux TDM/WDM PONs.

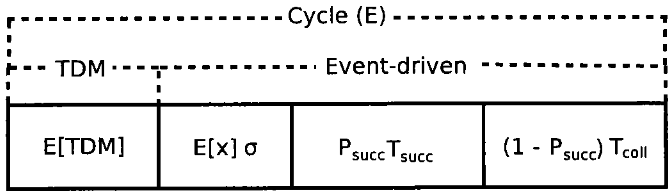

Figure 3.2 – Cycle de l'accès au canal pour modéliser les noeuds événements et par le temps.

Réseau sans fil Contrairement à [19], chaque cycle consiste en trois composantes : (i) temps moyen de période time division multiplexing (TDM) pour les transmissions des capteurs basés par le temps (ii) période aléatoire de résolution de contention sur le canal sans fil et (iii) une transmission avec succès ou une collision (Figure 3.2). De plus, contrairement à [19], chaque cycle contient seulement un sous-ensemble des noeuds qui rivalisent pour accéder au canal, où les autres n'ont pas de trames à transmettre dans leur file d'attente (cas non-saturé). Chaque noeud sans fil a C files d'attente, soit une par classe de trafic. Chaque classe c, $c = 1, ..., C$, a une priorité ascendante de $c = 1$ à $c = C$. $W_{k,c,s}$ dénote la valeur maximale de fenêtre de contention de la classe c au noeud k. De plus, $B_{k,c}(i)$ est la probabilité d'état d'équilibre de la classe c du noeud k de l'intervalle de temps i, où $0 \leq i \leq max_{s=0,...,R_{k,c}} W_{k,c,s}$. Pour simplifier la notation, on définit

$$\beta_{k,c}(i) = \begin{cases} 0 & i \leq 0 \\ \sum_{j=0}^{i-1} B_{k,c}(j) & i > 0 \\ 1 & i > \max_{s=0,1,...,R_{k,c}} W_{k,c,s}, \end{cases} \tag{3.14}$$

où $\beta_{k,c}(i)$ dénote la probabilité d'état d'équilibre de la file d'attente de la classe c du noeud k où le *backoff* slot a expiré à i. De plus, $\delta_{k,c}$ dénote le nombre minimum de *backoff* slots pour la classe c au noeud k, en plus du nombre AIFS.

Ensuite, $Q_{h,c}(i)$ dénote la probabilité que, de la perspective du noeud h, aucun autre noeud ne transmette avant l'intervalle de temps i. En utilisant $q_{k,c}$, soit la probabilité d'avoir une trame dans la file d'attente c au noeud k (définie sous peu), $Q_{h,c}(i)$ est défini par :

$$
\begin{aligned}
Q_{h,c}(i) &= \prod_{k\neq h}\prod_{z=1}^{C}[(1-q_{k,z})+q_{k,z}(1-\beta_{k,z}(i-\delta_{k,z}))]\cdot\prod_{z<c}[(1-q_{h,z})+q_{h,z}((1-\beta_{h,z}(i-\delta_{h,z}))+\\
&\quad \beta_{h,z}(i-\delta_{h,z})\beta_{h,c}(i-\delta_{h,c}))]\cdot\prod_{z>c}[(1-q_{h,z})+q_{h,z}(1-\beta_{h,z}(i-\delta_{h,z}))].
\end{aligned}
\tag{3.15}
$$

La probabilité que la file d'attente c du noeud h voit sa première transmission à un cycle exactement au slot i est définie par :

$$
T_{h,c}(i) = Q_{h,c}(i) - Q_{h,c}(i+1). \tag{3.16}
$$

On note $\Pi_{k,c}(s,j)$ la probabilité d'état d'équilibre lorsqu'il y a une trame en attente (partie du bas à la Figure 3.3) au noeud k de la classe c et est définie par :

$$
\begin{aligned}
\Pi_{k,c}(s,j), \qquad & s\in\{0,1,\ldots,R_{k,c}\}\\
& j\in\{0,1,\ldots,W_{k,c,s}\},
\end{aligned}
\tag{3.17}
$$

où s correspond au stage (maximalement $R_{k,c}$) et j la valeur de backoff. Pour $0 < s \leq R_{k,c}$ et $0 \leq j \leq W_{k,c,s}$, on a :

$$
\begin{aligned}
\Pi_{k,c}(s,j) &= \Pi_{k,c}(s,j)(1-Q_{k,c}(\delta_{k,c}))\\
&+ \sum_{r=1}^{W_{k,c,s}-j}\Pi_{k,c}(s,j+r)\cdot T_{k,c}(r-1+\delta_{k,c})\\
&+ \sum_{i=1}^{W_{k,c,s-1}}\left[\Pi_{k,c}(s-1,i)\cdot T_{k,c}(i+\delta_{k,c})\cdot\frac{1}{W_{k,c,s}+1}\right]
\end{aligned}
\tag{3.18}
$$

et pour $s=0$ et $0\leq j\leq W_{k,c,s}$ on a :

$$\begin{aligned}
\Pi_{k,c}(0,j) &= \Pi_{k,c}(0,j)(1-Q_{k,c}(\delta_{k,c})) \\
&+ \sum_{r=1}^{W_{k,c,0}-j} \Pi_{k,c}(0,j+r)\cdot T_{k,c}(r-1+\delta_{k,c}) \\
&+ \sum_{i=0}^{W_{k,c,R_{k,c}}} q_{k,c}\left[\Pi_{k,c}(R_{k,c},i)\cdot T_{k,c}(i+\delta_{k,c})\cdot \frac{1}{W_{k,c,0}+1}\right] \\
&+ \sum_{s=0}^{R_{k,c}} \sum_{i=0}^{W_{k,c,s}} q_{k,c}\left[\Pi_{k,c}(s,i)\cdot Q_{k,c}(i+1+\delta_{k,c})\cdot \frac{1}{W_{k,c,0}+1}\right] \\
&+ \Pi_{k,c}(0,j,0)\cdot\left(1-e^{-\lambda_{k,c}^{wi}E}\right), \qquad (3.19)
\end{aligned}$$

où E dénote le temps moyen de cycle (défini sous peu) et $\Pi_{k,c}(0,j,0)$ correspond aux nouveaux états pour tenir compte des cas où il n'y a pas de trame en attente (partie du haut à la Figure 3.3) pour $j \in \{0,...,W_{k,c,0}\}$:

$$\begin{aligned}
\Pi_{k,c}(0,j,0) &= \sum_{i=0}^{W_{k,c,R_{k,c}}} \left[\Pi_{k,c}(R_{k,c},i)\cdot T_{k,c}(i+\delta_{k,c})\cdot \frac{1-q_{k,c}}{W_{k,c,0}+1}\right] \\
&+ \sum_{s=0}^{R_{k,c}} \sum_{i=0}^{W_{k,c,s}} \left[\Pi_{k,c}(s,i)\cdot Q_{k,c}(i+1+\delta_{k,c})\cdot \frac{1-q_{k,c}}{W_{k,c,0}+1}\right] \\
&+ \Pi_{k,c}(0,j,0)\cdot e^{-\lambda_{k,c}^{wi}E}. \qquad (3.20)
\end{aligned}$$

Le premier terme de $\Pi_{k,c}(0,j,0)$ correspond au cas où une collision survient avec un noeud h, la retransmission maximale arrive ($R_{k,c}$) et aucune trame attend à la fin du cycle, le second correspond à une transmission avec succès et le troisième cas correspond à la probabilité de ne pas avoir de trame au début et à la fin.

On peut maintenant définir la probabilité d'avoir une valeur de backoff j, $0 \leq j \leq max_{s=0,\ldots,R_{k,c}} W_{k,c,s}$, au début d'un cycle :

$$B_{k,c}(j) = \sum_{s=0}^{R_{k,c}} \Pi_{k,c}(s,j) + \Pi_{k,c}(0,j,0). \qquad (3.21)$$

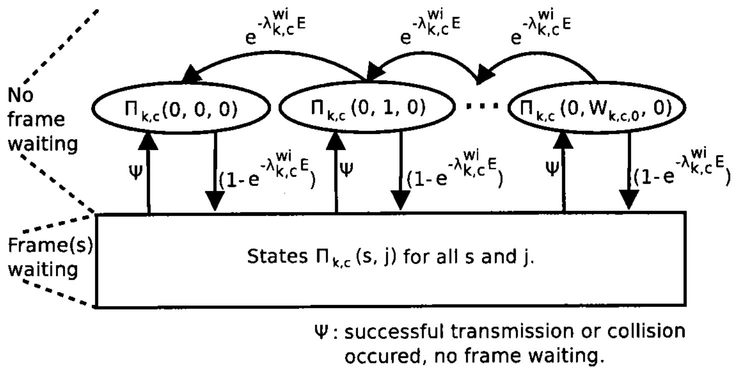

Figure 3.3 – Probabilités d'état d'équilibre des valeurs du compteur de backoff du modèle EDCA avec des conditions non-saturées.

Utilisant $P_{succ}(k, c)$ (en ajoutant c) de [19], on définit la probabilité d'avoir une transmission avec succès à la fin d'un cycle :

$$P_{succ} = 1 - \prod_{\forall k} \prod_{\forall c} \left[1 - P_{succ}(k, c)\right]. \tag{3.22}$$

Ceci permet de calculer la durée moyenne des cycles :

$$\begin{aligned} E &= \mathbb{E}[\text{TDM}] \\ &\quad + \mathbb{E}[\text{number of empty contention resolution slots}] \cdot \sigma \\ &\quad + P_{succ} \cdot T_{succ} + (1 - P_{succ}) \cdot T_{coll}, \end{aligned} \tag{3.23}$$

où $\mathbb{E}$[TDM] correspond au temps moyen des périodes sans contention dues aux allocations des capteurs périodiques qui est approximé par :

$$\mathbb{E}[\text{TDM}] = P_{TDM,z} \cdot (T_{succ} + D_{TDM}), \tag{3.24}$$

où $P_{TDM,z}$ dénote la probabilité qu'un noeud sans fil doit attendre dû à une période TDM dans la zone z :

$$P_{TDM,z} = \sum_{\forall s\ sensors} \lambda_{s,sen}^{wi} \cdot D_{TDM} + \frac{1}{(1/(\sum_{\forall s\ sensors} \lambda_{s,sen}^{wi} - D_{TDM}))/T_{succ}} \tag{3.25}$$

avec

$$D_{TDM} = \text{PHY Header} + \text{MAC Header}/r + \bar{L}/r + \text{FCS}/r + \delta. \tag{3.26}$$

$P_{TDM,z}$ définit l'interaction entre les cycles et les slots TDM. $P_{TDM,z} = \mathbb{E}[\text{TDM}] = 0$ si tous les capteurs sont événementiels dans la zone z.

σ dénote la durée d'une *time slot*, T_{succ} et T_{coll} représentent les temps lors d'une transmission avec succès et avec collision, respectivement. Utilisant une approche similaire à [61], T_{succ} et T_{coll} sont définis comme suit :

$$\begin{aligned} T_{succ} = {} & \text{RTS}/r + \text{SIFS} + \delta + \text{CTS}/r + \text{SIFS} + \delta + \text{PHY Header} + \text{MAC Header}/r \\ & + \bar{L}/r + \text{FCS}/r + \text{SIFS} + \delta + \text{ACK}/r + \text{AIFS} + \delta \end{aligned} \tag{3.27}$$

et

$$T_{coll} = \text{RTS}/r + \text{EIFS} + \delta, \tag{3.28}$$

où δ dénote le délai de propagation. La durée approximée de slots de contention est définie par :

$$\mathbb{E}[\text{number of empty contention resolution slots}] = \sum_{j=1}^{\max_{k,c}(W_{k,c,max}+\delta_{k,c})} Q_0(j), \tag{3.29}$$

avec

$$Q_0(j) = \prod_{\forall k} \prod_{\forall c} [1 - \beta_{k,c}(j - \delta_{k,c})]. \tag{3.30}$$

De plus, la probabilité d'avoir une trame attendant pour une transmission est exprimée par :

$$\begin{aligned} q_{k,c} &= 1 - Pr[\text{no frame waiting in queue } c \text{ of node } k \text{ after a cycle}] \\ &= 1 - \left[(1-q_{k,c}) \cdot \left(1 - \frac{1-e^{-\lambda_{k,c}^{wi}E}}{1-P_{TDM,z}}\right) + \; q_{k,c} \cdot P_{succ}(k,c)\right]. \end{aligned} \tag{3.31}$$

En isolant $q_{k,c}$, on obtient :

$$q_{k,c} = \frac{\left(1-e^{-\lambda_{k,c}^{wi}E}\right)/(1-P_{TDM,z})}{\left(1-e^{-\lambda_{k,c}^{wi}E}\right)/(1-P_{TDM,z}) + P_{succ}(k,c)}. \tag{3.32}$$

On peut donc déduire le délai pour les noeuds avec accès événementiel. La première composante de délai est le délai d'attente dû aux transmissions :

$$D_{k,c}^{sen} = P_z^{wait} \cdot (1 - P_{succ}(k,c)) \cdot \left(T_{succ} + \frac{W_{k,c,0}}{2}\sigma\right) \tag{3.33}$$

avec

$$P_z^{wait} = \frac{\sum_{k\ EDCA\ node \in z} \sum_c \lambda_{k,c}^{wi}}{1/T_{succ}}. \tag{3.34}$$

La probabilité d'attente P_z^{wait} est estimée par le ratio du taux de trafic sur le taux maximal. La seconde composante de délai est due aux collisions :

$$\begin{aligned} D_{k,c}^{back} &= \sum_{s=1}^{R_{k,c}} (p_{k,c})^s \cdot (1-p_{k,c}) \cdot \left[s\Big(T_{coll} + \delta_{k,c}\sigma + P_z^{wait} \cdot (1 - P_{succ}(k,c)) \cdot \; T_{succ}\Big) + \right. \\ & \left. \left(\sum_{j=1}^{s} \frac{W_{k,c,j}}{2}\right)\sigma \right], \end{aligned} \tag{3.35}$$

où la probabilité de collision $p_{k,c}$ est similaire à celle de [61] :

$$p_{k,c} = \sum_{i=0}^{W_{k,c,max}+\delta_{k,c}} \frac{T_{k,c}(i)}{Q_{k,c}(i)}. \tag{3.36}$$

Le délai d'accès total est finalement exprimé par :

$$D_{k,c}^{wi,a} = D_{k,c}^{sen} + D_{k,c}^{back} + \frac{T_{succ}}{P_{succ}(k,c)}. \tag{3.37}$$

Le délai total (file d'attente + transmission) est défini suivant une file d'attente M/M/1 :

$$D_{k,c}^{wi} = \frac{1}{1/D_{k,c}^{wi,a} - \lambda_{k,c}^{wi}}. \tag{3.38}$$

$D_{k,c}^{wi}$ correspond au délai pour les noeuds sans fil événementiels. En ce qui concerne les noeuds de type capteur périodique, l'équation (3.26) est utilisée.

Délai de bout-en-bout FiWi

— **Trafic régulier H2H :** Le délai moyen de bout-en-bout du trafic régulier de classe c, $c = 1, \ldots, C$, est exprimé par :

$$\begin{aligned} D_c \;=\; & \frac{1}{\sum_{\forall i,j \in \mathcal{N}\setminus\{\text{Sensors}\}} S_{ij}} \Bigg[\sum_{\substack{\forall \text{ STAs } i,j \\ \text{or ONU/AP } j \\ \text{in same zone}}} S_{ij} \cdot D_{i,c}^{wi} \\ & + \sum_{\forall \text{ STA } i} S_{i0} \left(D_{i,c}^{wi} + D^u \right) \\ & + \sum_{\substack{\forall \text{ STA } i \\ \text{and ONU/AP } j \\ \text{in other zones}}} S_{ij} \left(D_{i,c}^{wi} + D^u + D^d \right) \\ & + \sum_{\substack{\forall \text{ STA } i \\ \text{and STA } j \\ \text{in other zones}}} S_{ij} (D_{i,c}^{wi} + D^u + D^d + D_{\text{ONU/AP } j,c}^{wi}) \\ & + \sum_{\forall \text{ ONU } i} S_{i0} \cdot D^u + \sum_{\forall \text{ ONUs } i,j} S_{ij} \left(D^u + D^d \right) \\ & + \sum_{\substack{\forall \text{ ONU } i \\ \text{and STA } j \\ \text{in other zones}}} S_{ij} \left(D^u + D^d + D_{\text{ONU/AP } j,c}^{wi} \right) \\ & + \sum_{\forall \text{ ONU } j} S_{0j} \cdot D^d \\ & + \sum_{\forall \text{ STA } j} S_{0j} \left(D^d + D_{\text{ONU/AP } j,c}^{wi} \right) \Bigg], \end{aligned} \tag{3.39}$$

où chaque ligne correspond à un chemin possible.

— **Trafic M2M :** Le délai moyen de bout-en-bout des capteurs sans fil de classe c, $c = 1, \ldots, C$, est exprimé par :

$$\begin{aligned} D_c \;=\; & \frac{1}{\sum_{\substack{\forall \text{ sensor } i \\ \text{and OLT,} \\ \text{ONUs, STAs } j}} S_{ij}} \Bigg[\sum_{\forall \text{ sensor } i} D^{wi}_{i,c} \cdot \sum_{\substack{\forall \text{ STAs } j \\ \text{in same zone}}} S_{ij} \\ & + \sum_{\forall \text{ sensor } i} S_{i0} \left(D^{wi}_{i,c} + D^u \right) \\ & + \sum_{\substack{\forall \text{ sensor } i \\ \text{and ONU } j \\ \text{in other zones}}} S_{ij} \left(D^{wi}_{i,c} + D^u + D^d \right) \\ & + \sum_{\substack{\forall \text{ sensor } i \\ \text{and STA } j \\ \text{in other zones}}} S_{ij} (D^{wi}_{i,c} + D^u + D^d + D^{wi}_{\text{ONU/AP } j,c}) \Bigg]. \end{aligned} \tag{3.40}$$

Fiabilité des capteurs On définit la fiabilité comme étant la probabilité qu'un capteur transmette sans atteindre la limite de retransmission (où dans ce cas la trame est rejetée) :

$$\Theta_s = \begin{cases} \mathcal{R}_c & \text{pour des capteurs événementiels,} \\ \\ 1 & \text{pour des capteurs périodiques,} \end{cases} \tag{3.41}$$

où

$$\begin{aligned} \mathcal{R}_c \;=\; & \frac{1}{\sum_{\substack{\forall \text{ sensor } i \\ \text{and OLT,} \\ \text{ONUs, STAs } j}} S_{ij}} \Bigg[\sum_{\forall \text{ sensor } i} r^{wi}_{i,c} \cdot \sum_{\substack{\forall \text{ STAs } j \\ \text{in same zone}}} S_{ij} + \sum_{\forall \text{ sensor } i} S_{i0} \cdot r^{wi}_{i,c} \\ & + \sum_{\substack{\forall \text{ sensor } i \\ \text{and ONU } j \\ \text{in other zones}}} S_{ij} \cdot r^{wi}_{i,c} + \sum_{\substack{\forall \text{ sensor } i \\ \text{and STA } j \\ \text{in other zones}}} S_{ij} \cdot r^{wi}_{i,c} \cdot r^{wi}_{\text{ONU/AP } j,c} \Bigg], \end{aligned} \tag{3.42}$$

avec

$$r^{wi}_{i,c} = 1 - (p_{i,c})^{R_{i,c}+1}. \tag{3.43}$$

3.3.5 Calcul de la borne théorique supérieure du trafic M2M

Pour trouver la borne théorique supérieure du trafic M2M, le taux de trafic, $\lambda_{i,c}^{wi}$ doit être itérativement incrémenté jusqu'à ce que le seuil maximal de délai (noté $\mathcal{L}_r$) du trafic H2H soit atteint. On trouve cette borne théorique en utilisant la fonction *max* suivante :

$$max_{l \in [0..\infty]} \left(\lambda_{\forall i,c}^{wi} := l \right), D_c < \mathcal{L}_r, \tag{3.44}$$

où c est une classe de capteur donnée et i un capteur donné. En augmentant le taux de données des capteurs et en mettant à jour D_c itérativement, on trouve la borne théorique du débit de données maximal des capteurs sans violer la limite de délai du trafic H2H. Plus spécifiquement, $\lambda_{i,c}^{wi}$ est en premier lieu fixé à 0. Ensuite, la procédure suivante est exécutée :

- **Étape 1 :** Augmenter $\lambda_{i,c}^{wi}$ à $\lambda_{i,c}^{wi} + 1$.
- **Étape 2 :** Résoudre le modèle analytique et mettre à jour D_c, où c est une classe régulière de trafic.
- **Étape 3 :** Si D_c est plus petit que $\mathcal{L}_c$, aller à Étape 1.
- **Étape 4 :** $\lambda_{i,c}^{wi}$ correspond à la borne supérieure.

3.3.6 Résultats

Configurations

On considère en premier lieu un TDM PON 20 km avec 8 ONUs, où chaque ONU est équipé d'un AP déservant 2 STAs et 2 capteurs. Les paramètres EDCA sont les mêmes utilisés dans [19] avec une taille de trame de 1500 octets. Les STAs, ONUs et OLT envoient un trafic H2H uniformément distribué entre eux avec $\delta_{k,c} = 3$, $CW_{min} = 64$ et $CW_{max} = 256$. Pour le trafic des capteurs M2M, la destination est fixée au DMS avec $\delta_{k,c} = 0$, $CW_{min} = 8$ et $CW_{max} = 256$.

Le simulateur est basé sur OMNeT++ [1] et utilise le module de communications *inet* avec des extensions pour WiFi EDCA, TDM/WDM PONs et pour intégrer le routage FiWi. La partie PON correspond à une implémentation d'un réseau conventionnel EPON point-à-multipoint avec des

1. OMNeT++ est disponible à `http://www.omnetpp.org/`.

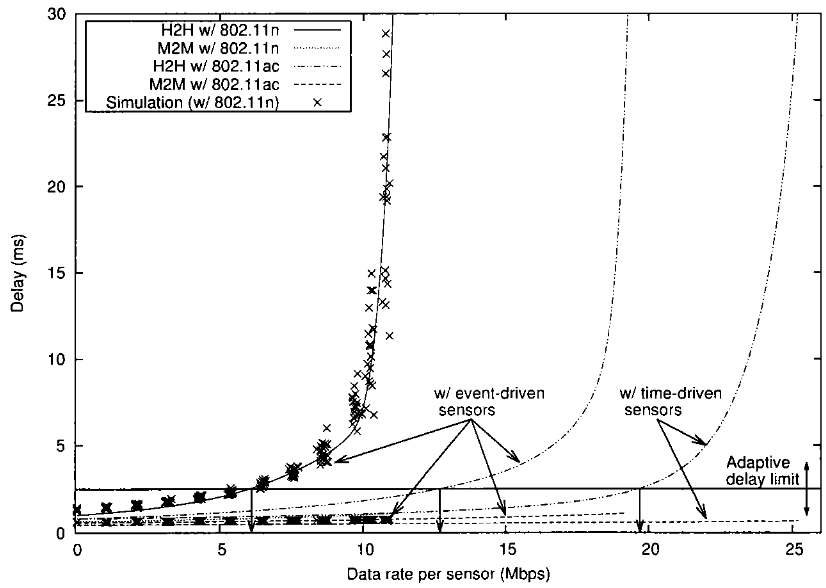

Figure 3.4 – Délai de bout-en-bout moyen vs. débit de données des capteurs.

échanges de messages de contrôle REPORT-GRANT. Pour le réseau WLAN EDCA, une machine à états finis est modélisée et disponible dans *inet*[2], implémentant les états de IEEE 802.11e, incluant *idle*, *defer*, *wait-AIFS*, *backoff*, *wait-ack*, *receive-ack*, *wait-SIFS* et *receive*. De plus, le modèle probabiliste est développé en Python avec le module de calcul scientifique NumPy[3].

Fiabilité et débit de données maximal du trafic M2M avec un réseau conventionnel EPON

La Figure 3.4 montre le délai de bout-en-bout du trafic H2H (charge fixée à 144 Mbps) et trafic M2M vs. le débit de données par capteur, incluant les simulations OMNeT++ de vérification. En augmentant le débit de données des capteurs, le délai du trafic H2H atteint une limite de délai, qui est adaptative selon les exigences du trafic H2H. Par exemple, pour une limite de 2.5 ms, les débits de données maximaux correspondent à 6.1, 12.7 et 19.7 Mbps et montre qu'un plus grand débit peut être supporté en utilisant VHT WLAN sans violer la limite de délai.

La Figure 3.5 montre la fiabilité des capteurs vs. le débit de données du trafic H2H en considérant que les capteurs envoient 350 mesures par seconde. On observe que les capteurs temporels ne sont

2. Le module inet est disponible à `http://inet.omnetpp.org/`.
3. Pour plus d'informations sur NumPy, voir `http://www.numpy.org/`.

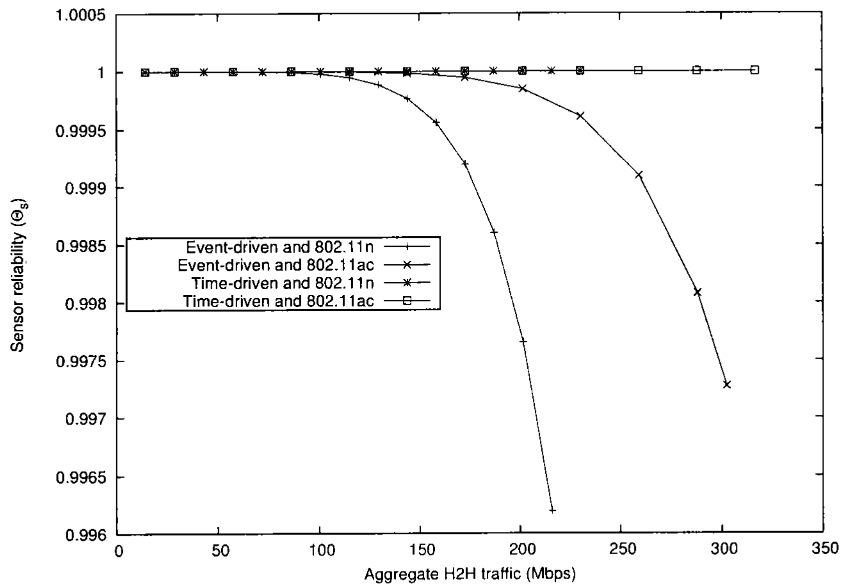

Figure 3.5 – Fiabilité des capteurs en fonction de la charge du trafic H2H.

pas affectés par le débit de données du trafic H2H puisqu'il n'y pas de contention. Cependant, pour ce qui est des capteurs événementiels, la fiabilité décroît en augmentant le trafic H2H, spécialement en utilisant IEEE 802.11n qui a un plus faible débit, ce qui augmente la probabilité de collision de paquet.

Configurations triple-play et smart grid

Pour considérer des configurations plus réalistes dans les sous-sections suivantes, on utilise des tailles moyennes de *payload* selon des mesures faites d'applications smart grids IEC 61850 (Tableau 3.3) [5].

Tableau 3.3 – Mesures expérimentales d'applications smart grids de surveillance suivant le standard IEC 61850 [5].

Noeud source	Taille moyenne de payload
HVA/LV	500 octets
Substation	5000 octets
DER	224 octets
Switch	100 octets

On considère deux classes de trafic, soit une classe régulière de *triple-play* (vidéo, voix et données) et une autre pour le trafic de surveillance smart grid. Pour la classe régulière, on fixe la taille de payload à 1500 octets, correspondant à la taille maximale de payload d'une trame Ethernet. Pour ce qui est du trafic de surveillance smart grid, on utilise les moyennes listées au Tableau 3.3. Le trafic capturé pour obtenir ces moyennes correspond à des applications expérimentales de télécontrôle de réseaux de distribution en France, détaillé plus en détail dans le chapitre suivant. Dans les sous-sections suivantes, on configure 500 octets pour le trafic smart grid, consistant 5 manufacturing message specifications (MMSs) contenant les métriques suivantes : puissance active et réactive, tension, courant et positionnement. Utilisant ces configurations, on calcule et utilise la moyenne $\bar{L}$ et la variance moyenne des messages smart grids.

Impact de la variation du trafic H2H avec différentes technologies PONs

On considère ensuite des réseaux TDM/WDM PONs comprenant 128 ONUs avec 2 capteurs événementiels et 2 STAs par ONU. Chaque capteur génère $\lambda_{i,c}^{wi} = 10$ trames de 500 octets par seconde. Puisque le trafic H2H est sporadique et peut significativement varier en fonction du temps, ce qui peut non seulement influencer le délai H2H, mais aussi le délai M2M de bout-en-bout. La moyenne du délai de bout-en-bout des capteurs événementiels avec différentes charges de trafic H2H et PONs est illustrée à la Figure 3.6.

Il est à noter que le délai de bout-en-bout est affiché uniquement pour des charges de trafic H2H où le délai des trames H2H est inférieur au seuil de 2.5 ms. Avec un réseau conventionnel TDM EPON 1 Gbps, le seuil de 2.5 ms du trafic H2H est obtenu avec un traffic H2H d'environ 1 Gbps, dû à la forte intensité de trafic du réseau PON ce qui affecte le délai des classes H2H et M2M. Considérant ensuite système TDM 10-G EPON et 40 Gbps WDM PON, le délai des capteurs demeure similaire indépendamment du trafic H2H. En fait, le goulot d'étranglement dans ce cas est situé aux STAs qui deviennent saturées, mais sans toutefois affecter les capteurs événementiels. On note de plus que mettre à jour les noeuds sans fil de 802.11n (capacité : 300 Mbps par zone) à 802.11ac (capacité : 6900 Mbps par zone) permet d'augmenter la charge de trafic H2H de seulement 1 Gbps avec les configurations considérées, puisque l'efficacité de ces protocoles MAC est faible.

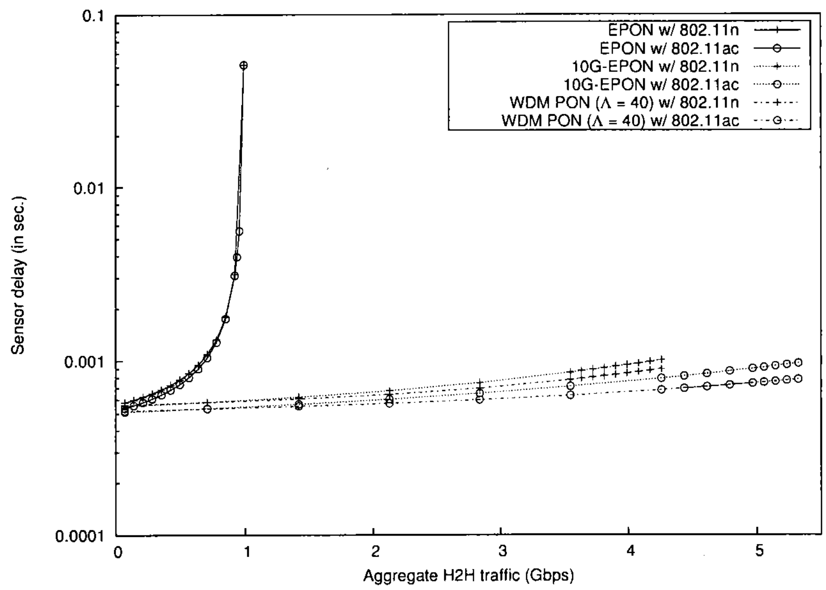

Figure 3.6 – Impact de différentes charges réseau de trafic H2H sur le délai des capteurs.

Analyse de la sensibilité de l'influence entre les noeuds événementiels et ceux périodiques

On analyse l'influence entre les noeuds événementiels et périodiques. Pour ce faire, on varie le nombre de noeuds H2H et M2M et on trouve la borne théorique du trafic M2M en utilisant l'équation (3.44). On fixe le trafic H2H à 500 Mbps et 802.11n est utilisé dans le WLAN.

Tableau 3.4 – Bornes théoriques supérieures (en Mbps) du trafic M2M avec un seuil de délai H2H de 2.5 ms.

	Capteurs par ONU $\left(\frac{\tilde{N}_s}{O}\right)$							
	Temporel				Événementiel			
	1	2	3	4	1	2	3	4
$\frac{\tilde{N}_r}{O} = 1$	67.2	33.6	22.4	16.8	25.4	8.0	4.6	3.3
$\frac{\tilde{N}_r}{O} = 2$	66.9	33.5	22.3	16.7	18.8	6.5	3.9	2.8
$\frac{\tilde{N}_r}{O} = 3$	66.9	33.5	22.3	16.7	16.6	6.0	3.6	2.5
$\frac{\tilde{N}_r}{O} = 4$	67.1	33.55	22.37	16.78	15.2	5.6	3.4	2.4

Au Tableau 3.4, la borne théorique du trafic M2M pour toutes les permutations de [1, 2, 3, 4] STAs/ONU et [1, 2, 3, 4] capteurs/ONU est calculée pour étudier l'impact sur la borne théorique. Dans le cas des capteurs périodiques, comme prévu, le comportement est linéaire, où la borne théorique supérieure du trafic M2M dépend du nombre de capteurs. Cependant, dans le cas des capteurs événementiels, ce comportement linéaire ne s'applique pas. Puisque la priorité EDCA des STAs est faible, la borne supérieure du trafic M2M décroît significativement de façon non linéaire en fonction du nombre de noeuds événementiels (STAs et capteurs). Par exemple, avec 2 capteurs et 1 STA, $8\ Mbps \cdot 2\ noeuds = 16\ Mbps$ est obtenu pour les deux capteurs (et $4 \cdot 3.3 = 13.2$ Mbps avec 4 capteurs), ce qui est inférieur comparativement avec 1 capteur événementiel (25.4 Mbps). De plus, on note que le nombre de capteurs événementiels influence plus significativement la borne supérieure théorique comparativement au nombre de STAs avec les configurations considérées.

3.4 Résumé

Le modèle analytique de trafic hétérogène avec infrastructure FiWi pour les réseaux intelligents permet de trouver la borne supérieure théorique du trafic M2M coexistant avec un trafic H2H. Les résultats obtenus pour avec réseau d'accès optique conventionnel EPON montrent que des débits de capteurs événementiels et TDM peuvent être aussi élevés que 12.7 et 19.7 Mbps, respectivement, sans violer une limite de délai H2H de 2.5 ms. Utilisant des mesures expérimentales réelles d'applications de télécontrôle smart grid pour fixer les tailles de *payload*, on a étudié l'impact de charge de trafic H2H variable sur le délai de bout-en-bout des capteurs. On a trouvé, avec les configurations utilisées, que l'utilisation d'un réseau d'accès EPON conventionnel peut causer un goulot d'étranglement et augmenter le délai de bout-en-bout de trafic H2H et M2M, tandis qu'avec des réseaux d'accès 10G-EPON et WDM PON le goulot d'étranglement se situe au niveau du réseau WLAN, ce qui représente ainsi des défis pour combiner ces deux réseaux efficacement. On a aussi étudié l'influence des capteurs événementiels et périodiques. On a montré qu'avec des capteurs périodiques, la borne théorique supérieure varie de façon linéaire en fonction du nombre de noeuds, tandis qu'avec des capteurs événementiels la borne théorique supérieure décroît non linéairement plus rapidement.

Dans ce chapitre, on a modélisé la perspective de communications pour un réseau d'accès convergent FiWi. Compte tenu que les réseaux intelligents comportent également les perspectives de technologies de l'information et de communications, le chapitre suivant porte sur l'étude multidisciplinaire de perspectives smart grids jointes via co-simulation.

Chapitre 4

Co-simulation Dynamique Smart Grid

Dans ce chapitre, un modèle de co- et multi-simulation smart grid est premièrement proposé, permettant de modéliser les performances d'une smart grid sous plusieurs perspectives de façon multidisciplinaire. Le design et l'implémentation des perspectives de technologies de l'information, de communications et du système électrique sont décrites. Ensuite, un cas d'usage d'une application de télécontrôle est décrit en tenant compte d'une topologies réelle en France et des mesures d'applications smart grids sont prises et injectées dans le modèle de co-simulation des perspectives de technologies de l'information et de communications. Finalement, des résultats de co-simulation d'une application de coordination de véhicules électriques sont présentés, modélisant les perspectives de communications et du système électrique de façon jointe et dynamique.

4.1 Introduction

L'élaboration d'un banc d'essai est utile pour expérimenter de nouvelles applications smart grids. Cependant, il n'est pas nécessairement toujours évident de concevoir de tels systèmes, notamment pour faire des tests avec des centaines, voire des milliers de noeuds. Une autre approche consiste à combiner plusieurs simulateurs pour étudier de façon multidisciplinaire une smart grid sous plusieurs perspectives (information, communications et système électrique) via multi-simulations [62].

La co-simulation des perspectives de communications et du système électrique s'est avérée utile notamment dans les travaux suivants :

— L'opération d'un mécanisme de protection des instabilités a été démontré comme étant grandement affectée par le taux de perte de communications via co-simulation [63].
— Avec l'utilisation d'un co-simulateur, un mécanisme de contrôle pour véhicules électriques est significativement influencé par le taux d'envoi des capteurs [64].
— Un mécanisme de protection a été validé pour divers scénarios en tenant compte d'un seuil de délai de 100 ms, où le délai principal provient de l'infrastructure de communications [65].
— Un mécanisme d'intégration V2G, G2V et de sources d'énergie renouvelables (nommé IntVGR) co-simulé opérant via une infrastructure FiWi a été proposé [23]. Ce travail est présenté en détail dans le chapitre II.9. La co-simulation permet de mesurer le débit de données et le délai nécessaires ainsi que les performances du système électrique de façon jointe.

La création d'un co-simulateur n'est cependant pas nécessairement triviale. Une problématique significative relevée dans plusieurs travaux est la synchronisation, puisque plusieurs trames de temps peuvent être modélisées. Trois approches ont été utilisées :

— *Avec discrétisation du temps.* Dans [66], le modèle *High Level Architecture* (HLA) a été proposé. L'approche consiste à discrétiser le temps en slots τ. Au début d'une slot donnée, les simulateurs notifient les événements prévus dans la slot. Ensuite, pour chaque événement le simulateur est arrêté pour le notifier aux simulateurs. Si un événement est créé durant la slot, il devra être reporté au début de la prochaine slot. Cette approche a été utilisée dans plusieurs travaux [62, 63, 67, 68, 69, 70, 71].
— *Avec temps global.* Dans cette approche, un seul temps est modélisé et utilisé par les deux simulateurs [65, 72].
— *Sans synchronisation.* Dans certaines modélisations de co-simulation, une seule trame du temps est nécessaire. Un exemple est l'utilisation d'un calculateur tel que OpenDSS qui ne modélise pas le temps, mais permet d'obtenir des statistiques sur les performances d'un réseau de distribution [23, 73, 74].

Dans cette section, l'accent est mis sur l'approche HLA compte tenu que chaque simulateur demeure indépendant de la multi-simulation. Il est à noter que HLA a été normalisé (IEEE 1516) et est supporté par certains simulateurs. Il existe également une autre norme, *Functional Mockup Interface* (FMI) qui permet d'exporter/importer des modèles de simulation [75]. Cependant, un

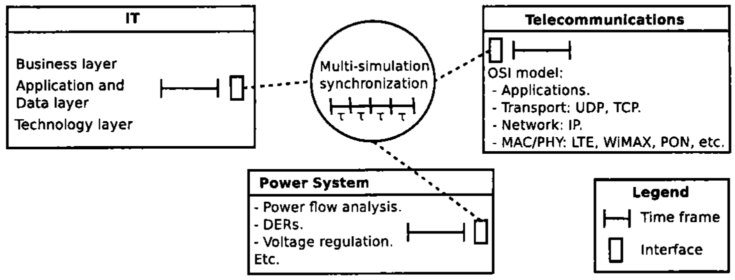

Figure 4.1 – Modèle de multi-simulation couvrant toutes les perspectives smart grids.

inconvénient majeur de FMI est qu'il ne fournit pas d'algorithme principal pour coordonner les simulateurs [67].

4.2 Modèle de multi-simulation smart grid

Le modèle de multi-simulation illustré à la Figure 4.1 permet de modéliser un smart grid complet sous toutes les perspectives telles que définies dans la norme IEEE P2030. L'ajout ici correspond à la perspective des technologies de l'information, qui permet de modéliser les flux complexes d'informations concernant les modèles d'affaire, échanges entre plusieurs entités smart grids, les processus, etc.

L'intérêt ici est d'utiliser la multi-simulation pour valider de nouveaux algorithmes smart grids avant de les déployer, et ainsi potentiellement prévenir des problèmes. Sur la Figure 4.2, les perspectives des technologies de l'information et des communications utilisent le modèle HLA, tandis que le modèle FMI peut être utilisé pour la perspective du système électrique. FMI et HLA peuvent alors communiquer via HLA. Une fonctionnalité importante est de vérifier le modèle de multi-simulation en injectant des mesures réelles et les comparer avec le modèle de multi-simulation.

4.3 Design et implémentation

Dans cette section, le design et l'implémentation de deux co-simulateurs développés sont décrits, permettant de co-simuler (*i*) les perspectives technologies de l'information et de communications et (*ii*) les perspectives de communications et du système électrique.

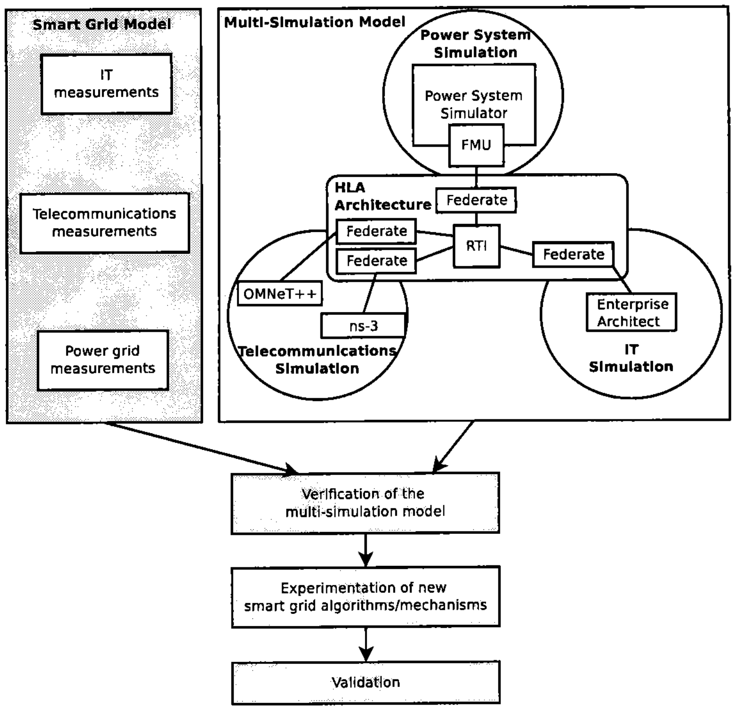

Figure 4.2 – Modèle de multi-simulation pour valider de bout-en-bout une smart grid.

4.3.1 Perspectives de technologies de l'information et de communications

La Figure 4.3 illustre les composantes primaires du co-simulateur de technologies de l'information et de communications. On note que la couche application (modèle OSI) peut être modélisée dans la couche application d'un simulateur de communications. Cependant, ceci nécessite de développer les modèles de technologies de l'information (IT) qui existent déjà dans les simulateurs ITs, tel que Enterprise Architect. De plus, les simulateurs IT contiennent des interfaces graphiques riches et peuvent être exécutés pendant les expériences de multi-simulation, et les programmes de conception ITs peuvent être utilisés sans réinventer la roue pour créer des scénarios de flux d'informations riches.

La perspective IT est modélisée par un ensemble de programmes Java générant des messages IEC 61850 entre les noeuds de la topologie, formant un système multi-couche. Toutes les couches reçoivent des messages GRANT du *federate* IT, ce qui permet au simulateur IT d'avancer dans le temps jusqu'au temps GRANT. Chaque couche IT peut transmettre les messages à la couche du haut et du bas, où une couche donnée peut ajouter des champs de données ou de contrôle aux messages.

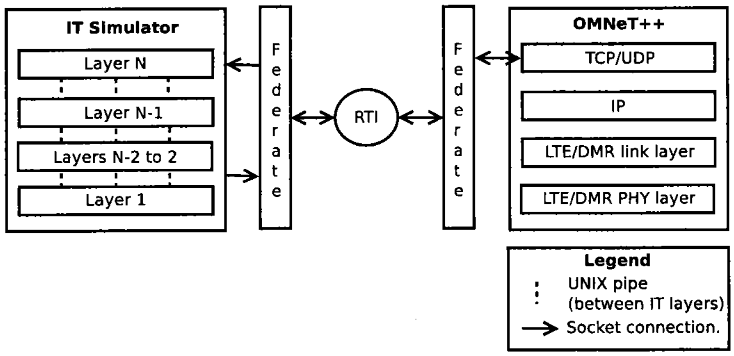

Figure 4.3 – Design de la co-simulation des perspectives de technologies de l'information et de communications.

Pour ce qui est de la perspective de communications, le modèle de simulation HLA-OMNeT++ [69] suivant la norme HLA. Comme l'étude de cas dans la section suivante porte sur les technologies LTE et digital mobile radio (DMR), ces modules ont été ajoutés. La composante de RTI gère le temps pour les deux simulateurs en discrétisant le temps en slots de τ.

4.3.2 Perspectives de communications et du système électrique

Pour modéliser les perspectives de communications et du système électrique de façon jointe, un co-simulateur basé sur OMNeT++ et OpenDSS, illustré à la Figure 4.4, a été développé. OMNeT++ est un simulateur *open source* extensible et OpenDSS est un simulateur de système de distribution électrique.

Contrairement au co-simulateur décrit à la sous-section précédente, celui-ci utilise l'approche avec une seule trame de temps modélisée par OMNeT++, puisque le temps n'est pas modélisé dans OpenDSS. Pour compiler et exécuter le co-simulateur, plusieurs composantes supplémentaires ont été ajoutées pour joindre les deux simulateurs. Les deux simulateurs sont fusionnés comme suit :

— *Communications and Power Distribution Network Co-simulator:* Ceci est exécuté en OMNeT++ et maintient une couche du système électrique en exécutant périodiquement OpenDSS à distance lorsque la charge dans le système électrique varie. L'appel à distance est fait par échange de requêtes hypertext transfer protocol (HTTP) avec les paramètres du système électrique ((1) dans Figure 4.4) et ensuite une réponse HTTP est retournée ((2) dans Figure 4.4).

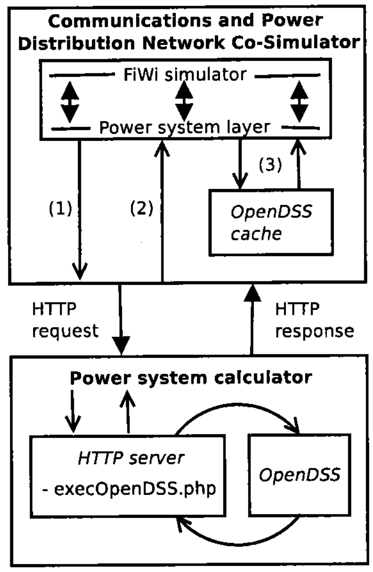

Figure 4.4 – Design de la co-simulation des perspectives de communications et du système électrique.

— *Power system simulator:* Il reçoit des requêtes HTTP avec les paramètres HTTP POST du système électrique à calculer. Ensuite, un script PHP écrit les configurations OpenDSS et OpenDSS est exécuté pour calculer le *power flow analysis* et successivement les résultats sont retournés.

Le co-simulateur a été proposé et présenté à [21].

4.4 Etude de cas

4.4.1 Télécontrôle du réseau de distribution

Le système considéré pour un système de distribution électrique est illustré à la Figure 4.5. L'application consiste à surveiller et contrôler un système de distribution pour les noeuds suivants :

— Transformateurs haute-tension (20 kV)/basse-tension (400 V).
— Poste électrique, tension de 225/63 kV à 20 kV.
— Futures fermes éoliennes et panneaux photovoltaïques.

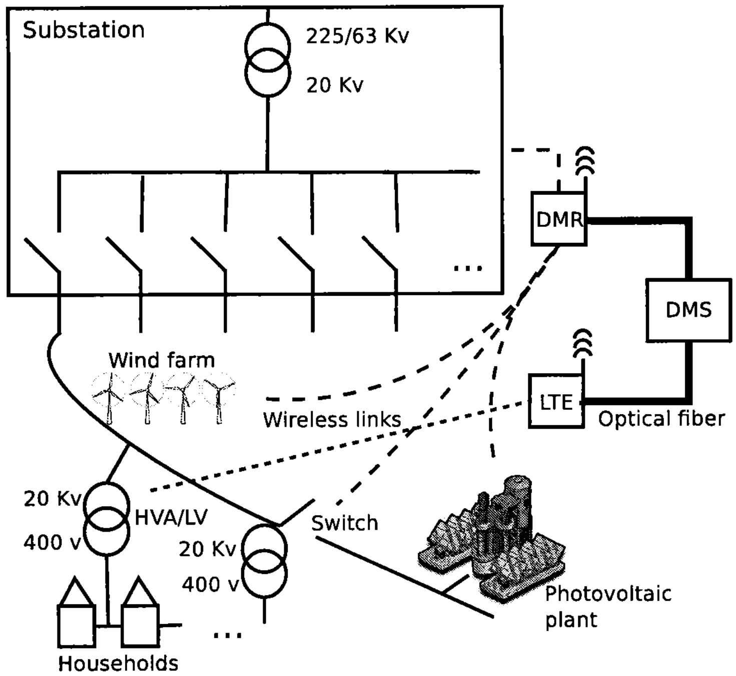

Figure 4.5 – Structure du réseau de distribution interconnecté via des liens sans fil LTE et DMR.

Tous les noeuds surveillés envoient des métriques au système DMS. Les métriques mesurées sont la puissance active/réactive, la tension, le courant et la position du noeud. En fonction des mesures reçues par le DMS, des messages de contrôle sont envoyés dans deux cas de figure :

— Des commandes manuelles et/ou automatiques pour contrôler l'activation et la désactivation des noeuds de coupure sont envoyées. Ces commandes permettent de replanifier le réseau pour maintenir et optimiser le réseau de distribution.

— Puisque les sources d'énergie renouvelables peuvent causer des problèmes de tension, le DMS envoie des commandes de contrôle de puissance active/réactive pour remettre la tension dans les limites permises.

La Figure 4.6 illustre la topologie utilisée des noeuds d'un poste électrique. Les noeuds ont deux interfaces de communications, une LTE et une *Digital Mobile Radio* (DMR). Le réseau LTE est utilisé pour transférer les mesures et le réseau DMR pour les messages de contrôle. Dans le cas où le réseau LTE devient indisponible, le réseau DMR est utilisé pour acheminer tous les paquets. A noter que le réseau DMR est dédié, mais a une capacité de 1.9 kbps, tandis que 50 kbps est assumée pour LTE.

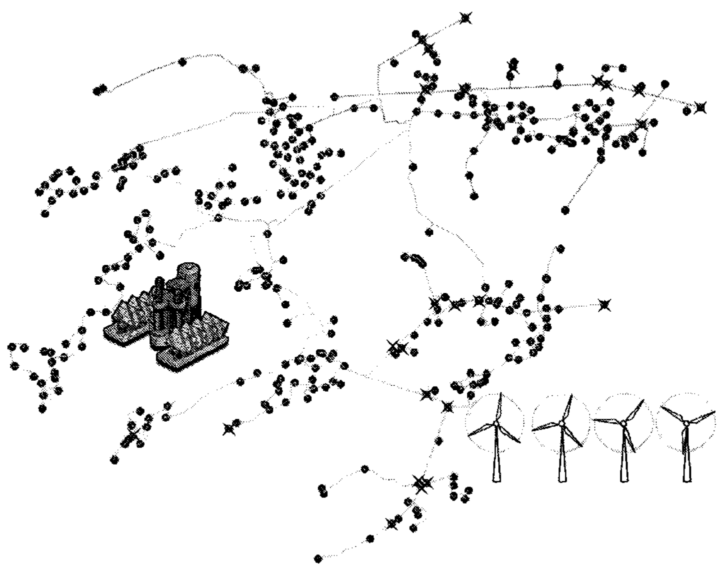

Figure 4.6 – Topologie du réseau de distribution basée sur de réelles configurations en France pour un poste électrique donné. Dimension : 15x15 kilomètres, nombre de clients en basse tension : 3139, nombre de noeuds haute tension/basse tension : 332 (noeuds pleins), nombre de noeuds de coupure : 26 (noeuds avec croix).

Tableau 4.1 – Mesures expérimentales, moyennes de la taille des corps des messages suivant la norme IEC 61850.

Variable	Valeur(s)
$\bar{L}_{dms}$	64/184 bytes
$\bar{L}_{hva/lv}$	500 bytes
$\bar{L}_{substation}$	5000 bytes
$\bar{L}_{der}$	224 bytes
$\bar{L}_{switch}$	100 bytes

Pour rendre l'expérience plus réaliste, les paquets d'applications smart grids suivant la norme IEC 61850 ont été capturés en utilisant l'outil Wireshark [1]. Les moyennes pour les noeuds DMS, haute-tension/basse-tension, poste électrique, sources d'énergie renouvelables et coupures sont notés par $\bar{L}_{dms}$, $\bar{L}_{hva/lv}$, $\bar{L}_{substation}$, $\bar{L}_{der}$ et $\bar{L}_{switch}$, respectivement, et sont utilisés dans la co-simulation (Tableau 4.1).

1. Ces mesures ont été faites sur des applications expérimentales smart grids à EDF R&D.

4.4.2 Véhicules électriques

Pour complémenter l'étude, une application de coordination de véhicules électriques est étudiée au niveau des perspectives de communications et du système électrique. Le réseau de distribution OpenDSS correspond à une version modifiée de *IEEE 13-Node radial distribution test feeder* [76] et décrite en détail dans [22]. Le but primaire est de comparer des algorithmes de coordination ainsi que de vérifier l'impact du taux de données des capteurs sur les performances de ces algorithmes.

4.5 Résultats

4.5.1 Télécontrôle du réseau de distribution

Cette section présente les résultats de l'étude de cas en utilisant une version préliminaire du modèle de multi-simulation, où les perspectives de technologies de l'information et de communications sont co-simulées via une architecture HLA.

La Figure 4.7 illustre les performances au niveau de la perspective de technologies de l'information en termes de fiabilité du système ([0..1]) en fonction d'un seuil maximal du délai de communications. On définit $\omega \in \{m, c\}$ et m, c qui correspondent aux classes de *monitoring* et de contrôle, respectivement. Pour une intervalle de co-simulation i, la fiabilité à un certain noeud n est définie comme suit :

$$\mathcal{R}_{i,n}^{\omega} = \frac{1}{|\mathcal{M}_{i,n}^{\omega}|} \cdot \sum_{m \in \mathcal{M}_{i,n}^{\omega}} \begin{cases} 1, & \text{if } d_{m,it} \leq \mathcal{L}_{\omega} \\ 0, & \text{otherwise} \end{cases}, \tag{4.1}$$

où $\mathcal{M}_{i,n}^{\omega}$ dénote l'ensemble des messages durant i de n et $d_{m,it}$ correspond au délai du message m de la perspective des technologies de l'information.

Pour chaque intervalle i, la fiabilité de la classe ω est définie selon une intervalle de confiance 95% :

$$\mathcal{R}_{i}^{\omega} = \mu(\Theta_i^{\omega}) \pm 1.96 \cdot \frac{\sigma(\Theta_i^{\omega})}{\sqrt{|\mathcal{N}_{\omega}|}}, \tag{4.2}$$

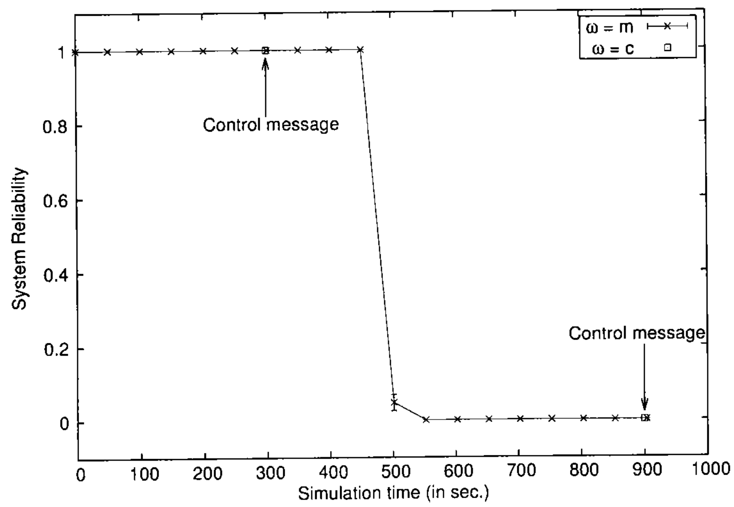

Figure 4.7 – Fiabilité du système sans utilisation de mécanisme de QdS. Le lien LTE devient indisponible au temps 500.

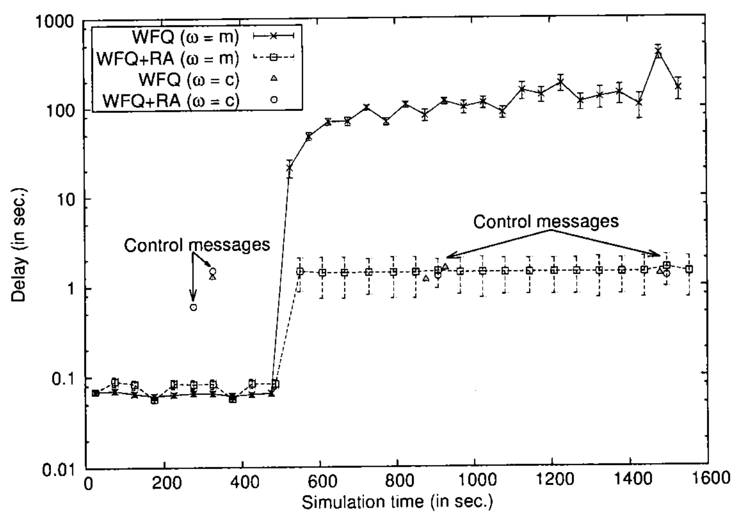

Figure 4.8 – Délai du système avec utilisation de mécanisme de QdS (WFQ: weighted fair queuing, RA: Rate adaptive).

où $\mathcal{N}_\omega$ est l'ensemble des noeuds et Θ_i^ω est la distribution des fiabilités à tous les noeuds :

$$\Theta_i^\omega = [\mathcal{R}_{i,n}^\omega], \forall n \in \mathcal{N}_\omega. \tag{4.3}$$

Aux temps 0-500 de la Figure 4.7, le système est fiable compte tenu que les deux réseaux sont disponibles. Cependant, à partir de 500, les paquets normalement acheminés en utilisant l'interface LTE sont envoyés à l'interface DMR, dont le lien devient saturé.

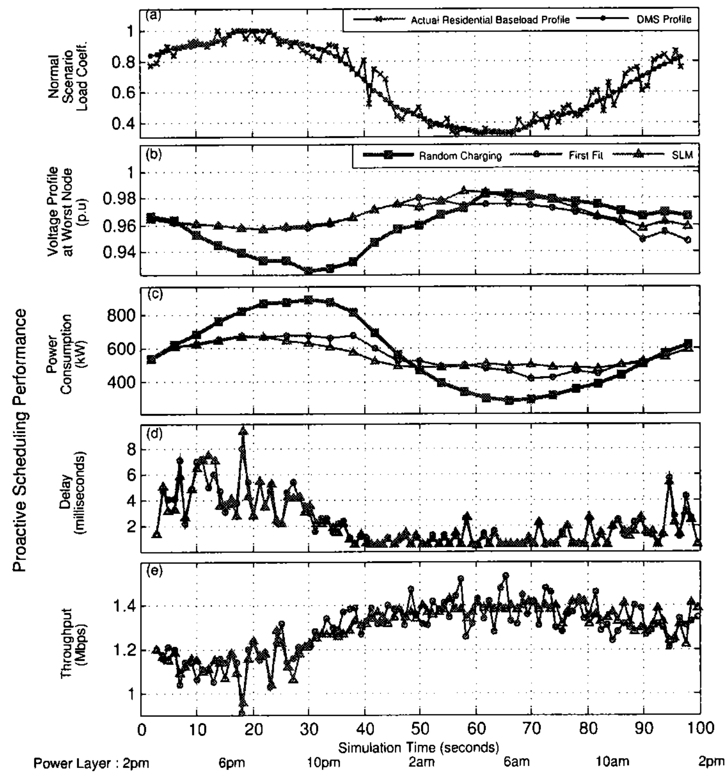

Figure 4.9 – Résultats selon les perspectives de communications et du système électrique avec différents algorithmes d'allocation de charge de véhicules électriques (niveau de pénétration : 66 %).

En utilisant un mécanisme de QdS à l'interface DMR avec adaptation du taux d'envoi (WFQ+RA), la fiabilité peut être significativement améliorée, tel qu'illustré à la Figure 4.8.

4.5.2 Véhicules électriques

Dans ce qui suit, on montre un exemple de résultat de co-simulation des perspectives de communications et du système électrique pour étudier différents algorithmes de véhicules électriques.

La Figure 4.9 compare les performances au niveau du système électrique en termes de tension et de charge de consommation, et au niveau du système de communications en termes de délai et de *throughput*. L'approche *smart load management* (SLM) [32], qui a pour but de minimiser la charge et les pertes, permet de diminuer la puissance maximale et mieux stabiliser la tension, comparativement aux approches *first fit* et *random charging*. Le délai et le débit ont été également mesurés de façon jointe, permettant de quantifier la bande passante nécessaire pour cette application donnée.

4.6 Résumé

Dans ce chapitre, un modèle de multi-simulation couvrant toutes les perspectives smart grids a été proposé suivant les modèles HLA et FMI normalisés. La multi-simulation permet d'expérimenter de nouveaux algorithmes smart grids à grande échelle. Une étude de cas de surveillance et de contrôle de réseau de distribution a été décrit et étudié en utilisant un modèle de co-simulation des perspectives de technologies de l'information et de communications. Ensuite, les perspectives de communications et du système électrique ont été étudiées dans un cas d'usage de coordination de véhicules électriques, permettant de quantifier les performances de divers algorithmes de coordination sous un angle de communications et du système électrique où les deux systèmes s'influencent. Des mesures expérimentales de messages d'applications smart grids ont été capturées et utilisées dans le co-simulateur pour rendre le cas d'usage réaliste. La co-simulation smart grid est étudiée plus en détail au Chapitre 9 où un algorithme de coordination centralisé de G2V, V2G et de sources d'énergie renouveables est proposé et étudié via co-simulation.

La co-simulation dynamique smart grid permet d'étudier de façon multidisciplinaire de nouveaux mécanismes smart grids. Cependant, cela ne permet pas de valider la faisabilité pratique de ces techniques, car il faut comparer ces performances de façon pratique pour améliorer la justesse du co-simulateur. La coordination de véhicules électriques n'a pas été expérimentée pratiquement. Dans le chapitre suivant, pour une première fois, on démontre la faisabilité de la coordination de véhicules électriques de façon pratique avec un banc d'essai expérimental d'un système de distribution réel (du Denemark) miniaturisé dans le laboratoire et communiquant entre les noeuds électriques via un réseau Ethernet multi-saut hétérogène.

Chapitre 5

Banc d'essai expérimental de véhicules électriques coordonnés

Dans ce chapitre, la faisabilité technique d'un nouvel algorithme de coordination de véhicules électriques est démontré expérimentalement sur un banc d'essai d'un système de distribution électrique réel miniaturisé et communiquant via un réseau d'accès Ethernet multi-saut hétérogène composé notamment d'un EPON.

5.1 Introduction

Très peu de tentatives ont été faites pour implémenter un banc d'essai smart grid. Dans [77], les auteurs ont proposé un laboratoire smart grid (SmartGridLab) pour concevoir et analyser de nouveaux protocoles dans un environnement expérimental. Une originalité significative dans leur conception est le contrôle d'*intelligent power switches* (IPSs) pour dynamiquement acheminer l'énergie en fonction de la disponibilité des sources d'énergie renouvelables. Cependant, le travail a mis l'accent au niveau de la conception seulement sans montrer expérimentalement des résultats. De plus, les résultats, éventuellement obtenus, ne permettraient pas d'être comparés à ceux d'un vrai système de distribution puisque le laboratoire est à un seul noeud et les propriétés (résistance et inductance) des lignes électriques ne sont pas modélisées. Un système pour surveiller et contrôler l'environnement d'un bâtiment et le lier au réseau intelligent a été proposé et implémenté [78]. Pour contrôler les appareils, un réseau ZigBee a été utilisé et des économies de 11-15 % ont été obtenues en optimisant les opérations des appareils en fonction de variations de prix. De plus, les auteurs ont démontré que les performances du réseau ZigBee peuvent décroître lorsque d'autres appareils sont en fonction, par exemple les micro-ondes. Dans [79], les auteurs ont conçu un microréseau en utilisant la radio cognitive. Bien que des efforts significatifs ont été menés pour concevoir des bancs d'essai smart grids, la démonstration expérimentale de la coordination de véhicules électriques n'a pas été expérimentée, ce qui est l'objet de cette section.

Plusieurs approches de chargement de véhicules électriques ont été investiguées par des modèles de simulation et de calculs [80, 81, 82, 83, 84]. Cependant, aucune de ces études n'a investigué de façon pratique la coordination de véhicules électriques. Une approche pour démontrer cela expérimentalement sans dépenser des sommes faramineuses dans de grands projets pilotes est de concevoir un modèle miniature d'un vrai système dans un environnement de laboratoire, qui est une façon moins risquée d'expérimenter de nouveaux mécanismes, tel qu'expérimenté dans [85] pour les sources d'énergie renouvelables. Les éléments nouveaux dans cette section sont définis comme suit :

— *Développement et implémentation d'un système de distribution réel de 13 noeuds miniaturisé avec intégration des perspectives des technologies de l'information et des communications. L'approche permet d'expérimenter des algorithmes et protocoles smart grids.*
— *Combinaison d'approches de contrôle centralisées et décentralisées validée via le banc d'essai. Ces techniques permettent la coordination en temps réel en tenant compte de la satisfaction des clients, des contraintes du réseau et de la minimisation des coûts de chargement.*

5.2 Banc d'essai expérimental

5.2.1 Réseau de distribution miniaturisé

Les configurations du système de distribution de basse tension Børup 250 kVA, 0.4 kV détenu par Danish Distribution SEAS-NVE est miniaturisé à 1 kVA 0.22 kV et implémenté dans le laboratoire. Pour miniaturiser, la technique *per unit* (PU) est utilisée. La Figure 5.1 correspond au schéma du réseau expérimental illustré à la Figure 5.2.

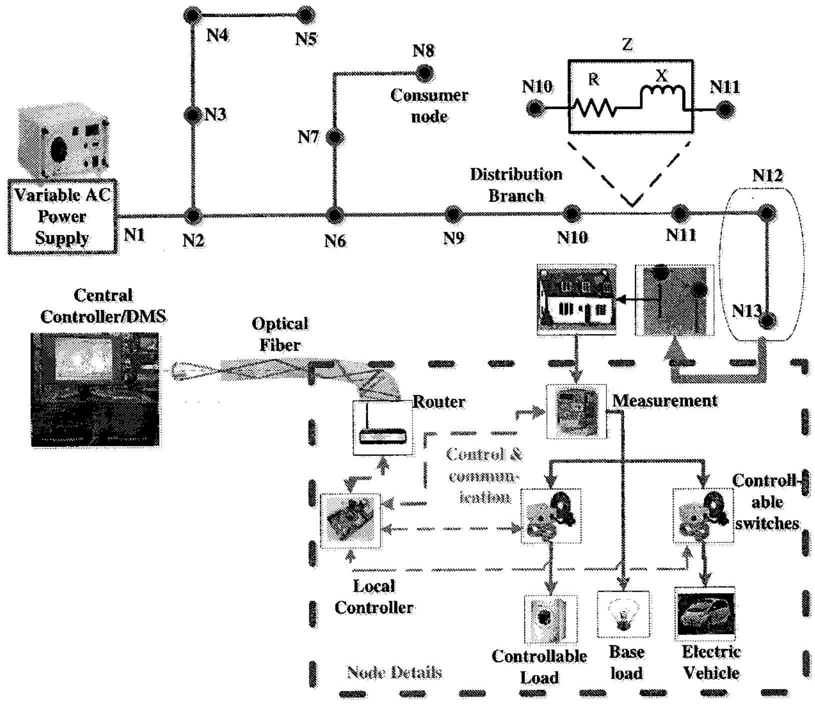

Figure 5.1 – Schéma du banc d'essai du réseau ingelligent miniaturisé de 13 noeuds.

Tableau 5.1 – Configurations avant et après miniaturisation des principaux paramètres du réseau de distribution.

Paramètre	Avant	Après
Capacité	250 (kVA)	1 (kVA)
Tension	0.4 (kV)	0.22 (kV)
Transformer R/X	4.64/18.64 (mΩ)	0.314/1.26 (Ω)
Câble R/X	207/78 (mΩ/km)	13.99/5.27 (Ω/km)

Distribution d'alimentation Les configurations des lignes sont représentées par des valeurs de résistance et d'inductance, voir N10-N11 à la Figure 5.1. Ces valeurs peuvent être calculées en utilisant la formule suivante :

$$R_{act,SD} = \left(R_{act} \cdot \frac{V_b^2}{S_b} \right) \cdot \frac{V_{b,SD}^2}{S_{b,SD}}, \tag{5.1}$$

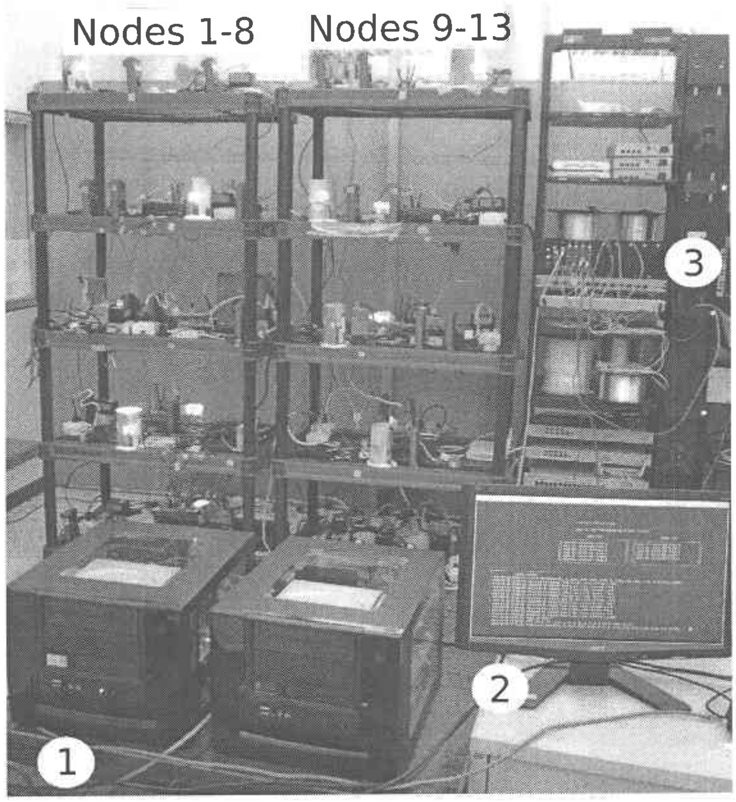

Figure 5.2 – Réseau de distribution miniaturisé composé d'un serveur DMS (1), d'une interface graphique (2), d'un EPON (3) et du réseau de distribution (nodes 1-13).

où R_{act} et $R_{act,SD}$ correspondent à la valeur de résistance avant et après miniaturisation. S_b et $S_{b,SD}$ sont la puissance de base avant et après miniaturisation, V_b et $V_{b,SD}$ sont la basse tension avant et après miniaturisation et finalement R_{PU} est la résistance PU. Les configurations principales du *test feeder* sont résumées au Tableau 5.1.

Charge La Figure 5.3 illustre la configuration complète du noeud 10. Une charge de base peut être configurée et connue en configurant à ON un certain nombre de moteurs. De plus, un profil de charge peut être configuré en mettant à ON/OFF de façon séquencielle à travers le temps des moteurs connectés aux interrupteurs. Les véhicules électriques sont modélisés par des batteries 4/7 Ah. De plus, des chargeurs 2/0.9 A sont contrôlés via un contrôleur local qui peut mettre à ON/OFF les interrupteurs électriques contrôlables. Ces contrôleurs locaux agissent en fonction de messages reçus par le *distribution management system* (DMS).

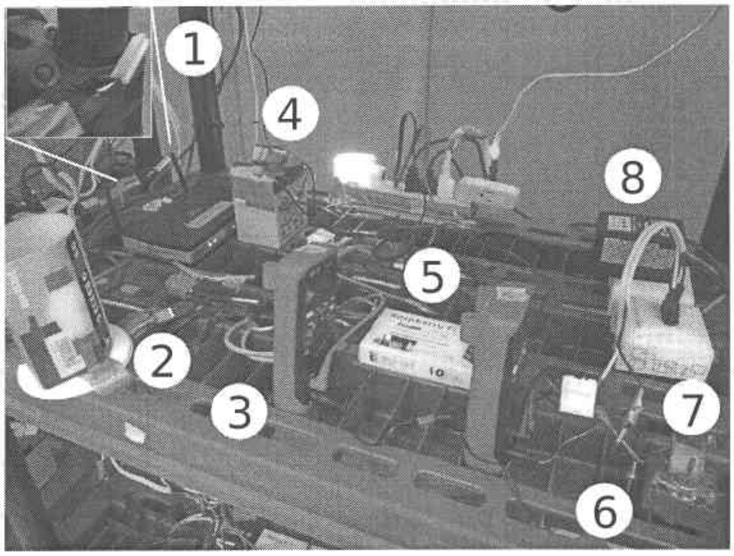

Figure 5.3 – Noeud intelligent (correspond au noeud 10) composé des configurations de résistance et d'inductance (1), appareil pour déchargement (2), capteurs (3), batterie (4), contrôleur local (5), charge dynamique (6), interrupteur électrique contrôlable (7) et chargeur (8).

5.2.2 Perspective de communications

L'infrastructure de communications, illustrée à la Figure 5.4, consiste en un EPON et d'un réseau NAN Ethernet filaire (qui pourra être remplacé par un réseau sans fil). Le EPON utilisé est un Sun Telecom GE8100/GE8200 Series, 4 ONUs, avec une distance de 20 kilomètres entre les noeuds ONUs et l'OLT. Le capacité est de 1 Gbps bidirectionnellement. Les contrôleurs locaux sont des Raspberry Pi model B (512 MB) et peuvent communiquer avec le DMS via le réseau NAN.

5.2.3 Perspective de technologies de l'information

Des *sockets Transmission Control Protocol* (TCP) sont établis entre les contrôleurs locaux et le DMS pour des communications fiables. Un délai d'aller-retour de 2 ms est mesuré lorsque la charge dans le réseau est faible ou moyenne. Le modèle est de type client-serveur implémenté avec le langage de programmation Python. Le DMS exécute l'application développée *SmartCoordinator* offrant les fonctionnalités suivantes :

— Interrogation périodique et synchronisée des contrôleurs locaux. Le temps est discrétisé en slots de 40 secondes, où le DMS interroge les contrôleurs locaux, dont ces derniers envoient le statut de chargement et des statistiques locales (tension, courant, etc.).

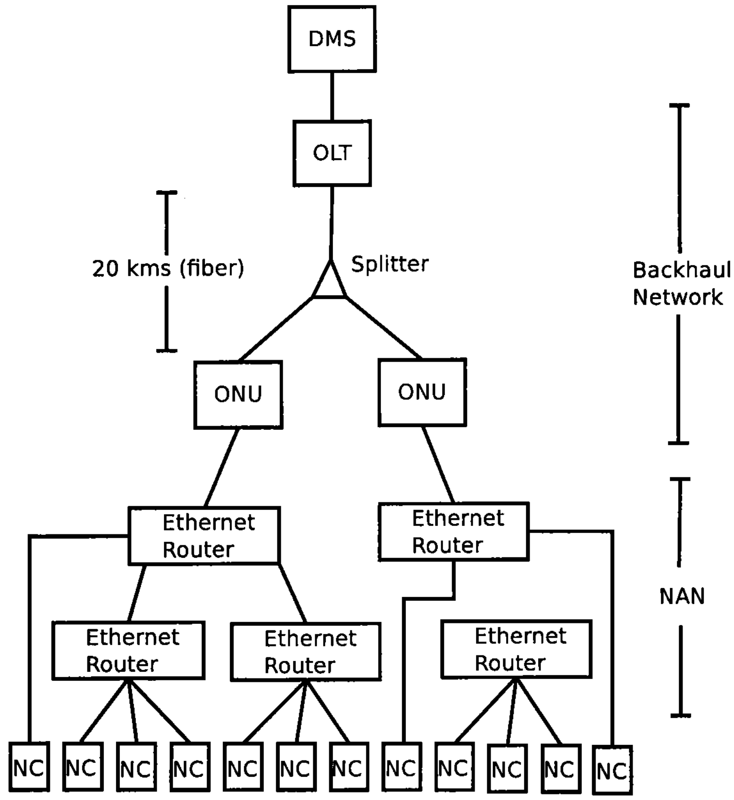

Figure 5.4 – Infrastructure de communications composée de nano-ordinateurs utilisés comme contrôleurs, de routeurs Ethernet et d'un EPON (NC : nano-computer).

— Exécution du modèle d'optimisation de coordination des véhicules électriques, implémenté en Matlab et décrit dans la Section 5.3.

— Interface graphique en temps réel affichant les statuts des noeuds et des événements majeurs.

De plus, chaque contrôleur local exécute l'application développée *SmartNode* suivante :

— Réception des interrogations du DMS et mise à jour du temps local.

— Interruption ON/OFF du chargement de batterie.

— Interruption ON/OFF du moteur pour créer un profil de charge.

— Lecture périodique du courant et de la tension.

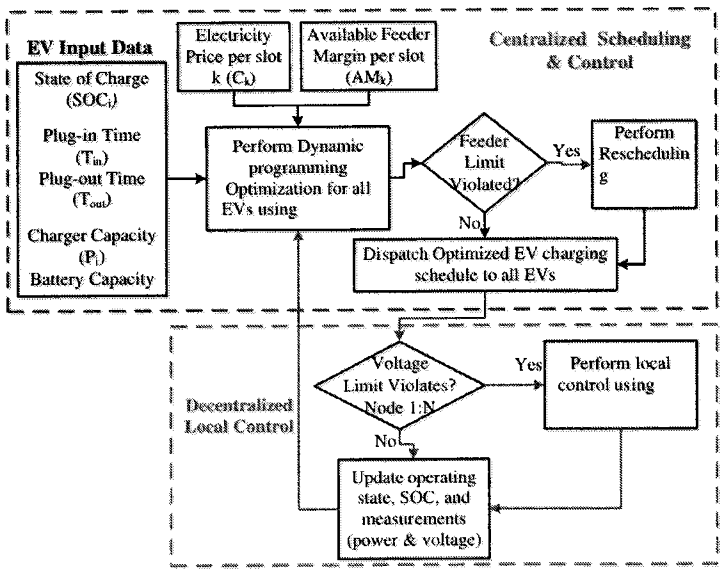

Figure 5.5 – Modèle de programmation dynamique pour coordination optimisée de chargement des véhicules électriques.

5.2.4 Synchronisation

Le DMS doit idéalement recevoir les mesures des capteurs de façon synchronisée pour avoir l'ensemble des mesures à un temps précis donné de l'ensemble du réseau. Dans cette section, deux méthodes de synchronisation simples, mais suffisantes pour l'application considérée :

- *Avec des capteurs à base de temps :* Chaque contrôleur local envoie les mesures à intervalle régulier sans tenir compte des autres capteurs.
- *Avec des capteurs coordonnés :* Dans ce scénario, le DMS diffuse un message de synchronisation à tous les capteurs et ceux-ci répondent au message en incluant les mesures.

5.3 Modèle de coordination optimisé de véhicules électriques

Le modèle de coordination, illustré à la Figure 5.5, est composé de 2 mécanismes. L'algorithme central est exécuté à chaque début de slot et l'algorithme décentralisé est exécuté périodiquement localement par les contrôleurs locaux. Ainsi, l'approche centrale agit par inter-slot et l'approche décentralisée agit par intra-slot.

5.3.1 Algorithme centralisé d'ordonnancement inter-slot

L'algorithme est exécuté par le DMS à chaque début de slot et les résultats d'ordonnancement sont envoyés aux contrôleurs locaux. L'algorithme est exécuté comme suit :

- Les véhicules électriques envoient au DMS leur état de chargement SOC_i, temps de *plug-in* $T_{in,i}$, temps de *plug-out* $T_{out,i}$, position dans le réseau, capacité de la batterie BC_i et la capacité de chargement P_i.
- Après réception des statistiques de tous les véhicules actifs, le DMS crée des ordonnancements pour les slots subséquentes.

Les ordonnancements sont créées en 2 étapes. La première étape consiste à minimiser en fonction du prix :

$$Minimize \sum_{k=T_{in,i}}^{T_{out,i}} P_{i,k} \cdot x_k \cdot t_k \cdot C_k \tag{5.2}$$

$$\begin{aligned} Subject\ to\ & P_{i,min} < P_i < P_{i,max} \\ & P_{i,avg} \leq P_{i,max} \\ & SOC_{i,T_{out}} = SOC_{i,max} \end{aligned} , \tag{5.3}$$

où $P_{i,k}$, t_k, x_k et C_k dénotent le vitesse de chargement du véhicule i, le temps de slot, l'état de k et le prix de l'électricité pour la période k, respectivement. $P_{i,min}$ et $P_{i,max}$ représentent les taux de chargement limites pour le véhicule i. Similairement, $P_{i,avg}$ est la moyenne de taux de chargement du véhicule i pour être entièrement chargé au temps de plug-out. $SOC_{i,T_{out}}$ et $SOC_{i,max}$ correspondent au niveau de charge lors du *plug-out* et au niveau de charge maximal, respectivement. Ces contraintes guident la procédure pour considérer les besoins du client.

La seconde étape consiste à considérer la perspective du réseau de distribution pour diminuer notamment la charge de pointe :

$$Minimize \sum_{k=1}^{N_{slt}} \sum_{i=1}^{N_{EV}} (P_{i,k} \cdot x_{i,k}) \cdot t_k \cdot C_k \tag{5.4}$$

$$Subject\ to \sum_{i=1}^{N_{EV}} P_{i,k} \leq AM_k,\ \forall k = 1 : N_{slt},, \tag{5.5}$$

où N_{EV} et N_{slt} dénotent le nombre de véhicules électriques connectés et le nombre de slots restantes. AM_k correspond à la charge disponible pour les véhicules électriques. Les contraintes dans Eq. (5.3) sont toujours utilisées.

5.3.2 Algorithme décentralisé intra-slot

L'algorithme décentralisé est exécuté par le contrôleur local. L'algorithme vérifie la tension et sa limite :

$$EV_i = \begin{cases} ON, & \text{if } V_i > 0.95 \\ OFF, & \text{sinon,} \end{cases} \tag{5.6}$$

où V_i est la tension au noeud i et 0.95 PU représente la limite minimale. Pour éviter que plusieurs contrôleurs basculent en même temps, Eq. (5.6) est utilisée si et seulement la même valeur est obtenue pendant d secondes, où d est aléatoirement choisi parmi $[0..S]$, où S est la valeur maximale d'attente.

5.4 Résultats expérimentaux

La Figure 5.6 comporte les configurations utilisées dans le banc d'essai pour les temps de charge et pour les profils de prix. Dans cette sous-section, les résultats des algorithmes proposés sont présentés.

5.4.1 Algorithmes proposés

La Figure 5.7 présente les résultats de l'approche centralisée. La Figure 5.7a démontre le charge du réseau. On dénote que la charge est supérieure de quelque peu à la limite maximale de 300 W dû aux pertes de puissance et au fait que l'efficacité de chargement est moins de 100 %. Figure 5.7b

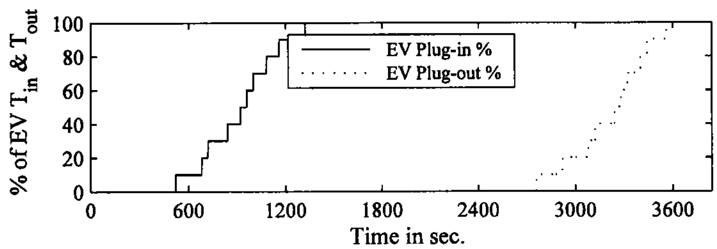

(a) Temps de départ et d'arrivée des véhicules électriques.

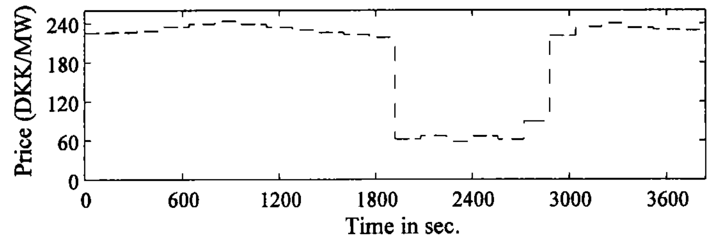

(b) Profil du prix de l'électricité.

Figure 5.6 – Configurations concernant les arrivées-départs des véhicules et profil de coût.

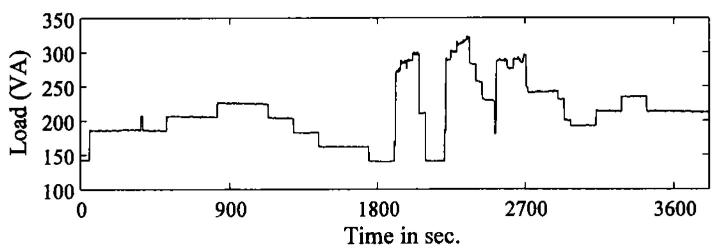

(a) Profil de la puissance.

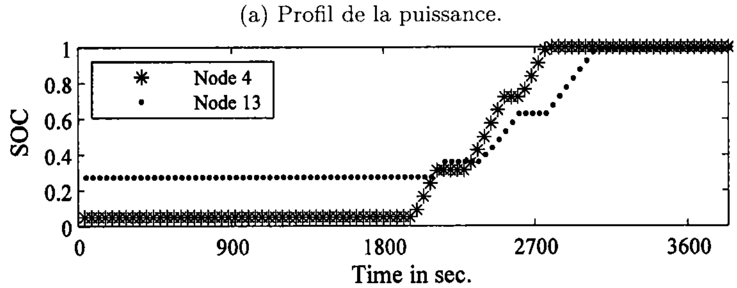

(b) Etat de chargement de batterie des noeuds 4 et 13.

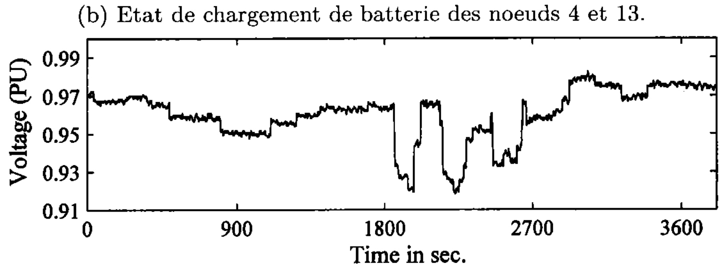

(c) Profil de tension du noeud 13.

Figure 5.7 – Optimisation centralisée des véhicules électriques.

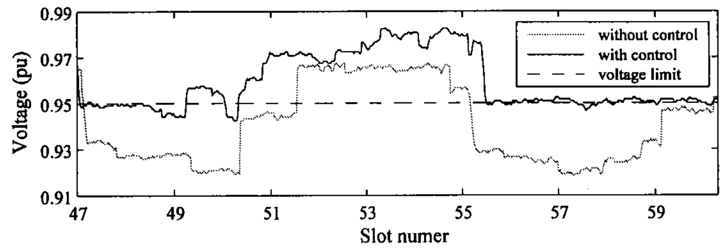

Figure 5.8 – Profil de tension de l'algorithme décentralisé.

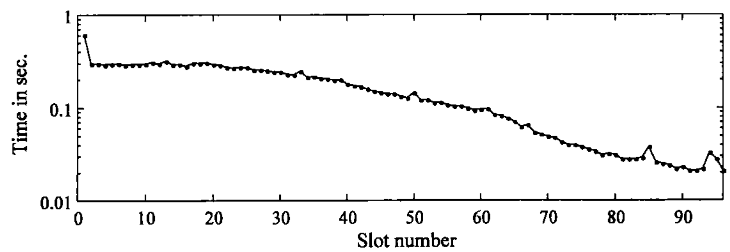

Figure 5.9 – Durée de calcul du processus d'optimisation centralisée.

illustre l'état de charge des batteries de deux noeuds, un noeud avec un chargeur 0.9 A (noeud 13) et le second avec un chageur 2 A (noeud 4). Figure 5.7c illustre le profil de la tension. On dénote que la tension est inférieure à la tension minimale (0.95 PU) puisque cette contrainte n'est pas incluse dans l'approche centrale, mais considéré dans l'approche décentralisée.

En activant l'algorithme décentralisé de contrôle de tension, on note une amélioration significative du profil de tension, tel qu'illustré à la Figure 5.8.

5.4.2 Complexité et synchronisation

La complexité de l'algorithme de coordination centralisée est mesurée en termes de durée de calcul (Figure 5.9) en fonction du numéro de slot. Effectivement, le temps de calcul est une métrique importante puisque les algorithmes smart grids doivent s'exécuter avec un temps de calcul raisonnable (qui varie en fonction de l'application). Avec les configurations utilisées, le temps maximal de calcul mesuré correspond à 0.6 secondes et ce temps décroît en fonction du numéro de slot, ce qui est suffisamment rapide pour l'application considérée.

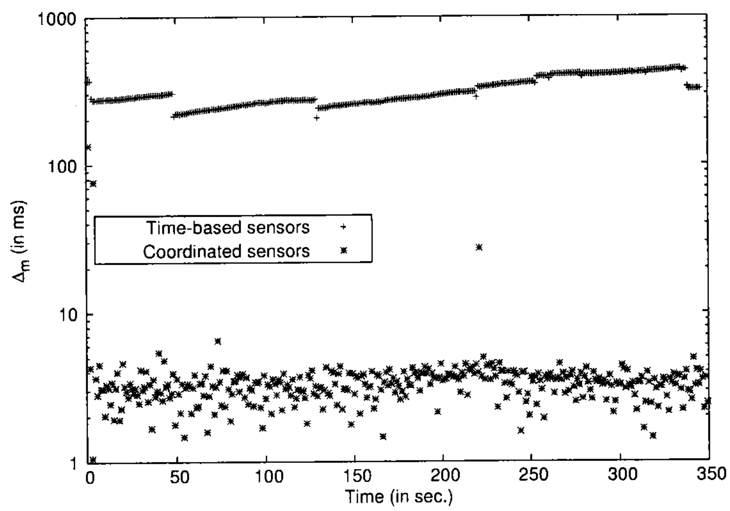

Figure 5.10 – Performance de synchronisation avec capteurs périodiques et coordonnés.

Les algorithmes de synchronisation sont investigués et mesurés à la Figure 5.10. Pour une certaine slot s, on définit l'intervalle moyen entre les mesures reçues comme suit :

$$\Delta_m = \frac{1}{|\mathcal{M}_s| \cdot (|\mathcal{M}_s| - 1)} \cdot \sum_{i \in \mathcal{M}_s} \sum_{j \in \mathcal{M}_s - \{i\}} |t_i - t_j|, \tag{5.7}$$

où $\mathcal{M}_s$ correspond aux mesures reçues par le DMS durant la slot s. $t_{i/j}$ correspond au temps reçu du message i/j. Le taux d'envoi utilisé est de 1 seconde. Ainsi, on dénote que l'approche coordonnée permet de synchroniser les mesures à environ 5 ms, contrairement à environ 500 ms avec l'approche non coordonnée. De plus, les packets transférés au port de sortie de DMS vers OLT ont été capturés, tel qu'illustré à la Figure 5.11. Le débit de transmission maximal mesuré est de 450 kbps, où le profil de trafic consiste à de longues périodes sans trafic suivies de courtes rafales.

5.5 Résumé

Un banc d'essai d'un réseau de distribution réel a été miniaturisé et couplé à un réseau de communications formé d'un EPON et NAN multi-sauts. L'algorithme de coordination centralisé et décentralisé permet de simultanément prendre en compte le coût de chargement, la congestion du réseau et la tension locale. Une méthode de synchronisation coordonnée simple et efficace permet de synchroniser les mesures de façon plus efficacement qu'avec une approche périodique non co-

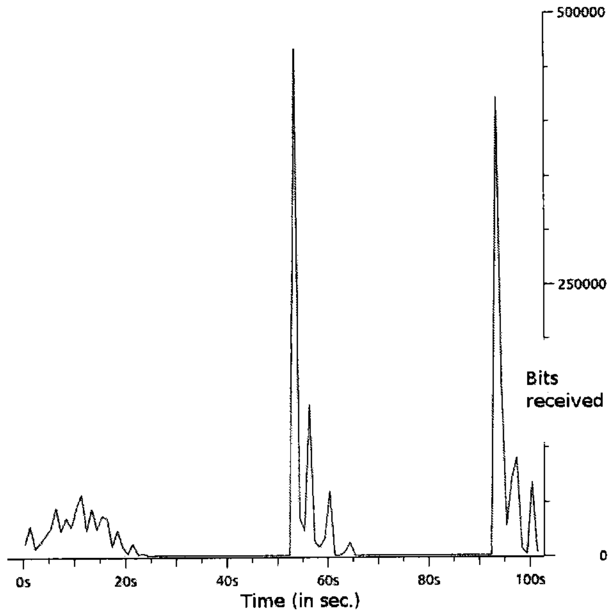

Figure 5.11 – Trafic capturé au port de sortie entre DMS et OLT.

ordonnée. Un débit maximal de l'ordre de 400 kbps avec un profil périodique fit mesuré avec les configurations investiguées.

Dans le chapitre suivant, les conclusions et les travaux futurs sont décrits. La partie II comporte de façon plus détaillée les journaux acceptés complétant plus en détails et de façon étendue les éléments présentés dans cette partie.

Chapitre 6

Conclusions et travaux futurs

6.1 Conclusions

Les réseaux optiques passifs de prochaines générations permettent une évolution à court terme et une révolution à long terme, où les réseaux optiques et sans fil (FiWi) intégrés représentent la finalité des réseaux d'accès. Dans le cadre de cette thèse, on a souligné l'opportunité d'intégrer des capteurs optiques et sans fil avec les réseaux d'accès FiWi et avons proposé le réseau Über-FiWi dont le potentiel permet de bénéficier non pas seulement pour le secteur des télécommunications, mais pour une multitude de secteurs économiques tels que l'énergie (smart grid) et le transport.

Le premier modèle analytique FiWi est proposé, permettant ainsi d'évaluer la performance de différents algorithmes de routage FiWi. Le modèle est très flexible et incorpore différentes distributions de taille de trame, de débits de données et d'échec de fibre optique. Le modèle analytique a été vérifié au moyen de simulations FiWi avec différentes architectures suivant des scénarios de trafic *peer-to-peer*, en amont, uniforme et non-uniforme. Un nouvel algorithme de routage, *optimized FiWi routing algorithm* (OFRA), a été proposé et surpasse les approches de minimisation par nombre de sauts ou par le délai en termes de débit maximal au détriment d'une augmentation mineure du délai pour des charges de trafic faible à moyenne.

Les performances de réseaux multi-niveau FiWi intégrés avec trafic *human-to-human* (H2H) et *machine-to-machine* (M2M) ont été étudiées en terme de délai, capacité et fiabilité. Considérant le protocole EDCA de IEEE 802.11e avec qualité de service, un modèle existant considérant un trafic saturé a été adapté et vérifié avec un trafic non-saturé. De plus, des capteurs événementiels (*event-driven*) et périodiques (*time-driven*) ont été considérés. L'analyse développée permet de quantifier la borne théorique du débit de données maximal du trafic M2M sans violer un seuil de délai du trafic H2H.

Un modèle probabiliste multi-classe original de la disponibilité a été proposé pour les réseaux PONs et WiMAX intégrés. Comparativement aux autres travaux, le modèle tient compte (*i*) des limites des protocoles MAC et (*ii*) des échecs probabilistes de fibres optiques et des stations de base. En utilisant les configurations réalistes mesurées d'applications smart grids dans [20], le modèle développé permet de quantifier le débit de données maximal des capteurs pouvant être généré permettant de respecter les exigences de disponibilité des capteurs et du trafic régulier.

La coordination et l'optimisation de véhicules électriques et sources d'énergie renouvelables ont été étudiées de façon multidisciplinaire. En premier temps, une co-simulation sans synchronisation a été proposé, combinant les simulateurs OMNeT++ et OpenDSS existants, permettant ainsi de montrer l'impact de capteurs périodiques vs. événementiels sur un algorithme de contrôle de tension. Ensuite, un multi-simulateur suivant une architecture High Level Architecture (HLA) a été proposé, permettant de synchroniser un ensemble de simulateurs pour modéliser toutes les perspectives smart grids. Un cas d'usage basé sur des configurations réelles en France a été développé, et notamment les caractérisques d'applications smart grids ont été mesurées et injectées dans le modèle de multi-simulation. Utilisant l'original co-simulateur OMNeT++-OpenDSS, un algorithme de coordination intégré pour véhicule et sources d'énergie renouvelables a été proposé et permet d'interagir via une infrastructure de communications convergente FiWi. L'algorithme a été évalué par co-simulation où la perspective du système de distribution électrique interagit dynamiquement avec le modèle d'infrastructure FiWi, où moins de 2 Mbps ont été nécessaire pour diminuer de 21 % la puissance durant la période de pointe. Ensuite, les configurations d'un système de distribution du Danemark ont été miniaturisées et un banc d'essai a été développé suivant ces configurations réalistes. Dans le cadre de ce travail, une méthode de coordination des capteurs a été proposé pour améliorer la synchronisation de mesures échangées via une architecture de communications multi-saut. De plus, un mécanisme original de programmation dynamique a été proposé pour tenir compte de façon jointe des performances du réseau de distribution et de la minimisation des coûts clients.

6.2 Suggestions pour les travaux futurs

Dans le futur, on planifie d'étudier la synchronisation des capteurs et noeuds smart grids communiquant sur une architecture multi-saut hétérogène. Les capteurs doivent être déployés dans divers terrain pour contrôler, surveiller et stocker des informations avec granularité fine à propos de l'ensemble du système électrique. Plusieurs applications telles que wide-area situational awareness (WASA) nécessitent de mettre à jour l'ensemble de la vue du réseau à chaque 15 ms de façon synchronisée. Etant donné que les délais entre les capteurs et le système de distribution électrique (DMS) varient, le DMS ne reçoit pas nécessairement les mesures de façon ordonnée, ce qui représente un défi majeur compte tenu que des décisions critiques sont prises en fonction de ces mesures. De plus, chaque horloge des capteurs a une déviation. Pour synchroniser au delà de plusieurs liens Ethernet, le protocole Precision Time Protocol (PTP) a été élaboré. Cependant, une hypothèse de ce protocole est qu'il suppose des liens symétriques, ce qui n'est pas toujours le cas. Un nouveau protocole de synchronisation est donc nécessaire pour les applications critiques telles que les smart grids communiquant sur une architecture partagée de communications.

On note également plusieurs améliorations et extensions possibles de cette thèse :

— Comparaison détaillée des bénéfices et des limitations de l'approche d'évaluation avec un banc d'essai vs. par co-simulation.

— Au niveau de la disponibilité probabiliste du réseau FiWi, il serait intéressant de considérer des échecs probabilistes corrélés pour rendre plus réalistes le modèle proposé.

— Pour ce qui est de la performance des protocoles MAC, il serait intéressant de considérer des distributions de trafic plus réalistes, par exemple Pareto. Pour effectuer ces extensions, des modifications au niveau de la probabilité de transmission et du délai de file d'attente doivent être effectuées.

Chapitre 7

Publications réalisées

Chapitre de livre

[BC1] **M. Lévesque**, L. Ivanescu, and M. Maier, "Next-Generation Optical Access Networks: Trends, Challenges, and Applications," *Hershey, PA: IGI Global, Encyclopedia of Information Science and Technology, Third Edition*, accepted for publication.

Journaux

[J8] **M. Lévesque**, M. Maier, C. Béchet, E. Suignard, A. Picault and G. Joós, "From Co- Towards Multi-Simulation of Smart Grids: A Telecontrol Case Study Based on Real World Configurations," *submitted to IEEE Transactions on Smart Grid.*

[J7] B. P. Bhattarai, **M. Lévesque**, M. Maier, B. Bak-Jensen, J. R. Pillai, "Optimizing Electric Vehicle Coordination over a Heterogeneous Mesh Network in a Scaled-down Smart Grid Testbed," *submitted to IEEE Transactions on Smart Grid.*

[J6] **M. Lévesque**, F. Aurzada, M. Maier, and G. Joós, "Coexistence Analysis of H2H and M2M Traffic in FiWi Smart Grid Communications Infrastructures Based on Multi-Tier Business Models," *IEEE Transactions on Communications*, in first revision.

[J5] **M. Lévesque** and M. Maier, "Probabilistic Availability Quantification of PON and WiMAX Based FiWi Access Networks for Future Smart Grid Applications," *IEEE Transactions on Communications*, accepted for publication.

[J4] M. Maier and **M. Lévesque**, "Dependable Fiber-Wireless (FiWi) Access Networks and Their Role in a Sustainable Third Industrial Revolution Economy (Invited Paper)," *IEEE Transactions on Reliability*, accepted for publication.

[J3] F. Aurzada, **M. Lévesque**, M. Maier, and M. Reisslein, "FiWi Access Networks Based on Next-Generation PON and Gigabit-Class WLAN Technologies: A Capacity and Delay Analysis," *IEEE/ACM Transactions on Networking*, accepted for publication.

[J2] D. Q. Xu, **M. Lévesque**, G. Joós, and M. Maier, "Integrated V2G, G2V, and Renewable Energy Sources Coordination over a Converged Fiber-Wireless Broadband Access Network," *IEEE Transactions on Smart Grid*, vol. 4, no. 3, pp. 1381-1390, May 2013.

[J1] M. Maier, **M. Lévesque**, and L. Ivanescu, "NG-PONs 1&2 and Beyond: The Dawn of the Über-FiWi Network," *IEEE Network, Special Issue on Next Generation Optical Access Networks: Dynamic Bandwidth Allocation, Resource Use Optimization and QoS Improvements*, vol. 26, no. 2, pp. 15-21, March/April 2012.

Actes de conférence

[C5] **M. Lévesque**, F. Aurzada, M. Maier, and M. Reisslein, "Analytical Framework for the Capacity and Delay Evaluation of Next-Generation FiWi Network Routing Algorithms," *Proc., IEEE Wireless Communications and Networking Conference (WCNC),* pp. 1926-1931, Shanghai, China, Apr. 2013.

[C4] **M. Lévesque**, D. Q. Xu, G. Joós, and M. Maier, "Co-Simulation of PEV Coordination Schemes over a FiWi Smart Grid Communications Infrastructure," *Proc., The 38th Annual Conference of the IEEE Industrial Electronics Society (IECON 2012),* pp. 2901-2906, Montréal, Canada, Oct. 2012.

[C3] **M. Lévesque** and M. Maier, "The Über-FiWi Network: QoS Guarantees for Triple-Play and Future Smart Grid Applications (Invited Paper)," *Proc., International Conference on Transparent Optical Networks (ICTON),* pp. 1-4, Coventry, United Kingdom, Jul. 2012.

[C2] **M. Lévesque**, M. Maier, Y. Desai, and G. Joós, "Adaptive Admission Control for a Smart Grid FiWi Communications Network facing Power Blackouts during a DDoS Attack," *Proc., IEEE Green Technologies Conference,* pp. 1-3, Tulsa, OK, USA, Apr. 2012.

[C1] **M. Lévesque**, D. Q. Xu, M. Maier, and G. Joós, "Communications and Power Distribution Network Co-Simulation for Multidisciplinary Smart Grid Experimentations," *Proc.,*

SCS/ACM Spring Simulation Multiconference (SpringSim), Annual Simulation Symposium, pp. 1-7, Orlando, FL, USA, Mar. 2012.

Bibliographie

[1] X. Fang, S. Misra, G. Xue, and D. Yang. Smart Grid - The New and Improved Power Grid: A Survey. *IEEE Communications Surveys & Tutorials*, 14(4):944–980, Fourth Quarter 2012.

[2] C.-K. Wen, J.-C. Chen, J.-H. Teng, and P. Ting. Decentralized Plug-in Electric Vehicle Charging Selection Algorithm in Power Systems. *IEEE Transactions on Smart Grid*, 3(4):1949–3053, December 2012.

[3] B. Mukherjee G. Kramer and G. Pesavento. IPACT A Dynamic Protocol For An Ethernet PON (EPON). *IEEE Communications Magazine*, 40(2):74–80, 2002.

[4] N. Ghazisaidi and M. Maier. Fiber-Wireless (FiWi) Access Networks: Challenges and Opportunities. *IEEE Network*, 25(1):36–42, Jan.-Feb. 2011.

[5] M. Lévesque and M. Maier. Probabilistic Availability Quantification of PON and WiMAX Based FiWi Access Networks for Future Smart Grid Applications. *IEEE Transactions on Communications*, to appear.

[6] S. Davies. Grid Looks to Smart Solutions. *IET Engineering & Technology*, 5(7):49–51, 2010.

[7] B. Xiao-Min, M. Jun-Xia, and Z. Ning-Hui. Functional Analysis of Advanced Metering Infrastructure in Smart Grid. In *Proc., IEEE International Conference on Power System Technology (POWERCON)*, Hangzhou, China, October 2010.

[8] U.S. Energy Information Administration. The International Energy Outlook 2010. *U.S. Department of Energy*, July 2010.

[9] B. Heile. Smart Grids for Green Communications. *IEEE Wireless Communications*, 17(3):4–6, June 2010.

[10] IEEE Standards Working Group. IEEE Guide for Smart Grid Interoperability of Energy Technology and Information Technology Operation with the Electric Power System (EPS), End-Use Applications, and Loads. *IEEE Std 2030-2011*, September 2011.

[11] M. Lévesque, L. Ivanescu, and M. Maier. Next-Generation Optical Access Networks: Trends, Challenges, and Applications. *Hershey, PA: IGI Global, Encyclopedia of Information Science and Technology, Third Edition, in print*, 2014.

[12] M. Maier and M. Lévesque. Dependable Fiber-Wireless (FiWi) Access Networks and Their Role in a Sustainable Third Industrial Revolution Economy. *IEEE Transactions on Reliability*, to appear, 2014.

[13] M. Maier, M. Lévesque, and L. Ivanescu. NG-PONs 1&2 and Beyond: The Dawn of the Über-FiWi Network. *IEEE Network, Special Issue on Next Generation Optical Access Networks: Dynamic Bandwidth Allocation, Resource Use Optimization and QoS Improvements*, 26(2):15–21, March/April 2012.

[14] M. Lévesque, M. Maier, Y. Desai, and G. Joós. Adaptive Admission Control for a Smart Grid FiWi Communications Network facing Power Blackouts during a DDoS Attack. In *Proc., IEEE Green Technologies Conference*, Tulsa, OK, USA, April 2012.

[15] M. Lévesque and M. Maier. The Über-FiWi Network: QoS Guarantees for Triple-Play and Future Smart Grid Applications (Invited Paper). In *Proc., International Conference on Transparent Optical Networks (ICTON)*, Coventry, United Kingdom, July 2012.

[16] M. Lévesque, F. Aurzada, M. Maier, and M. Reisslein. Analytical Framework for the Capacity and Delay Evaluation of Next-Generation FiWi Network Routing Algorithms. In *Proc., IEEE Wireless Communications and Networking Conference (WCNC)*, Shanghai, China, April 2013.

[17] F. Aurzada, M. Lévesque, M. Maier, and M. Reisslein. FiWi Access Networks Based on Next-Generation PON and Gigabit-Class WLAN Technologies: A Capacity and Delay Analysis. *IEEE/ACM Transactions on Networking (Early Access)*, 2014.

[18] M. Lévesque, F. Aurzada, M. Maier, and G. Joós. Coexistence Analysis of H2H and M2M Traffic in FiWi Smart Grid Communications Infrastructures Based on Multi-Tier Business Models. *IEEE Transactions on Communications*, in first revision.

[19] I. Tinnirello and G. Bianchi. Rethinking the IEEE 802.11e EDCA Performance Modeling Methodology. *IEEE/ACM Transactions on Networking*, 18(2):540–553, April 2010.

[20] M. Lévesque, M. Maier, C. Béchet, E. Suignard, A. Picault, and G. Joós. From Co- Towards Multi-Simulation of Smart Grids: A Telecontrol Case Study Based on Real World Configurations. *IEEE Transactions on Smart Grid*, submitted.

[21] M. Lévesque, D. Q. Xu, M. Maier, and G. Joós. Communications and Power Distribution Network Co-Simulation for Multidisciplinary Smart Grid Experimentationss. In *Proc., SCS/ACM Spring Simulation Multiconference (SpringSim), Annual Simulation Symposium*, Orlando, FL, USA, March 2012.

[22] M. Lévesque, D. Q. Xu, G. Joós, and Martin Maier. Co-Simulation of PEV Coordination Schemes over a FiWi Smart Grid Communications Infrastructure. In *Proc., The 38th Annual Conference of the IEEE Industrial Electronics Society (IECON)*, Montréal, QC, Canada, October 2012.

[23] D. Q. Xu, M. Lévesque, G. Joós, and M. Maier. Integrated V2G, G2V, and Renewable Energy Sources Coordination over a Converged Fiber-Wireless Broadband Access Network. *IEEE Transactions on Smart Grid*, 4(3):1381–1390, September 2013.

[24] B. P. Bhattarai, M. Lévesque, M. Maier, B. Bak-Jensen, and J. R. Pillai. Optimizing Electric Vehicle Coordination over a Heterogeneous Mesh Network in a Scaled-down Smart Grid Testbed. *IEEE Transactions on Smart Grid*, submitted.

[25] V. C. Gungor, D. Sahin, T. Kocak, S. Ergut, C. Buccella, C. Cecati, and G. P. Hancke. A Survey on Smart Grid Potential Applications and Communication Requirements. *IEEE Transactions on Industrial Informatics*, 9(1):28–42, February 2013.

[26] L. H. Tsoukalas and R. Gao. From Smart Grids to an Energy Internet: Assumptions, Architectures and Requirements. In *Proc., Third International Conference on Electric Utility Deregulation and Restructuring and Power Technologies*, Nanjuing, China, April 2008.

[27] R. Abe, H. Taoka, and D. McQuilkin. Digital Grid: Communicative Electrical Grids of the Future. *IEEE Transactions on Smart Grid*, 2(2):399–410, April 2011.

[28] National Institute of Standards & Technology. NIST Framework and Roadmap for Smart Grid Interoperability Standards, release 1.0. 2010.

[29] M. Afzal and V. Pothamsetty. Analytics for Distributed Smart Grid Sensing. In *Proc., IEEE PES Innovative Smart Grid Technologies (ISGT)*, Washington, DC, USA, January 2012.

[30] J. G. Pinto, V. Monteiro, H. Gonçalves, B. Exposto, D. Pedrosa, C. Couto, and J. L. Afonso. Bidirectional Battery Charger with Grid-to-Vehicle, Vehicle-to-Grid and Vehicle-to-Home Technologies. In *Proc., IEEE Industrial Electronics Society Annual Conference (IECON)*, Vienna, Austria, November 2013.

[31] K. Bao, S. Li, and H. Zheng. Battery Charge and Discharge Control for Energy Management in EV and Utility Integration. In *Proc., IEEE Power and Energy Society General Meeting*, San Diego, CA, USA, July 2012.

[32] S. Deilami, A. S. Masoum, P. S. Moses, and M. A. S. Masoum. Real-Time Coordination of Plug-In Electric Vehicle Charging in Smart Grids to Minimize Power Losses and Improve Voltage Profile. *IEEE Transactions on Smart Grid*, 2(3):456–467, August 2011.

[33] B. Wang, M. Sechilariu, and F. Locment. Intelligent DC Microgrid With Smart Grid Communications: Control Strategy Consideration and Design. *IEEE Transactions on Smart Grid*, 3(4):2148–2156, December 2012.

[34] F. Blaabjerg, R. Teodorescu, M. Liserre, and A. V. Timbus. Overview of Control and Grid Synchronization for Distributed Power Generation Systems. *IEEE Transactions on Industrial Electronics*, 53(5):1398–1409, October 2006.

[35] J. Bryan, R. Duke, and S. Round. Decentralized Generator Scheduling in a Nanogrid Using DC Bus Signaling. In *Proc., IEEE Power Engineering Society General Meeting*, Denver, Colorado, USA, June 2004.

[36] E. Hassan Et-Tolba, M. Maaroufi, and M. Ouassaid. Demand side management algorithms and modeling in smart grids A customer's behavior based study. In *Proc., International Renewable and Sustainable Energy Conference (IRSEC)*, Ouarzazate, Morocco, March 2013.

[37] T. Logenthiran, D. Srinivasan, and T. Z. Shun. Demand Side Management in Smart Grid Using Heuristic Optimization. *IEEE Transactions on Smart Grid*, 3(3):1244–1252, September 2012.

[38] S. Bu, F. R. Yu, and P. X. Liu. Dynamic Pricing for Demand-side Management in the Smart Grid. In *Proc., IEEE Online Conference on Green Communications*, New York, NY, USA, September 2011.

[39] V. C. Gungor, D. Sahin, T. Kocak, S. Ergut, and C. Buccella. Smart Grid Technologies: Communication Technologies and Standards. *IEEE Transactions on Industrial Informatics*, 7(4):529–539, November 2011.

[40] G. R. Hiertz, Y. Zang, S. Max, T. Junge, E. Weiss, and B. Wolz. IEEE 802.11s: WLAN Mesh Standardization and High Performance Extensions. *IEEE Network*, 22(3):12–19, May-June 2008.

[41] B. S. Kim, H. Y. Hwang, and D. K. Sung. Effect of Frame Aggregation on the Throughput Performance of IEEE 802.11n. In *Proc., IEEE Wireless Communications and Networking Conference (WCNC)*, Las Vegas, NV, USA, Mar.-Apr. 2008.

[42] Y. Kim, S. Choi, K. Jang, and H. Hwang. Throughput Enhancement of IEEE 802.11 WLAN via Frame Aggregation. In *Proc., IEEE Vehicular Technology Conference (VTC)*, Los Angeles, CA, USA, September 2004.

[43] N. Ramos, D. Panigrahi, and S. Dey. Quality of Service Provisioning in 802.11e Networks: Challenges, Approaches, and Future Directions. *IEEE Network*, 19(4):14–20, July-Aug. 2005.

[44] G. Giambene and S. Hadzic-Puzovic. WiMAX Non-Saturated Analysis. In *Proc., IEEE GLOBECOM Workshops*, Houston, TX, USA, December 2011.

[45] P. Cheng, L. Wang, B. Zhen, and S. Wang. Feasibility Study of Applying LTE to Smart Grid. In *Proc., IEEE International Workshop on Smart Grid Modeling and Simulation (SGMS)*, Brussels, Belgium, October 2011.

[46] J. Wakemen, M. Hodson, P. Shafer, and V. Hnatyshin. Ultra High-Powered Long-Range ZigBee Devices for Communication During Amateur Car Racing Events. In *Proc., International Conference on Wireless Communications, Vehicular Technology, Information Theory and Aerospace & Electronic Systems (VITAE)*, Atlantic City, NJ, USA, June 2013.

[47] C. Bianco, F. Cucchietti, and G. Griffa. Energy Consumption Trends in the Next Generation Access Network - A Telco Perspective. In *Proc., International Telecommunications Energy Conference*, Rome, Italia, October 2007.

[48] W. Bo. China Telecom FTTH Deployment - Lessons Learnt and Future Plans. In *Proc., Communications and Photonics Conference (ACP)*, Guangzhou, China, November 2012.

[49] H. Song, B.W. Kim, and B. Mukherjee. Multi-Thread Polling: A Dynamic Bandwidth Distribution Scheme in Long-Reach PON. *IEEE IEEE Journal on Selected Areas in Communications*, 27(2):134–142, February 2009.

[50] N. Ghazisaidi and M. Maier. Fiber-Wireless (FiWi) Access Networks: A Survey. *IEEE Communications Magazine*, 47(2):160–167, February 2009.

[51] M. Maier. Fiber-Wireless Sensor Networks (Fi-WSNs) for Smart Grids. In *Proc., International Conference on Transparent Optical Networks (ICTON)*, Stockholm, Sweden, June 2011.

[52] Y. Somemura. Key Roles of Green Technology for Access Network Systems. In *Proc., Conference on Optical Fiber Communication collocated National Fiber Optic Engineers Conference (OFC/NFOEC)*, San Diego, CA, USA, March 2010.

[53] V. K. Sood, D. Fischer, J. M. Eklund, and T. Brown. Developing a Communication Infrastructure for the Smart Grid. In *Proc., IEEE Electrical Power & Energy Conference*, pages 1–7, Montréal, QC, Canada, October 2009.

[54] G. Kramer, M. De Andrade, R. Roy, and P. Chowdhury. Evolution of Optical Access Networks: Architectures and Capacity Upgrades. *Proceedings of the IEEE*, 100(5):1188–1196, May 2012.

[55] M. Tahon, J. Van Ooteghem, K. Casier, L. Deschuttere, S. Verbrugge, D. Colle, M. Pickavet, and P. Demeester. Cost allocation model for a synergetic cooperation in the rollout of telecom and utility networks. In *Proc., Conference on Telecommunications Internet and Media Techno-Economics (CTTE)*, May 2011. Paper S3-2.

[56] P. Yi, A. Iwayemi, and C. Zhou. Developing ZigBee Deployment Guideline Under WiFi Interference for Smart Grid Applications. *IEEE Transactions on Smart Grid*, 2(1):110–120, March 2011.

[57] K. Moslehi and R. Kumar. Smart Grid - A Reliability Perspective. In *Proc., Innovative Smart Grid Technologies*, pages 1–8, January 2010.

[58] S. Rickers, C. Spiegel, G. Bruck, P. Jung, R. Lee, S. Park, and J. Yu. Multi Data Rate Signaling based on IEEE 802.15.4. In *Proc., International Symposium on Applied Sciences in Biomedical and Communication Technologies*, pages 1–4, November 2010.

[59] S. Tozlu, M. Senel, W. Mao, and A. Keshavarzian. Wi-Fi Enabled Sensors for Internet of Things: A Practical Perspective. *IEEE Communications Magazine*, 50(6):134–143, June 2012.

[60] L. Kleinrock. *Queueing Systems.* Wiley, 1975.

[61] G. Bianchi. Performance Analysis of the IEEE 802.11 Distributed Coordination Function. *IEEE Journal on Selected Areas in Communications*, 18(3):535–547, March 2000.

[62] V. Liberatore and A. Al-Hammouri. Smart Grid Communication and Co-Simulation. In *Proc., IEEE Energytech*, Cleveland, OH, USA, May 2011.

[63] K. Hopkinson, X. Wang, R. Giovanini, J. Thorp, K. Birman, and D. Coury. EPOCHS: A Platform for Agent-Based Electric Power and Communication Simulation Built from Commercial Off-the-Shelf Components. *IEEE Transactions on Power Systems*, 21(2):548–558, May 2006.

[64] M. Lévesque, D. Q. Xu, G. Joós, , and M. Maier. Co-Simulation of PEV Coordination Schemes Over a FiWi Smart Grid Communications Infrastructure. In *Proc., IEEE Industrial Electronics Society IECON*, Montréal, QC, Canada, October 2012.

[65] H. Lin, S. S. Veda, S. S. Shukla, L. Mili, and J. Thorp. GECO: Global Event-Driven Co-Simulation Framework for Interconnected Power System and Communication Network. *IEEE Transactions on Smart Grid*, 3(3):1444–1456, 2012.

[66] R. M. Fujimoto and R. M. Weatherly. Time Management in the DoD High Level Architecture. In *Proc., Workshop on Parallel and Distributed Simulation*, Philadelphia, PA, USA, May 1996.

[67] V. Liberatore and A. Al-Hammouri. The High Level Architecture RTI As a Master to the Functional Mock-Up Interface Components. In *Proc., International Conference on Computing, Networking and Communications (ICNC)*, San Diego, CA, USA, January 2013.

[68] X. Wang, P. Zhang, Z. Wang, V. Dinavahi, G. Chang, J. A. Martinez, A. Davoudi, A. Mehrizi-Sani, and S. Abhyankar. Interfacing Issues in Multiagent Simulation for Smart Grid Applications. *IEEE Transactions on Power Delivery*, 28(3):1918–1927, July 2013.

[69] E. Galli, G. Cavarretta, and S. Tucci. HLA-OMNET++: An HLA Compliant Network Simulator. In *Proc., 12th IEEE/ACM International Symposium on Distributed Simulation and Real-Time Applications*, Vancouver, BC, Canada, October 2008.

[70] H. Georg, C. Wietfeld, S. C. Muller, and C. Rehtanz. A HLA Based Simulator Architecture for Co-Simulating ICT Based Power System Control and Protection Systems. In *Proc., IEEE Third International Conference on Smart Grid Communications (SmartGridComm)*, Tainan, Taïwan, November 2012.

[71] C.-H. Yang, G. Zhabelova, C.-W. Yang, and V. Vyatkin. Co-Simulation Environment for Event-Driven Distributed Controls of Smart Grid. *IEEE Transactions on Industrial Informatics*, 9(3):1423–1435, August 2013.

[72] H. Lin, S. Sambamoorthy, S. Shukla, J. Thorp, and L. Mili. Power System and Communication Network Co-Simulation for Smart Grid Applications. In *Proc., IEEE PES Innovative Smart Grid Technologies (ISGT)*, Anaheim, CA, USA, January 2011.

[73] T. Godfrey, S. Mullen, D. W. Griffith, and N. Golmie. Modeling Smart Grid Applications with Co-Simulation. In *Proc., IEEE International Conference on Smart Grid Communications (SmartGridComm)*, Gaithersburg, MD, USA, October 2010.

[74] M. Lévesque, D. Q. Xu, G. Joós, and M. Maier. Communications and Power Distribution Network Co-Simulation for Multidisciplinary Smart Grid Experimentations. In *Proc., SCS/ACM Spring Simulation Multi-Conference*, Orlando, FL, USA, March 2012.

[75] T. Blochwitz, T. Neidhold, M. Otter, M. Arnold, C. Bausch, M. Monteiro, C. Clauß, S. Wolf, H. Elmqvist, H. Olsson, A. Junghanns, J. Mauss, D. Neumerkel, and J.-V. Peetz. The Functional Mockup Interface for Tool Independent Exchange of Simulation Models. In *Proc., The 8th International Modelica Conference*, Dresden, Germany, March 2011.

[76] W. H. Kersting. Radial Distribution Test Feeders. In *Proc., IEEE Power Engineering Society Winter Meeting*, Columbus, USA, January 2001.

[77] W.-Z. Song, D. De, S. Tan, S. K. Das, and L. Tong. A Wireless Smart Grid Testbed in Lab. *IEEE Wireless Communications*, 19(3):58–64, June 2012.

[78] I. Georgievski, V. Degeler, G. A. Pagani, T. A. Nguyen, A. Lazovik, , and M. Aiello. Optimizing Energy Costs for Offices Connected to the Smart Grid. *IEEE Transactions on Smart Grid*, 3(4):2273–2285, December 2012.

[79] R. C. Qiu, Z. Hu, Z. Chen, N. Guo, R. Ranganathan, S. Hou, and G. Zheng. Cognitive Radio Network for the Smart Grid: Experimental System Architecture, Control Algorithms, Security, and Microgrid Testbed. *IEEE Transactions on Smart Grid*, 2(4):724–740, December 2011.

[80] C. Wen, J. Chen, J. Teng, and P. Ting. Decentralized Plug-in Electric Vehicle Charging Selection Algorithm in Power Systems. *IEEE Transactions on Smart Grid*, 3(4):1779–1789, December 2012.

[81] C. Jin, J. Tang, and P. Ghosh. Optimizing Electric Vehicle Charging: A Customer's Perspective. *IEEE Transactions on Vehicular Technology*, 62(7):2919–2927, September 2013.

[82] B. Geng, J. K. Mills, and D. Sun. Two-Stage Charging Strategy for Plug-In Electric Vehicles at the Residential Transformer Level. *IEEE Transactions on Smart Grid*, 4(3):1442–1452, September 2013.

[83] P. Richardson, D. Flynn, and A. Keane. Local Versus Centralized Charging Strategies for Electric Vehicles in Low Voltage Distribution Systems. *IEEE Transactions on Smart Grid*, 3(2):1020–1028, 2012.

[84] O. Sundstrom and C. Binding. Flexible Charging Optimization for Electric Vehicles Considering Distribution Grid Constraints. *IEEE Transactions on Smart Grid*, 3(1):26 –37, 2013.

[85] F. W. Fuchs, N. Hoffmann, J. Reese, C. Wessels, R. Lohde, S. Grunau, , and F. Gebhardt. Research Laboratory for Grid-integration of Distributed Renewable Energy Resources - Integration Analysis of DERs. In *Proc., 15th International Conference on Power Electronics and Motion Control (EPE/PEMC)*, pages LS7a.4–1–8, Novi Sad, Serbia, 2012.

Deuxième partie

Articles

Chapitre 8

Probabilistic Availability Quantification of PON and WiMAX Based FiWi Access Networks for Future Smart Grid Applications

Publication:

— M. Lévesque and M. Maier, "Probabilistic Availability Quantification of PON and WiMAX Based FiWi Access Networks for Future Smart Grid Applications," *IEEE Transactions on Communications*, accepted for publication.

In the previous chapter, we proposed the first FiWi model allowing to evaluate the performance of any routing algorithms under non-saturated conditions. Note, however, that under saturated conditions the network becomes probabistically unavailable, even if we assume there is no physical failure. In this chapter, we quantify the probabilistic availability metric both in terms of physical failure and MAC performance limits. Given that WiMAX represents an interesting alternative wireless technology especially in Canada due to the fact that there exists a dedicated spectrum for utility communications, we study an integrated access network based on PON and WiMAX in this chapter.

Generally, information reliability has the following two main data characteristics: (i) availability and (ii) level of assurance. The IEEE P2030 standard qualitatively defines the availability requirement to be either low, medium, or high. A critical information requiring high availability may have a catastrophic impact if the requirement is not met. In previous related work, availability was studied in terms of communications reachability and using availability metrics to maximize the routing performance. In this chapter, however, we define availability by considering (i) the MAC performance limit using mathematical models such as the ones also studied in this thesis and (ii) probabilistic fiber and base station failures. The considered access network consists of a multi-stage TDM/WDM PON integrated with WiMAX. The obtained numerical results show several interesting availability behaviors. First, fiber backhaul failures have a significant impact on availability especially at high loads, while WiMAX BS failures have a lower impact at low and high loads. The model also enables to quantify availability depending on the number of BSs available, whereby selecting the right number of BSs helps maximize availability in a cost-effective manner. We also show that there exists a unique ratio of traffic destined towards a faulty link permitted to be re-routed for maximizing availability. We investigate also a smart grid scenario with payload length and data rate configurations based on traffic measurements captured from smart grid applications. By considering regular and smart grid traffic classes with different priorities and availability requirements, we show that under the investigated conditions the sensors' maximum monitoring data rate to meet the availability requirements can be quantified. The developed probabilistic availability model enables to verify whether requirements are met based on predicted traffic and equipment failure probabilities.

IEEE Transactions on Communications, accepted for publication.

8.1 Abstract

Availability is one of the most important quality attributes for smart grid communications, as qualitatively defined in the IEEE P2030 standard. However, the availability metric must be quantified in order to validate given smart grid application requirements. In recent related work, availability has been quantified for wireless and optical backhaul networks in terms of communications reachability, while in some other work availability was not formally defined in a fine-grained manner and was assumed to be known. In this paper, we develop a novel multi-class probabilistic availability model for integrated passive optical network (PON) and WiMAX networks in order to quantify this metric according to medium access control (MAC) protocol limits as well as fiber and base station failures. The obtained numeric results show interesting availability behaviors, including the impact on availability depending on the number of base stations. We also investigate optical traffic re-routing through WiMAX when fiber faults occur and show that there exists a maximum amount of re-routed traffic for maximizing availability. Furthermore, we investigate a scenario of real-world smart grid traffic configurations shared with regular traffic and find the maximum sensor data rate to meet the availability requirements.

Keywords: Communications availability, fiber-wireless communications, PON and WiMAX networks, smart grid communications.

8.2 Introduction

The research on a new power system paradigm, the smart grid (SG), has recently attracted significant attention in the information technology (IT), telecommunications, and power system communities [8]. The quantification of the communications requirements of several smart grid applications has been done in terms of security, reliability, bandwidth, and latency [1]. Quantifying the requirements of smart grid communications is crucial from a research perspective, since the predicted communications performance can be compared to given requirements and new communications mechanisms can be developed to meet these requirements. Efforts have also been made by standardization organizations. IEEE P2030 is one of the first attempts to standardize smart grids [2]. IEEE

IEEE Transactions on Communications, accepted for publication.

P2030 presents generic design and implementation guidelines among systems in order to exchange data between smart grid components. More specifically, the standard lists four main quality attributes: scalability, interoperability, information reliability, and security. In this work, we focus on the reliability quality attribute. Reliability is defined as the ability to execute a function under given conditions for a given period of time. Information reliability has the following two main data characteristics: (*i*) availability and (*ii*) level of assurance. The IEEE P2030 standard qualitatively defines the availability requirement to be either low, medium, or high. A critical information requiring high availability could, for instance, cause catastrophic impacts if the requirement is not met. Although qualitative requirements can be useful to give an idea about the critical importance of an operation, it is not sufficient from an engineering perspective though; instead qualitative requirements must be used in collaboration with quantitative models. In this paper, we are interested in quantitatively defining the availability metric for a specific next-generation communications architecture.

Availability is a well-known metric used by engineers to quantify the availability of a given piece of equipment [3]:

$$A = \frac{MTTF}{MTTF + MTTR}, \tag{8.1}$$

where $MTTF$ corresponds to the mean time to failure and $MTTR$ is defined as the mean time to repair. In telecommunications, information can be exchanged and thus is available if the network itself is available. In this paper, we quantify the network availability, that is, the probability for a given packet to reach a given destination without failure. There exist two main reasons that can cause a network failure if the network is properly installed and not mobile:

- One or several networking components physically fail. From the equipment specifications, one can determine availability A for certain components by using the given values of $MTTF$ and $MTTR$[1].
- One or several communications nodes are saturated/congested and thus packets are constantly dropped.

1. Examples are available for several N-Tron Ethernet switch series at: `http://www.n-tron.com/pdf/network_availability.pdf`.

IEEE Transactions on Communications, accepted for publication.

Note that it is not necessarily always trivial to find the exact values of $MTTF$ and $MTTR$. For example, a fiber cut could occur randomly and does not necessarily depend on the product specifications. Therefore, in this work, we define A in terms of probabilistic availability by combining parameters for both failure types listed above.

A variety of communications technologies could be used for smart grid communications. According to Ovum Telecoms, a leading analysis company in the telecommunications industry, as Chinese utility companies such as State Grid Corporation of China (SGCC) [2] are migrating toward smart grids, backhaul networks based on passive optical networks (PONs) are planned to be widely deployed for two purposes: to enable emerging smart grid applications and to offer fiber-to-the-home (FTTH) services to consumers as a long-term and cost-effective communications solution for both smart grid and triple-play services. China Telecom deployed more than 70 millions FTTH ports from 2004 to 2012 [4]. According to China Telecom, some of the major trends are: (*i*) increase of fiber penetration, whereby optical nodes get closer to customers to improve bandwidth and quality of network services, (*ii*) higher volume and speed, from legacy Ethernet/Gigabit PONs (EPONs/GPONs) to 10G-EPON towards 40G time division multiplexing (TDM) and wavelength division multiplexing (WDM) PONs to provide at least 40 Gbps in one PON system, and (*iii*) increased coverage by combining fixed, wireless (e.g., wireless local area network (WLAN)), and mobile (e.g., 3G and Long Term Evolution (LTE)) nodes.

In this paper, we focus on an integrated fiber-wireless (FiWi) communications architecture based on PONs and Worldwide Interoperability for Microwave Access (WiMAX) [5]. Broadband access networks based on PONs have multiple significant merits: low operational expenditures (OPEXs), future-proofness, longevity, and high *reliability* as they use completely passive (e.g., unpowered) network components. Network operators (e.g., China Telecom) are seeking next-generation PONs (NG-PONs) that can transparently coexist with legacy PONs such as IEEE 802.3ah/av 1/10 Gbps EPON architectures, enable gradual upgrades in order to avoid costly and time-consuming network modifications, and stay flexible for future evolution paths. The final frontier of NG-PONs is the integration with their wireless counterparts, giving rise to bimodal FiWi broadband access networks

2. Refer to: http://www.fiercetelecom.com/story/chinas-smart-grid-drive-creates-15-billion-opportunity-pon-vendors-says-ovu/2013-01-09.

[6]. Wireless networks such as WiMAX, ZigBee, and WLANs based on IEEE 802.11g/n/ac are highly *available* as they do not need to be physically connected and provide mobility, but they are less reliable due to channel interference. In this paper, for the wireless domain, we focus on WiMAX since in Canada a separate spectrum (30 MHz frequency spectrum in 1.8 GHz) is dedicated to the utilities and this technology provides long-range connectivity. Electricity companies in Australia have also proposed WiMAX-based smart grid solutions [7]. Note that LTE could also be used for smart grid communications. In [7], the authors have shown that LTE technologies can satisfy the latency and reliability requirements of distribution automation (DA) networks. The considered traffic load and latency requirements were 1-480 bps and 1-4 seconds, respectively, which can be provided over LTE. However, for novel smart grid applications requiring larger data rates, communications over LTE may not remain cost-effective. Furthermore, the minimum scheduling delays of LTE correspond to 65.5 ms and 16.5 ms for the upstream and downstream directions, respectively [7]. Some smart grid applications require lower latency in the order of 12-20 ms, such as real-time sensing/metering [8] and wide-area situational awareness (WASA). For comparison, the minimum upstream/downstream delay can be as low as $3 \cdot 2.5$ ms with IEEE 802.16-2004 WiMAX [9]. Combining both fiber and wireless networks is a promising long-term and cost-efficient solution for smart grid communications [10]. Therefore, we focus on this type of communications architecture in order to define network availability.

The performance of PON and WiMAX technologies have been widely studied in terms of different performance metrics over the last few years. In [11], the authors developed a novel techno-economic analysis to compare EPON and WiMAX technologies with regard to equipment, installation, power consumption, and repairing costs. The medium access control (MAC) protocol performance in terms of delay and capacity has also been modeled. The delay and throughput performance of WiMAX technologies under non-saturated [12] and saturated [13] conditions has been quantified. A capacity and delay analytical framework for TDM/WDM PONs was developed in [14], and the survivability performance of FiWi access networks was studied in [15]. In our previous work, we developed a novel capacity model for FiWi access networks based on TDM/WDM PONs and Gigabit WLANs to evaluate the performance of FiWi network routing algorithms [16]. Although these analytical models allow to evaluate the performance of different FiWi access network metrics, the network

IEEE Transactions on Communications, accepted for publication.

availability quantification studies presented up to date are limited and are briefly reviewed in the next section. This paper provides a probabilistic availability analytical framework for WiMAX as well as legacy and NG-PONs. Note that the model is applied to specific technologies, but several portions of the model can be adapted to other technologies and could be extended, for instance, to include also the probabilistic reachability between nodes. The main novelties of this paper are as follows:

— *Availability is not only modeled considering the physical equipment but also taking into account MAC protocol limits, which can affect availability depending on the amount of traffic routed in the network.*

— *The model considers both non-saturated and saturated traffic conditions as well as failure of optical fibers and WiMAX base stations (BSs).*

— *The traffic matrix takes into account multiple prioritized classes.*

— *In the presented numerical results, we investigate a scenario with traffic configurations based on smart grid traffic patterns of smart grid applications we recorded.*

— *The quantified availability metrics can be used to compare them with given smart grid requirements, as availability is one of the most important metrics of smart grid communications [2].*

The remainder of the paper is structured as follows. The considered communications architecture based on integrated TDM/WDM PON and WiMAX is described in Section 8.3. The network availability analysis is developed in Section 8.4. Section 8.5 presents numerical results. Section 8.6 concludes the paper.

8.3 Integrated TDM/WDM PON and WiMAX Network Architectures

There exist a variety of different ways to use/integrate PON and WiMAX technologies. In [17], the authors argue that both technologies are less likely to be integrated, as operators choose either WiMAX or PON since both share common characteristics. Both technologies have a point-to-

IEEE Transactions on Communications, accepted for publication.

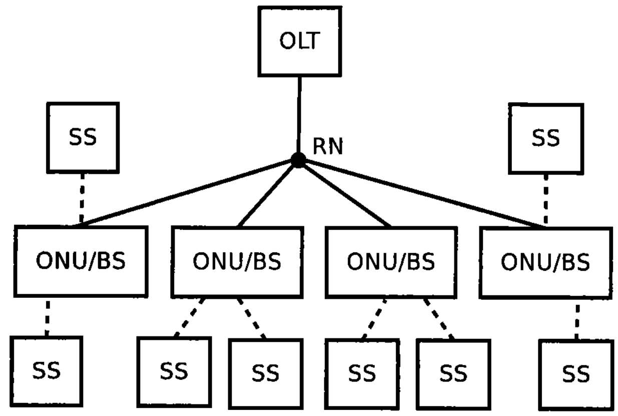

Figure 8.1 – Conventional cascaded PON and WiMAX architecture.

multipoint topology with a central node (optical line terminal (OLT) or BS) allocating bandwidth in the network. The end-users, connected to the optical network units (ONUs) for the PON case or subscriber stations (SSs) for the WiMAX case, send their bandwidth requirements to the central node, which in turn sends back the bandwidth allocations. The OLT in a PON system periodically polls ONUs, which subsequently send back their current queue lengths in order to allocate bandwidth, whereas WiMAX uses a random access mechanism compliant with IEEE 802.16 to send bandwidth request messages.

Clearly, such a non-cascaded architecture cannot take advantage of both networks. In [18], different types of possible EPON and WiMAX integrations were discussed, such as the one depicted in Fig 8.1. A first type of integration is to combine both networks independently, whereby ONUs and SSs remain unchanged and are interconnected to combine both technologies. A different type of integration is the hybrid architecture, whereby BSs and ONUs are merged, but the connection mechanisms are not unified. The unification of connections in EPON and WiMAX networks represent another type of integration. Integrating EPON and WiMAX allows to extend the EPON coverage at low cost, which can be very beneficial for example in rural areas to avoid deploying fibers for sparsely distributed homes. In legacy wavelength-broadcasting (WB) TDM PONs (e.g., EPON and GPON) or WDM PONs, ONUs share the wavelength(s) for both upstream and downstream traffic. Such an architecture typically can cover a distance of 20 kilometers.

As forecasted by major telecommunications providers such as China Telecom, networking trends include a deeper fiber penetration and growth of network speed. Wavelength-routing (WR) WDM

IEEE Transactions on Communications, accepted for publication.

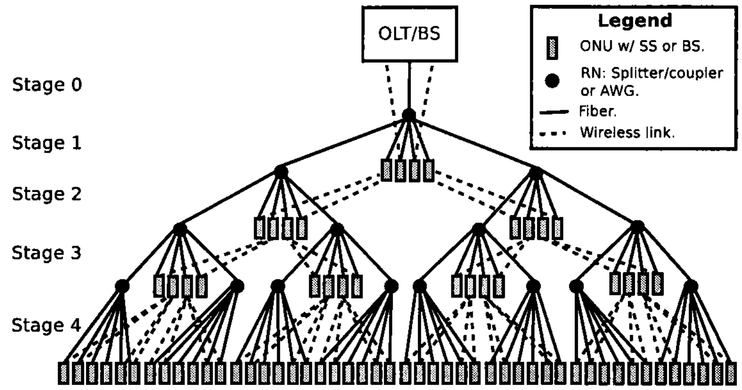

Figure 8.2 – Pyramid-based FiWi topology with WR WDM PON consisting of 76 ONUs, whereby ONUs have WiMAX interfaces and can act as SS or BS (splitting ratio: 6).

PONs are expected to play a key role in response to these trends. This type of PON system is characterized by the replacement of one or several splitters/combiners with passive arrayed-waveguide gratings (AWGs), which act as a wavelength (de)multiplexer, whereby each wavelength may be shared by a subset of ONUs [10]. Fig. 8.2 shows an example of such a WR WDM PON system composed of 5 stages with a splitting ratio of 6 in a pyramid-based topology (as proposed in [15]). A subset of ONUs have a WiMAX interface and can therefore act as SS or BS. Note that this type of multi-stage PON system offers a higher coverage of up to 100 kms, thus also referred to as Long-Reach PON. This kind of hybrid topology helps improve network availability as WiMAX can be used temporarily in case of fiber failures and vice versa, which we model in the next section.

8.4 Network Availability Analysis

Availability was the object of several recent research studies in the context of optical and wireless networks. An availability-aware routing algorithm for hybrid wireless-optical broadband access networks (WOBANs) was proposed in [19], where paths maximizing networking availability were selected. However, the availability metric itself was not modelled and was assumed to be known. In [20], availability was considered in a novel provisioning path protection scheme for optical WDM networks, whereby availability was computed based on a primary and a backup path according to the fiber length and optical cross-connect (OXC) ports. Availability was also studied for wireless networks according to the distance between nodes and depending on their transmission and reception capabilities [21, 22]. In the context of smart grids, it is important to know the availability between wireless nodes during installations. However, once installed, there is still a need to quantify the availability depending on the failure of the components and considering the limitations of the MAC protocols in use. In the following, we quantify the network availability considering the MAC protocols of PONs and WiMAX as well as random fiber and BS failures under the following assumptions:

— For WiMAX, only the upstream direction is modelled and thus no traffic can be routed in the downstream direction. Note that the main traffic generated from smart grid sensors is typically sent upstream from sensors to the distribution management system (DMS).

— We take into account two types of failure: (i) a fiber cut at stage s occurring with probability p_s^{op}, and (ii) a failure of a base station z occurring with probability p_z^{wi}. Both terms p_s^{op} and p_z^{wi} represent the long-term failure probabilities, that is, the probability that at any given time instant the component fails. These terms can be defined based on the $MTTF$ and $MTTR$ in Eq. (8.1) obtained from the component specifications. The developed analysis below accommodates any type of fiber and BS failure.

— The traffic is differentiated per class, whereby existing/regular $\mathcal{C}_r$ and smart grid $\mathcal{C}_{sg}$ traffic classes are considered. The overall traffic classes are given by $\mathcal{C} = \mathcal{C}_r + \mathcal{C}_{sg}$. All traffic classes $\mathcal{C}$ can be routed in the PON network, but only the smart grid traffic ($\mathcal{C}_{sg}$) can use WiMAX dedicated to smart grids. Each traffic class has an average payload length denoted by $\bar{L}_c, \forall c \in \mathcal{C}$.

— As we take into account the MAC protocol performance of both the PON and WiMAX networks, availability is defined by considering both frame drop and failure probabilities. It relates to Eq. (8.1) as it represents the long-term availability probability, but without explicitely defining $MTTF$ and $MTTR$.

— To find the MAC protocol limits, we adapt the analysis developed in [16] for PON and [12] for WiMAX.

— We assume each FiWi node has a maximum queue length of Q frames and thus frames are dropped according to the following blocking probability equation under nonsaturated ($0 \leq \rho < 1$, M/M/1/K model from [23, Eq. (3.43)]) and saturated conditions ($\rho \geq 1$):

$$B(\rho) = \begin{cases} \frac{(1-\rho)\cdot\rho^{Q+1}}{1-\rho^{Q+1+1}}, & \text{if } 0 \leq \rho < 1 \\ 1 - \frac{1}{\rho}, & \text{if } \rho \geq 1 \end{cases}, \tag{8.2}$$

where ρ represents the traffic intensity and $B(\rho)$ the blocking/dropping probability.

— WiMAX frames are composed of mini-slots and during a frame the mini-slots can be allocated to multiple SSs [24]. In this paper, similarly to [12], we assume a given frame is fully allocated to a single SS.

To introduce our model, Fig. 8.3 illustrates our probabilistic model for a single-stage WB TDM/WDM PON. The availability of such a topology can be found by executing the following steps:

— Calculate the blocking probability at the ouput ports of SSs, ONUs, and OLT, corresponding to $B(\rho_w^{wi})$, $B(\rho^{op,u})$, and $B(\rho^{op,d})$ (derived thereafter in this section), respectively. Note that these three terms correspond to the generic blocking probability term defined in Eq. 8.2, which is generally applicable to any traffic intensity.

— Define the fiber failure probability at stages 0 and 1, corresponding to p_0^{op} and p_1^{op} and derived thereafter in this section.

— Define the BS failure probability at each ONU/BS, corresponding to p_z^{wi} and derived thereafter in this section.

— Calculate the probabilistic availability which is derived thereafter in this section.

8.4.1 Network Model

Generic Definitions

In this paper, we focus on PONs consisting of Λ bidirectional wavelength channels, indexed as $\lambda = 1, 2, ..., \Lambda$. We consider two distinct flavors:

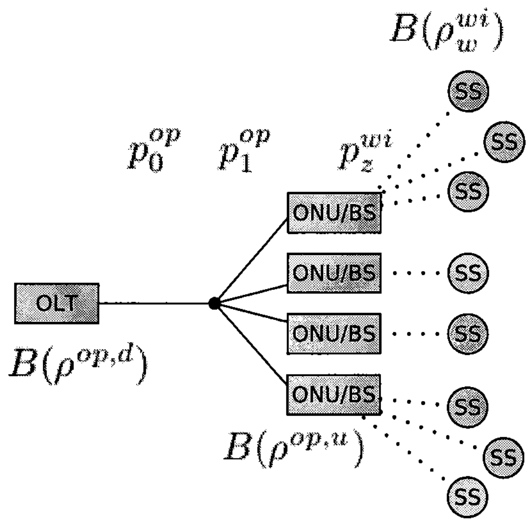

Figure 8.3 – Probabilistic model for a single-stage WB TDM/WDM PON. $B(\rho_w^{wi})$, $B(\rho^{op,u})$, **and** $B(\rho^{op,d})$ **correspond to the blocking probabilities at the output ports of the SSs, ONUs, and OLT, respectively;** $p_{0/1}^{op}$ **denotes the fiber failure probability at stage 0 or 1, and** p_z^{wi} **denotes the BS failure probability.**

— Wavelength-broadcasting (WB) single-stage TDM/WDM PON: A WB TDM/WDM PON consists of a legacy splitter/combiner as remote node (RN) and deploys Λ wavelengths, which can be used by all ONUs. For legacy EPONs and GPONs we have $\Lambda = 1$.

— Wavelength-routing (WR) multi-stage WDM PON: The conventional splitter/combiner at the RN is replaced with a wavelength (de)multiplexer. A typical wavelength (de)multiplexer is an arrayed-waveguide grating (AWG). A given wavelength λ can be used by a subset of the ONUs forming a sector at each AWG output port.

The PON can be either single-stage or multi-stage. We let Ξ denote the number of fiber stages, whereby we consider $\Xi = 2$ for WB PONs and $\Xi \geq 2$ for WR WDM PONs. Note that we have $\Xi = 2$ for single-stage PONs since there is a fiber between the OLT and RN and another one between the RN and ONUs. Note that a fiber stage corresponds to the maximum number of links between the OLT, intermediate RNs, and ONUs, whereby multiple wavelengths can be shared in each given link. A sector, using a given wavelength, corresponds to the set of ONUs (end-users) sharing a given wavelength. Let $\mathcal{S}_\lambda$ denote the set of ONUs in sector λ such that:

$$\mathcal{S}_1 \cup ... \cup \mathcal{S}_\Lambda = \mathcal{O}, \tag{8.3}$$

IEEE Transactions on Communications, accepted for publication.

whereby $\mathcal{O}$ denotes the set of ONUs. Each wavelength channel has a capacity of c_{op} (in bps). Furthermore, the stage of ONU o is defined as $s(o)$, $\forall o \in \mathcal{O}, s(o) \in \{1, ..., \Xi\}$. Note that an ONU cannot be installed at stage 0, which corresponds to the fiber between the OLT and first remote node.

As for the WiMAX network(s), let $\mathcal{B}$ denote the set of base stations:

$$\forall z \in \mathcal{B}, z \in \{0, 1, ..., |\mathcal{O}|\}, \tag{8.4}$$

where the index 0 corresponds to the OLT and z represents a zone aggregating traffic from subscriber stations (SSs), denoted as $\mathcal{W}_z$. SSs are either ONUs equipped with a WiMAX interface or SSs with a WiMAX interface only. Thereby, the set of WiMAX SSs having only a wireless interface is given by:

$$\mathcal{W} = \bigcup_{z \in \mathcal{B}} \mathcal{W}_z - \mathcal{O}. \tag{8.5}$$

This model is generic and can accommodate multiple different FiWi access network topologies, which we illustrate in Section 8.5.

Pyramid-based Topology

The analysis accommodates any type of topology. We describe below the pyramid-based topology since this type of topology presents interesting symmetric properties. As depicted in Fig. 8.2, the number of ONUs depends on the splitting ratio S and number of stages Ξ, and is given by:

$$2^{\Xi-2} \cdot S + \sum_{i=1}^{\Xi-2} 2^{i-1} \cdot (S-2), \tag{8.6}$$

where the first term corresponds to ONUs at the last stage ($i = \Xi - 1$) and the second term accounts for the ONUs at stages $[1..\Xi - 2]$.

IEEE Transactions on Communications, accepted for publication.

For a given set of ONUs attached to a RN, we let β denotes the ratio of the number of BSs versus S. For example in Fig. 8.2, we have $\beta = \frac{2}{6}$.

8.4.2 Traffic Matrix

We first define the set of FiWi nodes as follows:

$$\mathcal{N} = \{0\} \cup \mathcal{O} \cup \mathcal{W}. \tag{8.7}$$

Next, we define the traffic matrix consisting of source-destination connections characterized by a traffic rate (in frames/sec.): $M_{i,j,c}$, whereby $i, j \in \mathcal{N}$ and $c \in \mathcal{C}$. $M_{i,j,c} = 0$ for $i = j, \forall c \in \mathcal{C}$. For the traffic being forwarded first in the wireless domain, we define $\tilde{M}_{i,j,c}$ following a matrix with the same properties as $M_{i,j,c}$. Also, for all SSs w, $w \in \mathcal{W}$ and $i \in \mathcal{N}$, we have $M_{i,w,c} = 0$, that is, we do not model downstream WiMAX traffic.

8.4.3 Traffic Intensity

We next derive the traffic intensities for both PON and WiMAX systems. These traffic intensities are used to calculate blocking/dropping probabilities.

Each class $c \in \mathcal{C}$ has a priority α_c such that $\sum_{c \in \mathcal{C}} \alpha_c = 1$. A given frame of class c is assigned the following probability, used thereafter in the analysis:

$$\chi_c(R, \rho) = \frac{min(AdmS2_c(R, \rho), R_c \cdot \bar{L}_c)}{R_c \cdot \bar{L}_c}, \tag{8.8}$$

where R and ρ denote the set of traffic rates and traffic intensity at a given output port, respectively. The equation defines the ratio of the per-class admitted data rate and per-class load, whereby $AdmS2_c(R, \rho)$ gives the bandwidth scheduled for class c, which is given by:

$$AdmS2_c(R,\rho) = AdmS1_c(R,\rho) - \sum_{\forall i \neq c, \alpha_i = \alpha_c} min\left(AdmS1_c(R,\rho) \cdot \frac{1}{|[i \in \mathcal{C} | \alpha_i = \alpha_c]|}, R_i \cdot \bar{L}_i \right) \quad (8.9)$$

with $AdmS1_c$ as follows:

$$AdmS1_c(R,\rho) = (1 - B(\rho)) \cdot \sum_{i \in \mathcal{C}} R_i \cdot \bar{L}_i - \sum_{\forall i, \alpha_i > \alpha_c} R_i \cdot \bar{L}_i. \quad (8.10)$$

Wireless Domain

The traffic rate of class c destined to n from a given SS w with wireless support only is given by:

$$R^{wi}_{w,n,c} = \tilde{M}_{w,n,c}, \quad (8.11)$$

where $n \in \mathcal{N}$. For a given ONU o in zone z having a WiMAX interface sending to n (either a different ONU or the OLT), the traffic rate of class c takes into account the traffic forced to be sent to the wireless domain and optical traffic destined towards faulty (due to frame drop or fiber failure) fibers:

$$R^{wi}_{o,n,c} = \tilde{M}_{o,n,c} + R^{op,f}_{o,n,c}, \quad (8.12)$$

where the first term accounts for the traffic forced to be sent in the wireless domain. The second term corresponds to the optical traffic from ONU o destined towards faulty fibers being re-routed in the wireless domain and sent to a reachable base station z (if any):

$$R^{op,f}_{o,n,c} = \begin{cases} \varrho^{op,f}_{o,n,c}, & \text{if } \exists z \in \mathcal{W}_z \wedge o \in \mathcal{W}_z \\ 0, & \text{otherwise} \end{cases}. \tag{8.13}$$

$\varrho^{op,f}_{o,n,c}$ is given by:

$$\varrho^{op,f}_{o,n,c} = \delta^{wi}_{o,z} \cdot M_{o,n,c} \cdot \left(1 - \chi_c\Big(\Big[\sum_{\forall n'} R^{op,u}_{o,n',\forall c'}\Big], \rho^{op,u}_o\Big) \cdot \prod_{i=s(o)}^{0} \left(1 - p^{op}_i\right)\right), \tag{8.14}$$

where $\delta^{wi}_{o,z} \in [0..1]$ corresponds to the ratio of the optical traffic destined to faulty fibers permitted to be re-routed in the wireless domain toward BS z. The traffic intensity for a given wireless interface $w \in \mathcal{W}_z$ in zone z is defined as the traffic rate multiplied by the access delay:

$$\rho^{wi}_w = \sum_{c \in \mathcal{C}_{sg}} \sum_{n \in \{0\} \cup \mathcal{O}} R^{wi}_{w,n,c} \cdot E[T_{pkt}, z], \tag{8.15}$$

where $E[T_{pkt}, z]$ corresponds to the WiMAX access delay in a given zone z, given in Eq. (17) in [12]. Note that in [12], a single wireless zone was used, thus in this work, since we have several WiMAX zones, we have one access delay for each given zone. Note that we adapt the traffic rate at each SS of [12, $\frac{\lambda}{N}$] to:

$$\frac{1}{|\mathcal{W}_z|} \cdot \sum_{c \in \mathcal{C}_{sg}} \sum_{w \in \mathcal{W}_z} \sum_{n \in \{0\} \cup \mathcal{O}} \frac{\bar{L}_c}{T_{frame} \cdot c_{wi}} \cdot R^{wi}_{w,n,c}, \forall z \in \mathcal{B}, \tag{8.16}$$

where c_{wi} denotes the WiMAX capacity.

IEEE Transactions on Communications, accepted for publication.

Furthermore, we adapt the analysis in [12] for both non-saturated and saturated conditions (note that [12] applies only to non-saturated conditions). To do so, we bound the traffic intensity for a given SS, corresponding to [12, (16) and (17)], to be maximally $1/0.\bar{9}$ as follows:

$$P_0^* = \frac{1 - e^{-\frac{\lambda}{N} \cdot E[T_{pkt}]}}{min(1, \frac{\lambda}{N} \cdot E[T_{pkt}])} \cdot \left(1 - min\left(1, \frac{\lambda}{N} \cdot E[T_{pkt}]\right)\right) \tag{8.17}$$

and for T_3:

$$T_3 = \frac{1}{2} + \frac{1}{2 \cdot (1 - min(0.\bar{9}, P_0 \cdot \lambda \cdot T_{frame}))}. \tag{8.18}$$

Note that the variables in Eqs. (8.17, 8.18) refer to the variables in the WiMAX analysis [12].

Fiber Domain

The upstream traffic rate of class c from a given ONU o (in zone z if it has a wireless interface) to ONU/OLT $n \neq o$ is given by:

$$\begin{aligned} R_{o,n,c}^{op,u} &= M_{o,n} + \\ &\delta_{o,0}^{op} \cdot \tilde{M}_{o,n,c} \cdot \left[1 - \chi_c\left(\left[\sum_{\forall n'} R_{o,n',\forall c'}^{wi}\right], \rho_o^{wi}\right) \cdot \left(1 - p_z^{wi}\right)\right] + \\ &\sum_{w \in \mathcal{W}_o} \tilde{M}_{w,n,c} \cdot (1 - p_o^{wi}) \cdot \chi_c\left(\left[\sum_{\forall n'} R_{w,n',\forall c'}^{wi}\right], \rho_w^{wi}\right) + \\ &\sum_{o_2 \in \mathcal{W}_o} R_{o_2,n,c}^{op,e} \cdot \left[1 - \chi_c\left(\left[\sum_{\forall n'} R_{o_2,n',\forall c'}^{wi}\right], \rho_{o_2}^{wi}\right) \cdot (1 - p_o^{wi})\right], \end{aligned} \tag{8.19}$$

where the first term accounts for the optical traffic, the second term corresponds to the traffic destined to a faulty WiMAX node re-routed in the optical domain towards the OLT, the third term represents the traffic coming from SSs with WiMAX support only, and the fourth term accounts for the traffic previously re-routed from the optical domain to the wireless domain and sent to o. $\delta_{o,0}^{op}$ corresponds to the ratio of the permitted traffic re-routed from the wireless to the optical domain.

IEEE Transactions on Communications, accepted for publication.

Similarly to [16, Eq. (6)] (but extended to multiple classes), the upstream traffic intensity for WB PONs is given by:

$$\rho^{op,u} = \sum_{c\in\mathcal{C}} \frac{\bar{L}_c}{\Lambda \cdot c_{op}} \cdot \sum_{o\in\mathcal{O}} \sum_{n\in\{0\}\cup\mathcal{O}-\{o\}} R^{op,u}_{o,n,c} \tag{8.20}$$

and similarly to [16, Eq. (4)] (extended to multiple classes)

$$\rho^{op,u}_{\lambda} = \sum_{c\in\mathcal{C}} \frac{\bar{L}_c}{c_{op}} \cdot \sum_{o\in\mathcal{S}_\lambda} \sum_{n\in\{0\}\cup\mathcal{O}-\{o\}} R^{op,u}_{o,n,c} \tag{8.21}$$

for WR PONs.

The downstream traffic rate of class c for WB PONs is given by:

$$R^{op,d}_c = \sum_{o\in\mathcal{O}} M_{0,o,c} + \sum_{n\in\mathcal{O}} R^{op,u}_{n,o,c} \cdot \chi_c\left(\left[\sum_{\forall n'\in\mathcal{O}} R^{op,u}_{o,n',\forall c'}\right], \rho^{op,u}\right) \cdot \left(\prod_{i=1}^{0}(1-p_i^{op})\right),$$

where the first term accounts for the traffic from the OLT to ONUs and the second term for the traffic from ONUs to the OLT subsequently forwarded to another ONU. Similarly, the downstream traffic rate of class c for WR PONs is given by:

$$\begin{aligned} R^{op,d}_{\lambda,c} \;=\;& \sum_{o\in\mathcal{S}_\lambda} M_{0,o,c} + \\ & \sum_{l=1}^{\Lambda}\sum_{n\in\mathcal{S}_l} R^{op,u}_{n,o,c} \cdot \chi_c\left(\left[\sum_{\forall n'\in\mathcal{O}} R^{op,u}_{o,n',\forall c'}\right], \rho^{op,u}_l\right) \cdot \prod_{i=s(n)}^{0}(1-p_i^{op}) + \\ & \sum_{w\in\mathcal{W}_0} R^{wi}_{w,o,c} \cdot \chi_c\left(\left[\sum_{\forall n'\in\mathcal{O}} R^{wi}_{w,n',\forall c'}\right], \rho^{op,u}_w\right) \cdot (1-p_0^{wi}), \end{aligned} \tag{8.22}$$

where the additional third term accounts for the wireless traffic sent to the OLT/BS and subsequently optically forwarded to a given ONU. The downstream traffic intensity for WB PONs is defined similarly to [16, Eq. (7)] (extended to multiple classes):

$$\rho^{op,d} = \sum_{c \in C} \frac{\bar{L}_c}{\Lambda \cdot c_{op}} \cdot R_c^{op,d} \tag{8.23}$$

and similarly to [16, Eq. (5)]

$$\rho_\lambda^{op,d} = \sum_{c \in C} \frac{\bar{L}_c}{c_{op}} \cdot R_{\lambda,c}^{op,d} \tag{8.24}$$

for WR PONs.

In the remainder, for convenience, we use $\rho_\Theta^{op,u}$ and $\rho_\Theta^{op,d}$ to denote the upstream and downstream intensities, respectively. Θ represents the PON flavor (empty for WB and λ for WR) and thus the proper traffic intensity equation must be used.

8.4.4 Probabilistic Availability

We first derive the probabilistic availability of a single-hop wireless link as follows:

$$\mathcal{A}_{w,z,c}^{wi,wi} = \chi_c\Big(\Big[\sum_{\forall n'} R_{w,n',\forall c'}^{wi}\Big], \rho_w^{wi}\Big) \cdot \Big(1 - p_z^{wi}\Big), \tag{8.25}$$

representing the probability that no frame is dropped and that no BS failure occurs. The probabilistic availability for the downstream traffic is defined according to the dropping probability at the OLT and fiber failure(s):

$$\mathcal{A}_{0,o,c}^{olt,onu} = \chi_c\Big(\Big[R_{\Theta,\forall c'}^{op,d}\Big], \rho_{\Theta,c}^{op,d}\Big) \cdot \prod_{i=0}^{s(o)} \Big(1 - p_i^{op}\Big). \tag{8.26}$$

The probabilistic availability for the upstream ONU-OLT traffic is derived from both PON and WiMAX availabilities:

$$
\begin{aligned}
\mathcal{A}^{onu,olt}_{o,0,c} = & \Bigg[1 - \\
& \Bigg[1 - \chi_c\Bigg(\Bigg[\sum_{\forall n'} R^{op,u}_{o,n',\forall c'}\Bigg], \rho^{op,u}_{\Theta,c}\Bigg) \cdot (1 - p^{op}_z)^{s(z)+1}\Bigg] \cdot \\
& \Bigg[1 - \delta^{wi}_{o,0} \cdot \mathcal{A}^{wi,wi}_{o,0,c}\Bigg] \cdot \\
& \Bigg[1 - \delta^{wi}_{o,z} \cdot \mathcal{A}^{wi,wi}_{o,z,c} \cdot \chi_c\Bigg(\Bigg[\sum_{\forall n'} R^{op,u}_{z,n',\forall c'}\Bigg], \rho^{op,u}_{\Theta,c}\Bigg) \cdot (1 - p^{op}_z)^{s(z)+1}\Bigg]\Bigg],
\end{aligned}
\tag{8.27}
$$

where $o \in \mathcal{W}_z$. The equation defines the availability probability according to three unavailability probabilities: (*i*) the failure probability of using the fiber between ONU o and the OLT, (*ii*) the failure probability of using the WiMAX link between ONU o and the OLT, and (*iii*) the failure probability to first route wirelessly from ONU o to ONU o_2 and then optically forward the frame from o_2 to the OLT.

For improved readability, we derive some availability equations for the traffic between SSs and OLT:

$$
\mathcal{A}^{wi,olt}_{w,0,c} = \mathcal{A}^{wi,wi}_{w,z,c} \cdot \mathcal{A}^{onu,olt}_{z,0,c}, w \in \mathcal{W}_z \tag{8.28}
$$

and for the traffic from SSs to ONUs:

$$
\mathcal{A}^{wi,onu}_{w,o,c} = \mathcal{A}^{wi,olt}_{w,0,c} \cdot \mathcal{A}^{olt,onu}_{0,o,c}, w \in W_0. \tag{8.29}
$$

Finally, we derive the average probabilistic availability of class c in the FiWi access network as follows by taking into account all possible paths:

$$
\begin{aligned}
\mathcal{A}_c = & \frac{1}{\sum_{n_1 \in \mathcal{N}} \sum_{n_2 \in \mathcal{N}, n_1 \neq n_2} M_{n_1,n_2,c}} \cdot \\
& \Bigg(\sum_{z \in \mathcal{B}} \sum_{w \in \mathcal{W}_z, w \in \mathcal{W}} M_{w,z,c} \cdot \mathcal{A}^{wi,wi}_{w,z,c} + \\
& \sum_{z \in \mathcal{B}} \sum_{w \in \mathcal{W}_z, w \in \mathcal{W}} M_{w,0,c} \cdot A^{wi,olt}_{w,0,c} + \\
& \sum_{z \in \mathcal{B}} \sum_{w \in \mathcal{W}_z, w \in \mathcal{W}} \sum_{o \in \mathcal{O} - \{z\}} M_{w,o,c} \cdot \mathcal{A}^{wi,onu}_{w,o,c} + \\
& \sum_{o \in \mathcal{O}} M_{o,0,c} \cdot \mathcal{A}^{onu,olt}_{o,0,c} + \\
& \sum_{o_1 \in \mathcal{O}} \sum_{o_2 \in \mathcal{O}, o_2 \neq o_1} M_{o_1,o_2,c} \cdot \mathcal{A}^{onu,olt}_{o_1,0,c} \cdot \mathcal{A}^{olt,onu}_{0,o_2,c} + \\
& \sum_{o \in \mathcal{O}} M_{0,o,c} \cdot \mathcal{A}^{olt,onu}_{0,o,c} \Bigg),
\end{aligned} \tag{8.30}
$$

whereby the individual availabilities are as follows:

— Single-hop wireless communications,

— Wireless communications destined to the OLT,

— Wireless communications destined to ONUs,

— Optical traffic destined to the OLT,

— Optical traffic from ONUs to ONUs, and

— Optical traffic from the OLT to ONUs.

Note that $\mathcal{A}$ represents the average network availability. We derive a second availability metric representing the probabilistic availability on a per-node and class basis with confidence interval:

$$
\mathcal{A}_{pn,c} = \mu(\vartheta_c) \pm z \cdot \frac{\sigma(\vartheta_c)}{\sqrt{|\vartheta_c|}}, \tag{8.31}
$$

where z is the z-score value (e.g., $z = 1.96$ for a 95 % confidence interval) and ϑ_c denotes a vector containing the probabilistic availability for all nodes for a given class c, defined as follows:

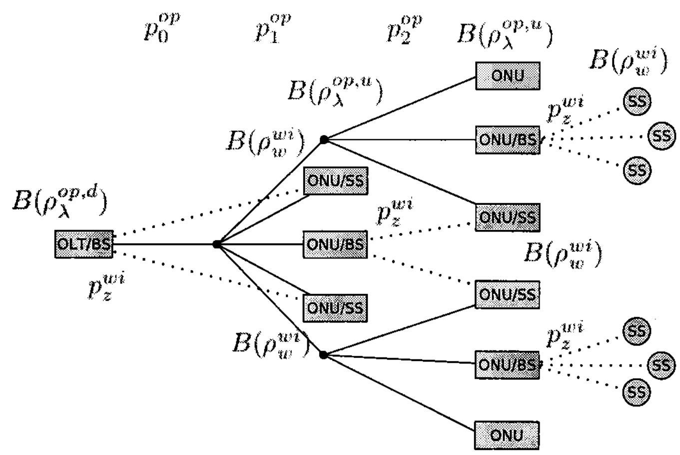

Figure 8.4 – Probabilistic model for a WR WDM PON ($\Xi = 3$).

$$\vartheta_c = \Big[[\mathcal{A}_{w,z,c}^{wi,wi} | z \in \mathcal{B}, w \in \mathcal{W}_z, w \in \mathcal{W}, c \in \mathcal{C}], \\ [\mathcal{A}_{o,0,c}^{onu,olt} | o \in \mathcal{O}], [\mathcal{A}_{0,o,c}^{olt,onu} | o \in \mathcal{O}] \Big]. \tag{8.32}$$

Note that the notation $[[.], [.], ..., [.]]$ corresponds to a vector built by concatenating the elements contained in a set of vectors.

Fig. 8.4 illustrates our probabilistic model for a WR WDM PON ($\Xi = 3$). As can be seen, the case of WR WDM PON is more complex compared with a WB TDM/PON (Fig. 8.3) as multiple stages are modeled and both WiMAX and PON systems overlap.

8.4.5 Adaptation of Framework to Mesh-based Topologies

The structure of the FiWi network considered in this paper is tree-based. Note, however, that traffic can be routed either via WiMAX or PON. The framework can be also adapted to mesh-based

IEEE Transactions on Communications, accepted for publication.

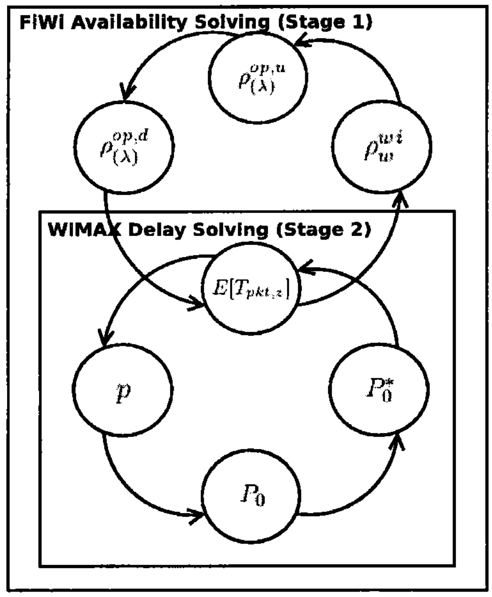

Figure 8.5 – Two-stage fixed-point iterations technique to solve the nonlinear equation system.

structures. Toward this end, from a given node n to node d the availability equations would need to consider multiple alternate adjacent nodes $a_{n,d}$ as follows:

$$\left(1 - \prod_{i \in a_{n,d}} (1 - \mathcal{A}_i)\right). \tag{8.33}$$

Furthermore, the traffic rates need to be adapted in a similar fashion as done in Eq. (8.19), whereby the traffic can be routed towards either the PON or WiMAX interface.

8.4.6 Solving the Analytical Framework

In order to solve the above developed nonlinear equation system, we use a two-stage fixed-point iterations technique, as illustrated in Fig. 8.5. We first solve Eqs. (8.20, 8.21, 8.23, 8.24) for the upstream and downstream PON traffic intensities. Next, we solve the set of WiMAX nonlinear systems in order to find the access delay for each zone. By means of fixed-point iterations, we calculate the three unknown variables from [12, Eqs. (14-16)] followed by the recalculation of $E[T_{pkt}, z]$ until $E[T_{pkt}, z]$ does not vary much (e.g., 10^{-8}). Once stable, we go back to the first stage in order to calculate Eq. (8.15). These steps are executed until the traffic intensities do not

IEEE Transactions on Communications, accepted for publication.

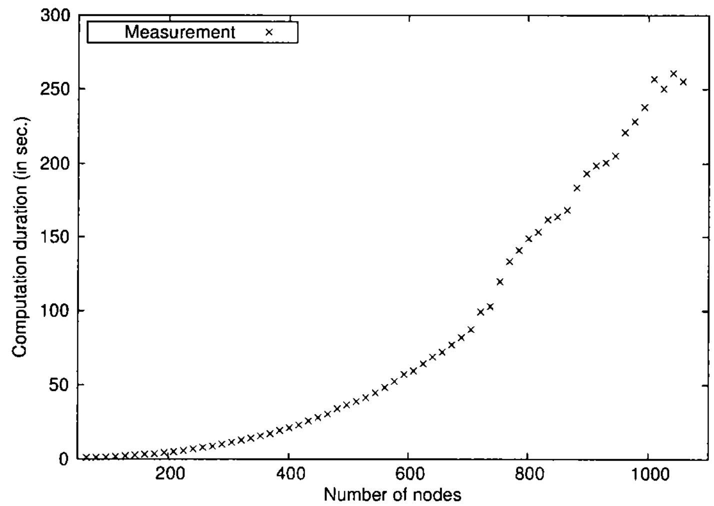

Figure 8.6 – Computation duration (complexity) versus topology size (number of nodes).

vary much. We note that we did not experience any computation problems as the equation systems converge quickly within a few iterations.

To provide insights into the computation requirements, we measured the computation duration as a function of the topology size (i.e., number of nodes), as depicted in Fig. 8.6. We observe from the figure that the complexity of the system grows linearly for medium to large number of nodes. For about 1000 nodes, the availability performance can be computed within 4 minutes using a 800 MHz processor and 5.4 GB random access memory (RAM).

8.5 Numerical Results

This section presents numerical results on the network availability equation $\mathcal{A}$ from Eq. (8.30) for WB and WR PONs integrated with WiMAX.

8.5.1 Configurations

We set the WiMAX capacity per channel/zone to 75 Mbps assuming 64-QAM modulation [25]. Furthermore, according to the WiMAX specifications, the frame duration varies between 5 and 20 ms. For ease of calculation, we set the mean frame duration in the wireless networks to

IEEE Transactions on Communications, accepted for publication.

Tableau 8.1 – Configurations

Parameter	Value
Q	100 frames
T_{frame} (in [12])	0.005 sec.
c_{op}	10^9 bps
c_{wi}	$75 \cdot 10^6$ bps

$T_{frame} = 0.005$ and first set the average FiWi frame length to $T_{frame} \cdot 75 \cdot 10^6$ bits. We first assume a single traffic class. Table 8.1 presents the main parameters used in all scenarios described below. For the other WiMAX configurations, we use the same ones as considered in [12]. We use a traffic matrix with $M_{i,j,c} = \Phi$, $i \in \mathcal{N}$ and $j \in \{0\} \cup \mathcal{O}$, whereby Φ represents a variable traffic rate given in frames/sec.

8.5.2 WB TDM/WDM PONs

We first consider a single-stage WB TDM PON supporting 1 Gbps per wavelength, which can be upgraded to a WDM PON supporting multiple bidirectional wavelengths. We examine the WiMAX and PON networks independently without any interaction between them. Fig. 8.7 shows the availability of each network versus offered load (OL). Note that the WiMAX case corresponds to a single zone with 16 SSs. Expectedly, the WiMAX availability drops more quickly compared to the PONs due to its low capacity. The availability of PONs drops when the offered load gets close to their capacity.

Next, we consider a topology with a similar structure as depicted in Fig. 8.1, whereby the number of ONU/BSs is set to 16 and each ONU/BS aggregates traffic from 3 SSs. Fig. 8.8 compares the availability of an EPON and WDM PON. The availability drops at approximately 1 Gbps for the EPON due to optical capacity saturation and the availability drops at 1.3 Gbps in the WDM PON case due to WiMAX capacity saturation.

Next, we investigate the fiber and BS failure probabilities in Figs. 8.9 and 8.10 for different traffic matrices. Overall, the impact of fiber failures is significantly larger compared to BS failures, which is explained by the fact that a larger number of connections uses the PON. The impact is especially apparent when the network is highly loaded.

IEEE Transactions on Communications, accepted for publication.

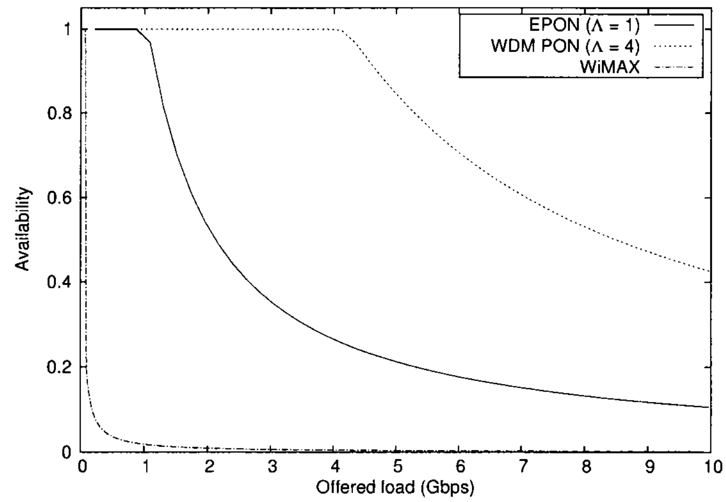

Figure 8.7 – WiMAX, WB TDM, and WDM PON availability performance vs. the offered load ($p^{wi} = p^{op} = 10^{-5}$).

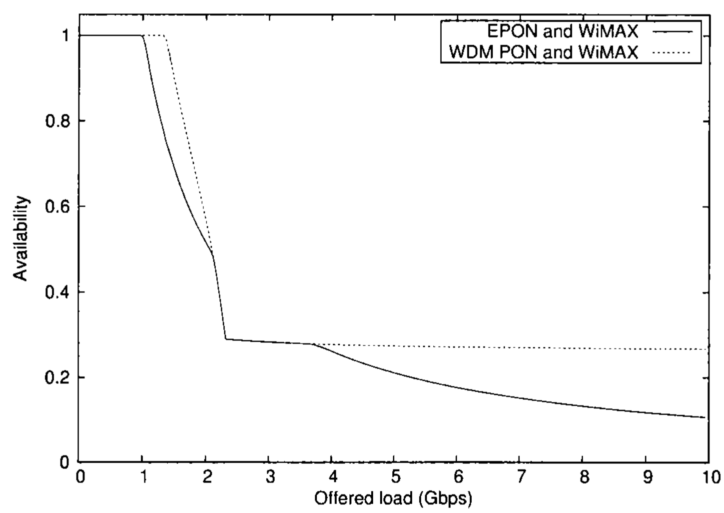

Figure 8.8 – Integrated WB TDM/WDM PON availability performance vs. the offered load ($p^{wi} = p^{op} = 10^{-5}$, $|\mathcal{W}| = 16 \cdot 3$).

8.5.3 Next-Generation FiWi Settings with Integrated WR WDM PONs

In the remainder, we focus on a topology with a WR WDM PON following the same structure as in Fig. 8.2 (a pyramid-based topology) with a splitting ratio of 16 ($S = 16$). As opposed to the previous subsection, each ONU has a WiMAX interface, either acting as a SS or BS, therefore all parts of the analysis are used. The number of stages is set to 4 ($\Xi = 4$), thus a total of $14 + 2 \cdot 14 + 4 \cdot 16 = 106$ ONUs are installed. Stages 0-2 use AWGs as a remote node and the last stage

IEEE Transactions on Communications, accepted for publication.

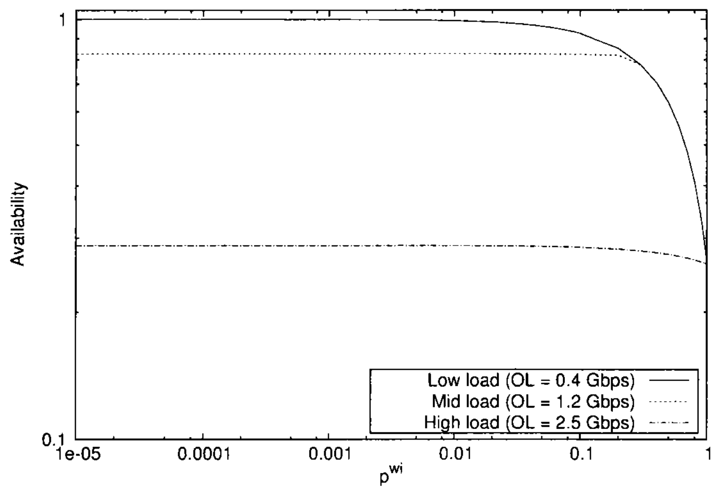

Figure 8.9 – Impact of WiMAX BS failure probability on overall network availability for different network offered loads ($p^{wi} = p_z^{wi}, \forall z \in \mathcal{B}$).

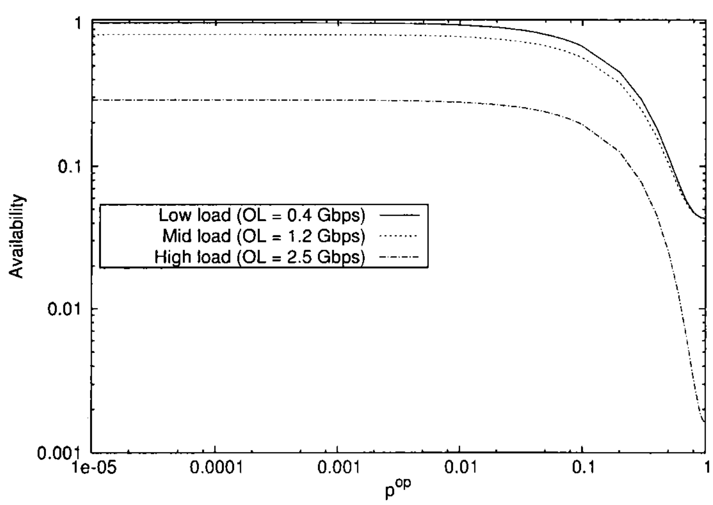

Figure 8.10 – Impact of fiber failure probability on overall network availability for different offered loads ($p^{op} = p_s^{op}, \forall s \in \{0, ..., \Xi - 1\}$).

uses conventional splitters. Hence, a total of $14 + 2 \cdot 14 + 4 = 46$ wavelengths are available, each dedicated to a different sector, whereby the wavelengths at the last stage are shared by 16 ONUs. Furthermore, a total of 64 SSs with WiMAX support only are attached to the last PON stage. Fig. 8.11 shows the probabilistic availability versus the offered load. The first availability drop close to 1 Gbps is due to the saturation of the WiMAX channels for zones attached to ONUs at the last stage. The second drop close to 10 Gbps is due to the successive saturation of PON channels.

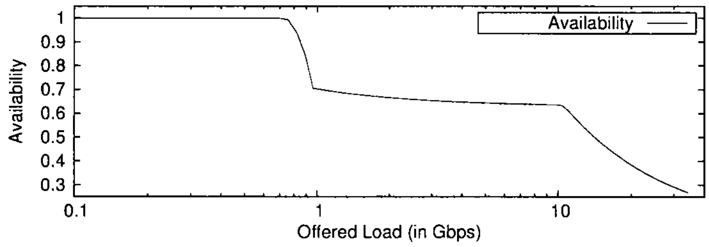

Figure 8.11 – Availability performance vs. the offered load for a pyramid-based WR WDM PON consisting of 106 ONUs with a splitting ratio of 16.

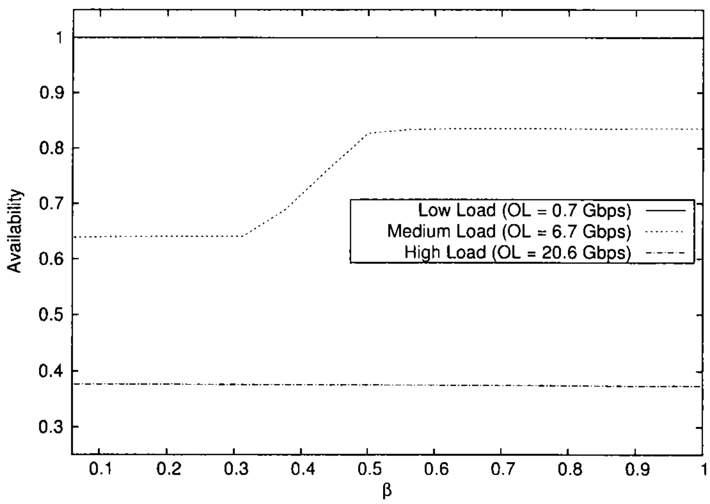

Figure 8.12 – Impact of the number of BSs per S (β) on availability.

We investigate the impact of the parameter β in Fig. 8.12. We observe that under low and high traffic loads, increasing the number of BSs does not significantly improve the overall network availability. However, at medium traffic loads, we observe a significant network availability improvement by adding 4-7 BSs ($0.3 \leq \beta \leq 0.5$). A surprising behaviour is observed for $\beta > 0.5$, where an increasing number of BSs does not further improve network availability.

Another important parameter is the ratio of the traffic destined towards faulty fibers permitted to be re-routed in the wireless domain, denoted as δ^{wi} and illustrated in Fig. 8.13 for different values of β. We observe that for each given configuration depending on the number of BSs installed, there exists a δ^{wi} that maximizes network availability, namely 0.17 for $\beta = \frac{3}{16}$, 0.37 for $\beta = \frac{7}{16}$, and 0.7 for $\beta = \frac{11}{16}$.

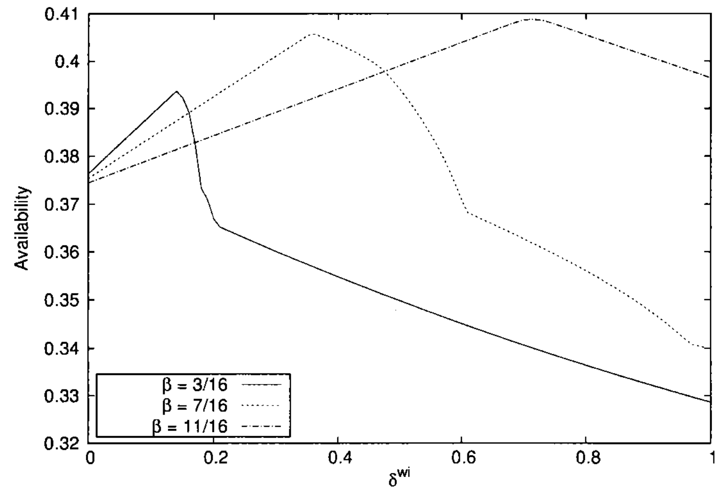

Figure 8.13 – Impact of the ratio of the traffic destined towards faulty fibers permitted be re-routed in the wireless domain (OL = 20.5 Gbps, $\delta^{wi} = \delta^{wi}_{i,j}, \forall i,j \in \mathcal{N}$).

Tableau 8.2 – Experimental measurements of smart grid applications based on the IEC 61850 standard.

Source node	Average payload length	Rate per sec.
HVA/LV	500 bytes	$\frac{1}{30}$
Substation	5000 bytes	$\frac{1}{30}$
DER	224 bytes	$2 \cdot \frac{1}{60 \cdot 10}$
Switch	100 bytes	$2 \cdot \frac{1}{60 \cdot 10}$

8.5.4 Impact of Fiber and BS Failures

In this subsection, we study equipment failures using the same topology as in the previous subsection. We calculate the availability by varying the values of p^{wi} and p^{op} from 10^{-6} to 1 for low (OL = 686 Mbps) and high (OL = 20.5 Gbps) traffic loads, as depicted in Figs. 8.14 and 8.15. For both traffic loads, we denote a higher reduction of the availability as p^{op} increases, as compared to p^{wi}. Furthermore, the variation of the BS failure probability has a significant impact on the availability only at low loads, as depicted in Fig. 8.14, which was already observed in the case of the WB WDM PON (See Fig. 8.9).

IEEE Transactions on Communications, accepted for publication.

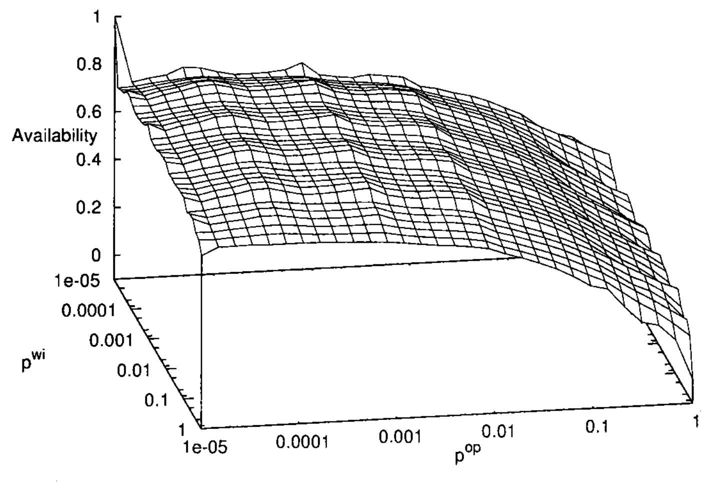

Figure 8.14 – Availability as a function of fiber and BS failures ($OL = 686$ Mbps).

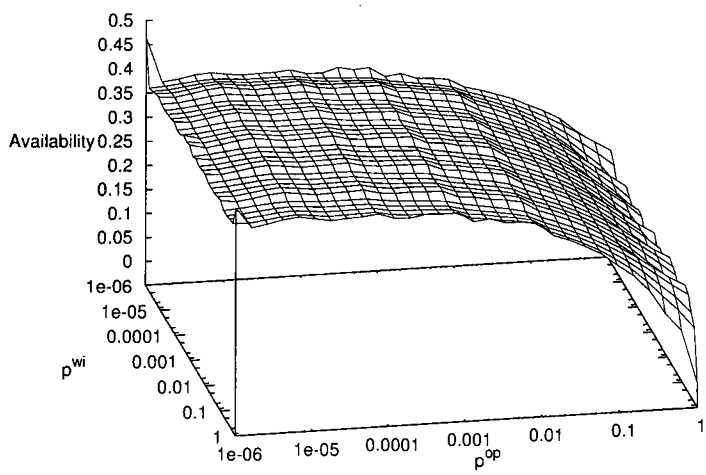

Figure 8.15 – Availability as a funciton of fiber and BS failures ($OL = 20.5$ Gbps).

8.5.5 Coexistence of Human-to-Human (H2H) and Smart Grid Traffic

In the following, we consider three traffic classes: one regular class for triple-play (video, voice, and data) traffic and two others for control and monitoring SG traffic. The control traffic can be used, for instance, to turn ON/OFF controllable power switches. Therefore, the data rate of this type of traffic is generally small and event-driven, but with high priority. As for the monitoring traffic, typical smart grid sensors are time-based with configurable data rates. We captured the traffic of experimental telecontrol smart grid applications. Table 8.2 shows the average payload length

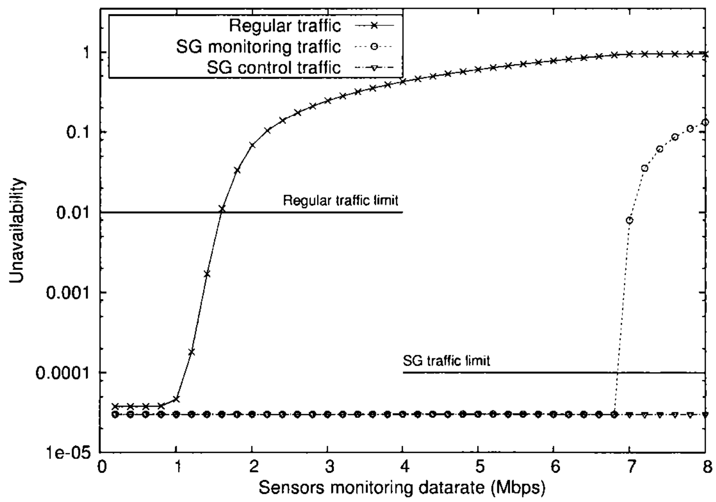

Figure 8.16 – Unavailability as a function of sensor data rate ($p^{op} = p^{wi} = 10^{-5}$). Regular traffic has an availability requirement of 99.99 % and 99.9999 % for SG traffic.

originating from high-voltage/low-voltage (HV/LV) transformers, substation, distributed energy resources (DERs), and controllable switches. A single variable-value pair (following the format of manufacturing message specification messages (MMSs) of IEC 61850) accounts for 100 bytes. The measured payload length of 500 bytes for the HV/LV nodes corresponds to active/reactive power, voltage, current, and location.

We assume a WB PON of 16 ONUs, with bidirectional 1 Gbps link, and 10 SSs are aggregated per ONU. For the payload length, we use $\bar{L}_r = 1500 \cdot 8$, $\bar{L}_m = 500 \cdot 8$, and $\bar{L}_c = 100 \cdot 8$ for the regular, SG monitoring, and SG control traffic, respectively, whereby the SG traffic payload lengths correspond to the ones listed in Table 8.2. The traffic rate for the regular traffic follows a uniform distribution in the WB PON, whereby $\forall i, j \in \mathcal{O} + \{0\}, M_{i,j,r} = 250$ (Total traffic: 816 Mbps). As for the SG classes, we have one SS i per ONU sending control frames to the OLT ($M_{i,0,c} = \frac{1}{60 \cdot 10}$) and SG monitoring frames are destined to the OLT, whereby the data rate is varied, as depicted in Fig. 8.16. We set the class priorities to $\alpha_r = 0.2$ and $\alpha_m = \alpha_c = 0.4$ for the regular and SG classes, respectively.

We assume that the availability requirements of the regular and SG traffic are different and are hence set to 99.99% and 99.9999%, respectively. To meet these requirements under the conditions used in our scenario, the data rate should be set to maximally 1.5 Mbps per sensor. Note that

IEEE Transactions on Communications, accepted for publication.

the frames of lower priorities are dropped first. Therefore, at a sensor monitoring data rate of 1.5 Mbps, frames belonging to the regular class are dropped in order to be able to accommodate SG monitoring frames.

8.6 Conclusions

Backhaul networks based on PONs are expected to be widely deployed for emerging smart grid applications and to offer FTTH services. There is a continuous trend of increasing communications coverage, by integrating FiWi-based communications architectures. In this paper, we developed a novel multi-class probabilistic availability model to quantify the availability metric defined in the IEEE P2030 standard. The model takes into account the MAC protocol limits of integrated PON and WiMAX networks as well as fiber and base station failures. The obtained examples show several interesting availability behaviors. First, fiber backhaul failures have a significant impact on availability especially at high loads, while WiMAX BS failures have a lower impact at low and high loads. The model also enables to quantify availability depending on the number of BSs available, whereby selecting the right number of BSs helps maximize availability in a cost-effective manner. We have also shown that there exists a unique ratio of traffic destined towards a faulty link permitted to be re-routed for maximizing availability. Each smart grid application has a certain given availability requirement. We investigated a smart grid scenario with payload length and data rate configurations based on traffic measurements captured from smart grid applications. By considering regular and smart grid traffic classes with different priorities and availability requirements, we have shown that under the investigated conditions the sensors' maximum monitoring data rate to meet the availability requirements can be quantified. The developed probabilistic availability model enables to verify wether or not requirements are met based on predicted traffic and equipment failure probabilities.

References

[1] V. C. Gungor, D. Sahin, T. Kocak, S. Ergut, C. Buccella, C. Cecati, and G. P. Hancke, "A Survey on Smart Grid Potential Applications and Communication Requirements," *IEEE Transactions on Industrial Informatics*, vol. 9, no. 1, pp. 28–42, Feb. 2013.

[2] IEEE-SA Standards Board, "IEEE Guide for Smart Grid Interoperability of Energy Technology and Information Technology Operation with the Electric Power System (EPS), End-Use Applications, and Loads," *IEEE Std 2030-2011*, pp. 1–126, Sep. 2011.

[3] S. Cabuk, "Simple Test of Hypotheses on System Availability and Mean Time to Repair," *IEEE Transactions on Reliability*, vol. 35, no. 5, pp. 581–583, Dec. 1986.

[4] W. Bo, "China Telecom FTTH Deployment - Lessons Learnt and Future Plans," in *Proc., Asia Communications and Photonics Conference (ACP)*, Guangzhou, China, Nov. 2012, pp. 1–3.

[5] M. Maier, "Reliable Fiber-Wireless Access Networks: Less an End than a Means to an End," in *Proc., International Conference on the Design of Reliable Communication Networks (DRCN)*, Budapest, Hungary, Mar. 2013, pp. 119–130.

[6] N. Ghazisaidi, M. Maier, and C. M. Assi, "Fiber-Wireless (FiWi) Access Networks: A Survey," *IEEE Communications Magazine*, vol. 47, no. 2, pp. 160–167, Feb. 2009.

[7] P. Cheng, L. Wang, B. Zhen, and S. Wang, "Feasibility Study of Applying LTE to Smart Grid," in *Proc., IEEE First International Workshop on Smart Grid Modeling and Simulation (SGMS)*, Brussels, Belgium, Oct. 2011, pp. 108–113.

IEEE Transactions on Communications, accepted for publication.

[8] Y. Yan, Y. Qian, H. Sharif, and D. Tipper, "A Survey on Smart Grid Communication Infrastructures: Motivations, Requirements and Challenges," *IEEE Communications Surveys & Tutorials*, vol. 15, no. 1, pp. 5–20, Feb. 2012.

[9] WiMAX Forum, "Mobile WiMAX - Part I: A Technical Overview and Performance Evaluation," *Technical Report*, Aug. 2006.

[10] M. Maier, M. Lévesque, and L. Ivanescu, "NG-PONs 1&2 and Beyond: The Dawn of the Über-FiWi Network," *IEEE Network*, vol. 26, no. 2, pp. 15–21, Mar./Apr. 2012.

[11] N. Ghazisaidi and M. Maier, "Fiber-Wireless (FiWi) Networks: A Comparative Techno-Economic Analysis of EPON and WiMAX," in *Proc., IEEE GLOBECOM*, Honolulu, HI, USA, Nov./Dec. 2009, pp. 1–6.

[12] G. Giambene and S. Hadzic-Puzovic, "WiMAX Non-Saturated Analysis," in *Proc., IEEE GLOBECOM Workshops*, Houston, USA, Dec. 2011, pp. 1325–1329.

[13] H. L. Vu, S. Chan, and L. L. H. Andrew, "Performance Analysis of Best-Effort Service in Saturated IEEE 802.16 Networks," *IEEE Transactions on Vehicular Technology*, vol. 59, no. 1, pp. 460–472, Jan. 2010.

[14] F. Aurzada, M. Scheutzow, M. Reisslein, N. Ghazisaidi, and M. Maier, "Capacity and Delay Analysis of Next-Generation Passive Optical Networks (NG-PONs)," *IEEE Transactions on Communications*, vol. 59, no. 5, pp. 1378–1388, May 2011.

[15] N. Ghazisaidi, M. Scheutzow, and M. Maier, "Survivability Analysis of Next-Generation Passive Optical Networks and Fiber-Wireless Access Networks," *IEEE Transactions on Reliability*, vol. 60, no. 2, pp. 479–492, Jun. 2011.

[16] F. Aurzada, M. Lévesque, M. Maier, and M. Reisslein, "FiWi Access Networks Based on Next-Generation PON and Gigabit-Class WLAN Technologies: A Capacity and Delay Analysis," *IEEE/ACM Transactions on Networking (Early Access)*, Jul. 2013.

[17] M. Maier, N. Ghazisaidi, and M. Reisslein, "The Audacity of Fiber-Wireless (FiWi) Networks," *Springer AccessNets: Lecture Notes of the ICST*, vol. 6, pp. 16–35, Sep. 2009.

IEEE Transactions on Communications, accepted for publication.

[18] G. Shen, R. S. Tucker, and C.-J. Chae, "Fixed Mobile Convergence Architectures for Broadband Access: Integration of EPON and WiMAX," *IEEE Communications Magazine*, vol. 45, no. 8, pp. 44–50, Aug. 2007.

[19] X. Shao, Y. K. Yeo, L. H. Ngoh, X. Cheng, W. Rong, and L. Zhou, "Availability-Aware Routing for Large-Scale Hybrid Wireless-Optical Broadband Access Network," in *Proc., Conference on Optical Fiber Communication (OFC), collocated National Fiber Optic Engineers Conference (OFC/NFOEC)*, San Diego, CA, USA, Mar. 2010, pp. 1–3.

[20] Y. Huang, J. P. Heritage, and B. Mukherjee, "Availability-Guaranteed Service Provisioning with Shared-Path Protection in Optical WDM Networks," in *Proc., Optical Fiber Communication Conference (OFC)*, Los Angeles, CA, USA, Feb. 2004, pp. 1–3.

[21] M. Kiese, E. Georgieva, D. Schupke, B. Mukherjee, and J. Eberspächer, "Availability Evaluation of Hybrid Wireless Optical Broadband Access Networks," in *Proc., IEEE International Conference on Communications (ICC)*, Dresden, Germany, Jun. 2009, pp. 1–6.

[22] O. Salami, A. Bagula, and H. A. Chan, "Link and Route Availability for Inter-working Multihop Wireless Networks," in *Proc., International Conference on Parallel Processing Workshops*, Vienna, Austria, Sep. 2009, pp. 356–361.

[23] L. Kleinrock, *Queuing Systems: Theory.* Wiley, 1976, vol. 1.

[24] A. Vinel, Q. Ni, D. Staehle, and A. Turlikov, "Capacity Analysis of Reservation-based Random Access for Broadband Wireless Access Networks," *IEEE Journal on Selected Areas in Communications*, vol. 27, no. 2, pp. 172–181, Feb. 2009.

[25] H.-T. Lin, C.-L. Lai, and Y.-C. Huang, "Dynamic Bandwidth Allocation with QoS Support for Integrated EPON/WiMAX Networks," in *Proc., IEEE International Conference on High Performance Switching and Routing (HPSR)*, Taipei, Taiwan, Jul. 2013, pp. 74–79.

Chapitre 9

Integrated V2G, G2V, and Renewable Energy Sources Coordination over a Converged Fiber-Wireless Broadband Access Network

Publication:

— D. Q. Xu, M. Lévesque, G. Joós, and M. Maier, "Integrated V2G, G2V, and Renewable Energy Sources Coordination over a Converged Fiber-Wireless Broadband Access Network," *IEEE Transactions on Smart Grid*, vol. 4, no. 3, pp. 1381-1390, May 2013.

The focus of the two previous chapters was on the performance evaluation of integrated fiber-wireless access networks in terms of delay-throughput and availability. As stated in IEEE P2030, there is a strong need to study the future power grid and its applications in a comprehensive manner that considers power systems, communications, and information technologies as a whole physical-cyber system. All the aforementioned studies, however, have focused on proposing or optimizing plug-in electric vehicle (PEV) coordination algorithms only from the perspective of power systems, while neglecting the requirement and performance of the supporting communications network. The main novelties in the following paper are as follows :

— An integrated V2G, G2V, and RES (IntVGR) algorithm is proposed, which aims at smoothening the overall demand profile (peak shaving and valley filling) and making maximum utilization of local RES capacity by coordinating PEVs between V2G and G2V operation modes, whilst taking into account both power grid technical constraints and PEV owners' requests and satisfaction.

— Implementation of the proposed scheme is based on exchanging notification and control packets between PEVs, households, and a central controlling system over a converged cost-effective broadband access network based on optical fiber and wireless technologies.

— This is the first work that attemps to actually implement a specific PEV coordination scheme by simulating real-time information interactions in a novel co-simulation framework, and examine its performance from both power systems and communications viewpoints.

More specifically regarding the contributions from M. Lévesque, they are listed as follows:

— Proposition of the networking architecture covering the power distribution network.

— Development and proposition of the co-simulation environment in OMNeT++ (for communications) and its integration with OpenDSS.

— Suggestions and discussions regarding the integrated coordination scheme (IntVGR).

The co-simulation results show that, from the perspective of power systems, the proposed IntVGR scheduling scheme is able to achieve a 15% improvement compared to the uncoordinated scenario in terms of flattening the overall demand profile without compromising on PEV owner's satisfaction. The scheme is also demonstrated effective in helping PEVs utilize local RES capacity to its full extent. From the viewpoint of the supporting communications infrastructure, a throughput of 1-2 Mbps is required to execute IntVGR for a distribution grid consisting of 342 households, with a low end-to-end delay of 1 ms.

IEEE Transactions on Smart Grid, vol. 4, no. 3, pp. 1381-1390.

9.1 Abstract

In this paper, an integrated vehicle-to-grid, grid-to-vehicle, and renewable energy sources (IntVGR) coordination algorithm is proposed. The focus of this work is to provide a multidisciplinary study on implementing the proposed IntVGR scheme over a broadband fiber-wireless communications infrastructure by co-simulating both power and communications perspectives. For the power systems perspective, results show that the scheme is able to achieve a 21% reduction in peak demand compared to uncontrolled charging, and a better performance in flattening the overall demand profile and maintaining network constraints in comparison to a benchmark scenario. The scheme has also been demonstrated to successfully coordinate PEVs to take maximum utilization of local renewable energy. For the communications perspective, the measured upstream traffic for executing the proposed IntVGR scheme on a residential area of 342 households is found to be 1-2 Mbps with an end-to-end latency level of 1 ms. The scheme has also been validated from both perspectives in a sensitivity analysis with a higher PEV adoption rate.

Keywords: Co-simulation, demand side management, plug-in electric vehicles, smart grid communications.

9.2 Introduction

The emergence of plug-in electric vehicles (PEVs) is envisioned to become a promising alternative to conventional fuel-based automobiles. Proliferation of PEVs, however, provokes new challenges to the current electric power systems operation and planning, especially at the low-voltage (LV) distribution level from the perspective of demand side management (DSM) [1]. Charging activities of PEVs with poor regulation might impose severe stress on the distribution grid, resulting in degraded system efficiency and deterioration of power quality on a local scale [2, 3, 4].

In order to mitigate the aforementioned detrimental impacts due to PEV loads, some recent works have proposed various optimized and coordinated charging strategies from the viewpoint of different stakeholders, based on minimization of system-level power losses [5, 6], minimization of charging costs for PEV owners [7], and maximization of the state-of-charge (SOC) level of PEV batteries [8].

Next-generation PEVs with vehicle-to-grid (V2G) technology enabled, in addition to simply acting as a load operated in the grid-to-vehicle (G2V) charging mode, are of great potential to offer many benefits to the power grid, including peak shaving and load leveling, voltage regulation, providing frequency regulation and other ancillary services (e.g., spinning reserves), and serving as distributed storage units for backup capacity [9]. The authors in [10] propose a coordinated charging and discharging scheme based on minimization of PEV charging costs, whilst taking network constraints into account such as voltage profile patterns along the grid.

The most sustainable solution toward deployment of PEVs is to realize "Green E-mobility" by combining PEVs with renewable energy sources (RESs). PEVs are able to serve as dispersed energy storage units and help integrate RESs in the energy mix as stable base load generation capacity by performing controlled G2V/V2G operations. They can also be controlled as flexible loads to utilize local RES capacity to avoid requiring long-distance transport of electricity, reduce the risk of inducing local grid problems, and minimize the charging cost for PEV owners as well [11].

Realization of coordination of G2V, V2G, and RESs as previously discussed, relies on the creation of a bi-directional smart grid communications infrastructure capable of handling all kinds of information that needs to be exchanged among different entities [3]. As stated in IEEE P2030 released recently [12], there is a strong need to study the future power grid and its applications in a comprehensive manner that considers power systems, communications, and information technologies as a whole physical-cyber system. All the aforementioned researches, however, have focused on proposing or optimizing PEV coordination algorithms only from the perspective of power systems, while neglecting the requirement and performance of the supporting communications network. The problem states that a multidisciplinary study is required, which has also been considered one of the main challenges for future DSM [13].

In this paper, we extend our previous work [14] by proposing an integrated V2G, G2V, and RESs (IntVGR) coordination scheme, which is supported by a converged fiber-wireless (FiWi) communications infrastructure, and examining its performance from both power systems and communications perspectives in a co-simulation environment developed in our recent work [15]. The main contributions of this paper are as follows:

— The proposed IntVGR scheme aims to smoothen the overall demand profile (peak shaving and valley filling) and make maximum utilization of local RES capacity by coordinating PEVs between V2G and G2V operation modes, whilst taking into account both power grid technical constraints and PEV owners' requests and satisfaction.

— Implementation of the proposed scheme is based on exchanging notification and control packets between PEVs, households, and a central controlling system over a converged cost-effective broadband access network based on optical fiber and wireless technologies.

— In comparison to existing studies where only the power systems perspective has been considered, this is the first work that attempts to actually implement a specific PEV coordination scheme by simulating real-time information interactions in a novel co-simulation framework, and examine its performance from both power systems and communications viewpoints.

Our co-simulation results show that, from the perspective of power systems, the proposed IntVGR scheduling scheme is able to achieve a 15% improvement compared to the uncoordinated scenario in terms of flattening the overall demand profile without compromising on PEV owner's satisfaction. The scheme is also demonstrated effective in helping PEVs utilize local RES capacity to its full extent. From the viewpoint of the supporting communications infrastructure, a throughput of 1-2 Mbps is required to execute the IntVGR scheme for a distribution grid consisting of 342 households, with a fairly low end-to-end delay of 1 ms.

The remainder of this paper is organized as follows. A description of information interactions between the power systems layer and the communications network layer for implementation of the proposed IntVGR scheme is given in Section 9.3. Section 9.4 describes the proposed IntVGR algorithm with mathematical formulations provided. Co-simulation results are shown and discussed in Section 9.5. Conclusions are finally drawn in Section 9.6.

IEEE Transactions on Smart Grid, vol. 4, no. 3, pp. 1381-1390.

9.3 Power Distribution and Communications Interactions

To implement smart PEV coordination schemes in the distribution grid, a viable bi-directional communications infrastructure beyond substations is indispensable, along with advanced information and communications technologies (ICTs). We recently proposed a FiWi communications infrastructure for distribution networks based on standardized and low-cost Ethernet passive optical network (EPON), WiMAX, and wireless mesh network technologies as well as an optical metropolitan area ring network. Due to space limitations, interested readers are referred to [16] for a detailed description of our proposed FiWi infrastructure.

As this work attempts to deploy an intelligent PEV coordination scheme by exchanging real-time information packets between the superior controlling unit and PEVs, in this section we focus on explaining some main information interactions over the FiWi network, as depicted in Fig. 9.1, for implementing our proposed algorithm to be described in greater details in Section 9.4.

9.3.1 Workplace/public parking garage

When a PEV arrives at the workplace, a G2V request is sent to the distribution management system (DMS) containing its identifier, status of the battery, and its desired time to be picked up. Each PEV reaches an optical network unit (ONU) by communicating in the wireless domain with a mesh portal point (MPP). The G2V request packet is then transmitted across the EPON network after a polling period and subsequently forwarded to the DMS through the optical line terminal (OLT). Upon receiving the G2V request, the DMS schedules the charging period for that PEV based on maximum utilization of generation capacity from local RES units (described in Section 9.4). Finally, the DMS sends back a G2V response, containing the time interval when the corresponding PEV will be charged during the parking period at the public garage. After receiving the G2V response, the corresponding PEV follows the charging schedule calculated by the DMS.

IEEE Transactions on Smart Grid, vol. 4, no. 3, pp. 1381-1390.

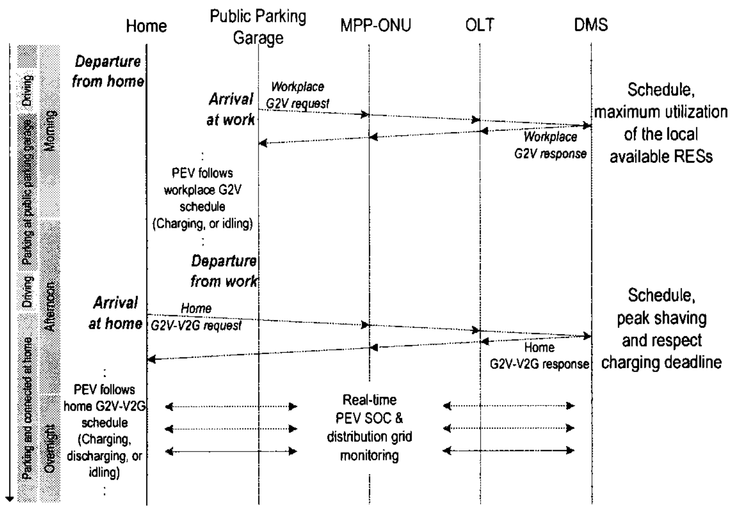

Figure 9.1 – Interactions between the FiWi network nodes and the DMS to implement the proposed PEV coordination algorithm.

9.3.2 Home

When a PEV arrives at home, a home G2V-V2G request message is sent to the DMS, containing its identifier, status of the battery, and deadline when the PEV is desired to be disconnected for the next trip. Upon receiving this message, the DMS performs the coordination algorithm (described in Section 9.4) to find both the V2G and G2V slots. The central DMS then sends back the slot information to the grid-connected PEV. Finally, based on the information given in the home G2V-V2G response, a specific V2G and/or G2V schedule will be followed by the corresponding PEV to get charged, stay idle, or contribute in peak shaving together with other PEVs. Also, periodically, notification messages containing the network information such as nodal voltage magnitudes and power consumptions are sent from each household to the DMS, which might be realized by some smart metering infrastructure [15]. These messages are sent at a specific rate (denoted by λ_{notif}) depending on the required sensitivity by the utility operator.

9.4 Integrated V2G, G2V, and RES Scheduling Algorithm

In this section, our proposed integrated V2G, G2V, and RES (IntVGR) scheduling algorithm is described, which takes into account not only the performance of the distribution grid but also vehicle owner's satisfaction. G2V and V2G are both considered and coordinated in such a way that better peak shaving and valley filling are realized whilst maintaining an acceptable power quality. The schematic of the proposed IntVGR algorithm with an emphasis on the part of home scheduling is illustrated in Fig. 9.2, which demonstrates different V2G/G2V schedules that will be assigned to a given PEV in terms of uncertainties related to its arrival time, its desirable disconnection deadline, and the amount of energy that it needs to be replenished.

To define our proposed IntVGR scheduling algorithm, we provide below the main parameters involved, objective functions, and system constraints. Note that following cost functions cannot be solved directly using an integer programming solver as multiple parameters are to be obtained by performing power flow analysis.

9.4.1 IntVGR main parameters

The main parameters of our proposed IntVGR scheduling algorithm are listed below.

- $\mathcal{H}$: Set of residential network nodes.
- $\mathcal{L}$: Set of power distribution lines.
- $t_{arr,i}$: Home arrival time of PEV i, where $i \in \mathcal{H}$.
- $t_{deadline,i}$: Deadline/disconnection time of PEV i.
- $SOC_{i,t}$: Battery SOC level of PEV i at time t.
- $P_{desired}$: Desired system-level peak demand (in kW). This is similar to the circuit level demand threshold specified in [17], which represents the network supply limit based on the existing generation capacity. $P_{desired}$ might also be a predefined level set by utility operators for other grid control purposes.
- $t_{V2G,S}$ and $t_{V2G,E}$: Start time and end time of the V2G period, which are defined as the time point when the system-level base load demand (non-PEV load consumption) becomes higher and drops lower than $P_{desired}$, respectively. $t_{V2G,S}$ and $t_{V2G,E}$ are known parameters prior to the optimization process based on historical residential base load profiles (discussed in co-simulation configurations in Section 9.5) and the predefined $P_{desired}$.

— T_{slot}: Interval of time slot. The time frame $\mathcal{T}$ is discretized into time slots for convenience of calculation and ease of implementation.

9.4.2 Objective function

The objectives of the proposed IntVGR algorithm are different for home scheduling and coordination at public parking garages, which will be explained and mathematically formulated in this section.

Home V2G scheduling

The objective for home scheduling within the V2G period is to shave the peak demand to the level of $P_{desired}$ as close as possible by aggregating feasible PEVs to feed energy back to the grid and is expressed as follows:

$$\begin{aligned} &min\left(\sum_{t=t_{V2G,S}}^{t_{V2G,E}}\left(\sum_{k}^{|\mathcal{H}|}P_{k,t}-P_{desired}\right)^2\right), \\ &\forall k\in\mathcal{H}, t\in[t_{V2G,S},t_{V2G,E}] \end{aligned} \tag{9.1}$$

where $P_{k,t}$ represents the power demand at node $k \in \mathcal{H}$ at time $t \in [t_{V2G,S}, t_{V2G,E}]$. Note that $P_{k,t}$ consists of two components:

$$P_{k,t} = P_{base,k,t} + P_{PEV,k,t}, \tag{9.2}$$

in which $P_{base,k,t}$ denotes the base load demand at node k at time t and $P_{PEV,k,t}$ represents the PEV load and is given by:

$$P_{PEV,k,t} = \begin{cases} R_{ch} & \text{if charging at node } k \text{ at time } t \\ -R_{dis} & \text{if discharging at node } k \text{ at time } t \\ 0 & \text{otherwise} \end{cases}, \tag{9.3}$$

where R_{ch} and R_{dis} represent the charging and discharging power level, respectively. Note that $-R_{dis}$ indicates that the PEV is actually feeding power back to the grid as a distributed generator. It is worth noting that the aforementioned "otherwise" circumstance accounts for the situation where no PEV is assigned to node k at all or the PEV associated with node k has not yet been connected to the grid at time t, e.g., currently driving on the road. This circumstance also ensures the causality of the scheduling. For example, if PEV k arrives after $t_{V2G,S}$ (but prior to $t_{V2G,E}$), the start time of Eq. (9.1) for scheduling PEV k is its actual arrival time instead of $t_{V2G,S}$ because the past cannot be changed. In that case, therefore, $P_{PEV,k,t}$ equals zero for all the slots between $t_{V2G,S}$ and its arrival time, according to the "otherwise" circumstance. At any given time point t, the term $P_{PEV,k,t}$ includes all the PEVs that have already been scheduled by the DMS, and we do not consider future unscheduled PEVs in scheduling a newly arrived one.

Home G2V scheduling

Having determined all the discharging slots for PEV i, for G2V scheduling, the objective is to minimize the total system losses while filling the valley, which was originally proposed in [5], and can be formulated as:

$$\begin{aligned} &min \left(\sum_{t}^{|\mathcal{T}-[t_{V2G,S},t_{V2G,E}]|} \left(\sum_{l}^{|\mathcal{L}|} I_{l,t}^{2} \left(\sum_{k}^{|\mathcal{H}|} P_{k,t} \right) \cdot R_l \right) \right), \\ &\forall k \in \mathcal{H}, t \in \mathcal{T} - [t_{V2G,S}, t_{V2G,E}] \end{aligned} \tag{9.4}$$

where $I_{l,t}$ represents the current flowing along line $l \in \mathcal{L}$ at time t, and its value is obtained from load flow analysis based on the value of $P_{PEV,k,t}$ (a component of $P_{k,t}$). Note that Eq. (9.4) cannot be solved explicitly, but instead the optimal $P_{PEV,k,t}$ is obtained by performing iterative load flow analysis, which results in minimum system-level power losses among all the scheduling permutations.

It is worth emphasizing that the decision variable for Eqs. (9.1) and (9.4) is the slot assignment represented by $P_{PEV,k,t}$, i.e., charging, discharging, or being idle, according to Eq. (9.3) for all the time slots when the corresponding PEV is grid-connected. Charging and discharging power levels (R_{ch} and R_{dis}) are not decision variables, but instead they are fixed at the maximum power ratings

IEEE Transactions on Smart Grid, vol. 4, no. 3, pp. 1381-1390.

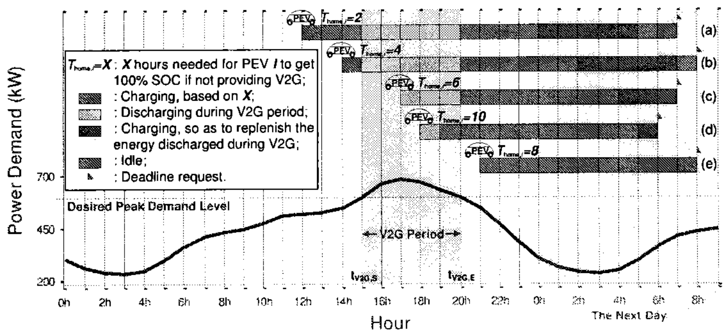

Figure 9.2 – Schematic of the proposed scheduling algorithm.

for ease of calculation. Adjustable charging/discharging rates might be adopted, which would result in more scheduling flexibility at the expense of higher computation complexity.

Workplace scheduling with RES

When RES units are available at the public parking garage/workplace, the objective is to make maximum utilization of available solar power generated locally. In case that there is a shortage of RES generation, given the fact that the majority of PEVs will be parking at the garage for a long period during the day (e.g., the typical daily work duration is approximately 8 hours), some PEVs might be postponed to a later time when the generation capacity from PV panels rises (i.e., solar intensity reaches its highest level around noon time). Consequently, the overall charging profile at the parking garage will track and match the RES unit output profile by controlling the charging time of garage-connected PEVs. The objective function can be therefore formulated as:

$$min\left(\sum_{t}^{|T|}(P_{RES,t}-P_{garage,t})^2\right), \tag{9.5}$$

where $P_{RES,t}$ represents the power generated locally from RES units at time t, and $P_{garage,t}$ denotes the total PEV charging load at public garages at time t. Note that each PEV will be parked at the public parking garage for a specific duration of time. The algorithm attempts to postpone, if necessary, those PEVs with longer parking duration and higher SOC level, in order to ensure that all PEVs have reached a full or near-full SOC level upon being picked up by the vehicle owner and thereby to alleviate the stress on the distribution grid during peak hours.

IEEE Transactions on Smart Grid, vol. 4, no. 3, pp. 1381-1390.

9.4.3 Constraints

The following constraints are considered in the proposed IntVGR algorithm:

(i) To ensure an acceptable power quality at the household utilization level, the per-unit magnitude of voltage at each node must be always maintained within the acceptable range given by [18]:

$$V_{min} \leq V_{k,t} \leq V_{max}, \forall k \in \mathcal{H}, t \in \mathcal{T}, \tag{9.6}$$

where V_{min} and V_{max} represent the minimum and maximum limit, respectively. Note that as the distribution grid topology in this study is based on single phase, asymmetric voltage on the other phase due to PEV loads is not considered.

(ii) The total system-level power demand can not be higher than the original base load peak demand level P_{orig} at all times:

$$\sum_{k}^{|\mathcal{H}|} P_{k,t} \leq P_{orig}, \forall t \in \mathcal{T}. \tag{9.7}$$

(iii) To optimize the battery lifetime, the battery can never be over-charged (SOC_{max}) or over-depleted (SOC_{min}):

$$SOC_{min} \leq SOC_{i,t} \leq SOC_{max}, \forall i \in \mathcal{N}, t \in \mathcal{T}, \tag{9.8}$$

where $SOC_{i,t}$ denotes the battery SOC of PEV i at time t.

(iv) For each PEV i, the number of charging as usual, discharging and idle slots scheduled by the proposed algorithm, denoted by $N_{ch,i}$, $N_{dis,i}$, and $N_{idle,i}$, respectively, should satisfy the following relationship:

$$N_{ch,i} + 2 \cdot N_{dis,i} + N_{idle,i} = \left(\frac{t_{deadline,i} - t_{arr,i}}{T_{slot}} \right), \\ \forall i \in \mathcal{N}. \tag{9.9}$$

Note that $N_{dis,i}$ is doubled in Eq. (9.9) to account for the number of charging slots for the sake of replenishing the discharged energy if R_{ch} and R_{dis} are equal.

IEEE Transactions on Smart Grid, vol. 4, no. 3, pp. 1381-1390.

(v) Local capacity of transformers and cables, for instance, might become barriers to the adoption rate of PEVs. Our additional impact studies, which are not provided in this paper due to space limitations, have not observed any local overloading events in the scenario of random charging for the specific distribution network in this study. Therefore, local element capacity limits will not be formulated as constraints in this paper, but might be easily taken into account for other heavily loaded distribution networks.

9.4.4 Electricity market concerns

In the future PEVs may be grouped and coordinated by some aggregating agents, especially when the V2G operation mode is enabled, due to the fact that a single PEV does not have adequate capacity to exploit business opportunities in the electricity markets. The aggregating agent can be either a utility, such as the distribution system operator (DSO), or some third party for-profit entities [19, 20, 21]. As previously mentioned, the aggregator as the superior controlling unit in this study is served by the DMS, which is directly controlled by the DSO [3]. The DSO has the right to schedule PEVs on the basis of its own constraints: mostly peak shaving to reduce the power variation on the transmission grid and the variation in power purchases from the power producers, but also other criteria, such as reducing power losses and asset congestions in the distribution grid.

It is worth noting that the objectives of the scheduling scheme currently proposed in this work is from the technical point of view, while electricity markets and market-based financial benefits to PEV owners or the aggregation unit are not taken into account. Therefore, our current approach is valid in jurisdictions where no electricity markets are involved. In addition, as stated in [3] where a hierarchical technical and market management structure was proposed, our approach is also valid when the power grid is approaching its technical restrictions or the grid is operated in abnormal or emergency conditions (e.g., contingencies and islanded operation), in which case the DMS headed by the DSO will act over, and if necessary, override V2G/G2V decisions from market-oriented aggregators with pure economic interests, if there are any.

In spite of this, the authors acknowledge that it is still important for our future work to integrate electricity market features in the scheduling scheme facilitated by the aggregation unit. Some recent works have already studied the market model of the aggregator, for example, based on maximization of financial profits from providing ancillary services (frequency regulation and spinning reserves) [22] or energy trading-related profits [19]. However, these analyses were performed at the bulk power level and ignored technical constraints at the distribution level. The authors in [19] concluded that current market policies and mechanisms with regard to PEV deployment need to be revised so as to provide sufficient incentives, especially for those third-party aggregating business, to take into account the technical perspective of the power grid in order to prevent imposing detrimental impacts on grid operations due to their for-profit V2G/G2V decisions.

Under current policies, the DSO is not allowed to be able to compete with other players in the market due to its advantage of having access to the network details. Instead, as previously mentioned and discussed in [3], the DSO sees the third party aggregator as an important actor in the distribution grid operation. Prior to approving the for-profit aggregator to proceed to any market negotiation, the DSO will perform an ex ante validation of V2G/G2V decisions (sell/buy bids) proposed by the aggregation unit, and if necessary, the DSO will ask the aggregator to make proper changes on the proposal until a safe technical feasibility is guaranteed (e.g., branch congestions, voltage profiles, etc.) [20, 21]. The DSO might mandate the aggregator to make further changes on its plan according to some other grid control purposes. This is how the technical and the market perspectives are integrated.

Therefore, to integrate the electricity market perspective into our current scheduling scheme, the aforementioned technical and market management structure could be modeled. The objectives will differ from those proposed in this work, and instead the scheduling might be based on maximization of the financial profits for the aggregator by optimizing energy and ancillary service scheduling, or minimization of the charging costs for the PEV owner [21]. The technical aspects, i.e., network constraints and some specific targets imposed by the DSO for a given feeder, such as peak shaving and minimized power losses as formulated in Eqs. (9.1) and (9.4), can be easily integrated into the optimization formulation by adapting the objective functions to additional constraints. These technical constraints, however, do not imply that the aggregator will have access to the network details as the DSO does, but rather represent the aforementioned ex ante validation procedure by the DSO, which ensures a safe grid operation. Another option to deal with the technical perspective might be based on transforming the technical constraints into equivalent monetary costs and keep them also in the objective function, similar to the work in [23].

It is worth emphasizing that the main focus of this work is on co-simulating the information interactions required to facilitate a specific PEV scheduling scheme and examining its performance from both power systems and communications viewpoints. In our future work, hence, instead of combining the technical and the market perspectives together in the scheduling formulation as previously explained, it is also possible to co-simulate the interactions among all the involved entities within the technical and market management framework, where the ex ante proposal/validation process between the DSO and the for-profit aggregator will also be modeled by simulating the information exchange between them, and to investigate the impacts of the scheduling decisions from the for-profit aggregator on the distribution grid operations and constraints.

9.5 Co-simulation Results

This section provides co-simulation results for our proposed IntVGR scheduling algorithm. We also consider a well-performing smart charging scheme recently proposed in [5] for benchmark comparison.

9.5.1 Co-simulation configurations

The proposed IntVGR scheduling algorithm is tested in our recently developed co-simulation environment, which is built using OMNeT++, while the power systems layer is modeled and load flow analysis is performed in OpenDSS. The architecture of the co-simulation platform is explained in details in our previous work [15]. We provide below a brief summary on the specific configurations used in this paper regarding the distribution network, the FiWi communications infrastructure, and the investigated scenarios.

IEEE Transactions on Smart Grid, vol. 4, no. 3, pp. 1381-1390.

Distribution grid configurations

Our co-simulation model is configured according to the following settings for the power distribution network:

— *Distribution network topology*: The distribution network is a modified IEEE 13-node radial distribution feeder [24], as depicted in Fig. 9.3. It has 18 LV residential networks, each of which consists of 19 customer households, representing 342 households in total.

— *PEVs*: PEVs are modeled based on the specification of a commercial PEV model, Nissan LEAF [1] (Table 9.1). Each PEV is associated with a specific home arrival time, home departure time, and daily driving distance based on realistic data extracted from the National Household Travel Survey (NHTS) 2001 [2].

— *Public parking garages*: Two public parking garages are available at node 632 and 684, respectively, where vehicle owners can park and charge their PEVs during work time.

— *RES*: PV panels are assumed available at parking garages. Each PV panel is configured to have an area of 500 m^2, with a conversion efficiency of 12% and an inverter efficiency of 95% [3]. Based on the sun irradiance level in Montréal [4], the hourly distribution of the generation capacity from PV panels can be determined, as shown in Fig. 9.4.

— *Residential base load*: A base load profile is applied at each household to model its daily base load consumption. The load shape is obtained from the RELOAD [5] database for both summer and winter. For each season, two additional load curves are generated by time shifting the original load shape by +/- 1 hour to account for discrepancies in residential daily routines. At each household and hour, the load randomly varies among the three aforementioned load profiles based on a uniform distribution. The maximum power demand and power factor are set to 2 kW and 0.95 [5], respectively, at each household.

1. LEAF's manual is available at `http://www.nissanusa.com/leaf-electric-car`.
2. The NHTS dataset is available at `http://nhts.ornl.gov`.
3. Efficiencies are given at `http://www.solarbuzz.com/`.
4. Sun irradiance level data is available at `http://www.climate.weatheroffice.qc.ca/`.
5. RELOAD Database Documentation and Evaluation and Use in NEMS is available at `http://www.onlocationinc.com/LoadShapesReload2001.pdf`.

IEEE Transactions on Smart Grid, vol. 4, no. 3, pp. 1381-1390.

Tableau 9.1 – PEV Model Configuration

Model	Nissan LEAF
Battery capacity	24 kWh
Maximum depletable capacity	80%
Electric drive efficiency	0.26 kWh/mile [25]
Charge/Discharge efficiency	90% [26]
Charging infrastructure	Level 1 [27]
Power rating	1.44 kW (120VAC/12A)

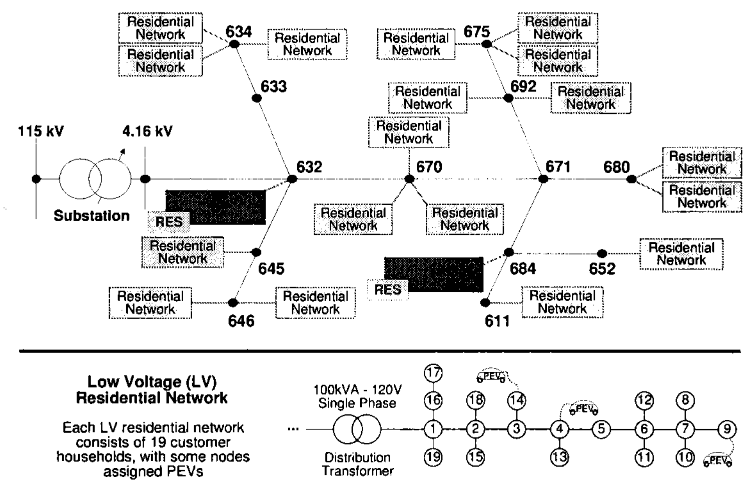

Figure 9.3 – Single line diagram of the 342-node distribution network topology.

FiWi-based communications infrastructure configurations

An EPON of 32 ONUs with a line rate of 1 Gbps is used for the fiber backhaul. The ONU nodes are distributed uniformly to cover the entire distribution grid of 342 customer households. A wireless mesh network based on IEEE 802.11g with a line rate of 54 Mbps is used to aggregate sensor data for those customer households without a direct connection to an ONU. The wireless mesh network forwards their packets through the closest ONU collocated with an MPP. The notification message rate, λ_{notif}, is set to 1 message per second. Due to space limitations, we do not evaluate the impact of λ_{notif} on our proposed IntVGR scheme. Nodal voltage and power consumption measurements are assumed to be available directly without any sensing delay or error.

IEEE Transactions on Smart Grid, vol. 4, no. 3, pp. 1381-1390.

Definition of investigated scenarios

Two penetration levels (PLs), i.e., 42% and 84%, are tested in the simulation. We introduce a coefficient η, which specifies the ratio of $P_{desired}$ to P_{orig}. The smaller the value of η is, the lower the peak demand level is desired and the longer the V2G period is extended. To be more specific, $P_{desired} = (342 \times 2) \cdot \eta$ in kW, where 342×2 corresponds to the system-level peak demand for non-PEV loads. η is varied from 0.80 to 0.95.

The following simulation scenarios are considered:

— *H-R:* This scenario serves as the business-as-usual (BAU) scenario, in which case PEVs are charged in a random and uncoordinated manner immediately upon arrival at home until being fully replenished, and therefore, no ICTs are involved.

— *H-S:* A smart charging scheme recently proposed in [5] is applied to home scheduling, which attempts to maintain the original base load peak demand level while minimizing the total power losses. This scenario serves as a benchmark test case for efficacy validation of the proposed IntVGR scheduling algorithm. The reason for taking this scheme as benchmark is that its objective is also from the technical viewpoint of power system (network constraints) instead of cost-benefit analysis as proposed in some other studies, and it has been demonstrated to successfully control the system peak demand level and regulate voltage deviations.

— *W-R/H-S:* Added to the aforementioned *H-S* scenario, public parking garages become available and thus enable parked PEVs to get charged in an uncoordinated manner during work hours.

— *IntVGR(η, w/o RES):* The proposed IntVGR algorithm is applied but no local RES generation unit is available.

— *IntVGR(η, w/ RES):* The proposed IntVGR is implemented with its full functionality.

Computation complexity

The proposed IntVGR algorithm may require a significant amount of calculations to find optimal solutions, depending on the value of parameters involved in scheduling. To decrease the computation

IEEE Transactions on Smart Grid, vol. 4, no. 3, pp. 1381-1390.

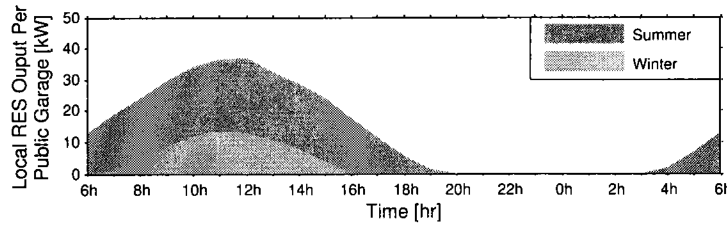

Figure 9.4 – Hourly distribution of the generation capacity from the local RES unit at the public parking garage (workplace).

complexity, first of all, the considered time frame, $\mathcal{T}$, must be finite, and intuitively, $\mathcal{T}$ could be set to 24 hours in order to schedule PEVs on a daily basis. Meanwhile, discretization of $\mathcal{T}$ into time slots (T_{slot}) significantly reduces the number of required power flow analyses. Furthermore, in order to cut down even more the number of calculations, we created a caching system in our co-simulator, exposed in our previous work [15], which avoids rerunning the same power flow analysis two times. In our numerical simulations, a T_{slot} of 15 minutes, which has also been suggested as a likely interval for PEV scheduling in [3], and a $\mathcal{T}$ set to 24 hours along with the aforementioned caching system have not led to a large computation time.

9.5.2 Results for the performance of distribution grid

The following performance metrics are measured and examined: (*i*) D_{peak} denotes the peak power demand in kW needed from the main source, (*ii*) L_{max} denotes the maximum system losses in kW, including both line losses and transformer losses, (*iii*) V_{min} represents the minimum per unit (p.u.) value of voltage at the node with the worst daily voltage profile, (*iv*) $V2G_{max}$ denotes the maximum power in kW fed back to the grid by aggregated PEVs, and (*v*) SOC_{final} indicates the average SOC in percentage upon PEV's deadline.

Table 9.2 shows the results for the aforementioned scenarios based on a PL of 42% and a summer base load profile. One of the main objectives of the proposed IntVGR algorithm is to smoothen the overall demand profile by shaving the peak. Despite that the benchmark *H-S* scenario successfully maintains the same peak level as P_{orig} (681.49 kW), our proposed IntVGR algorithm is able to achieve much more. The performance in terms of peak shaving and valley filling for different charging strategies is shown in Fig. 9.5. It can be observed that the *H-R* scenario increases D_{peak} significantly

IEEE Transactions on Smart Grid, vol. 4, no. 3, pp. 1381-1390.

and the *W-R/H-R* scenario enables public parking garages to share some of the charging burden during periods of already high demand. The *H-S* scenario successfully avoids the situation where PEV charging activities coincide with household peaks. In comparison, the *IntVGR(0.90, w/o RES)* scenario achieves a peak demand even lower than P_{orig} by coordinating feasible PEVs to provide V2G services during peak hours. Fig. 9.6 provides a closer look at the IntVGR algorithm between G2V and V2G modes. D_{peak} is further shaved as η decreases. With η equal to 0.80, D_{peak} is brought down to 605.79 kW, decreased by 21% compared to that in the BAU scenario.

The second metric in Table 9.2, L_{max}, is reduced by 30% from 22.65 kW in the *IntVGR(0.80, w/o RES)* scenario compared to that in the BAU scenario. The distribution system operator is concerned about power losses, which could be potentially compensated by increasing the electricity tariffs at customer premises. Based on the deployment of ICTs, intolerable voltage deviations are avoided and V_{min} at all nodes is always maintained within the acceptable limit ([0.95, 1.05] p.u under normal conditions), as shown in Fig. 9.7. Compared to the benchmark *H-S* scenario, the proposed IntVGR algorithm achieves a better performance in voltage regulation.

It is worth noting that for some η, $P_{desired}$ cannot be always reached. For example, with η equal to 0.80, D_{peak} is only shaved to 605.79 kW, or equivalently 85% of D_{orig}, and $V2G_{max}$ increases by only 4.32 kW, corresponding to three more PEVs, as η decreases from 0.85 to 0.80. This can be explained by the fact that our proposed IntVGR algorithm also takes PEV owner's need into account, which is illustrated in Fig. 9.8. It can also be observed from Table 9.2 that SOC_{final} is not sacrificed but maintained at a fairly satisfying level (above 99.88%).

Tableau 9.2 – Co-simulation results for a PL of 42% and a summer base load profile.

	w/o ICTs	w/ ICTs									
	H-R	*H-S*		*IntVGR(η, w/o RES)*				*IntVGR(η, w/ RES)*			
		w/o *W-R*	w/ *W-R*	η=0.95	η=0.90	η=0.85	η=0.80	η=0.95	η=0.90	η=0.85	η=0.80
D_{peak} [kw]	759.87	681.49	678.16	666.54	635.20	633.84	605.79	653.27	630.55	609.09	584.09
L_{max} [kw]	32.34	27.22	26.90	26.12	24.05	24.00	22.65	26.29	24.59	23.92	22.49
V_{min} [pu]	0.9443	0.9507	0.9531	0.9522	0.9548	0.9553	0.9558	0.9521	0.9528	0.9528	0.9552
$V2G_{max}$ [kw]	0	0	0	38.88	69.12	87.84	92.16	21.60	50.40	73.44	87.84
SOC_{final} [%]	100.00	99.63	100.00	100.00	99.95	99.88	99.90	100.00	100.00	99.94	100.00

IEEE Transactions on Smart Grid, vol. 4, no. 3, pp. 1381-1390.

Another objective of the proposed IntVGR algorithm is to take maximum utilization of low-cost energy generated locally from RES units, considering the fact that most PEVs are parked for quite a long period during the day and as such give sufficient flexibility of their charging time. As shown in Fig. 9.9, in an uncoordinated and random manner, there is a garage charging peak at 9 a.m. due to most PEVs arriving at work around that time, and thereby, some PEVs need to take power from the grid as a result of not sufficient capacity from local RES units. The *IntVGR(0.90, w/ RES)* scenario, in contrast, is able to track the RES output profile by putting off those PEVs with relatively longer parking duration to a later time when the RES output increases. For example at 9 a.m., only 38 out of 80 PEVs are enabled by the IntVGR algorithm to charge while the remaining 42 ones are delayed. Note that with the same η, *IntVGR(η, w/ RES)* scenarios result in lower D_{peak} and $V2G_{max}$ than *IntVGR(η, w/o RES)* scenarios do, as can be observed in Table 9.2, which can be explained by the fact that a surplus of RES output, if applicable, is fed back to the grid and to some extent contributes in peak shaving.

The sensitivity to the PEV adoption rate of our proposed IntVGR algorithm is then tested with a higher PL of 84%, the results of which are given in Table 9.3. Besides similar results to those previously mentioned, we make some new observations. As the PL is high, a higher morning peak exists as a result of PEVs charging at public parking garages (e.g., D_{peak} is 651.40 kW in *IntVGR(η, w/o RES)* scenarios with η equal to 0.90, 0.85, and 0.80). Although the garage charging demand is more than the amount that local RES units can provide, the IntVGR algorithm makes its best effort in coordinating PEVs for utilization of local renewables and preventing the occurrence of the aforementioned peak during morning hours, as depicted in Fig. 9.10.

As the PL rises, more efforts are required to aggregate PEVs to provide V2G services. We note that as the PL is doubled from 42% to 84%, $V2G_{max}$, however, is not doubled, which can be explained by the fact that a higher PL results in a higher probability that PEVs have to be interrupted from V2G mode and switched back to G2V mode within the V2G period for the sake of reaching a satisfying SOC level by the desired deadline. As observed in Table 9.3, SOC_{final} is slightly worsened by only 1%.

IEEE Transactions on Smart Grid, vol. 4, no. 3, pp. 1381-1390.

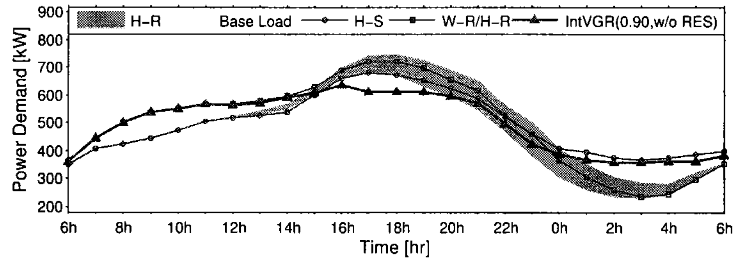

Figure 9.5 – The overall demand profile in different simulation scenarios based on a PEV penetration level of 42% and a summer base load profile.

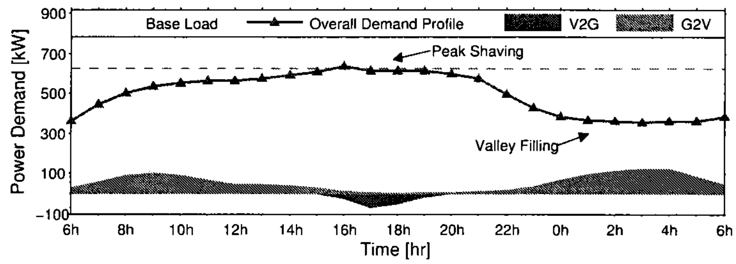

Figure 9.6 – Operation of G2V and V2G modes in the *IntVGR(0.90, w/o RES)* scenario based on a PEV penetration level of 42% and a summer base load profile.

We also validate the efficacy of our proposed algorithm with a winter base load profile. Similar findings to Table 9.2 and 9.3 were obtained, but results are not given in this paper due to space limitations.

To sum up, our proposed IntVGR algorithm has been demonstrated to successfully smoothen the overall demand profile by peak shaving and valley filling, the peak-to-average ratio (PAR) of which can be brought down to 1.28 with η equal to 0.90 and even lower as η further decreases. This is much improved compared to a PAR of 1.50 for the BAU scenario and 1.38 for the benchmark scenario, allowing the utility to run the power grid at decreased peak provisioning with higher system efficiency, lower costs, and also reduced carbon emissions. It has also been proved effective in coordinating PEV charging loads based on tracking the generation profile of local RES units. Note that in simulations, we use a forecast output profile known in advance for local RES units. To deal with unpredictable uncertainties/deviations involved in generation/load profiles, we have proposed and examined in our previous work [14] a reactive coordination scheme, which is able to adjust the scheduling results with respect to unknown variations, but this is not the main focus of this paper.

IEEE Transactions on Smart Grid, vol. 4, no. 3, pp. 1381-1390.

Tableau 9.3 – Co-simulation results for a PL of 84% and a summer base load profile.

	w/o ICTs	w/ ICTs									
	H-R	*H-S*		*IntVGR(η, w/o RES)*				*IntVGR(η, w/ RES)*			
		w/o *W-R*	w/ *W-R*	η=0.95	η=0.90	η=0.85	η=0.80	η=0.95	η=0.90	η=0.85	η=0.80
D_{peak} [kw]	850.08	683.29	679.13	667.46	651.40	651.40	651.40	668.71	641.59	624.28	595.51
L_{max} [kw]	38.89	27.21	26.88	26.17	24.26	23.40	20.48	25.86	24.24	23.19	20.53
V_{min} [pu]	0.9397	0.9503	0.9531	0.9527	0.9536	0.9542	0.9533	0.9484	0.9518	0.9537	0.9544
$V2G_{max}$ [kw]	0	0	0	40.32	83.53	119.52	138.24	48.96	90.72	122.40	151.20
SOC_{final} [%]	99.87	98.82	99.93	99.92	99.87	99.66	99.24	99.72	99.57	99.30	98.88

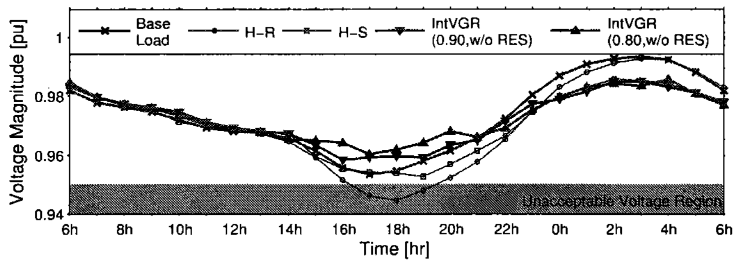

Figure 9.7 – Worst nodal voltage profile based on a PEV penetration level of 42% and a summer base load profile.

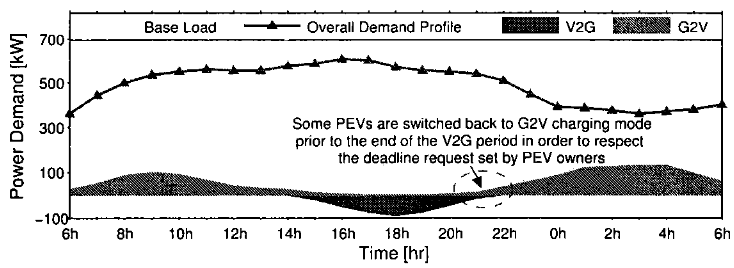

Figure 9.8 – Operation of G2V and V2G modes in the *IntVGR(0.80, w/o RES)* scenario based on a PEV penetration level of 42% and a summer base load profile.

9.5.3 Interoperability with the supporting communications infrastructure

The performance of the communications infrastructure also plays a critical role for deployment of the proposed scheduling algorithm. Two main performance metrics are examined, namely, channel throughput and delay. Due to space limitations, we show selected results for the aforementioned scenarios from a communications perspective.

For all the simulation scenarios, the bandwidth utilization is observed to vary significantly with the PL and whether garage scheduling with RESs is deployed, as depicted in Fig. 9.11. During the simulation interval from 26 to 42 seconds, corresponding to 6 to 10 a.m. on the virtual distribution

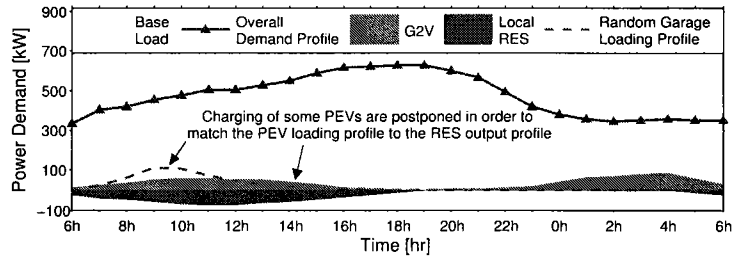

Figure 9.9 – Workplace scheduling with RESs in the *IntVGR(0.90, w/o RES)* scenario based on a PEV penetration level of 42% and a summer base load profile.

system layer (VDSL), bandwidth utilization is higher for scenarios with RESs scheduling enabled and remains unchanged if PEVs are charged in an uncoordinated manner at public garages. Note that 1 simulation second corresponds to 15 minutes on the VDSL and the interval up to 26 seconds is basically used for simulation initialization and thus not shown in the figure. During peak hours, starting from 70 seconds, the throughput significantly increases for both PLs as a large volume of home G2V-V2G requests/responses as well as other messages such as SOC information packets are exchanged between PEVs and the DMS. The channel throughput reaches the peak at around 114 seconds (4 a.m. on the VDSL). This is caused by the fact that the number of PEVs that are in charging (G2V) mode reaches the maximum at 4 a.m. and thereby the number of SOC messages exchanged between PEVs and the DMS also reaches the maximum amount, which is consistent with the findings in Fig. 9.8 where G2V charging load reaches the maximum at 4 a.m.. When the PL is doubled from 42% to 84%, the number of PEVs is doubled, which might explain the observation that the channel throughput due to exchanging PEV-related messages is also roughly doubled at critical time points. Note that the bandwidth taken up by information interactions other than PEV-related messages, such as notification messages containg the sensor data for grid monitoring (loads, nodal voltages, etc.), is approximately 1.3 Mbps, and it remains unchanged over time for both two PLs as the number of household is fixed.

With regard to the second metric, as shown in Fig. 9.12, the upstream end-to-end delay measured at the DMS is approximately 1 ms and, as expected, is slightly higher on average for a higher PL, which is consistent with observations for the channel throughput. Note that the end-to-end delay takes into account the transmission, propagation, and queuing delays. We do not evaluate computation times. The delay reaches its highest level during 66 to 90 simulation seconds (4 p.m.

IEEE Transactions on Smart Grid, vol. 4, no. 3, pp. 1381-1390.

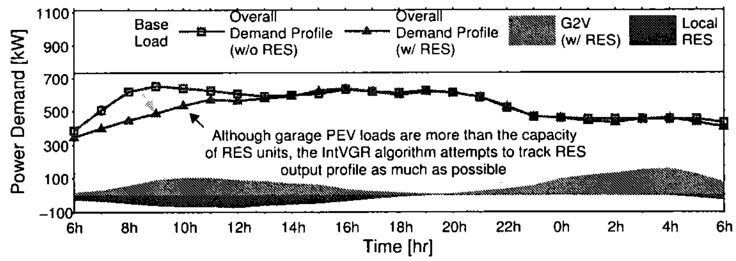

Figure 9.10 – Workplace scheduling with RESs based on a PEV penetration level of 84% and a summer base load profile, $\eta = 0.90$.

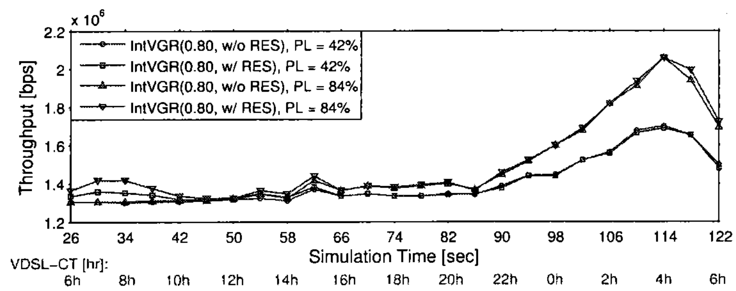

Figure 9.11 – Upstream throughput measured at the DMS for different PLs.

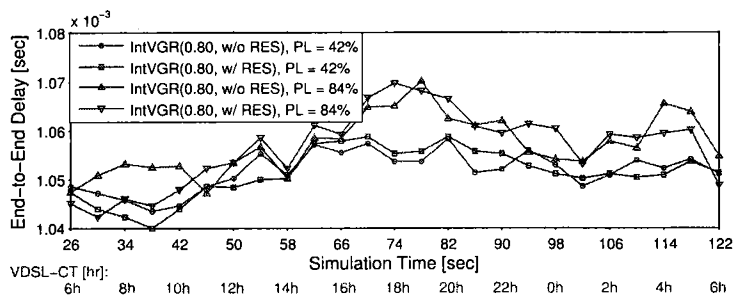

Figure 9.12 – Upstream end-to-end delay measured at the DMS for different PLs.

to 22 p.m. on the VDSL). This can be explained by the fact that most PEVs arrive at home during this period and contend for the wireless network channel bandwidth to exchange their messages to the DMS through an ONU, and therefore packet collision is more likely to occur as multiple PEVs attempt to transmit their messages to an ONU simultaneously.

Note that 1-2 Mbps were required by the proposed algorithm with the aforementioned configurations. Depending on the sensitivity required by the utility, λ_{notif} can be changed. As our proposed communications infrastructure has the potential of sharing its bandwidth with other applications, such as voice and video, quality-of-service issues could be noted. We addressed this problem in our previous work [28], to which interested readers are referred for further details.

9.6 Conclusions

In this paper, our proposed IntVGR algorithm has been implemented in a co-simulation environment by exchanging real-time message and data between the DMS and PEVs over a converged FiWi broadband access network. Its performance from both power systems and communications perspectives has been examined. Results demonstrate its effectiveness in smoothening the overall demand profile and controlling PEVs to make maximum utilization of local RES capacity. Grid constraints as well as vehicle owners's satisfaction are both taken into account. To deploy the proposed scheme over a distribution grid consisting of 342 customer households, the utilized upstream bandwidth is found to be 1-2 Mbps, which occupies a fairly low level of the EPON channel resources and a low end-to-end delay of 1 ms is obtained. The multidisciplinary study performed in this paper can be further extended to accommodate various smart grid applications and services in more complex physical-cyber systems.

References

[1] A. G. Boulanger, A. C. Chu, S. Maxx, and D. L. Waltz, "Vehicle Electrification: Status and Issues," *Proc. IEEE*, vol. 99, no. 6, pp. 1116–1138, Jun. 2011.

[2] L. Pieltain Fernández *et al.*, "Assessment of the Impact of Plug-in Electric Vehicles on Distribution Networks," *IEEE Trans. Smart Grid*, vol. 26, no. 1, pp. 206–213, Feb. 2011.

[3] J. A. P. Lopes, F. J. Soares, and P. M. R. Almeida, "Integration of Electric Vehicles in the Electric Power System," *Proc. IEEE*, vol. 99, no. 1, pp. 168–183, Jan. 2011.

[4] K. Clement-Nyns, E. Haesen, and J. Driesen, "The Impact of Charging Plug-In Hybrid Electric Vehicles on a Residential Distribution Grid," *IEEE Trans. Power Syst.*, vol. 25, no. 1, pp. 371–380, Feb. 2010.

[5] S. Deilami *et al.*, "Real-Time Coordination of Plug-In Electric Vehicle Charging in Smart Grids to Minimize Power Losses and Improve Voltage Profile," *IEEE Trans. Smart Grid*, vol. 2, no. 3, pp. 456–467, Sep. 2011.

[6] E. Sortomme, M. M. Hindi, S. D. J. MacPherson, and S. S. Venkata, "Coordinated Charging of Plug-In Hybrid Electric Vehicles to Minimize Distribution System Losses," *IEEE Trans. Smart Grid*, vol. 2, no. 1, pp. 198–205, Mar. 2011.

[7] Y. Cao *et al.*, "An Optimized EV Charging Model Considering TOU Price and SOC Curve," *IEEE Trans. Smart Grid*, vol. 3, no. 1, pp. 388–393, Mar. 2011.

[8] W. Su and M. Y. Chow, "Performance Evaluation of an EDA-Based Large-Scale Plug-In Hybrid Electric Vehicle Charging Algorithm," *IEEE Trans. Smart Grid*, vol. 3, no. 1, pp. 308–315, Mar. 2012.

IEEE Transactions on Smart Grid, vol. 4, no. 3, pp. 1381-1390.

[9] D. P. Tuttle and R. Baldick, "The Evolution of Plug-In Electric Vehicle-Grid Interactions," *IEEE Trans. Smart Grid*, vol. 3, no. 1, pp. 500–505, Mar. 2012.

[10] K. Clement-Nyns, E. Haesen, and J. Driesen, "The Impact of Vehicle-to-grid on the Distribution Grid," *Electr. Power Syst. Res.*, vol. 81, no. 1, pp. 185–192, Jan. 2011.

[11] A. Y. Saber and G. K. Venayagamoorthy, "Plug-in Vehicles and Renewable Energy Sources for Cost and Emission Reductions," *IEEE Trans. Ind. Electron.*, vol. 58, no. 4, pp. 1229–1238, Apr. 2011.

[12] IEEE 2030, "Guide for Smart Grid Interoperability of Energy Technology and Information Technology Operation with the Electric Power System (EPS), and End-Use Applications and Loads," *IEEE Standards Association*, Sep. 2011.

[13] P. Palensky and D. Dietrich, "Demand Side Management: Demand Response, Intelligent Energy Systems, and Smart Loads," *IEEE Trans. Ind. Inf.*, vol. 7, no. 3, pp. 381–388, Aug. 2011.

[14] M. Lévesque, D. Xu, G. Joós, and M. Maier, "Co-Simulation of PEV Coordination Schemes over a FiWi Smart Grid Communications Infrastructure," in *Proc., IEEE Ind. Electron. Soc. Annu. Conf. (IECON)*, Montreal, QC, Canada, Oct. 2012.

[15] M. Lévesque, D. Xu, M. Maier, and G. Joós, "Communications and Power Distribution Network Co-Simulation for Multidisciplinary Smart Grid Experimentations," in *Proc., SCS/ACM Spring Simulation Multi-Conf.*, Orlando, FL, USA, Mar. 2012.

[16] M. Maier, M. Lévesque, and L. Ivănescu, "NG-PONs 1&2 and Beyond: The Dawn of the Über-FiWi Network," *IEEE Netw.*, vol. 26, no. 2, pp. 15–21, March/April 2012.

[17] S. Shao, M. Pipattanasomporn, and S. Rahman, "Grid Integration of Electric Vehicles and Demand Response With Customer Choice," *IEEE Trans. Smart Grid*, vol. 3, no. 1, pp. 543–550, Mar. 2012.

[18] American National Standards Institute, "National Electrical Manufacturers Association (NEMA) ANSI C84.1-1995-American National Standard for Electric Power Systems and Equipment-Voltage Ratings (60 Hertz)," *American Nat. Standards Inst., Nat. Elect. Manufacturers Assoc.*, 2006.

IEEE Transactions on Smart Grid, vol. 4, no. 3, pp. 1381-1390.

[19] D. Wu, D. C. Aliprantis, and L. Ying, "Load Scheduling and Dispatch for Aggregators of Plug-in Electric Vehicles," *IEEE Trans. Smart Grid*, vol. 3, no. 1, pp. 368–376, Mar. 2012.

[20] R. J. Bessa, M. A. Matos, F. J. Soares, and J. A. P. Lopes, "Optimized Bidding of a EV Aggregation Agent in the Electricity Market," *IEEE Trans. Smart Grid*, vol. 3, no. 1, pp. 443–452, Mar. 2012.

[21] E. Sortomme and M. A. El-Sharkawi, "Optimal Scheduling of Vehicle-to-Grid Energy and Ancillary Services," *IEEE Trans. Smart Grid*, vol. 3, no. 1, pp. 351–359, Mar. 2012.

[22] S. Han, S. Han, and K. Sezaki, "Development of an Optimal Vehicle-to-Grid Aggregator for Frequency Regulation," *IEEE Trans. Smart Grid*, vol. 1, no. 1, pp. 65–72, 2010.

[23] J. Xu and V. W. S. Wong, "An Approximate Dynamic Programming Approach for Coordinated Charging Control At Vehicle-to-Grid Aggregator," in *Proc., IEEE International Conf. on Smart Grid Communications*, Brussels, Belgium, Oct. 2011, pp. 279–284.

[24] W. H. Kersting, "Radial Distribution Test Feeders," *IEEE Trans. Power Syst.*, vol. 6, no. 3, pp. 975–985, Aug. 1991.

[25] M. Duvall, "Advanced Batteries for Electric-Drive Vehicles," *Final Rep. 1009299, Elect. Power Res. Inst.*, May 2004.

[26] W. X. Shen, C. C. Chan, E. W. C. Lo, and K. T. Chau, "Estimation of Battery Available Capacity under Variable Discharge Currents," *J. Power Sources*, vol. 103, no. 2, pp. 180–187, Mar. 2002.

[27] SAE J1772, "Electric Vehicle Conductive Charge Coupler," *SAE Recommended Practice*, 2009.

[28] M. Lévesque, M. Maier, Y. Desai, and G. Joos, "Adaptive Admission Control for a Smart Grid FiWi Communications Network facing Power Blackouts during a DDoS Attack," in *Proc., IEEE Green Technologies Conference*, Tulsa, OK, USA, Apr. 2012.

Troisième partie

Appendices

Chapitre 10

FiWi Access Networks Based on Next-Generation PON and Gigabit-Class WLAN Technologies: A Capacity and Delay Analysis

Publication:

— F. Aurzada, M. Lévesque, M. Maier, and M. Reisslein, "FiWi Access Networks Based on Next-Generation PON and Gigabit-Class WLAN Technologies: A Capacity and Delay Analysis," *IEEE/ACM Transactions on Networking*, accepted for publication.

In part I, the smart grid and potential communications technologies were first introduced, whereby we focused on the potential of fiber-wireless (FiWi) access networks integrated with optical and wireless sensors for cost-effective and reliable smart grid communications. More specifically, in Chapter 3, we developed a probabilistic framework allowing to find the theoretical upper bound of the machine-to-machine (M2M) traffic. This work was extended from the paper presented in this chapter, whereby the probabilistic FiWi framework is generic and can be applied to any single-class traffic applications.

IEEE/ACM Transactions on Networking, accepted for publication.

In this paper, we present the first analytical framework to quantify the performance of FiWi network routing algorithms, validate previous simulations studies, and provide insighful guidelines for the design of novel integrated optical-wireless routing algorithms for future FiWi access networks leveraging next-generation PONs, notably long-reach 10+ Gbps TDM/WDM PONs, and emerging Gigabit-class WLAN technologies. The analytical framework is flexible and can be applied to any existing or new optical-wireless routing algorithm. Furthermore, it takes the different characteristics of disparate optical and wireless networking technologies into account. Beside their capacity mismatch and bit error rate differences, the framework also incorporates arbitrary frame size distributions, traffic matrices, optical/wireless propagation delays, data rates, and fiber cuts. We investigate the performance of minimum hop, minimum interference (wireless hop), minimum delay, and our proposed OFRA routing algorithms. The obtained results show that OFRA yields the highest maximum aggregate throughput for both conventional and long-reach wavelength-routing WDM PONs under balanced and unbalanced traffic loads. For a higher loaded fiber backhaul, however, OFRA gives priority to lightly loaded wireless links, leading to an increased mean delay at small to medium wireless traffic loads. We also observe that using very high throughput WLAN helps increase the maximum mean aggregate throughput significantly, while high-speed 10 Gb/s WDM PON helps lower the mean delay especially at medium traffic loads.

IEEE/ACM Transactions on Networking, accepted for publication.

10.1 Abstract

Current Gigabit-class passive optical networks (PONs) evolve into next-generation PONs, whereby high-speed 10+ Gb/s time division multiplexing (TDM) and long-reach wavelength-broadcasting/routing wavelength division multiplexing (WDM) PONs are promising near-term candidates. On the other hand, next-generation wireless local area networks (WLANs) based on frame aggregation techniques will leverage physical layer enhancements, giving rise to Gigabit-class very high throughput (VHT) WLANs. In this paper, we develop an analytical framework for evaluating the capacity and delay performance of a wide range of routing algorithms in converged fiber-wireless (FiWi) broadband access networks based on different next-generation PONs and a Gigabit-class multi-radio multi-channel WLAN-mesh front-end. Our framework is very flexible and incorporates arbitrary frame size distributions, traffic matrices, optical/wireless propagation delays, data rates, and fiber faults. We verify the accuracy of our probabilistic analysis by means of simulation for the wireless and wireless-optical-wireless operation modes of various FiWi network architectures under peer-to-peer, upstream, uniform, and nonuniform traffic scenarios. The results indicate that our proposed optimized FiWi routing algorithm (OFRA) outperforms minimum (wireless) hop and delay routing in terms of throughput for balanced and unbalanced traffic loads, at the expense of a slightly increased mean delay at small to medium traffic loads.

Keywords: Availability, fiber-wireless (FiWi) access networks, frame aggregation, integrated routing algorithms, next-generation PONs, VHT WLAN.

10.2 Introduction

Fiber-wireless (FiWi) access networks, also referred to as wireless-optical broadband access networks (WOBANs), combine the reliability, robustness, and high capacity of optical fiber networks and the flexibility, ubiquity, and cost savings of wireless networks [1]. To deliver peak data rates up to 200 Mb/s per user and realize the vision of complete fixed-mobile convergence, it is crucial to replace today's legacy wireline and microwave backhaul technologies with integrated FiWi broadband access networks [2].

Significant progress has been made on the design of advanced FiWi network architectures as well as access techniques and routing protocols/algorithms over the last few years [3]. Among others, the beneficial impact of advanced hierarchical frame aggregation techniques on the end-to-end throughput-delay performance of an integrated Ethernet passive optical network (EPON)/wireless mesh network (WMN)-based FiWi network was demonstrated by means of simulation and experiment for voice, video, and data traffic [4]. A linear programming based routing algorithm was proposed in [5, 6] with the objective of maximizing the throughput of a FiWi network based on a cascaded EPON and single-radio single-channel WMN. Extensive simulations were conducted to study the throughput gain in FiWi networks under peer-to-peer traffic among wireless mesh clients and compare the achievable throughput gain with conventional WMNs without any optical backhaul. The presented simulation results show that FiWi and conventional WMN networks achieve the same throughput when all traffic is destined to the Internet, i.e., no peer-to-peer traffic, since the interference in the wireless front-end is the major bandwidth bottleneck. However, with increasing peer-to-peer traffic the interferences in the wireless mesh front-end increase and the throughput of WMNs decreases significantly, as opposed to their FiWi counterpart whose network throughput decreases to a much lesser extent for increasing peer-to-peer traffic.

The design of routing algorithms for the wireless front-end only or for both the wireless and optical domains of FiWi access networks has received a great deal of attention, resulting in a large number of wireless, integrated optical-wireless, multipath, and energy-aware routing algorithms. Important examples of wireless routing algorithms for FiWi access networks are the so-called delay-aware routing algorithm (DARA) [7], delay-differentiated routing algorithm (DDRA) [8], capacity and delay aware routing (CaDAR) [9], and risk-and-delay aware routing (RADAR) algorithm [10]. Recently proposed integrated routing algorithms for path computation across the optical-wireless interface include the so-called availability-aware routing [11], multipath routing [12], and energy-aware routing algorithms [13]. Most of these previous studies formulated routing in FiWi access networks as an optimization problem and obtained results mainly by means of simulation.

In this paper, we present to the best of our knowledge the first analytical framework that allows to evaluate the capacity and delay performance of a wide range of FiWi network routing algorithms and provides important design guidelines for novel FiWi network routing algorithms that leverage the different unique characteristics of disparate optical fiber and wireless technologies. Although a few FiWi architectural studies exist on the integration of EPON with long-term evolution (LTE) (e.g., [2]) or worldwide interoperability for microwave access (WiMAX) wireless front-end networks (e.g., [14]), the vast majority of studies, including but not limited to those mentioned in the above paragraph, considered FiWi access networks consisting of a conventional IEEE 802.3ah EPON fiber backhaul network and an IEEE 802.11b/g wireless local area network (WLAN)-based wireless mesh front-end network [15]. Our framework encompasses not only legacy EPON and WLAN networks, but also emerging next-generation optical and wireless technologies such as long-reach and multi-stage 10+ Gb/s time and/or wavelength division multiplexing (TDM/WDM) PONs as well as Gigabit-class very high throughput (VHT) WLAN.

Our contributions are threefold. First, we develop a unified analytical framework that comprehensively accounts for both optical and wireless broadband access networking technologies. We note that recent studies focused either on TDM/WDM PONs only, e.g., [16], or on WLANs only, e.g., [17]. However, there is a need for a comprehensive analytical framework that gives insights into the performance of bimodal FiWi access networks built from disparate yet complementary optical and wireless technologies. Toward this end, our framework is flexibly designed such that it not only takes the capacity mismatch and bit error rate differences between optical and wireless networks into account, but also includes possible fiber cuts of optical (wired) infrastructures.

Second, our analysis emphasizes future and emerging next-generation PON and WLAN technologies, as opposed to many previous studies that assumed state-of-the-art solutions, e.g., conventional IEEE 802.11a WLAN without frame aggregation [17]. Our analytical approach in part builds on previous studies and includes significant original analysis components to achieve accurate throughput-delay modeling and cover the scope of FiWi networks. Specifically, we build on analytical models of the distributed coordination function in WLANs, e.g., [18, 19], and WLAN frame aggregation, e.g., [20]. We develop an accurate delay model for multihop wireless front-ends under nonsaturated and stable conditions for traffic loads from both optical and wireless network nodes, as detailed in Section 10.7.

Third, we verify our analysis by means of simulations and present extensive numerical results to shed some light on the interplay between different next-generation optical and wireless access networking technologies and configurations for a variety of traffic scenarios. We propose an *optimized FiWi routing algorithm (OFRA)* based on our developed analytical framework. The obtained results show that OFRA outperforms previously proposed routing algorithms, such as DARA [8], CaDAR [9], and RADAR [10]. They also illustrate that it is key to carefully select appropriate paths across the fiber backhaul in order to minimize link traffic intensities and thus help stabilize the entire FiWi access network.

To our best knowledge, the presented unified analytical framework is the first to allow capacity and delay evaluations of a wide range of FiWi network routing algorithms, both previously proposed and new ones. Our analytical framework covers not only legacy EPON and WLAN, but also next-generation high-speed long-reach WDM PON and emerging Gigabit-class VHT WLAN technologies.

The remainder of the paper is structured as follows. In Section 10.3, we discuss related work and recent progress on FiWi access networks. Section 10.4 describes FiWi access networks based on next-generation PON and Gigabit-class WLAN technologies in greater detail. Section 10.5 outlines our network model as well as traffic and routing assumptions. The capacity and delay of the constituent fiber backhaul and wireless front-end networks are analyzed in Sections 10.6 and 10.7, respectively, while the stability and end-to-end delay of the entire FiWi access network are evaluated in Section 10.8. Section 10.9 presents numerical and verifying simulation results. Section 10.10 concludes the paper.

10.3 Related Work

The recent survey of hybrid optical-wireless access networks [21] explains the key underlying photonic and wireless access technologies and describes important FiWi access network architectures. Energy-efficient FiWi network architectures as well as energy-efficient medium access control (MAC) and routing protocols were reviewed in [22]. Recent efforts on energy-efficient routing in FiWi access networks focused on routing algorithms for cloud-integrated FiWi networks that of-

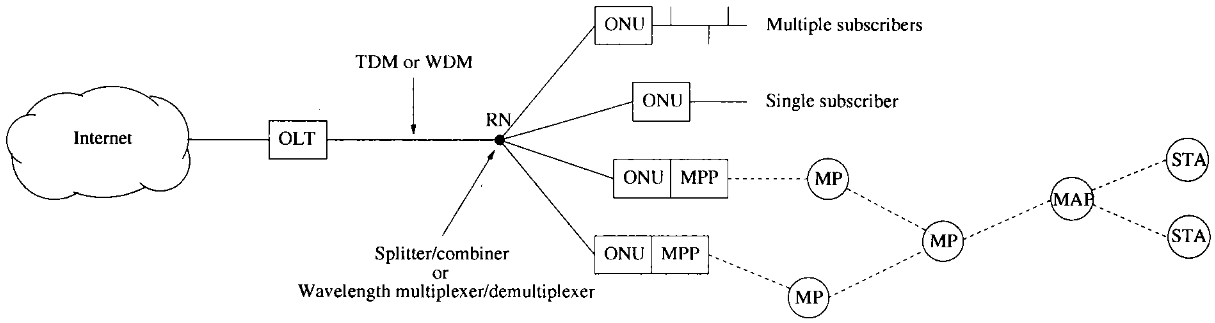

Figure 10.1 – FiWi network architecture based on single- or multi-stage TDM or WDM PON and multihop WMN.

fload the wireless mesh front-end and the optical-wireless gateways by placing cloud components, such as storage and servers, closer to mobile end-users, while at the same time maintaining low average packet delays [23, 24]. A delay-based admission control scheme for providing guaranteed quality-of-service (QoS) in FiWi networks that deploy EPON as backhaul for connecting multiple WiMAX base stations was studied in [25].

A promising approach to increase throughput, decrease delay, and achieve better load balancing and resilience is the use of multipath routing schemes in the wireless mesh front-end of FiWi networks. However, due to different delays along multiple paths, packets may arrive at the destination out of order, which deteriorates the performance of the Transmission Control Protocol (TCP). A centralized scheduling algorithm at the optical line terminal (OLT) of an EPON that resequences the in-transit packets of each flow to ensure in-order packet arrivals at the corresponding destination was examined in [26]. In addition, [26] studied a dynamic bandwidth allocation (DBA) algorithm that prioritizes flows that may trigger TCP's fast retransmit and fast recovery, thereby further improving TCP performance.

Given the increasing traffic amounts on FiWi networks, their survivability has become increasingly important [27, 28]. Cost-effective protection schemes against link and node failures in the optical part of FiWi networks have been proposed and optimized in [29, 30, 31, 32]. The survivability of FiWi networks based on multi-stage PONs, taking not only partial optical protection but also protection through a wireless mesh network into account, was probabilistically analyzed in [33]. Deployment of both back-up fibers and radios was examined in [34].

IEEE/ACM Transactions on Networking, accepted for publication.

Recent research efforts have focused on the integration of performance-enhancing network coding techniques to increase the throughput and decrease the delay of FiWi access networks for unicast and multicast traffic [35, 36].

10.4 FiWi Access Networks

Most previous FiWi access network studies considered a cascaded architecture consisting of a single-stage PON and a multihop WMN, as shown in Fig. 10.1. Typically, the PON is a conventional IEEE 802.3ah compliant wavelength-broadcasting TDM EPON based on a wavelength splitter/combiner at the remote node (RN), using one time-shared wavelength channel for upstream (ONUs to OLT) transmissions and another time-shared wavelength channel for downstream (OLT to ONUs) transmissions, both operating at a data rate of 1 Gb/s. A subset of ONUs may be located at the premises of residential or business subscribers, whereby each ONU provides fiber-to-the-home/business (FTTH/B) services to a single or multiple attached wired subscribers. Some ONUs have a mesh portal point (MPP) to interface with the WMN. The WMN consists of mesh access points (MAPs) that provide wireless FiWi network access to stations (STAs). Mesh points (MPs) relay the traffic between MPPs and MAPs through wireless transmissions. Most previous FiWi studies assumed a WMN based on IEEE 802.11a/b/g WLAN technologies, offering a maximum raw data rate of 54 Mb/s at the physical layer.

Future FiWi access networks will leverage next-generation PON and WLAN technologies to meet the ever increasing bandwidth requirements. A variety of next-generation PON technologies are currently investigated to enable short-term evolutionary and long-term revolutionary upgrades of coexistent Gigabit-class TDM PONs [37]. Promising solutions for PON evolution toward higher bandwidth per user are (*i*) data rate upgrades to 10 Gb/s and higher, and (*ii*) multi-wavelength channel migration toward wavelength-routing or wavelength-broadcasting WDM PONs with or without cascaded TDM PONs [38, 39]. Similarly, to alleviate the bandwidth bottleneck of the wireless mesh front-end, future FiWi networks are expected to be based on next-generation IEEE 802.11n WLANs, which offer data rates of 100 Mb/s or higher at the MAC service access point, as

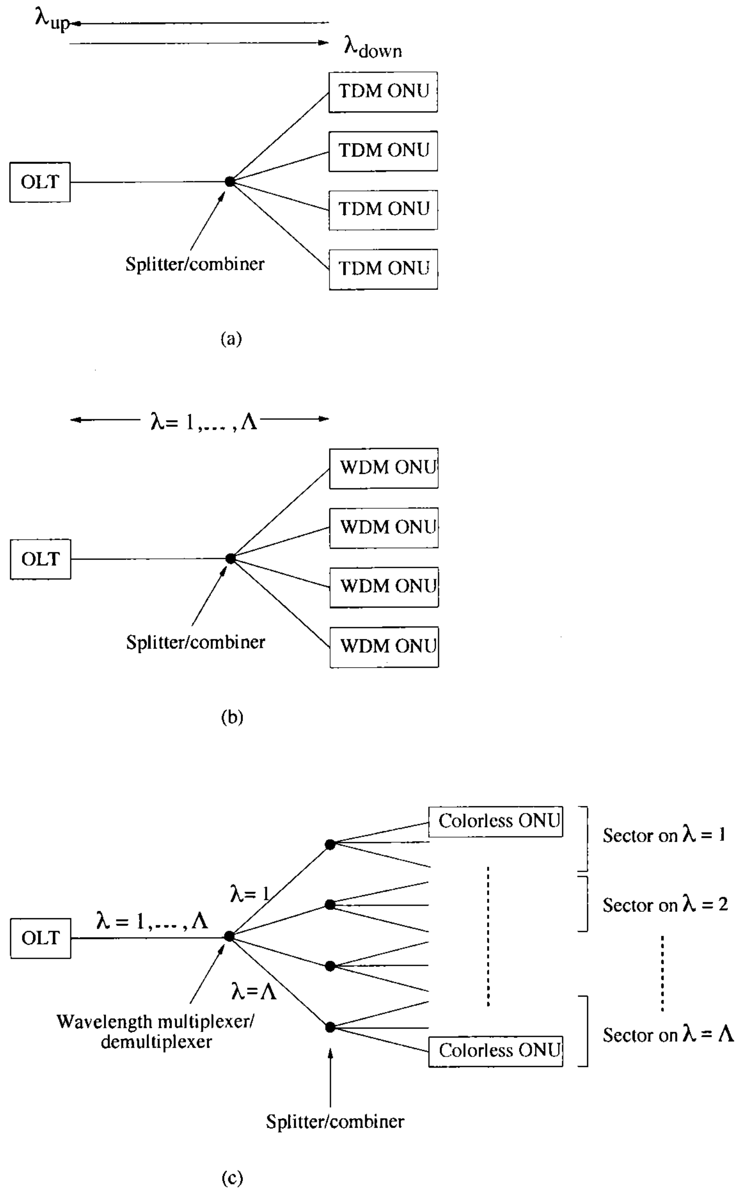

Figure 10.2 – Next-generation PONs: (a) High-speed TDM PON, (b) wavelength-broadcasting WDM PON, and (c) wavelength-routing multi-stage WDM PON.

well as emerging IEEE 802.11ac VHT WLAN technologies that achieve raw data rates up to 6900 Mb/s.

10.4.1 Next-Generation PONs

As shown in Fig. 10.1, current TDM PONs may evolve into next-generation single- or multi-stage PONs of extended reach by exploiting high-speed TDM and/or multichannel WDM technologies and replacing the splitter/combiner at the RN with a wavelength multiplexer/demultiplexer, giving rise to the following three types of next-generation PONs:

High-speed TDM PON

Fig. 10.2(a) depicts a high-speed TDM PON, which maintains the network architecture of conventional TDM PONs except that both the time-shared upstream wavelength channel λ_{up} and downstream wavelength channel λ_{down} and attached OLT and TDM ONUs operate at data rates of 10 Gb/s or higher [40].

Wavelength-broadcasting WDM PON

A wavelength-broadcasting WDM PON has a splitter/combiner at the RN and deploys multiple wavelength channels $\lambda = 1, \ldots, \Lambda$, as shown in Fig. 10.2(b). Each of these Λ wavelength channels is broadcast to all connected WDM ONUs and is used for bidirectional transmission. Each WDM ONU selects a wavelength with a tunable bandpass filter (e.g., fiber Bragg grating) and reuses the downstream modulated signal coming from the OLT for upstream data transmission by means of remodulation techniques, e.g., FSK for downstream and OOK for upstream [41].

Wavelength-routing multi-stage WDM PON

Fig. 10.2(c) shows a wavelength-routing WDM PON, where the conventional splitter/combiner at the RN is replaced with a wavelength multiplexer/demultiplexer, e.g., arrayed-waveguide grating (AWG), such that each of the Λ wavelength channels on the common feeder fiber is routed to a different distribution fiber. A given wavelength channel may be dedicated to a single ONU (e.g., business subscriber) or be time shared by multiple ONUs (e.g., residential subscribers). In the latter case, the distribution fibers contain one or more additional stages, whereby each stage consists of a wavelength-broadcasting splitter/combiner and each wavelength channel serves a different sector, see Fig. 10.2(c). Note that due to the wavelength-routing characteristics of the wavelength multiplexer/demultiplexer, ONUs can be made colorless (i.e., wavelength-independent) by using, for example, low-cost reflective semiconductor optical amplifiers (RSOAs) that are suitable for bidirectional transmission via remodulation [38]. Wavelength-routing multi-stage WDM PONs enable next-generation PONs with an extended optical range of up to 100 km, thus giving rise to *long-reach WDM PONs* at the expense of additional in-line optical amplifiers. Long-reach WDM PONs promise major cost savings by consolidating optical access and metropolitan area networks [42].

10.4.2 Gigabit-Class WLAN

IEEE 802.11n specifies a number of PHY and MAC enhancements for next-generation WLANs. Applying orthogonal frequency division multiplexing (OFDM) and multiple-input multiple-output (MIMO) antennas in the PHY layer of IEEE 802.11n provides various capabilities, such as antenna diversity (selection) and spatial multiplexing. Using multiple antennas also provides multipath capability and increases both throughput and transmission range. The enhanced PHY layer applies two adaptive coding schemes: space time block coding (STBC) and low density parity check coding (LDPC). IEEE 802.11n WLANs are able to co-exist with IEEE 802.11 legacy WLANs, though in greenfield deployments it is possible to increase the channel bandwidth from 20 MHz to 40 MHz via channel bonding, resulting in significantly increased raw data rates of up to 600 Mb/s at the PHY layer.

A main MAC enhancement of 802.11n is frame aggregation, which comes in two flavors, as shown in Figs. 10.3-10.4.

Aggregate MAC Service Data Unit (A-MSDU): Multiple MSDUs, each up to 2304 octets long, are joined and encapsulated into a separate subframe, see Fig. 10.3. Specifically, multiple MSDUs are packed into an A-MSDU, which is encapsulated into a PHY service data unit (PSDU). All constituent MSDUs must have the same traffic identifier (TID) value (i.e., same QoS level) and the resultant A-MSDU must not exceed the maximum size of 7935 octets. Each PSDU is prepended

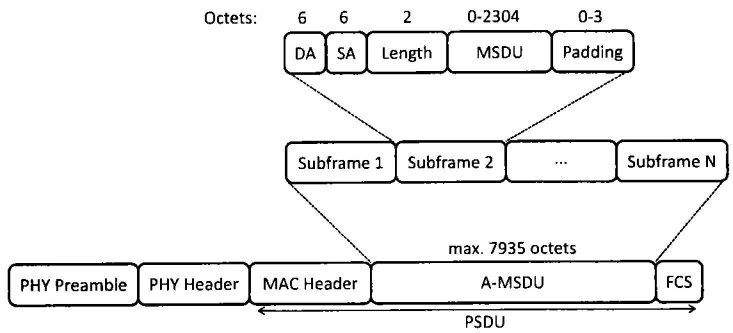

Figure 10.3 – A-MSDU frame aggregation scheme.

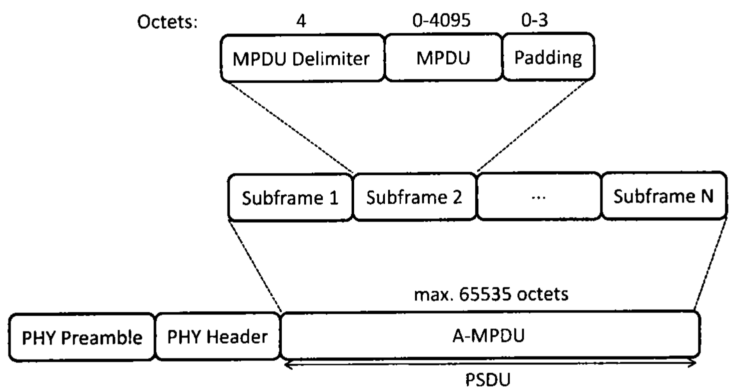

Figure 10.4 – A-MPDU frame aggregation scheme.

with a PHY preamble and PHY header. Although the fragmentation of MSDUs with the same destination address is allowed, A-MSDUs must not be fragmented.

Aggregate MAC Protocol Data Unit (A-MPDU): Multiple MPDUs, each up to 4095 octets long, are joined and inserted in a separate subframe, see Fig. 10.4. Specifically, multiple MPDUs are aggregated into one PSDU of a maximum size 65535 octets. Aggregation of multiple MPDUs with different TID values into one PSDU is allowed by using multi-TID block acknowledgment (MTBA).

Both A-MSDU and A-MPDU require only a single PHY preamble and PHY header. In A-MSDU, the PSDU includes a single MAC header and frame check sequence (FCS), as opposed to A-MPDU where each MPDU contains its own MAC header and FCS. A-MPDU and A-MSDU can be used separately or jointly.

Future Gigabit-class WMNs may be upgraded with emerging IEEE 802.11ac VHT WLAN technologies that exploit further PHY enhancements to achieve raw data rates up to 6900 Mb/s and provide an increased maximum A-MSDU/A-MPDU size of 11406/1048575 octets [43].

10.5 Network Model

10.5.1 Network Architecture

We consider a PON consisting of one OLT and O attached ONUs. The TDM PON carries one upstream wavelength channel and a separate downstream wavelength channel. We suppose that both the wavelength-broadcasting and the wavelength-routing multi-stage WDM PONs carry Λ bidirectional wavelength channels $\lambda = 1, \ldots, \Lambda$. In the wavelength-routing multi-stage WDM PON, the O ONUs are divided into Λ sectors. We use λ to index the wavelength channel as well as the corresponding sector. In our model, sector λ, $\lambda = 1, \ldots, \Lambda$, accommodates O_λ ONUs. Specifically, ONUs with indices o between $\sum_{v=1}^{\lambda-1} O_v$ and $\sum_{v=1}^{\lambda} O_v$ belong to sector λ, i.e., form the set of nodes

$$\mathcal{S}_\lambda := \left\{ o \middle| \sum_{v=1}^{\lambda-1} O_v < o \leq \sum_{v=1}^{\lambda} O_v \right\}. \tag{10.1}$$

Thus, sector $\lambda = 1$ comprises ONUs $o \in \mathcal{S}_1 = \{1, \ldots, O_1\}$, sector $\lambda = 2$ comprises ONUs $o \in \mathcal{S}_2 = \{O_1 + 1, \ldots, O_1 + O_2\}$, and so on, while we assign the index $o = 0$ to the OLT. The one-way propagation delay between OLT and ONUs of sector λ is $\psi^{(\lambda)}$ (in seconds) and the data rate of the associated wavelength channel λ is denoted by $c^{(\lambda)}$ (in bit/s). Hence, each sector of the wavelength-routing multi-stage WDM PON is allowed to operate at a different data rate serving a subset of ONUs located at a different distance from the OLT (e.g., business vs. residential service areas). For ease of exposition, we assume that in the wavelength-broadcasting TDM and WDM PONs all wavelength channels operate at the same data rate c (in bit/s) and that all ONUs have the one-way propagation delay ψ (in seconds) from the OLT.

All or a subset of the O ONUs are equipped with an MPP to interface with the WMN. The WMN is composed of different zones z, whereby each zone operates on a distinct frequency such that the frequencies of neighboring zones do not overlap. Frequencies may be spatially reused in nonadjacent zones. A subset of MPs are assumed to be equipped with multiple radios to enable them to send and receive data in more than one zone and thereby serve as relay nodes between adjacent zones. We denote each radio operating in a given relay MP in a given zone z by a unique ω. The remaining MPs as well as all MPPs, MAPs, and STAs are assumed to have only a single radio ω operating on the frequency of their corresponding zone. All wireless nodes are assumed to be stationary; incorporating mobility is left for future research. Adopting the notation proposed in [44], we let $\mathcal{R}_z$ denote the set of multi-radio relay MPs and $\mathcal{L}_z$ denote the set of single-radio MPs, MPPs, MAPs, and STAs in zone z. Note that set $\mathcal{R}_z$ is empty if there are only single-radio MPs in zone z. Note that due to this set definition each multi-radio MP is designated by multiple ω; one ω and corresponding set R_z for each zone z in which it can send and receive. The WMN operates at a data rate r (in bit/s).

In the WMN, we assume that the bit error rate (BER) of the wireless channel is $p_b > 0$. On the contrary, the BER of the PON is assumed to be negligible and is therefore set to zero. However, individual fiber links may fail due to fiber cuts and become unavailable for routing traffic across the PON, as described next in more detail. Throughout, we neglect nodal processing delays.

10.5.2 Traffic Model and Routing

We denote $\mathcal{N}$ for the set of FiWi network nodes that act as traffic sources and destinations. Specifically, we consider $\mathcal{N}$ to contain the OLT, the O ONUs (whereby a given ONU models the set of end users with wired access to the ONU), and a given number N of STAs. In our model, MPPs, MPs, and MAPs forward in-transit traffic, without generating their own traffic. Hence, the number of traffic sources/destinations is given by $|\mathcal{N}| = 1+O+N$. Furthermore, we define the traffic matrix $\mathbf{S} = (S_{ij}),\ i,j \in \mathcal{N}$, where S_{ij} represents the number of frames per second that are generated at FiWi network node i and destined to FiWi network node j (note that $S_{ij} = 0$ for $i = j$). We allow for any arbitrary distribution F of the frame length L (in bit) and denote $\bar{L}$ and ς_L^2 for the mean and variance of the length of a frame, respectively. The traffic generation is assumed to be ergodic and stationary.

Our capacity and delay analysis flexibly accommodates any routing algorithm. For each pair of FiWi network source node i and destination node j, a particular considered routing algorithm results in a specific traffic rate (in frames/s) Γ_{ij} sent in the fiber domain and traffic rate $\tilde{\Gamma}_{ij}$ sent in the wireless domain such that $S_{ij} = \Gamma_{ij} + \tilde{\Gamma}_{ij}$. A conventional ONU o without an additional MPP cannot send in the wireless domain, i.e., $\tilde{\Gamma}_{oj} = 0$, and sends its entire generated traffic to the OLT, i.e., $S_{oj} = \Gamma_{oj}$. On the other hand, an ONU o equipped with an MPP can send in the wireless domain, i.e., $\tilde{\Gamma}_{oj} \geq 0$. Note that we allow for multipath routing in both the fiber and wireless domains, whereby traffic coming from or going to the OLT may be sent across a single or multiple ONUs and their collocated MPPs. We consider throughout first-come-first-served service in each network node.

10.6 Fiber Backhaul Network

10.6.1 Capacity Analysis

For the wavelength-routing multi-stage WDM PON, we define the normalized downstream traffic rate (intensity) in sector $\lambda, \lambda = 1, \ldots, \Lambda$, as

$$\rho^{d,\lambda} := \frac{\bar{L}}{c^{(\lambda)}} \left(\sum_{o \in \mathcal{S}_\lambda} \Gamma_{0o} + \sum_{q=1}^{O} \sum_{o \in \mathcal{S}_\lambda} \Gamma_{qo} \right), \tag{10.2}$$

where the first term represents the traffic generated by the OLT for sector λ and the second term accounts for the traffic from all ONUs sent to sector λ via the OLT. We define the upstream traffic rate (in frames/s) of ONU o as

$$R_o^u := \Gamma_{o0} + \sum_{q=1}^{O} \Gamma_{oq}, \tag{10.3}$$

where the first term denotes traffic destined to the OLT and the second term represents the traffic sent to other ONUs via the OLT. The normalized upstream traffic rate (intensity) of sector λ is

$$\rho^{u,\lambda} := \frac{\bar{L}}{c^{(\lambda)}} \sum_{o \in \mathcal{S}_\lambda} R_o^u. \tag{10.4}$$

For stability, the normalized downstream and upstream traffic rates have to satisfy

$$\rho^{d,\lambda} < 1 \text{ and } \rho^{u,\lambda} < 1 \tag{10.5}$$

in each sector λ, $\lambda = 1, \ldots, \Lambda$, of the wavelength-routing multi-stage WDM PON.

In the wavelength-broadcasting TDM PON ($\Lambda = 1$) and WDM PON ($\Lambda > 1$), we define the upstream traffic intensity ρ^u and downstream traffic intensity ρ^d as:

$$\rho^u := \frac{\bar{L}}{\Lambda \cdot c} \sum_{o=1}^{O} \sum_{q=0}^{O} \Gamma_{oq} \tag{10.6}$$

$$\rho^d := \frac{\bar{L}}{\Lambda \cdot c} \sum_{q=0}^{O} \sum_{o=1}^{O} \Gamma_{qo}. \tag{10.7}$$

The TDM and WDM PONs are stable if $\rho^u < 1$ and $\rho^d < 1$.

10.6.2 Delay Analysis

In the wavelength-routing multi-stage WDM PON, the OLT sends a downstream frame to an ONU in sector λ by transmitting the frame on wavelength λ, which is received by all ONUs in the sector. We model all downstream transmissions in sector λ to emanate from a single queue. For Poisson frame traffic, the downstream queueing delay is thus modeled by an M/G/1 queue characterized by the Pollaczek-Khintchine formula [45]

$$\Phi(\rho) := \frac{\rho}{2c^{(\lambda)}(1-\rho)} \left(\frac{\varsigma_{L}^{2}}{\bar{L}} + \bar{L} \right) \tag{10.8}$$

giving the total downstream frame delay

$$D^{d,\lambda} = \Phi\left(\rho^{d,\lambda}\right) + \frac{\bar{L}}{c^{(\lambda)}} + \psi^{(\lambda)}. \tag{10.9}$$

Weighing the downstream delays $D^{d,\lambda}$ in the sectors λ by the relative downstream traffic intensities $\rho^{d,\lambda} / \sum_{\lambda=1}^{\Lambda} \rho^{d,\lambda}$ in the sectors, gives the average downstream delay of the wavelength-routing multi-stage WDM PON

$$D^d = \frac{1}{\sum_{\lambda=1}^{\Lambda} \rho^{d,\lambda}} \sum_{\lambda=1}^{\Lambda} \rho^{d,\lambda} \cdot D^{d,\lambda}. \tag{10.10}$$

For the upstream delay, we model each wavelength channel λ, $\lambda = 1, \ldots, \Lambda$, as a single upstream wavelength channel of a conventional EPON. Accordingly, from Eq. (39) in [46], we obtain for the mean upstream delay of sector λ

$$D^{u,\lambda} = 2\psi^{(\lambda)} \cdot \frac{2-\rho^{u,\lambda}}{1-\rho^{u,\lambda}} + \Phi\left(\rho^{u,\lambda}\right) + \frac{\bar{L}}{c^{(\lambda)}} \tag{10.11}$$

and the average upstream delay of the wavelength-routing multi-stage WDM PON equals

$$D^u = \frac{1}{\sum_{\lambda=1}^{\Lambda} \rho^{u,\lambda}} \sum_{\lambda=1}^{\Lambda} \rho^{u,\lambda} \cdot D^{u,\lambda}. \tag{10.12}$$

To improve the accuracy of our delay analysis, we take into account that traffic coming from an ONU o in sector υ and destined to ONU q in sector λ is queued at the intermediate OLT before being sent downstream to ONU q, i.e., the OLT acts like an insertion buffer between ONUs o and q. Consequently, to compensate for the queueing delay at the OLT we apply the method proposed in [47] by subtracting the correction term

$$B^{d,\lambda} = \sum_{\upsilon=1}^{\Lambda} \Phi\left(\rho^{\upsilon\rightarrow\lambda}\right), \tag{10.13}$$

whereby for the setting that $c^{(\lambda)} = c$ for all channels λ

$$\rho^{\upsilon\rightarrow\lambda} = \frac{\bar{L}}{c} \cdot \sum_{o\in\mathcal{S}_\upsilon} \sum_{q\in\mathcal{S}_\lambda} \Gamma_{oq} \tag{10.14}$$

denotes the rate of upstream traffic in sector υ destined for sector λ, from the above calculated mean downstream delay. Thus, for sector λ, $\lambda = 1, \ldots, \Lambda$, the corrected mean downstream delay $\tilde{D}^{d,\lambda}$ is given by

$$\tilde{D}^{d,\lambda} = D^{d,\lambda} - B^{d,\lambda}. \tag{10.15}$$

By replacing $D^{d,\lambda}$ with $\tilde{D}^{d,\lambda}$ in Eq. (10.10) we obtain a more accurate calculation of the average downstream delay for the wavelength-routing multi-stage WDM PON, as examined in Section 10.9.

Next, we evaluate the average downstream and upstream delays for the wavelength-broadcasting TDM PON ($\Lambda = 1$) and WDM PON ($\Lambda > 1$). With the aforementioned correction term the average downstream and upstream delays are given by

$$D^d = \Phi\left(\rho^d\right) + \frac{\bar{L}}{c} + \psi - B^d \tag{10.16}$$

and

$$D^u = \Phi\left(\rho^u\right) + \frac{\bar{L}}{c} + 2\psi\frac{2-\rho^u}{1-\rho^u} - B^u, \tag{10.17}$$

respectively, whereby

$$B^d = B^u = \Phi\left(\frac{\bar{L}}{\Lambda \cdot c}\sum_{o=1}^{O}\sum_{q=1}^{O}\Gamma_{oq}\right). \tag{10.18}$$

10.7 Wireless Front-End Network

So far, we have analyzed only the optical fiber backhaul of the FiWi network. Next, we focus on the wireless front-end. More specifically, in Sections 10.7.1–10.7.4 we build on and adapt existing models of distributed coordination [18, 19, 44] and frame aggregation [20] in WLANs to formulate the basic frame aggregate transmission and collision probabilities as well as time slot duration in the distributed access system. We note that these existing models have primarily focused on accurately representing the collision probabilities and system throughput; we found that directly adapting these existing models gives delay characterizations that are reasonably accurate only for specific scenarios, such as single-hop networking, but very coarse for multi-hop networking. In Sections 10.7.5–10.7.7 we develop a general multihop delay model that is simple, yet accurate by considering the complete service time of a frame aggregate in the wireless front-end network carrying traffic streams from and to both wireless and optical network nodes.

10.7.1 Frame Traffic Modeling

As defined in Section 10.5.1, we denote the radio operating in a given STA or ONU equipped with an MPP by a unique ω. Moreover, we denote each radio operating in a given relay MP in a unique zone z by a unique ω. For ease of exposition, we refer to "radio ω" henceforth as "node ω."

Similar to [44], we model time as being slotted and denote E_ω for the mean duration of a time slot at node ω. The mean time slot duration E_ω corresponds to the average time period required for a successful frame transmission, a collided frame transmission, or an idle waiting slot at node ω and is evaluated in Section 10.7.4. We let q_ω denote the probability that there is a frame waiting for transmission at node ω in a time slot.

For an STA or ONU with collocated MPP ω we denote σ_ω for the traffic load that emanates from node ω, i.e.,

$$\sigma_\omega := \sum_{\forall i} \tilde{\Gamma}_{\omega i}. \tag{10.19}$$

For a relay MP we obtain for a given wireless mesh routing algorithm the frame arrival rate for each of the MP's radios $\omega \in \mathcal{R}_z$ associated with a different zone z:

$$\sigma_\omega := \sum_{\forall i,j} \tilde{\Gamma}_{ij}, \tag{10.20}$$

whereby i and j denote any pair of STA or ONU with collocated MPP that send traffic on a path via relay MP ω, as computed by the given routing algorithm for the wireless mesh front-end of the FiWi network.

For exponentially distributed inter-frame arrival times with mean $1/\sigma_\omega$ (which occur for a Poisson process with rate σ_ω), q_ω is related to the offered frame load at node ω during mean time slot duration E_ω via

$$1 - q_\omega = e^{-\sigma_\omega \cdot E_\omega}. \tag{10.21}$$

10.7.2 Frame Aggregate Error Probability

In this section, we first characterize the sizes of the frame aggregates and then the frame aggregate error probability. For a prescribed distribution $F(l)$ of the size (in bit) of a single frame, e.g., the typical trimodal IP packet size distribution, the distribution $A(l)$ of the size (in bit) of a transmitted A-MSDU or A-MPDU can be obtained as the convolution of F with itself, i.e.,

$$A(l) = (F * F * \ldots * F)(l). \tag{10.22}$$

The number of required convolutions equals the number of frames carried in the aggregate, which in turn depends on the minimum frame size, including the MAC-layer overhead of the corresponding frame aggregation scheme, and the maximum size of an A-MSDU/A-MPDU $A_{\text{max}}^{\text{A-MSDU/A-MPDU}}$ (see Figs. 10.3-10.4). From the distribution $A(l)$ we obtain the average frame aggregate sizes $E[\text{A-MSDU}]$ and $E[\text{A-MPDU}]$. Correspondingly, we divide the traffic rate $\tilde{\Gamma}_{ij}$ (in frames/s) by the average number of frames in an aggregate to obtain the traffic rate in frame aggregates per second.

Moreover, as ground work for Section 10.7.4 we obtain the average size of the longest A-MSDU, $E[\text{A-MSDU}^*]$, and longest A-MPDU, $E[\text{A-MPDU}^*]$, involved in a collision with the simplifying assumption of neglecting the collision probability of more than two packets [18] as

$$E[\text{A-MSDU}^*/\text{A-MPDU}^*] = \int_0^{A_{\text{max}}^{\text{A-MSDU/A-MPDU}}} \left(1 - A(x)^2\right) dx. \tag{10.23}$$

The probability p_e of an erroneously transmitted frame aggregate, referred to henceforth as "transmission error", can be evaluated in terms of bit error probability p_b and size A of a transmitted A-MSDU (with distribution $A(l)$) with [48, Eqn. (16)]; for A-MPDU, p_e can be evaluated in terms of p_b and the sizes L_i of the aggregated frames with [48, Eqn. (18)].

10.7.3 Probabilities for Frame Aggregate Collision and Successful Frame Aggregate Transmission

Following [44], we note that the transmission of any transmitting node $\omega \in \mathcal{R}_z \cup \mathcal{L}_z$ in zone z cannot collide if none of the other nodes $\nu \in \mathcal{R}_z \cup \mathcal{L}_z, \nu \neq \omega$ transmits, i.e., we obtain the collision probability $p_{c,\omega}$ as

$$1 - p_{c,\omega} = \prod_{\substack{\nu \in \mathcal{R}_z \cup \mathcal{L}_z \\ \nu \neq \omega}} (1 - \tau_\nu), \tag{10.24}$$

where τ_ν denotes the transmission probability of WMN node ν. Note that if the considered node is a relay MP, Eq. (10.24) holds for each associated zone z (and corresponding radio ω). We define the probability of either a collision or transmission error p_ω, in brief collision/transmission error probability, as

$$1 - p_\omega = (1 - p_e) \cdot (1 - p_{c,\omega}). \tag{10.25}$$

The transmission probability τ_ω for any node $\omega \in \mathcal{R}_z \cup \mathcal{L}_z$ can be evaluated as a function of the frame waiting probability q_ω, the frame collision/transmission error probability p_ω, the minimum contention window W_0, and the maximum backoff stage H by [44, Eqn. (1)], as explained in [19].

The probability that there is at least one transmission taking place in zone z in a given time slot is given by

$$P_{tr,z} = 1 - \prod_{\omega \in \mathcal{R}_z \cup \mathcal{L}_z} (1 - \tau_\omega). \tag{10.26}$$

A successful frame aggregate transmission occurs if exactly one node ω transmits (and all other nodes $\nu \neq \omega$ are silent), given that there is a transmission, i.e.,

$$P_{s,z} = \frac{1}{P_{tr,z}} \left(\sum_{\omega \in \mathcal{R}_z \cup \mathcal{L}_z} \tau_\omega \cdot \prod_{\substack{\nu \in \mathcal{R}_z \cup \mathcal{L}_z \\ \nu \neq \omega}} (1 - \tau_\nu) \right). \tag{10.27}$$

10.7.4 Duration of Single Frame Aggregate Transmission

We denote ϵ for the duration of an empty time slot without any data transmission on the wireless channel in zone z, which occurs with probability $1 - P_{tr,z}$. With probability $P_{tr,z}$ there is a transmission in a given time slot in zone z, which is successful with probability $P_{s,z}$ and unsuccessful (resulting in a collision) with the complementary probability $1 - P_{s,z}$.

We denote $T_{s,z}$ for the mean duration of a successful frame aggregate transmission and $T_{c,z}$ is the mean duration of a frame aggregate transmission with collision in zone z. Note that $T_{s,z}$ and $T_{c,z}$ depend on the frame aggregation technique (A-MSDU or A-MPDU) and on the access mechanism α (basic access denoted by α = basic or RTS/CTS denoted by α = RTS/CTS). For the basic access mechanism, we define $\Theta_s^{\text{basic}} = \text{DIFS} + \text{PHY Header} + \text{SIFS} + \delta + \text{ACK}/r + \delta$, where δ denotes the propagation delay and r the WMN data rate. For the RTS/CTS access mechanism, we define $\Theta_s^{\text{RTS/CTS}} = \text{DIFS} + \text{RTS}/r + \text{SIFS} + \delta + \text{CTS}/r + \text{SIFS} + \delta + \text{PHY Header} + \text{SIFS} + \delta + \text{ACK}/r + \delta$. (Note that in IEEE 802.11n the parameters ACK, RTS, and CTS as well as the MAC Header and FCS below are given in bits, while the other parameters are given in seconds.) Then, for a successful frame aggregate transmission we have:

$$T_{s,z}^{\alpha} = \begin{cases} \Theta_s^{\alpha} + (\text{MAC Header} + \\ E[\text{A-MSDU}] + \text{FCS})/r & \text{for A-MSDU} \\ \\ \Theta_s^{\alpha} + E[\text{A-MPDU}]/r & \text{for A-MPDU.} \end{cases} \tag{10.28}$$

Moreover, with $\Theta_c^{\text{basic}} = \text{PHY Header} + \text{DIFS} + \delta$, for a collided frame aggregate transmission we have:

$$T_{c,z}^{\text{basic}} = \begin{cases} \Theta_c^{\text{basic}} + (\text{MAC Header} + \\ E[\text{A-MSDU}^*] + \text{FCS})/r & \text{for A-MSDU,} \\ \\ \Theta_c^{\text{basic}} + E[\text{A-MPDU}^*]/r & \text{for A-MPDU} \end{cases} \tag{10.29}$$

as well as for both A-MSDU and A-MPDU,

$$T_{c,z}^{\text{RTS/CTS}} = \text{RTS}/r + \text{DIFS} + \delta. \tag{10.30}$$

Thus, we obtain the expected time slot duration E_ω at node ω in zone z of our network model (corresponding to [18, Eq. (13)]) as

$$E_\omega = (1 - P_{tr,z})\epsilon + P_{tr,z}\left[P_{s,z}T^{\alpha}_{s,z} + (1 - P_{s,z})T^{\alpha}_{c,z}\right]. \tag{10.31}$$

Equations (10.21), (10.25), [44, Eqn. (1)], and (10.31) can be solved numerically for the unknown variables q_ω, p_ω, τ_ω, and E_ω for each given set of values for the known network model parameters. We use the obtained numerical solutions to evaluate the mean delay at node ω as analyzed in the following Sections 10.7.5 and 10.7.6.

10.7.5 Service Time for Frame Aggregate

We proceed to evaluate the expected service (transmission) time for a frame aggregate, which may require several transmission attempts, at a given node ω. With the basic access mechanism, the transmission of the frame aggregate occurs without a collision ($j = 0$) or transmission error with probability $1 - p_\omega$ (10.25), requiring one $T^{\text{basic}}_{s,z}$. With probability $p^j_\omega(1 - p_\omega)$, the frame aggregate suffers j, $j = 1, 2, \ldots$, collisions or transmission errors, requiring j backoff procedures and retransmissions. Thus, the expected service time for basic access is

$$\Delta^{\text{basic}}_{\text{ser},\omega} = \sum_{j=0}^{\infty} p^j_\omega(1 - p_\omega)\left(jT^{\text{basic}}_{c,z} + \sum_{b=1}^{j}\frac{2^{\min(b,H)}W_0 - 1}{2}\epsilon\right) + T^{\text{basic}}_{s,z}. \tag{10.32}$$

For the RTS/CTS access mechanism, collisions can occur only for the RTS or CTS frames (which are short and have negligible probability of transmission errors), whereas transmission errors may occur for the frame aggregates. Collisions require only retransmissions of the RTS frame, whereas transmission errors require retransmissions of the entire frame aggregate. More specifically, only one frame transmission ($k = 1$) is required if no transmission error occurs; this event has probability $1 - p_e$. This transmission without transmission error may involve j, $j = 0, 1, 2, \ldots$, collisions of the RTS/CTS frames. On the other hand, two frame transmissions ($k = 2$) are required if there is once a transmission error; this event has probability $p_e(1-p_e)$. This $k=2$ scenario requires twice an RTS/CTS reservation, which each time may experience $j, j = 0, 1, 2, \ldots$ collisions, as well as two full frame transmission delays $T_{s,z}$. Generally, $k,\ k = 1, 2, \ldots$, frame transmissions are required if $k-1$ times there is a frame transmission error. Each of the k frame transmission attempts requires an RTS/CTS reservation and a full frame transmission delay $T_{s,z}$. In summary, we evaluate the mean service delay for a frame aggregate with RTS/CTS access as

$$\Delta_{\mathrm{ser},\omega}^{\mathrm{RTS/CTS}} = \sum_{k=1}^{\infty} p_e^{k-1}(1-p_e)k \left[\sum_{j=0}^{\infty} p_{c,\omega}^{j}(1-p_{c,\omega}) \right.$$
$$\left. \left(\sum_{b=1}^{j} \frac{2^{\min(b,H)}W_0 - 1}{2}\epsilon + jT_{c,z}^{\mathrm{RTS/CTS}} \right) + T_{s,z} \right]. \tag{10.33}$$

10.7.6 Delay at WMN Node

We first evaluate the overall service time Δ_ω from the time instant when a frame aggregate arrives at the head of the queue at node ω to the completion of its successful transmission. Subsequently, with Δ_ω characterizing the overall service time at node ω, we evaluate the queueing delay D_ω^{wi}.

The overall service time Δ_ω is given by the service time $\Delta_{ser,\omega}$ required for transmitting a frame aggregate and the sensing delay $\Delta_{sen,\omega}^{\alpha}$ required for the reception of frame aggregates by node ω from other nodes, i.e.,

$$\Delta_\omega = \Delta_{\mathrm{ser},\omega}^{\alpha} + \Delta_{\mathrm{sen},\omega}. \tag{10.34}$$

As a first step towards modeling the sensing delay at a node v, we consider the service times $\Delta_{ser,v_1}^{\alpha}$ at nodes $v_1 \neq \nu$ and scale these service times linearly with the corresponding traffic intensities $\sigma_{v_1}/(1/\Delta_{ser,v_1})$ to obtain the sensing delay component

$$D_{sen,\nu} = \sum_{\forall_{v_1 \neq \nu} \text{ in} z} \frac{\sigma_{v_1}}{1/\Delta_{ser,v_1}^{\alpha}} \Delta_{ser,v_1}^{\alpha}. \tag{10.35}$$

As a second modeling step, we consider the service times plus sensing delay components scaled by the respective traffic intensities to obtain the sensing delay

$$\Delta_{\text{sen},\omega} = \sum_{\forall_{\nu \neq \omega \text{inz}}} \frac{\sigma_\nu}{1/(\Delta^\alpha_{\text{ser},\nu} + D_{\text{sen},\nu})} (\Delta^\alpha_{\text{ser},\nu} + D_{\text{sen},\nu}) \tag{10.36}$$

employed in the evaluation of the overall service delay (10.34).

We approximate the queue at node ω by an M/M/1 queue with mean arrival rate σ_ω and mean service time Δ_ω. This queue is stable if

$$\sigma_\omega \cdot \Delta_\omega < 1. \tag{10.37}$$

The total delay (for queueing plus service) at node ω is then given by

$$D^{\text{wi}}_\omega = \frac{1}{\frac{1}{\Delta_\omega} - \sigma_\omega}. \tag{10.38}$$

If node ω is an ONU with a collocated MPP the accuracy of the queueing delay calculation is improved by subtracting a correction term:

$$\tilde{D}^{\text{wi}}_\omega = D^{\text{wi}}_\omega - \Phi\left(\frac{\bar{L}}{c}\sum_{\forall i,j} S_{ij}\right) \tag{10.39}$$

for the wavelength-broadcasting TDM PON and WDM PON, or

$$\tilde{D}^{\text{wi}}_\omega = D^{\text{wi}}_\omega - \Phi\left(\frac{\bar{L}}{c^{(\lambda)}}\sum_{\forall i,j} S_{ij}\right) \tag{10.40}$$

for the wavelength-routing multi-stage WDM PON, whose sector λ accommodates the ONU with collocated MPP. Note that $\frac{\bar{L}}{c}\sum_{\forall i,j} S_{ij}$ or $\frac{\bar{L}}{c^{(\lambda)}}\sum_{\forall i,j} S_{ij}$ accounts for the traffic of all pairs of source node i and destination node j traversing ONU ω from the fiber backhaul towards the wireless front-end network.

10.7.7 Delay on WMN Path

In order to obtain the delay in the wireless front-end of our FiWi network, we have to average the sums of the nodal delays of all possible paths for all pairs of source node i and destination node j:

$$D^{\mathrm{wi}} = \sum_{i,j} \frac{\tilde{\Gamma}_{ij}}{\sum_{i,j} \tilde{\Gamma}_{ij}} \left(\sum_{\substack{\forall \omega \text{ on path} \\ \text{from } i \text{ to } j}} \left(D^{\mathrm{wi}}_{\omega} - B^{\mathrm{wi}}_{ij\omega} \right) \right), \tag{10.41}$$

with the queueing delay correction terms

$$B^{\mathrm{wi}}_{ij\omega} = \frac{\tilde{\Gamma}_{ij} \cdot \Delta_{\omega}}{\frac{1}{\Delta_{\omega}} - \tilde{\Gamma}_{ij}}, \tag{10.42}$$

whereby $\tilde{\Gamma}_{ij} \cdot \Delta_{\omega}$ is the traffic intensity at node ω due to traffic flowing from source node i to destination node j.

10.8 FiWi Network Stability and Delay

The entire FiWi access network is stable if and only if all of its optical and wireless subnetworks are stable. If the optical backhaul consists of a wavelength-routing multi-stage WDM PON the stability conditions in Eq. (10.5) must be satisfied. In the case of the wavelength-broadcasting TDM and WDM PON, the optical backhaul is stable if both ρ^u and ρ^d defined in Eqs. (10.6) and (10.7), respectively, are smaller than one. The wireless mesh front-end is stable if the stability condition in Eq. (10.37) is satisfied for each WMN node.

We obtain the mean end-to-end delay of the entire bimodal FiWi access network as

$$D = D^d + D^u + D^{\mathrm{wi}}. \tag{10.43}$$

Tableau 10.1 – FiWi Network Parameters

Parameter	Value
Min. contention window W_0	16
Max. backoff state H	6
Empty slot duration ϵ	9 μs
SIFS	16 μs
DIFS	34 μs
PHY Header	20 μs
MAC Header	36 bytes
RTS	20 bytes
CTS	14 bytes
ACK	14 bytes
FCS	4 bytes

10.9 Numerical and Simulation Results

We set the parameters of the FiWi mesh front-end to the default values for next-generation WLANs [49], see Table 10.1. We consider a distance of 1 km between any pair of adjacent WMN nodes (which is well within the maximum distance of presently available outdoor wireless access points), translating into a propagation delay of $\delta = 1/3 \cdot 10^{-5}$ s.

10.9.1 Model Verification

Configuration

In our initial verifying simulations, we consider the FiWi network configuration of Fig. 10.5. The fiber backhaul is a TDM PON, or a wavelength-broadcasting/routing WDM PON with $\Lambda = 2$ bidirectional wavelength channels ($\lambda = 1$, $\lambda = 2$), each operating at $c = c^{(\lambda)} = 1$ Gb/s (compliant with IEEE 802.3ah). In the case of the wavelength-routing (WR) WDM PON, the two sectors are defined as: $\lambda = 1$: $\{ONU_1, ONU_2\}$ and $\lambda = 2$: $\{ONU_3, ONU_4\}$. All four ONUs are located 20 km from the OLT (translating into a one-way propagation delay $\psi = \psi^{(\lambda)} = 0.1$ ms) and are equipped with an MPP. The WMN is composed of the aforementioned 4 MPPs plus 16 STAs and 4 MPs, which are distributed over 11 wireless zones, as shown in Fig. 10.5. For instance, the WMN zone containing ONU_1 comprises 1 MPP, 2 STAs, and 1 MP. MPPs and STAs use a single radio, whereas MPs use 3, 4, 4, 3 radios from left to right in Fig. 10.5. All WMN nodes apply the RTS/CTS access mechanism. The WMN operates at $r = 300$ Mb/s (compliant with IEEE 802.11n) with a bit error rate of $p_b = 10^{-6}$.

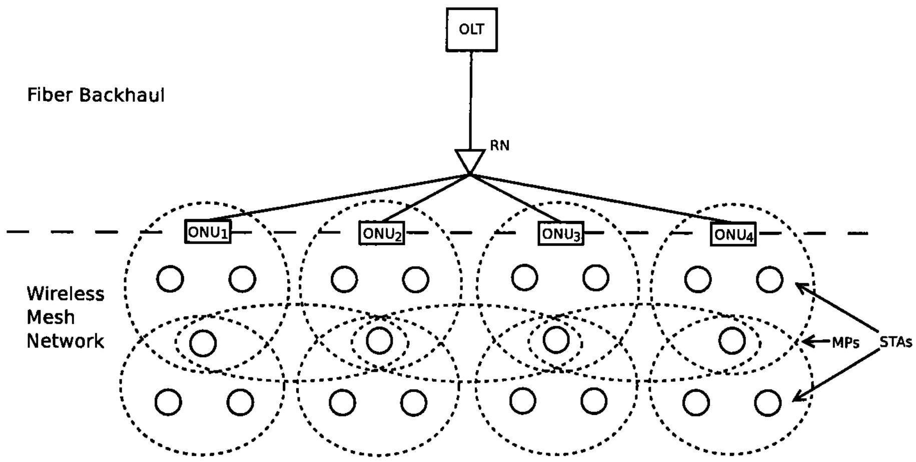

Figure 10.5 – FiWi network configuration for verifying simulations: 4 ONU/MPPs, 4 MPs, and 16 STAs distributed over 11 wireless zones (dashed circles).

Traffic and Routing Assumptions

We consider Poisson traffic with fixed-size frames of 1500 bytes (octets). We use A-MSDU for frame aggregation, whereby each A-MSDU carries the maximum permissible payload of 5 frames, see Fig. 10.3. Similar to [5], we consider two operation modes: (*i*) *WMN-only mode* which has no fiber backhaul in place; (*ii*) *wireless-optical-wireless mode* which deploys the FiWi network configuration of Fig. 10.5. For both modes, we consider the minimum interference routing algorithm [6], which selects the path with the minimum number of wireless hops. We compare different routing algorithms in Section 10.9.2.

Verifying Simulations

The simulation results presented in [5] indicate that the throughput performance of WMNs deteriorates much faster for increasing peer-to-peer traffic among STAs than that of FiWi networks, while WMN and FiWi networks achieve the same throughput when all traffic is destined to the Internet. For comparison with [5], we consider *peer-to-peer (P2P) traffic*, where each frame generated by a given STA is destined to any other of the remaining 15 STAs with equal probability 1/15, and *upstream traffic*, where all frames generated by the STAs are destined to the OLT. Fig. 10.6 depicts the results of our probabilistic analysis for the mean delay as a function of the mean aggregate throughput of a stand-alone WMN network and a TDM PON based FiWi network for P2P and upstream traffic. The figure also shows verifying simulation results and their 95% confidence intervals, whereby simulations were run 100 times for each considered traffic load [1].

We observe from Fig. 10.6 that the mean delay of the WMN increases sharply as the mean aggregate throughput asymptotically approaches its maximum data rate of 300 Mb/s. We also confirm the findings of [5] that under P2P traffic the mean aggregate throughput can be increased by using a TDM PON as fiber backhaul to offload the wireless mesh front-end at the expense of a slightly increased mean delay due to the introduced upstream and downstream PON delay to and from the OLT. As opposed to [5], however, Fig. 10.6 shows that the throughput-delay performance of the considered FiWi network is further improved significantly under upstream traffic. These different observations are due to the fact that in [5] the single-radio single-channel WMN based on legacy IEEE 802.11a WLAN with a limited data rate of 54 Mb/s suffered from severe channel congestion close to the MPPs, which is alleviated in the multi-radio multi-channel WMN based on next-generation high-throughput WLAN technologies.

Next, we verify different FiWi network architectures and their constituent subnetworks for *uniform* and *nonuniform traffic* for minimum (wireless or optical) hop routing [5]. Fig. 10.7 depicts the throughput-delay performance of a stand-alone WMN front-end, stand-alone TDM PON, and a variety of integrated FiWi network architectures using different fiber backhaul solutions, including conventional TDM PON, wavelength-broadcasting WDM PON (WDM PON), and wavelength-

1. Our simulator is based on OMNeT++ and uses the communication networks package *inetmanet* with extensions for frame aggregation, wireless multihop routing, TDM/WDM PONs, and integrated WMN/PON routing.

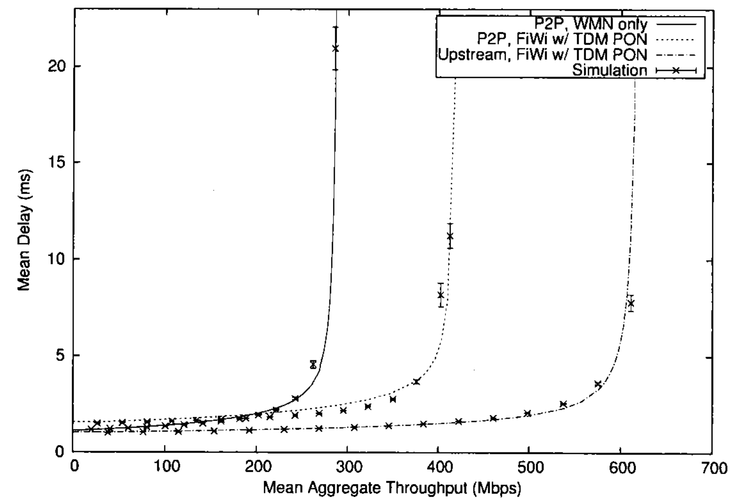

Figure 10.6 – Mean delay vs. mean aggregate throughput performance of WMN and TDM PON based FiWi networks for peer-to-peer (P2P) and upstream traffic.

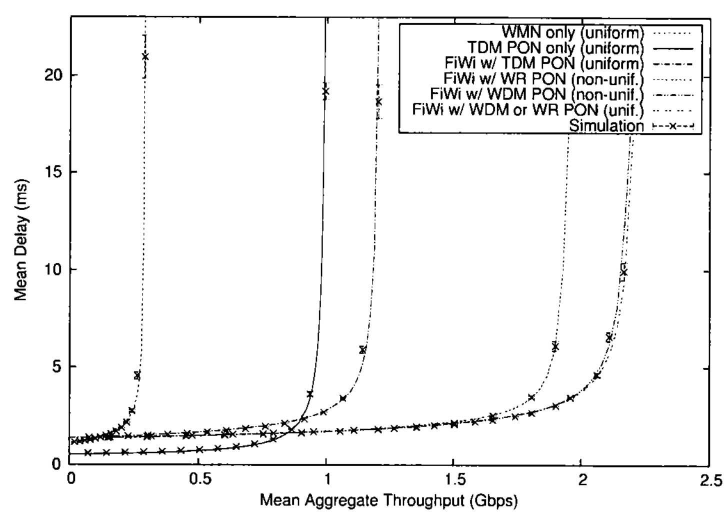

Figure 10.7 – Mean delay vs. mean aggregate throughput performance of different FiWi network architectures for uniform and nonuniform traffic.

routing WDM PON (WR PON). In the TDM PON only (WMN only) scenario under uniform traffic, each ONU (STA) generates the same amount of traffic and each generated frame is destined to any of the remaining ONUs (STAs) with equal probability. As expected, the WMN and TDM PON saturate at roughly 300 Mb/s and 1 Gb/s, respectively, and the TDM PON is able to support much higher data rates per source node (ONU) at lower delays than the WMN. Furthermore, we observe from Fig. 10.7 that under uniform traffic conditions, where STAs and ONUs send unicast traffic randomly uniformly distributed among themselves, FiWi networks based on a wavelength-broadcasting WDM PON or a WR PON give the same throughput-delay performance, clearly outperforming their single-channel TDM PON based counterpart. However, there is a clear difference between WDM PON and WR PON fiber backhauls when traffic becomes unbalanced. To see this, let us consider a nonuniform traffic scenario, where ONU_1 and ONU_2 and their 4 associated STAs (see Fig. 10.5) generate 30% more traffic than the remaining ONUs and STAs. Under such a nonuniform traffic scenario, a FiWi network based on a wavelength-broadcasting WDM PON performs better, as shown in Fig. 10.7. This is due to the fact that the WDM PON provides the two heavily loaded ONU_1 and ONU_2 with access to both wavelength channels, as opposed to the WR PON, thus resulting in an improved throughput-delay performance.

Overall, we note that the analysis and verifying simulation results presented in Figs. 10.6 and 10.7 match very well for a wide range of FiWi network architectures and traffic scenarios.

10.9.2 FiWi Routing Algorithms

Recall from Section 10.5.2 that our capacity and delay analysis flexibly accommodates any routing algorithm and allows for multipath routing in both the fiber and wireless domains. In this section, we study the impact of different routing algorithms on the throughput-delay performance of next-generation FiWi access networks in greater detail. We examine the following single-path routing algorithms:

Minimum hop routing: Conventional shortest path routing selects for each source-destination node pair the path minimizing the required number of wireless and/or optical hops.

Minimum interference routing [6]: The path with the minimum wireless hop count is selected. The rationale behind this algorithm is that the maximum throughput of wireless networks is typically much lower compared to the throughput in optical networks. Thus, minimizing the wireless hop count tends to increase the maximum FiWi network throughput.

Minimum delay routing: Similar to the previously proposed WMN routing algorithms DARA [7], CaDAR [9], and RADAR [10], we apply a slightly extended minimum delay routing algorithm, which aims at selecting the path that minimizes the end-to-end delay of Eq. (10.43) across the entire bimodal FiWi access network. The applied minimum delay routing algorithm is a greedy algorithm and proceeds in two steps. In the initialization step, paths are set to the minimum hop routes. The second step computes for each source-destination node pair the path with the minimum end-to-end delay under given traffic demands.

Optimized FiWi routing algorithm (OFRA): We propose the optimized FiWi routing algorithm (OFRA), which proceeds in two steps similar to minimum delay routing. After the initialization step to minimum hop routes, the second step of OFRA computes for each source-destination node pair the path p with the minimization objective

$$\min_{p} \left(\sum_{\forall n \in p} (\rho_n) + \max_{\forall n \in p}(\rho_n) \right), \qquad (10.44)$$

where ρ_n represents the long-run traffic intensity at a generic FiWi network node n, which may be either an optical node belonging to the fiber backhaul or a wireless node belonging to the wireless mesh front-end. Based on a combination of historic traffic patterns as well as traffic measurements and estimations similar to [50, 51, 52], the traffic intensities ρ_n used in OFRA can be periodically updated with strategies similar to [9, 53]. These long-run traffic intensities vary typically slowly, e.g., with a diurnal pattern, allowing essentially offline computation of the OFRA paths.

OFRA's path length measure includes the maximum traffic intensity $\max_{\forall n \in p}(\rho_n)$ along a path p in order to penalize paths with a high traffic intensity at one or more FiWi network nodes. For a given set of traffic flows, OFRA minimizes the traffic intensities, particularly the high ones, at the FiWi network nodes. Decreasing the traffic intensities tends to allow for a higher number of supported traffic flows and thus higher throughput.

To allow for a larger number of possible paths for the following numerical investigations of the different considered routing algorithms, we double the FiWi network configuration of Fig. 10.5. We consider a wavelength-routing (WR) WDM PON with a total of 8 ONU/MPPs, 8 MPs, and 32 STAs in 22 wireless zones, whereby ONU/MPPs 1-4 and ONU/MPPs 5-8 are served on wavelength channel $\lambda = 1$ and $\lambda = 2$, respectively. Furthermore, to evaluate different traffic loads in the optical

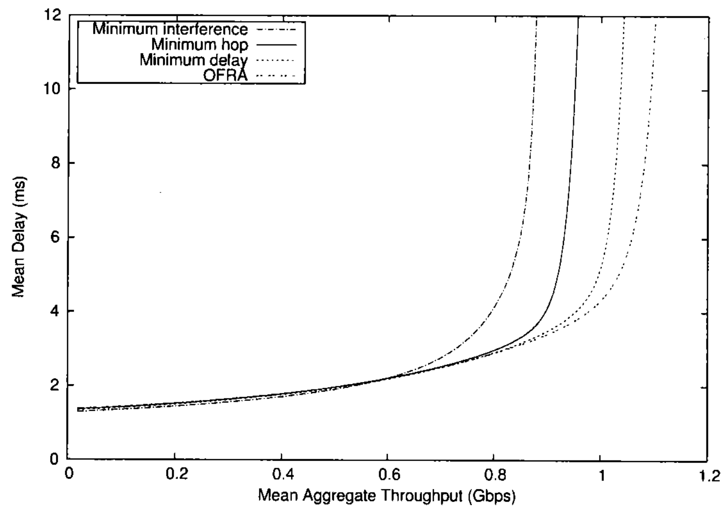

Figure 10.8 – Mean delay vs. mean aggregate throughput performance of different FiWi routing algorithms for a conventional wavelength-routing (WR) WDM PON of 20 km range and $B = 1$.

and wireless domains, we consider the following traffic matrix for the OLT, O ONUs, and N STAs:

$$
\begin{array}{cc}
 & \begin{array}{ccccccc} 0 & 1 & \dots & O & O+1 & \dots & O+N \end{array} \\
\begin{array}{c} 0 \\ 1 \\ \vdots \\ O \\ O+1 \\ \vdots \\ O+N \end{array} &
\begin{pmatrix}
0 & B\alpha & B\alpha & B\alpha & \alpha & \alpha & \alpha \\
B\alpha & 0 & B\alpha & B\alpha & \alpha & \alpha & \alpha \\
B\alpha & B\alpha & 0 & B\alpha & \alpha & \alpha & \alpha \\
B\alpha & B\alpha & B\alpha & 0 & \alpha & \alpha & \alpha \\
\alpha & \alpha & \alpha & \alpha & 0 & \alpha & \alpha \\
\alpha & \alpha & \alpha & \alpha & \alpha & 0 & \alpha \\
\alpha & \alpha & \alpha & \alpha & \alpha & \alpha & 0
\end{pmatrix}
\end{array},
$$

where $\alpha \geq 0$ denotes the mean traffic rate (in frames/second). The parameter $B \geq 1$ can be used to test different traffic intensities in the PON, since the ONUs could be underutilized compared to the WMN in the considered topology. Recall from Fig. 10.1 that ONUs may serve multiple subscribers with wired ONU access, whose aggregate traffic leads to an increased load at ONUs.

For a conventional WR WDM PON with a typical optical fiber range of 20 km, Fig. 10.8 illustrates that OFRA yields the best throughput-delay performance for $B = 1$, i.e., every optical and wireless FiWi node generates the same amount of traffic. Minimum interference routing tends to overload the wireless MPP interfaces as it does not count the fiber backhaul as a hop, resulting in high delays.

The throughput-delay performance of the four considered FiWi routing algorithms largely depends on the given traffic loads and length of the fiber backhaul. Fig. 10.9 depicts their throughput-delay performance for (*i*) a conventional 20 km range and (*ii*) a 100 km long-reach WR WDM PON, whereby in both configurations we set $B = 100$, i.e., the amount of generated traffic among optical nodes (OLT and ONUs) is 100 times higher than that between node pairs involving at least one wireless node (STA). More precisely, all the (increased) inter-ONU/OLT traffic is sent across the WDM PON only, thus creating a higher loaded fiber backhaul. We observe from Fig. 10.9 that in general all four routing algorithms achieve a higher maximum aggregate throughput due to the increased traffic load carried on the fiber backhaul.

We observe that for a conventional 20 km range WR WDM PON with small to medium traffic loads, OFRA gives slightly higher delays than the other considered routing algorithms. This observation is in contrast to Fig. 10.8, though in both figures OFRA yields the highest maximum aggregate throughput. We have measured the traffic on the optical and wireless network interfaces of each ONU/MPP. Our measurements show that at low to medium traffic loads with $B = 100$, OFRA routes significantly less traffic across the WDM PON than the other routing algorithms, but instead uses the less loaded wireless mesh front-end. This is due to the objective of OFRA to give preference to links with lower traffic intensities. As a consequence, for $B = 100$, OFRA routes relatively more traffic over lightly loaded wireless links, even though this implies more wireless hops, resulting in a slightly increased mean delay compared to the other routing algorithms at low to medium loads.

Fig. 10.9 also shows the impact of the increased propagation delay in a long-reach WDM PON with a fiber range of 100 km between OLT and ONUs. Aside from a generally increased mean delay, we observe that minimum hop and minimum interference routing as well as OFRA provide comparable delays at low to medium traffic loads, while the maximum achievable throughput differences at high traffic loads are more pronounced than for the 20 km range. The favorable performance

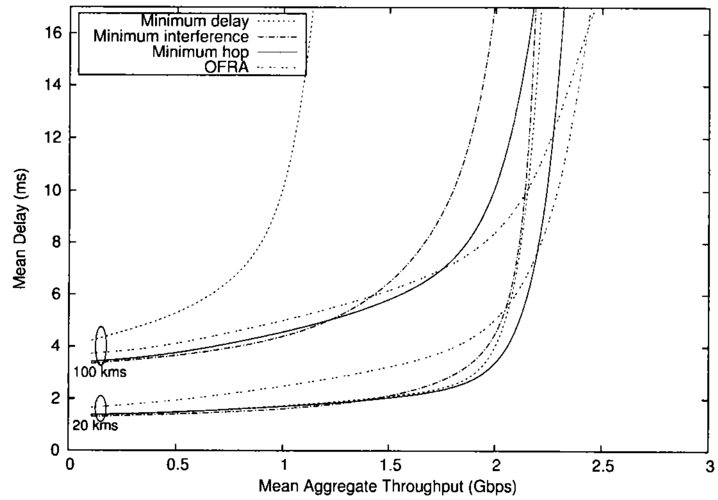

Figure 10.9 – Mean delay vs. mean aggregate throughput performance of different FiWi routing algorithms for (*i*) a conventional 20 km range and (*ii*) a 100 km long-reach wavelength-routing (WR) WDM PON and $B = 100$.

of OFRA at high traffic loads is potentially of high practical relevance since access networks are the bottlenecks in many networking scenarios and thus experience relatively high loads while core networks operate at low to medium loads.

Fig. 10.9 illustrates that minimum delay routing performs poorly in long-reach WDM PON based FiWi access networks. Our measurements indicate that minimum delay routing utilizes the huge bandwidth of the long-reach WDM PON much less than the other routing algorithms in order to avoid the increased propagation delay. As a consequence, with minimum delay routing most traffic is sent across the WMN, which offers significantly lower data rates than the fiber backhaul, resulting in a congested wireless front-end and thereby an inferior throughput-delay performance.

10.9.3 Fiber Failures

To highlight the flexibility of our analysis, we note that it accommodates any type and number of fiber failures. Fiber failures represent one of the major differences between optical (wired) fiber and wireless networks and affect the availability of bimodal FiWi networks. In the event of one or more distribution fiber cuts, the corresponding disconnected ONU/MPP(s) turn(s) into a conventional wireless MP without offering gateway functions to the fiber backhaul any longer.

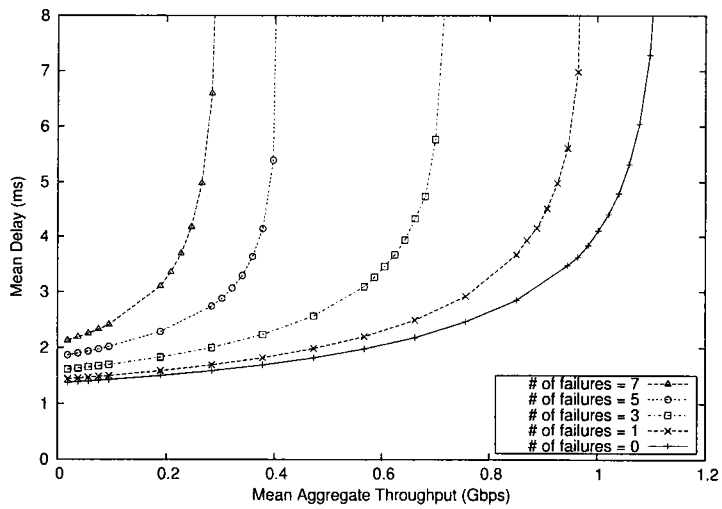

Figure 10.10 – Impact of distribution fiber failures on throughput-delay performance of a 20 km range wavelength-routing WDM PON using OFRA with $B = 1$.

Fig. 10.10 illustrates the detrimental impact of distribution fiber failures on the throughput-delay performance of a 20 km range wavelength-routing WDM PON, which is typically left unprotected due to the small number of cost-sharing subscribers and cost-sensitivity of access networks. We also note that the analytical framework is able to account for other types of network failure, e.g., ONU/MPP failures. In this case, malfunctioning ONU/MPPs become unavailable for both optical and wireless routing.

In principle, FiWi access networks can be made more robust against fiber failures through various optical redundancy strategies, such as ONU dual homing, point-to-point interconnection fibers between pairs of ONUs, fiber protection rings to interconnect a group of closely located ONUs by a short-distance fiber ring, or meshed PON topologies [28]. These redundancy strategies in general imply major architectural and ONU modifications of the FiWi access network of Fig. 10.1 under consideration. To incorporate such topological PON modifications, the fiber part of the capacity and delay analysis needed to be modified accordingly.

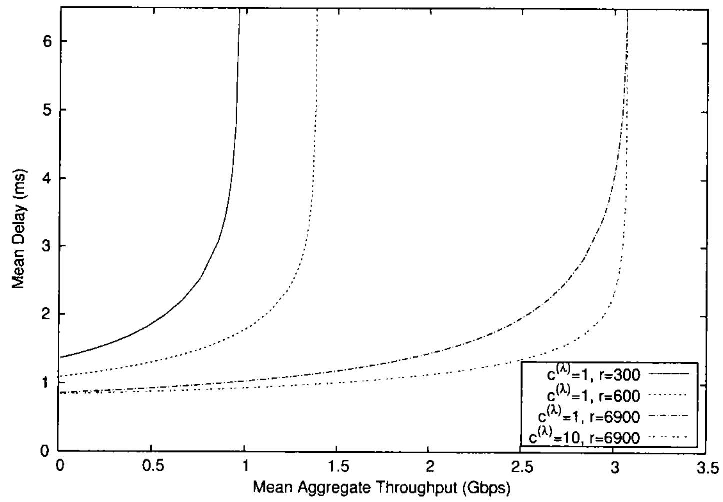

Figure 10.11 – Throughput-delay performance of next-generation FiWi access networks based on high-speed wavelength-routing WDM PON and VHT WLAN technologies using minimum hop routing with $B = 1$ (optical and wireless data rates , $c^{(\lambda)}$ and r, are given in Gb/s and Mb/s, respectively).

10.9.4 Very High Throughput WLAN

Our analysis is also applicable to the emerging IEEE standard 802.11ac for future VHT WLANs with raw data rates up to 6900 Mb/s. In addition to a number of PHY layer enhancements, IEEE 802.11ac will increase the maximum A-MSDU size from 7935 to 11406 octets and the maximum A-MPDU size from 65535 octets to 1048575 octets. Both enhancements can be readily accommodated in our analysis by setting the parameters $A_{\max}^{\text{A-MSDU/A-MPDU}}$ and r accordingly.

Fig. 10.11 illustrates the FiWi network performance gain achieved with a wireless front-end based on VHT WLAN instead of IEEE 802.11n WLAN with maximum data rate of 600 Mb/s, for minimum hop routing, an optical range of 20 km, and $B = 1$. For a wavelength-routing WDM PON operating at a wavelength channel data rate of 1 Gb/s, we observe from Fig. 10.11 that VHT WLAN roughly triples the maximum mean aggregate throughput and clearly outperforms 600 Mb/s 802.11n WLAN in terms of both throughput and delay. Furthermore, the figure shows that replacing the 1 Gb/s wavelength-routing WDM PON with its high-speed 10 Gb/s counterpart (compliant with the IEEE 802.3av 10G-EPON standard) does not yield a higher maximum aggregate throughput, but it does lower the mean delay especially at medium traffic loads before wireless links at the optical-wireless interfaces get increasingly congested at higher traffic loads.

IEEE/ACM Transactions on Networking, accepted for publication.

10.10 Conclusions

A variety of routing algorithms have recently been proposed for integrated FiWi access networks based on complementary EPON and WLAN-mesh networks. In this article, we presented the first analytical framework to quantify the performance of FiWi network routing algorithms, validate previous simulation studies, and provide insightful guidelines for the design of novel integrated optical-wireless routing algorithms for future FiWi access networks leveraging next-generation PONs, notably long-reach 10+ Gb/s TDM/WDM PONs, and emerging Gigabit-class WLAN technologies. Our analytical framework is very flexible and can be applied to any existing or new optical-wireless routing algorithm. Furthermore, it takes the different characteristics of disparate optical and wireless networking technologies into account. Beside their capacity mismatch and bit error rate differences, the framework also incorporates arbitrary frame size distributions, traffic matrices, optical/wireless propagation delays, data rates, and fiber cuts. We investigated the performance of minimum hop, minimum interference (wireless hop), minimum delay, and our proposed OFRA routing algorithms. The obtained results showed that OFRA yields the highest maximum aggregate throughput for both conventional and long-reach wavelength-routing WDM PONs under balanced and unbalanced traffic loads. For a higher loaded fiber backhaul, however, OFRA gives priority to lightly loaded wireless links, leading to an increased mean delay at small to medium wireless traffic loads. We also observed that using VHT WLAN helps increase the maximum mean aggregate throughput significantly, while high-speed 10 Gb/s WDM PON helps lower the mean delay especially at medium traffic loads.

References

[1] S. Sarkar, H.-H. Yen, S. Dixit, and B. Mukherjee, "Hybrid Wireless-Optical Broadband Access Network (WOBAN): Network Planning Using Lagrangean Relaxation," *IEEE/ACM Transactions on Networking*, vol. 17, no. 4, pp. 1094–1105, Aug. 2009.

[2] M. A. Ali, G. Ellinas, H. Erkan, A. Hadjiantonis, and R. Dorsinville, "On the Vision of Complete Fixed-Mobile Convergence," *IEEE/OSA J. Lightwave Technol.*, vol. 28, no. 16, pp. 2343–2357, Aug. 2010.

[3] N. Ghazisaidi and M. Maier, "Fiber-Wireless (FiWi) Networks: Challenges and Opportunities," *IEEE Network*, vol. 25, no. 1, pp. 36–42, Jan./Feb. 2011.

[4] N. Ghazisaidi and M. Maier, "Hierarchical Frame Aggregation Techniques for Hybrid Fiber-Wireless Access Networks," *IEEE Communications Magazine*, vol. 49, no. 9, pp. 64–73, Sep. 2011.

[5] Z. Zheng, J. Wang, and J. Wang, "A Study of Network Throughput Gain in Optical-Wireless (FiWi) Networks Subject to Peer-to-Peer Communications," in *Proc., IEEE ICC*, Jun. 2009, pp. 1–6.

[6] Z. Zheng, J. Wang, and X. Wang, "ONU Placement in Fiber-Wireless (FiWi) Networks Considering Peer-to-Peer Communications," in *Proc., IEEE GLOBECOM*, Nov./Dec. 2009, pp. 1–7.

[7] S. Sarkar and et al., "A Novel Delay-Aware Routing Algorithm (DARA) for a Hybrid Wireless-Optical Broadband Access Network (WOBAN)," *IEEE Network*, vol. 22, no. 3, pp. 20–28, Jan./Feb. 2008.

IEEE/ACM Transactions on Networking, accepted for publication.

[8] X. Chen and et al., "Delay-Differentiated Routing Algorithm to Enhance Delay Performance of WOBAN," in *Proc., International Conference on Optical Internet (COIN)*, Jul. 2010, pp. 1–4.

[9] A. Reaz, V. Ramamurthi, S. Sarkar, D. Ghosal, S. Dixit, and B. Mukherjee, "CaDAR: An Efficient Routing Algorithm for a Wireless-Optical Broadband Access Network (WOBAN)," *IEEE/OSA Journal of Optical Communications and Networking*, vol. 1, no. 5, pp. 392–403, Oct. 2009.

[10] S. Sarkar and et al., "RADAR: Risk-and-Delay Aware Routing Algorithm in a Hybrid Wireless-Optical Broadband Access Network (WOBAN)," in *Proc., OFC/NFOEC*, Mar. 2007, pp. 1–3.

[11] X. Shao, Y. K. Yeo, L. H. Ngoh, X. Cheng, W. Rong, and L. Zhou, "Availability-Aware Routing for Large-Scale Hybrid Wireless-Optical Broadband Access Network," in *Proc., OFC*, Mar. 2010, pp. 1–3.

[12] J. Wang, K. Wu, S. Li, and C. Qiao, "Performance Modeling and Analysis of Multi-Path Routing in Integrated Fiber-Wireless Networks," in *Proc., Mini-Conference at IEEE INFOCOM*, Mar. 2010, pp. 1–5.

[13] P. Chowdhury, M. Tornatore, S. Sarkar, and B. Mukherjee, "Building a Green Wireless-Optical Broadband Access Network (WOBAN)," *IEEE J. Lightw. Techn.*, vol. 28, no. 16, pp. 2219–2229, Aug. 2010.

[14] G. Shen, R. S. Tucker, and C.-J. Chae, "Fixed Mobile Convergence Architectures for Broadband Access: Integration of EPON and WiMAX," *IEEE Communications Magazine*, vol. 45, no. 8, pp. 44–50, Aug. 2007.

[15] M. Maier and N. Ghazisaidi, *FiWi Access Networks*. Cambridge University Press, 2012.

[16] J. Zhang and N. Ansari, "Scheduling Hybrid WDM/TDM Passive Optical Networks With Nonzero Laser Tuning Time," *IEEE/ACM Transactions on Networking*, vol. 19, no. 4, pp. 1014–1027, Aug. 2011.

IEEE/ACM Transactions on Networking, accepted for publication.

[17] B. Jang and M. L. Sichitiu, "IEEE 802.11 Saturation Throughput Analysis in the Presence of Hidden Terminals," *IEEE/ACM Transactions on Networking*, vol. 20, no. 2, pp. 557–570, Apr. 2012.

[18] G. Bianchi, "Performance Analysis of the IEEE 802.11 Distributed Coordination Function," *IEEE Journal on Selected Areas in Communications*, vol. 18, no. 3, pp. 535–547, Mar. 2000.

[19] D. Malone, K. Duffy, and D. Leith, "Modeling the 802.11 Distributed Coordination Function in Nonsaturated Heterogeneous Conditions," *IEEE/ACM Trans. Netw.*, vol. 15, no. 1, pp. 159–172, Feb. 2007.

[20] Y. Lin and V. W. S. Wong, "Utility-Optimal Cross-Layer Design for WLAN with MIMO Channels," in *Proc., IEEE ICC*, May 2008, pp. 2612–2617.

[21] L. Kazovsky and et al., "Hybrid Optical-Wireless Access Networks," *Proceedings of the IEEE*, vol. 100, no. 5, pp. 1197–1225, May 2012.

[22] B. Katarci and H. T. Mouftah, "Energy Efficiency in the Extended-Reach Fiber Wireless Access Networks," *IEEE Network*, vol. 26, no. 2, pp. 28–35, March/April 2012.

[23] A. Reaz, V. Ramamurthi, M. Tornatore, and B. Mukherjee, "Green Provisioning of Cloud Services over Wireless-Optical Broadband Access Networks," in *Proc., IEEE GLOBECOM*, Dec. 2011, pp. 1–5.

[24] A. Reaz, V. Ramamurthi, and M. Tornatore, "Cloud-over-WOBAN (CoW): an Offloading-Enabled Access Network Design," in *Proc., IEEE International Conference on Communications (ICC)*, Jun. 2011, pp. 1–5.

[25] A. R. Dhaini, P.-H. Ho, and X. Jiang, "QoS Control for Guaranteed Service Bundles Over Fiber-Wireless (FiWi) Broadband Access Networks," *IEEE J. Lightw. Techn.*, vol. 29, no. 10, pp. 1500–1513, May 2011.

[26] S. Li, J. Wang, C. Qiao, and Y. Xu, "Mitigating Packet Reordering in FiWi Networks," *IEEE/OSA Journal of Optical Communications and Networking*, vol. 3, no. 2, pp. 134–144, Feb. 2011.

IEEE/ACM Transactions on Networking, accepted for publication.

[27] Y. Liu, L. Guo, B. Gong, R. Ma, X. Gong, L. Zhang, and J. Yang, "Green survivability in fiber-wireless (FiWi) broadband access network," *Optical Fiber Technology*, vol. 18, no. 2, pp. 68–80, Mar. 2012.

[28] M. Maier, "Survivability Techniques for NG-PONs and FiWi Access Networks," in *Proc., IEEE ICC*, Jun. 2012, pp. 1–6.

[29] T. Feng and L. Ruan, "Design of a Survivable Hybrid Wireless-Optical Broadband-Access Network," *IEEE/OSA Journal of Optical Communications and Networking*, vol. 3, no. 5, pp. 458–464, May 2011.

[30] B. Kantarci and H. Mouftah, "Reliable and fast restoration for a survivable wireless-optical broadband access network," in *Proc. Int. Conf. on Transparent Optical Networks (ICTON)*, 2010, pp. 1–4.

[31] Y. Liu, L. Guo, R. Ma, and W. Hou, "Auxiliary graph based protection for survivable fiber-wireless (FiWi) access network considering different levels of failures," *Opt. Fiber Techn.*, vol. 18, no. 6, pp. 430–439, 2012.

[32] Z. Yubin, H. Li, X. Ruitao, Q. Yaojun, and J. Yuefeng, "Wireless protection switching for video service in wireless-optical broadband access network," in *Proc. Int. Conf. on Broadband Network Multimedia Technology (IC-BNMT)*, 2009, pp. 760–764.

[33] N. Ghazisaidi, M. Scheutzow, and M. Maier, "Survivability Analysis of Next-Generation Passive Optical Networks and Fiber-Wireless Access Networks," *IEEE Trans. Reliab.*, vol. 60, no. 2, pp. 479–492, June 2011.

[34] Y. Liu, Q. Song, R. Ma, B. Li, and B. Gong, "Protection based on backup radios and backup fibers for survivable fiber-wireless (FiWi) access network," *J. Network and Computer Appl., in print*, 2013.

[35] K. Fouli, M. Maier, and M. Médard, "Network Coding in Next-Generation Passive Optical Networks," *IEEE Communications Magazine*, vol. 49, no. 9, pp. 38–46, Sep. 2011.

IEEE/ACM Transactions on Networking, accepted for publication.

[36] J. Zhang, W. Xu, and X. Wang, "Distributed Online Optimization of Wireless Optical Networks with Network Coding," *IEEE/OSA Journal of Lightwave Technology*, vol. 30, no. 14, pp. 2246–2255, Jul. 2012.

[37] M. Maier, M. Lévesque, and L. Ivanescu, "NG-PONs 1&2 and Beyond: The Dawn of the Über-FiWi Network," *IEEE Network*, vol. 26, no. 2, pp. 15–21, March/April 2012.

[38] M. D. Andrade, G. Kramer, L. Wosinska, J. Chen, S. Sallent, and B. Mukherjee, "Evaluating Strategies for Evolution of Passive Optical Networks," *IEEE Comm. Mag.*, vol. 49, no. 7, pp. 176–184, Jul. 2011.

[39] G. Kramer, M. De Andrade, R. Roy, and P. Chowdhury, "Evolution of Optical Access Networks: Architectures and Capacity Upgrades," *Proceedings of the IEEE*, vol. 100, no. 5, pp. 1188–1196, May 2012.

[40] F. J. Effenberger, "The XG-PON System: Cost Effective 10 Gb/s Access," *IEEE J. Lightw. Techn.*, vol. 29, pp. 403–409, Feb. 2011.

[41] K. Grobe and J.-P. Elbers, "PON in Adolescence: From TDMA to WDM-PON," *IEEE Comm. Mag.*, vol. 46, no. 1, pp. 26–34, Jan. 2008.

[42] D. P. Shea and J. E. Mitchell, "Long-Reach Optical Access Technologies," *IEEE Network*, vol. 21, no. 5, pp. 5–11, Sept./Oct. 2007.

[43] E. H. Ong, J. Kneckt, O. Alanen, Z. Chang, T. Huovinen, and T. Nihilä, "IEEE 802.11ac: Enhancements for Very High Throughput WLANs," in *Proc., IEEE PIMRC*, Sep. 2011, pp. 849–853.

[44] K. Duffy, D. J. Leith, T. Li, and D. Malone, "Modeling 802.11 Mesh Networks," *IEEE Comm. Let.*, vol. 10, no. 8, pp. 635–637, Aug. 2006.

[45] L. Kleinrock, *Queueing Systems.* Wiley, 1975.

[46] F. Aurzada, M. Scheutzow, M. Herzog, M. Maier, and M. Reisslein, "Delay analysis of Ethernet passive optical networks with gated service," *OSA Journal of Optical Networking*, vol. 7, no. 1, pp. 25–41, Jan. 2008.

IEEE/ACM Transactions on Networking, accepted for publication.

[47] W. Bux and M. Schlatter, "An Approximate Method for the Performance Analysis of Buffer Insertion Rings," *IEEE Transactions on Communications*, vol. COM-31, no. 1, pp. 50–55, Jan. 1983.

[48] Y. Lin and V. W. S. Wong, "Frame Aggregation and Optimal Frame Size Adaptation for IEEE 802.11n WLANs," in *Proc., IEEE GLOBECOM*, San Francisco, CA, USA, Dec. 2006, pp. 1–6.

[49] E. Perahia and R. Stacey, *Next Generation Wireless LANs.* Cambridge University Press, 2008.

[50] A. Bianco, J. Finochietto, G. Giarratana, F. Neri, and C. Piglione, "Measurement-based reconfiguration in optical ring metro networks," *IEEE/OSA J. Lightwave Tech.*, vol. 23, no. 10, pp. 3156–3166, 2005.

[51] A. Elwalid, D. Mitra, I. Saniee, and I. Widjaja, "Routing and protection in GMPLS networks: from shortest paths to optimized designs," *IEEE/OSA J. Lightwave Tech.*, vol. 21, no. 11, pp. 2828–2838, 2003.

[52] A. Gencata and B. Mukherjee, "Virtual-topology adaptation for WDM mesh networks under dynamic traffic," *IEEE/ACM Trans. Netw.*, vol. 11, no. 2, pp. 236–247, 2003.

[53] S. Floyd and V. Jacobson, "The synchronization of periodic routing messages," *IEEE/ACM Trans. Netw.*, vol. 2, no. 2, pp. 122–136, 1994.

Chapitre 11

Dependable Fiber-Wireless (FiWi) Access Networks and Their Role in a Sustainable Third Industrial Revolution Economy

Publication:

— M. Maier and M. Lévesque, "Dependable Fiber-Wireless (FiWi) Access Networks and Their Role in a Sustainable Third Industrial Revolution Economy (Invited Paper)," *IEEE Transactions on Reliability*, accepted for publication.

In this chapter, we focus on the implications of the emerging Third Industrial Revolution (TIR) economy, which goes well beyond current austerity measures, and has recently been officially endorsed by the European Commission as the economic growth roadmap toward a competitive low carbon society by 2050. This roadmap has been receiving an increasing amount of attention by other key players, including the Government of China most recently. More specifically, a variety of advanced techniques to render converged bimodal fiber-wireless (FiWi) broadband access networks dependable are described, including optical coding based fiber fault monitoring techniques, localized optical redundancy strategies, wireless extensions, and availability-aware routing algorithms, to improve their reliability, availability, survivability, security, and safety.

IEEE Transactions on Reliability, accepted for publication.

11.1 Abstract

According to the Organisation for Economic Co-operation and Development (OECD), broadband access networks enable the emergence of new business models, processes, inventions, as well as improved goods and services. In fact, broadband access is viewed as a so-called general purpose technology (GPT) that has the potential to fundamentally change how and where economic activity is organized. In this paper, we focus on the implications of the emerging *Third Industrial Revolution (TIR)* economy, which goes well beyond current austerity measures, and has recently been officially endorsed by the European Commission as the economic growth roadmap toward a competitive low carbon society by 2050. This roadmap has been receiving an increasing amount of attention by other key players, e.g., the Government of China most recently. More specifically, we describe a variety of advanced techniques to render converged bimodal fiber-wireless (FiWi) broadband access networks dependable, including optical coding based fiber fault monitoring techniques, localized optical redundancy strategies, wireless extensions, and availability-aware routing algorithms, to improve their reliability, availability, survivability, security, and safety. Next, we elaborate on how the resultant dependent FiWi access networks can be exploited to enhance the dependability of other critical infrastructures of our society, most notably the future smart power grid and its envisioned electric transportation, by means of probabilistic analysis, co-simulation, and experimental demonstration.

Keywords: Energy internet, fiber-wireless (FiWi) access networks, human-to-human (H2H) services, internet of things (IoT), machine-to-machine (M2M) communications, multi-tier business models, network survivability, smart grid.

Acronyms and Abbreviations

AMI	Advanced Metering Infrastructure
A-MPDU	Aggregate MAC Protocol Data Unit
A-MSDU	Aggregate MAC Service Data Unit
AP	Access Point
BER	Bit Error Rate
BPL	Broadband Power Line
CAPEX	Capital Expenditures
CO	Central Office
DDoS	Distributed Denial-of-Service
DER	Distributed Energy Resource
DMS	Distribution Management System
DSL	Digital Subscriber Line
EPON	Ethernet Passive Optical Network
FBG	Fiber Bragg Grating
FiWi	Fiber-Wireless
Fi-WSN	Fiber-Wireless Sensor Network
FTTB	Fiber-To-The-Building
FTTH	Fiber-To-The-Home
G2V	Grid-To-Vehicle

GPT	General Purpose Technology
H2H	Human-To-Human
HAN	Home Area Network
IoT	Internet of Things
LAN	Local Area Network
M2M	Machine-To-Machine
MAC	Medium Access Control
MAP	Mesh Access Point
MP	Mesh Point
MPP	Mesh Portal Point
NAN	Neighborhood Area Network
NG-PON	Next-Generation Passive Optical Network
OC	Optical Coding
OECD	Organisation for Economic Co-operation and Development
OFDM	Orthogonal Frequency Division Multiplexing
OLT	Optical Line Terminal
ONU	Optical Network Unit
OPEX	Operational Expenditures
OTDR	Optical Time Domain Reflectometry

PEV	Plug-in Electric Vehicle
PLC	Power Line Communications
PON	Passive Optical Network
QoS	Quality of service
RN	Remote Node
SLA	Service Level Agreement
SMS	Short Message Service
STA	Station
TDM	Time Division Multiplexing
TIR	Third Industrial Revolution
V2G	Vehicle-To-Grid
VDSL	Very High Bit-Rate Digital Subscriber Line
VHT	Very High Throughput
WASA	Wide-Area Situational Awareness
WDM	Wavelength Division Multiplexing
WiMAX	Worldwide Interoperability for Microwave Access
WLAN	Wireless Local Area Network
WMN	Wireless Mesh Network
WSN	Wireless Sensor Network

NOTATION

A	Size of a transmitted A-MSDU
D	Number of failure-free connections between pairs of ONUs
E_ω	Mean duration of a time slot at WMN node ω
H	Maximum backoff stage of WMN nodes
L_i	Size of i-th frame in a transmitted A-MPDU
M	Number of ONU-MPPs
N	Number of ONUs
$\mathcal{O}$	Subset of ONUs optically connected to OLT after fiber failure(s)
p_b	Probability of bit error in WMN (BER)
$p_{c,\omega}$	Probability of a collision at WMN node ω
p_e	Probability of erroneously transmitted frame aggregate in WMN
p_i	Probability of fiber link failure in stage i
p_ω	Probability of either a collision or transmission error at WMN node ω
q_ω	Probability that a frame is waiting for transmission at WMN node ω in a time slot
W_0	Minimum contention window of WMN nodes
$\mathcal{W}$	Set of ONU-MPPs
σ_ω	Frame arrival rate at WMN node ω

IEEE Transactions on Reliability, accepted for publication.

11.2 Introduction

Many vital building blocks, organizations, and activities of today's society depend on the continued operation of various large, widespread, critical infrastructures, including telecommunications networks, and transportation systems. In particular, energy generation and distribution systems play a crucial role. Electrical power grids represent one of the most important critical infrastructures of our society. Current power grids, with their aging infrastructure, become increasingly unreliable, and are poorly suited to face increasingly frequent outages. Examples include the three-day blackout due to trees falling on power lines in the Washington D.C. area in early July 2012, the lengthy power blackout in the states of New York and New Jersey due to hurricane Sandy in October 2012, or more recently the 34 minute power outage during the Super Bowl in 2013.

In coming years, power grids in the United States, Europe, and other regions worldwide are expected to undergo major paradigm shifts. Today, Internet technology and renewable energies are beginning to merge to create the infrastructure for the so-called *Third Industrial Revolution (TIR)* economy, which goes well beyond current austerity measures, and has been officially endorsed by the European Commission as an economic growth roadmap toward a competitive low carbon society by 2050. TIR has already been implemented by several early-adopting countries such as Germany, England, and Italy, as well as cities such as San Antonio, TX, USA, among others [1]. In the coming era, millions of consumers will produce their own renewable energy, and share it with each other via an integrated, seamless *Energy Internet*, similar to the way we create and share information online.

The future Energy Internet aims at not only addressing the aforementioned reliability issues of current power grids but also offering several additional major benefits. The Energy Internet will be instrumental in realizing the vision of the *smart grid* by incorporating sophisticated sensing, monitoring, information, and communications technologies to provide better power grid performance, engage customers to play an interactive role, and support a wide range of additional services to both utilities and consumers. Potential smart grid applications include substation and distribution automation, advanced metering infrastructure (AMI), wide-area situational awareness (WASA), home energy and demand response management, outage management, distributed generation and renewables, and grid-to-vehicle (G2V) and vehicle-to-grid (V2G) electricity storage and charging applications for plug-in electric vehicles (PEVs) [2]. The authors also quantified the communications requirements of the aforementioned smart grid applications in terms of latency, bandwidth, reliability, and security; and concluded that a *reliable*, *fast* smart grid communications infrastructure is necessary to enable real-time exchange of data among distributed power grid elements, e.g., power generators, energy storage systems, and users.

A plethora of wired and wireless networking technologies exists to realize smart grid communications infrastructures [3]. It is important to note, however, that in general the goal of utilities is to use only a small number of low-cost, simple, reliable, and future-proof smart grid communications technologies that remain in place for decades after installation. It is also worthwhile to mention that IEEE P2030, one of the first smart grid standards, does not specify any communications technology of choice for the future smart grid gradually evolving between now and 2030, though it is favorable to rely on the exceptionally low latency characteristics of fiber optic facilities, either owned or leased by the smart grid operator, and wireless technologies, where fiber is available to some but not all points in the system [4].

In this paper, we focus on the distribution and customer levels of today's power grid given that utilities do not have visibility into their power distribution networks, where the majority of power outages occur, and where most of the opportunities for energy efficiency and integration of renewable distributed energy resources (DERs), e.g., solar panels and wind turbines, can be found [5]. Furthermore, we will pay particular attention to homes because the majority of the generated electricity is currently consumed in homes. Moreover, PEVs will be charged mostly at homes after business hours, and homes will host the largest number of renewable DERs [6]. Given the huge number of homes, smart grid communications solutions must be scalable, and use access technologies that meet a number of specific requirements. After providing a brief overview of a wide range of available smart grid communications technologies, and discussing their respective pros and cons, we elaborate on the evolution of current broadband access networks toward integrated bimodal *fiber-wireless (FiWi)* access networks within the next 10-20 years in line with the emergence of the smart grid by 2030, while copper remains the energy (but not necessarily data) transmission medium of choice in future smart power grids. We describe various techniques to improve the availability and survivability of bimodal FiWi access networks. More interestingly, and getting back to what we have briefly touched upon at the beginning of this section, we elaborate on how the resultant dependent FiWi broadband access networks can be used to enable and enhance the dependability of other critical infrastructures, most notably power grids. In fact, NSERC, Canada's federal research agency, postulates that broadband access networks become *less an end in itself than a means to an end* by exploiting them not only for telecommunications per se but also across other relevant economic sectors such as energy and transportation, as also envisioned by the Third Industrial Revolution. In doing so, we unleash the full potential of broadband access networks, which according to the Organisation for Economic Co-operation and Development (OECD) may be viewed as a so-called *general purpose technology (GPT)* that enables the emergence of new business models, processes, inventions, as well as improved goods and services; and empowers societies to fundamentally change how and where economic activity is organized.

The remainder of the paper is structured as follows. Section 11.3 briefly describes the shortcomings of various wired and wireless candidate smart grid communications technologies, and then outlines the migration of current broadband access networks toward FiWi access networks based on next-generation optical and wireless technologies, including a detailed description of their limitations in terms of availability and survivability. In Section 11.4, we elaborate on powerful means to improve the dependability of FiWi access networks, and explain various advanced techniques such as optical coding based fiber fault monitoring techniques, localized optical redundancy strategies, wireless extensions, and availability-aware routing algorithms, in greater detail. Section 11.5 introduces FiWi smart grid communications infrastructures, paying particular attention to the benefits of emerging multi-tier business models, and presents analytical, co-simulation, and experimental results on both the communications and power system perspectives of the future smart grid towards enhancing its dependability significantly. Section 11.6 concludes the paper.

11.3 FiWi Access Networks

A variety of readily available wired and wireless communications technologies exists to realize smart grid communications infrastructures. In the following, we briefly overview previously proposed candidate technologies, and outline their respective shortcomings with regard to smart grid communications requirements.

Clearly, an obvious choice may be the use of power line communications (PLC) technologies, which leverage the existing electrical power grid infrastructure for communications. The emerging ITU-T recommendation G.hnem is expected to exploit orthogonal frequency division multiplexing (OFDM) based technologies to target smart grid applications such as smart metering, distributed automation, in-home energy management, home automation, or PEV charging [7]. However, it is well known that PLC suffers from a fundamental drawback: in the event of (increasingly frequent) electrical power grid blackouts, PLC based solutions inherently become unavailable; and this is when they would be needed most for coordinating fast recovery and first response actions. ZigBee Smart Energy was developed for communications between the home area network (HAN) and the home's gateway over a wireless sensor network (WSN) [6]. However, measurements have shown that WSNs may suffer from high bit error rates when applied in harsh electric power system environments [8]. Cognitive radio might be useful for rural areas, but falls short for more densely populated areas [9]. Cellular networks and SMS text messages have been proposed for PEV charging, but the delays of 6 seconds or more reported in [10] render this solution unsuitable for real-time smart grid applications, including power network fault detection.

Currently, there are many technologies for the last mile to connect home gateways to the smart grid, all of them trying to play a role in the smart grid market, thus leaving utilities in an uncertain situation [11]. Recall from above that in general the goal of utilities is to use only a small number of low-cost, simple, reliable, and future-proof access technologies for holistic long-term solutions. We have already outlined the shortcomings of some network technologies above. In addition, to build their SmartGridCity (SGC), one of the most advanced smart grid pilot projects, Xcel Energy ruled out several access technologies. Upon email inquiry, Xcel Energy informed us that, during the initial design of the system, Xcel Energy looked at a number of alternatives to fiber optic cable, including satellite, cable, wireless, and digital subscriber line (DSL). The most promising looked to be utilizing a portion of the fiber backbone being built by Qwest in Boulder as part of their DSL upgrade. The topologies, type of fiber, available dark fibers, and location of termination points were reviewed against the needs of the SGC initiative. In addition, the Qwest build plan was

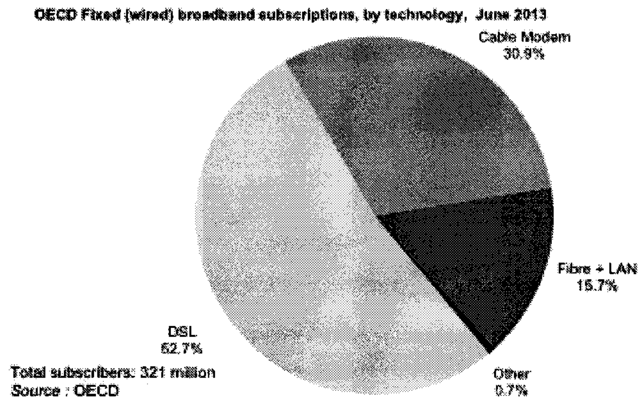

Figure 11.1 – Broadband subscribers across OECD countries by technology: fixed wired access technologies used in 2013 [13].

compared to the SGC plan. While the fiber from Qwest could be suitable for SGC, the location of the Qwest fiber termination points were not close enough to the SGC injection points to offer any practical advantages; and further, the timing of the builds were not sufficiently aligned to allow the two systems to leverage the same fiber routes. Other solutions such as satellite (high latency, and inability to deal with underground), cable (proximity, meter attachment, and inability to deal with underground or transformers), wireless (some potential latency issues, inability to deal with underground, lack of cards for existing meter types, potential coverage issues, and potential security issues), and DSL (lack of complete coverage, no ruggedized service offering) were considered by Xcel Energy. Finally, taking the aforementioned constraints and shortcomings into account, Xcel Energy decided to deploy their own fiber optic cable, and utilize broadband power line (BPL) to the individual premises within the SGC project's footprint.

Keeping in mind that utilities typically have developed their own roadmap to establish the smart grid within the next 10-25 years, e.g., Toronto's sustainable energy strategy [12], it is crucial to understand how broadband access networks will evolve over the next couple of decades to make the right investment decisions and technology choices for the long term. According to the OECD Broadband Portal, back in 2010 the majority of fixed broadband subscribers deployed DSL or cable modems, while only 9% of the 271 million subscribers were connected via fiber-to-the-premises solutions, i.e., fiber-to-the-home (FTTH) or fiber-to-the-building (FTTB), with local area network (LAN) deployment in apartments. (For completeness, we note that the remaining 2% of subscribers were provided broadband access via satellite, WiMAX, or BPL.) However, this situation is changing rapidly. For illustration, Fig. 11.1 shows the latest OECD data on fixed wired broadband subscriptions as of June 2013. Clearly, this figure illustrates that an increasing percentage of broadband subscribers rely on fiber access technologies, at the expense of legacy DSL solutions. This trend is expected to become even more pronounced over the next couple of decades. In the short- to mid-term, current state-of-the-art very high bit-rate DSL (VDSL) may be superseded by next-generation copper based solutions supported by deep fiber access networks getting increasingly closer to subscribers. According to [14], however, there is no doubt that FTTH or FTTB will eventually become the predominant fixed broadband technology of choice by 2035, paving the way toward all-fiber wired infrastructures, as already witnessed in the Asia-Pacific region and some east European countries that directly opted for FTTH or FTTB solutions to leapfrog legacy broadband access technologies. It is worth mentioning that FTTH or FTTB networks are increasingly installed by utilities and municipalities, rather than incumbents, by leveraging their existing duct, sewer, and other infrastructure. An interesting example is the national Swiss Fibre Net of OPENAXS, an association of currently 22 regional electricity utilities throughout Switzerland [1]. The goal of Swiss Fibre Net is to create added value for consumers by having 30% FTTH or FTTB connected households by 2013, and 80% by 2020.

Typically, FTTH or FTTB networks are realized via passive optical networks (PONs) due to their well-known merits, e.g., low operational expenditures (OPEX), longevity, and future-proofness. In addition, PONs provide the lowest energy consuming solution for broadband access, clearly outperforming optical point-to-point access networks, hybrid fiber-copper based access technologies, and wireless access solutions, e.g., WiMAX, in terms of energy per bit [15, 16]. This property assures that PONs will play an important role in response to concerns about the greenhouse impact of the Internet, especially given that access networks dominate the total power consumption of today's Internet [16]. More importantly, PONs are inherently highly *reliable* due to their completely passive (i.e., unpowered) network infrastructure.

Conventional IEEE and ITU-T standardized Gigabit-class time division multiplexing (TDM) PONs currently evolve into next-generation PONs (NG-PONs). A variety of NG-PON technologies

1. Visit `http://www.openaxs.ch` for further information.

have been investigated to enable short-term evolutionary and long-term revolutionary upgrades of co-existent Gigabit-class TDM PONs, e.g., long-reach PON or OFDM PON [17]. However, the most promising solutions for PON evolution toward higher bandwidth per user are (*i*) data rate upgrades to 10 Gb/s and higher, and (*ii*) multi-wavelength channel migration toward wavelength-routing or wavelength-broadcasting wavelength division multiplexing (WDM) PONs, with or without cascaded TDM PONs [18, 19].

Despite their aforementioned desirable properties, and numerous currently ongoing PON (r)evolution activities, state-of-the-art PONs as well as NG-PONs generally fall short of availability and survivability.

— **Availability-** In power-splitting PONs, e.g., conventional wavelength-broadcasting TDM PONs or multi-stage WDM PONs containing splitters at one or more stages, it is difficult to identify and localize faults within the optical infrastructure. To see this, note that well-known maintenance techniques, most notably optical time domain reflectometry (OTDR) based techniques for troubleshooting, work fine in wavelength-routing WDM PONs that deploy a wavelength (de)multiplexer at the remote node (RN), whereby each wavelength channel forms a logical point-to-point link whose individual backscattered signal enables both fault detection and fault localization on the respective feeder fiber branching out from the RN. OTDR becomes less effective for power-splitting PONs because a branch's backscattering signal can be partially or totally masked by other branch signals, thus making it difficult to differentiate them. As a result, PON network operators may have to rely on disconnected subscribers to call in and report on the fault, and then send technicians in the field to fix it. Clearly, this approach satisfies the cost constraints of highly cost-sensitive access networks that serve a relatively small number of cost-sharing subscribers, at the expense of slow fault recovery times and therefore lowered availability.

— **Survivability-** For the very same cost reasons, PONs are typically unprotected, even though network operators have the choice to deploy one of the four standardized types of protection referred to as Type A, B, C, and D in ITU-T recommendation G.983.1. These protection types improve the survivability of PONs in general against link and node failures by means of redundancy, whereby protection Types B and C represent the most promising solutions to provide an acceptable trade-off between achievable survivability and required redundancy. In most practical deployments, however, PONs are left unprotected due to the cost-sensitivity of optical access networks. In current PONs, the number of optical network units (ONUs), the customer premises equipment of PON-connected buildings, is rather small (typically 16 to 64 ONUs per PON), thus limiting the local impact of failures to a rather small number of subscribers. As a result, without protection, currently deployed PONs are fault-intolerant, e.g., a single feeder fiber cut disconnects all ONUs from the central optical line terminal (OLT).

There is a tacit consensus among researchers and practitioners in the PON community that the fault-tolerant design and key dependability properties such as availability and survivability will become increasingly important in emerging NG-PONs. More specifically, service and business continuity guarantees are expected to play a more prominent role in future optical access networks given that NG-PONs carry significantly increased traffic loads on multiple WDM channels, each operating at 10 Gb/s or higher. Long-reach NG-PONs hold great promise to achieve major cost savings by consolidating access and metropolitan area networks, and thereby serving much larger areas covering hundreds or even thousands of ONUs. Nevertheless, it remains to be seen whether these developments will justify the use of costly optical protection techniques given the cost sensitivity of access networks and the number of cost-sharing subscribers. A more viable solution appears to be to (*i*) rely on *localized optical redundancy* strategies based on (historical or estimated) fiber failure probabilities, and (*ii*) exploit *wireless extensions* of carefully selected optical network nodes to provide a less costly fiber-lean survivability approach for NG-PONs via converged FiWi access networks.

FiWi access networks aim at combining the reliability, robustness, and high capacity of optical fiber networks with the flexibility, ubiquity, and cost savings of wireless networks [20]. Fig. 11.2 depicts the architecture of a typical FiWi access network. The PON may be a conventional IEEE 802.3ah compliant wavelength-broadcasting TDM Ethernet PON (EPON) based on a wavelength splitter-combiner at the RN, using one time-shared wavelength channel for upstream transmissions (from the ONUs to the OLT), and another separate time-shared wavelength channel for downstream transmissions (from the OLT to the ONUs), both operating at a data rate of 1 Gb/s. A subset of

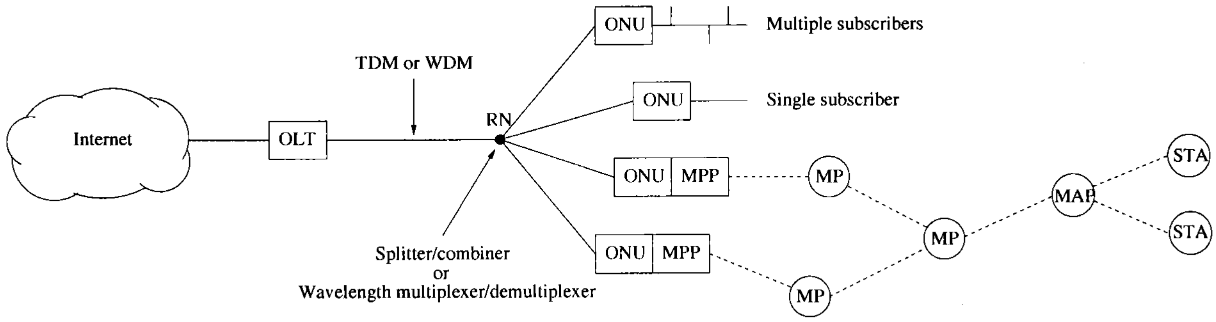

Figure 11.2 – FiWi access network architecture based on single- or multi-stage TDM or WDM PON and multihop WMN using legacy or VHT WLAN technologies.

ONUs may be located at the premises of residential or business subscribers, whereby each ONU provides FTTH or FTTB services to a single or multiple attached wired subscribers. For these ONUs, it will be crucial to have appropriate PON monitoring and protection techniques in place to provide a sufficient level of availability and survivability at reasonable costs. The remaining ONUs may be equipped with a mesh portal point (MPP) to interface with the wireless mesh network (WMN), which in turn consists of relay mesh points (MPs) and mesh access points (MAPs) to provide stations (STAs) with wireless access to the FiWi network. The WMN can be used for wireless protection of optically disconnected ONUs. Most previous FiWi studies assumed a WMN based on IEEE 802.11a/b/g wireless local area network (WLAN) technologies, offering a maximum raw data rate of 54 Mb/s at the physical layer.

Future FiWi access networks will leverage next-generation PON and WLAN technologies to meet the ever increasing bandwidth requirements of new and emerging applications and services. To alleviate the bandwidth bottleneck of wireless mesh front-end networks, future FiWi access networks are expected to be based on next-generation IEEE 802.11n WLAN, which offers data rates of 100 Mb/s or higher at the medium access control (MAC) service access point. Furthermore, access network designs will exploit emerging IEEE 802.11ac very high throughput (VHT) WLAN technologies, which achieve significantly increased raw data rates. More specifically, beside various PHY layer enhancements, IEEE 802.11n next-generation WLAN provides two frame aggregation techniques, Aggregate MAC Service Data Unit (A-MSDU) and Aggregate MAC Protocol Data Unit (A-MPDU), as the main MAC enhancements. The WMN may be upgraded with emerging IEEE

802.11ac VHT WLAN technologies that achieve raw data rates of up to 6900 Mb/s, and provide an increased maximum A-MSDU/A-MPDU size [21].

11.4 FiWi Network Dependability Techniques

In this section, we elaborate on the aforementioned localized optical redundancy strategies and wireless extensions in technically greater detail. We describe several techniques to render FiWi access networks dependable. These techniques can be used separately or jointly to achieve different levels of FiWi network dependability in a modular fashion for given cost constraints and performance requirements, ranging from low-cost broadband access deployments to highly critical smart grid communications infrastructures. In the following, we pay close attention to the fact that dependability has many facets, and includes several important system properties, most notably reliability, availability, survivability, security, and safety.

11.4.1 Reliability

Recall from above that PONs are inherently highly reliable due to their completely passive network infrastructure. Conversely, wireless channels are much less reliable due to a variety of severe physical transmission impairments, e.g., multipath fading or interference. For an improved reliability of bimodal FiWi access networks, the design of appropriate routing algorithms plays a major role. For instance, routing algorithms that mitigate interferences in the wireless front-end by selecting paths with a minimum number of wireless hops and offloading it by steering as much traffic as possible across the fiber backhaul represent a promising solution, as investigated in more depth shortly.

11.4.2 Availability

To enable both fiber fault detection and localization with minimum delay, and thereby help improve the availability of NG-PONs, advanced monitoring techniques need to be designed. The

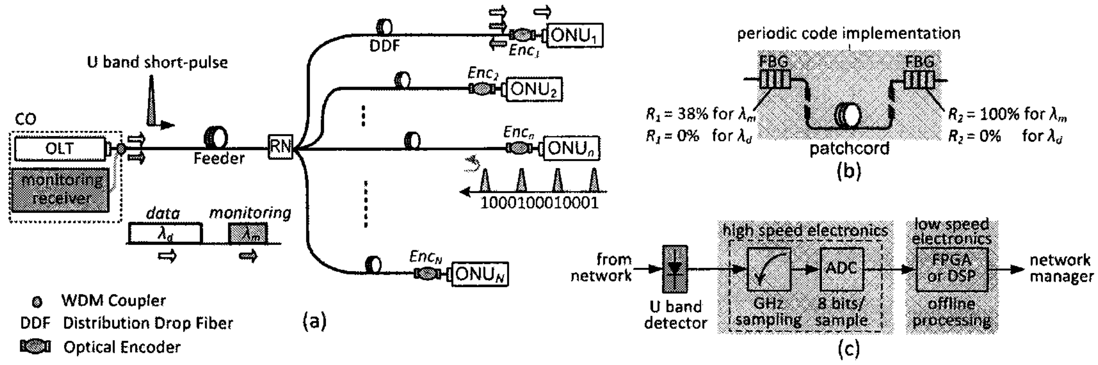

Figure 11.3 – Optical coding based PON monitoring: (a) architecture, (b) encoder, and (c) monitoring receiver.

aforementioned ITU-T recommendation G.983.1 does not specify how to identify and localize faults within the optical infrastructure, and defers the task to maintenance standards (ITU-T L series). ITU-T L.53 (2003) was the first standard to specifically address the maintenance of PONs by recommending the use of OTDR based techniques for troubleshooting. In-service monitoring of NG-PONs' fiber infrastructure without disturbing ongoing services is expected to become increasingly important to avoid the OPEX and large service restoration times of offline troubleshooting. Accordingly, ITU-T recommendation L.66 was approved in 2007 to reserve the U-band (1625-1675 nm) for in-service maintenance of PONs, and to specify methods for implementation, e.g., OTDR. OTDR works fine in single-stage WDM PONs that deploy a wavelength (de)multiplexer at the RN such that each wavelength channel forms a logical point-to-point link. By using a tunable multi-wavelength OTDR source at the OLT, this approach provides a centralized monitoring system that enables both fault detection and fault localization in feeder as well as distribution fibers. However, recall from above that OTDR becomes less effective for power-splitting PONs. In addition, the huge loss by splitters leads to a significant drop in measured backscattered light from each branch, though some manufacturers offer so-called *PON-tuned OTDR* solutions that allow for tests across splitters with losses of up to 20 dB.

In [22], we reported on the requirements and challenges of modified OTDR solutions, and also described alternative non-OTDR based PON monitoring techniques. A promising technique is optical coding (OC) based PON monitoring, where passive out-of-band encoders (Enc) are placed at the end of each PON distribution fiber to identify and monitor it, as shown in Fig. 11.3(a). The data, and monitoring signals occupy separate wavelength bands λ_d, and λ_m, respectively, consistent with emerging standards. At the central office (CO), an optical source transmits out-of-band pulses downstream, and a monitoring receiver processes the aggregate upstream reflected signals. Note that the encoders both reflect and imprint a unique code specific to the PON distribution fiber on the source pulses. While several encoders, e.g., fiber Bragg grating (FBG), and receivers have been proposed, the most cost-effective, high-performance solution that has emerged is a combination of periodic codes and an electronic receiver, as illustrated in Fig. 11.3(b) and (c).

11.4.3 Survivability

After detecting and localizing a fiber fault, partial optical or wireless protection techniques are triggered for fault recovery, as explained in more detail in the following. Fig. 11.4 depicts the generic tree-and-branch topology of a multi-stage NG-PON, which might be a long-reach PON with or without WDM and high-speed TDM upgrades. Note that each of the N ONUs is allowed to be at a different distance from the OLT, spanning a different number of stages. The generic topology also includes the special case of conventional TDM PONs, where each ONU is located at two stages from the OLT, whereby stage 0 ranges from the OLT to the RN, and stage 1 fans out from the RN to the ONUs. Without loss of generality, the RN is assumed to be a power splitter, but it might be also a wavelength (de)multiplexer or any cascaded multi-stage configuration thereof. Furthermore, we assume that each stage i, $i = 0, 1, \ldots$, can be assigned a certain fiber failure probability p_i based on historical records or estimates. That is, each fiber link of stage i is assumed to fail with the same probability p_i, though p_i may be different for each separate stage. We also assume that a subset of $0 \leq M \leq N$ selected ONUs may be interconnected via a wireless mesh front-end.

Next, let $\mathcal{O}$ be the random subset of ONUs, which are connected to the OLT optically after one or more fiber link failures have occurred. We denote $\mathcal{W}$ for the set of ONUs that have been selected to be equipped with an MPP to interface with the front-end WMN, where $|\mathcal{W}| = M \leq N$. Generally speaking, $\mathcal{W}$ should be chosen as small as possible to satisfy given cost constraints, while at the same time guaranteeing a high degree of survivability.

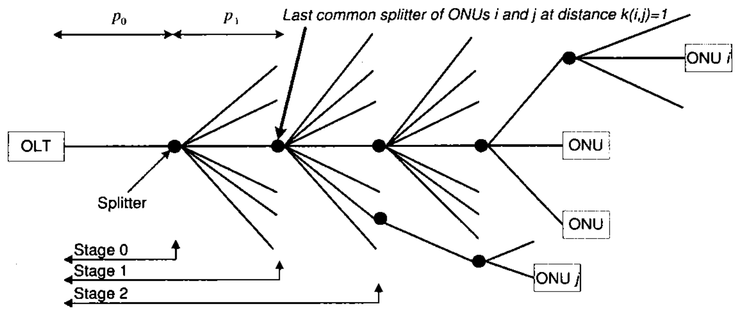

Figure 11.4 – Generic multi-stage NG-PON topology with historical or estimated fiber failure probability p_i assigned to each stage i.

The average number of failure-free connections among ONUs (i.e., pairs of ONUs connected by optical or wireless links) can be defined as

$$D := \mathbb{E}\left[\left(\sum_{i=1}^{N} \mathbb{1}_{\mathcal{O}\cup\mathcal{W}}(i)\right)\left(\left(\sum_{j=1}^{N} \mathbb{1}_{\mathcal{O}\cup\mathcal{W}}(j)\right) - 1\right)\right], \tag{11.1}$$

where $\mathbb{1}_{\mathcal{O}\cup\mathcal{W}}(i)$ denotes the indicator function of subset $\mathcal{O}\cup\mathcal{W}$ for a given ONU i and is given by

$$\mathbb{1}_{\mathcal{O}\cup\mathcal{W}}(i) = \begin{cases} 1, i \in (\mathcal{O}\cup\mathcal{W}) \\ 0, i \notin (\mathcal{O}\cup\mathcal{W}). \end{cases} \tag{11.2}$$

For further details on the computation of D, refer to [23]. In the following, we briefly highlight the merits of partial optical and wireless protection towards improving the survivability of FiWi access networks. For illustration, Fig. 11.5 shows the average number D of failure-free connections vs. the number $0 \le M \le N$ of wirelessly upgraded ONUs with and without optical protection for a 5-stage PON of $N = 465$ ONUs, whereby the M ONUs with the smallest probability of being (optically) connected to the OLT are wirelessly upgraded with an MPP. With optical protection, the wirelessly upgraded ONUs are additionally optically protected by means of back-up fibers such that their optical connection to the OLT can be considered safe, whereby OP denotes the number of optically protected ONUs. Under the assumption of an ascending fiber failure probability from OLT towards ONUs, Fig. 11.5 clearly demonstrates that deploying partial optical protection in combination with

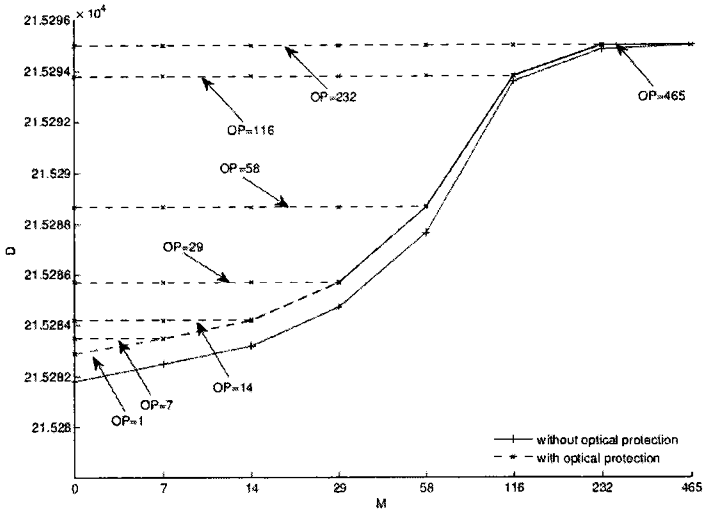

Figure 11.5 – Average number D of failure-free connections vs. number M of wirelessly upgraded ONUs for a five-stage NG-PON topology ($N = 465$) with and without partial optical protection.

using a wireless mesh front-end to re-route traffic affected by fiber failures increases D significantly, while requiring only a small to medium number M of wirelessly upgraded ONUs.

In our somewhat simplistic discussion above, we have assumed that WMNs do not suffer from any link failures, and therefore are always available. Clearly, wireless channels are much less reliable than their optical fiber counterparts due to several severe transmission impairments. By capitalizing on the aforementioned fiber fault detection, localization, and partial optical protection techniques, NG-PONs can be designed to meet high levels of availability. It is well understood that consequently the availability of optical links and wireless links differ significantly from each other; and that *availability-aware routing* should be applied not only to meet the specified availability, an important parameter in many service level agreements (SLAs) between network operator and subscribers, but also to increase the overall availability and survivability of FiWi access networks by making more use of monitored and protected NG-PONs [24]. While NG-PONs are able to provide high availability and survivability levels, the performance of wireless links depends on a variety of external parameters, which in many cases can be only modelled statistically [25].

In the WMN, we capture the impact of various external parameters on the wireless channel by its bit error rate (BER) $p_b > 0$, while the BER of the NG-PON can be considered negligible, and therefore is set to zero. However, individual fiber links may fail due to fiber cuts and become unavailable for routing traffic across the NG-PON. For a WMN using A-MSDU or A-MPDU, the probability p_e of an erroneously transmitted frame aggregate is given by [26]

$$p_e = \begin{cases} 1-(1-p_b)^A & \text{for A-MSDU,} \\ \prod_i \left(1-(1-p_b)^{L_i}\right) & \text{for A-MPDU,} \end{cases} \tag{11.3}$$

where A is the size of a transmitted A-MSDU, index i runs from one to the total number of aggregated frames, and L_i is the size of the i-th frame in a transmitted A-MPDU. By using p_e, the probability of either a collision or transmission error, p_ω, at WMN node ω can be computed as

$$1 - p_\omega = (1-p_e)\cdot(1-p_{c,\omega}), \tag{11.4}$$

whereby the collision probability $p_{c,\omega}$ is given by

$$1 - p_{c,\omega} = \prod_{\nu\neq\omega}(1-\tau_\nu). \tag{11.5}$$

For any WMN node ω, we have

$$\tau_\omega = \frac{1}{\eta}\left(\frac{q_\omega^2\cdot W_0}{(1-q_\omega)(1-p_\omega)[1-(1-q_\omega)^{W_0}]} - \frac{q_\omega^2(1-p_\omega)}{1-q_\omega}\right) \tag{11.6}$$

with

$$\begin{aligned}\eta = {} & \frac{q_\omega W_0}{1-(1-q_\omega)^{W_0}} + \frac{q_\omega W_0(q_\omega W_0 + 3q_\omega - 2)}{2(1-q_\omega)[1-(1-q_\omega)^{W_0}]} \\ & +(1-q_\omega) \\ & +\frac{q_\omega(W_0+1)[p_\omega(1-q_\omega)-q_\omega(1-p_\omega)^2]}{2(1-q_\omega)} \\ & +\frac{p_\omega q_\omega^2}{2(1-q_\omega)(1-p_\omega)}\left(\frac{W_0}{1-(1-q_\omega)^{W_0}} - (1-p_\omega)^2\right) \\ & \cdot\left(\frac{2W_0[1-p_\omega-p_\omega(2p_\omega)^{H-1}]}{1-2p_\omega}+1\right),\end{aligned} \tag{11.7}$$

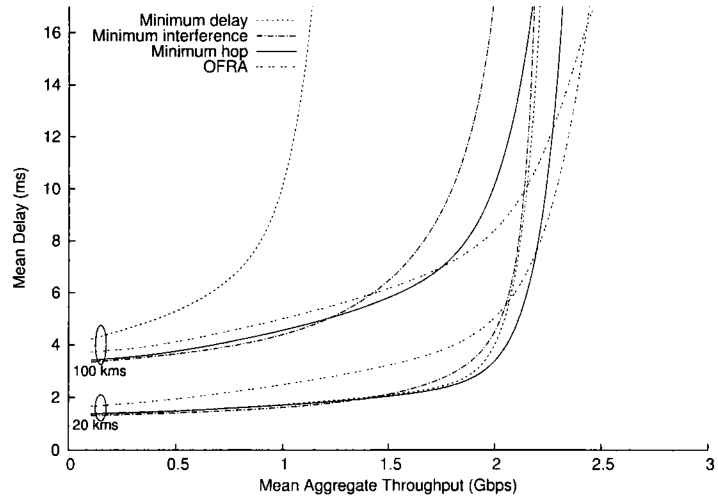

Figure 11.6 – Mean delay vs. mean aggregate throughput performance of different FiWi routing algorithms for (*i*) a conventional 20 km range, and (*ii*) a 100 km long-reach wavelength-routing WDM PON.

where, for exponentially distributed inter-frame arrival times with mean $1/\sigma_\omega$, the probability q_ω that there is a frame waiting for transmission at WMN node ω is related to its offered frame load σ_ω during mean slot duration E_ω via

$$1 - q_\omega = e^{-\sigma_\omega \cdot E_\omega}. \tag{11.8}$$

Furthermore, W_0 is node ω's minimum contention window, $W_0 2^H$ is the node's maximum window size, and H is the maximum backoff stage [27].

Building on these basic probabilities, we have recently developed an analytical framework for the capacity and delay evaluation of routing algorithms for FiWi access networks based on NG-PON and high-throughput WLAN technologies. We refer the interested reader for further details, including verifying simulations, to [28], and continue to briefly describe some of the obtained major results. Fig. 11.6 shows the throughput-delay performance of an IEEE 802.11n based WMN front-end with a physical data rate of r = 300 Mb/s using either (*i*) a conventional 20 km range IEEE 802.3ah TDM EPON, or (*ii*) a 100 km long-reach wavelength-routing WDM PON with two bidirectional wavelength channels, each operating at a data rate of $c^{(\lambda)}$ = 1 Gb/s. We set the BER of the WMN to $p_b = 10^{-6}$. To illustrate the flexibility of our analytical framework and study the impact of different routing algorithms on the throughput-delay performance of next-generation FiWi access networks, we consider the following four routing algorithms: (*i*) *minimum delay routing* similar to DARA [29], (*ii*) *minimum (wireless) interference routing* [30], (*iii*) *minimum (wireless or optical) hop routing*, and (*iv*) an *optimized FiWi routing algorithm (OFRA)*, whose objective function

$$min_p \left(\sum_{\forall n \in p} (\rho_n) + max_{\forall n \in p}(\rho_n) \right) \tag{11.9}$$

aims at finding the path p with the minimum traffic intensity ρ at intermediate optical and wireless nodes n. Given that the capacity of optical access networks is typically higher than that of their wireless counterparts, OFRA gives preference to steering traffic toward the fiber backhaul, and offloading the wireless front-end. Fig. 11.6 clearly illustrates that minimum delay routing performs poorly in terms of delay and throughput, and is ill-suited for long-reach WDM PON based FiWi networks because it steers most traffic across the WMN to avoid the optical propagation delay. As a result, the huge bandwidth of the long-reach WDM PON is heavily under-utilized while the wireless front-end gets congested, translating into a deteriorated throughput-delay performance. Note that OFRA is able to maximize the aggregate throughput of both conventional and especially long-reach PONs by routing more traffic across the more reliable fiber backhaul, and exploiting its high capacity and availability. For the long-reach WDM PON, we observe that minimum hop and minimum interference routing as well as OFRA provide comparable delays at low to medium traffic loads, while the maximum achievable throughput differences at high traffic loads are more pronounced than for the 20 km range. The favorable performance of OFRA at high traffic loads is potentially of high practical relevance because access networks are the bottlenecks in many networking scenarios, and thus experience relatively high loads while core networks operate at a low to medium bandwidth utilization.

Under the assumption of minimum hop routing, Fig. 11.7 depicts the performance gain achieved by using a wireless front-end based on VHT WLAN instead of state-of-the-art 802.11n WLAN, whose maximum data rate is limited to 600 Mb/s. For a wavelength-routing WDM PON operating at a wavelength channel data rate of 1 Gb/s, we observe from Fig. 11.7 that VHT WLAN roughly triples the maximum mean aggregate throughput, and clearly outperforms 600 Mb/s 802.11n WLAN

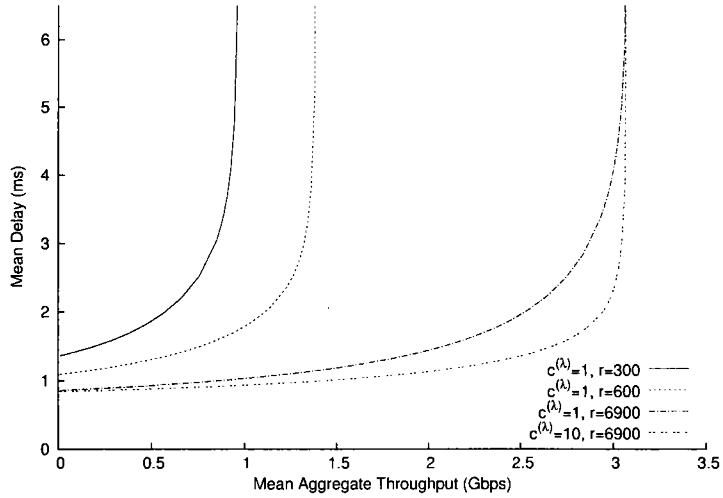

Figure 11.7 – Mean delay vs. mean aggregate throughput performance of next-generation FiWi access networks based on high-speed wavelength-routing WDM PON and VHT WLAN technologies ($c^{(\lambda)}$, and r are given in Gb/s, and Mb/s, respectively).

in terms of both throughput and delay. Furthermore, the figure shows that replacing the 1 Gb/s wavelength-routing WDM PON with its high-speed 10 Gb/s counterpart (both with an optical range of 20 km) does not yield a higher maximum aggregate throughput, but it does help lower the mean delay, especially at medium traffic loads before wireless links at the optical-wireless interfaces get increasingly congested at higher traffic loads.

11.4.4 Security and Safety

For enhanced cyber security, the various PONs and WLANs may apply IEEE standard 802.1AE and 802.11i, respectively, in conjunction with the aforementioned optical and wireless networking standards. Furthermore, public key infrastructure technologies along with trusted computing elements, were shown to be effective to secure the smart grid and its underlying communications infrastructures [31].

In terms of physical safety, FiWi access networks can be used to monitor the power grid and detect anomalies that may pose a threat to the system, as well as technicians and end users, e.g., power outages, voltage fluctuations, or electric discharges. Toward this end, FiWi access networks may be enriched by fiber optic and wireless sensors, giving rise to fiber-wireless sensor networks

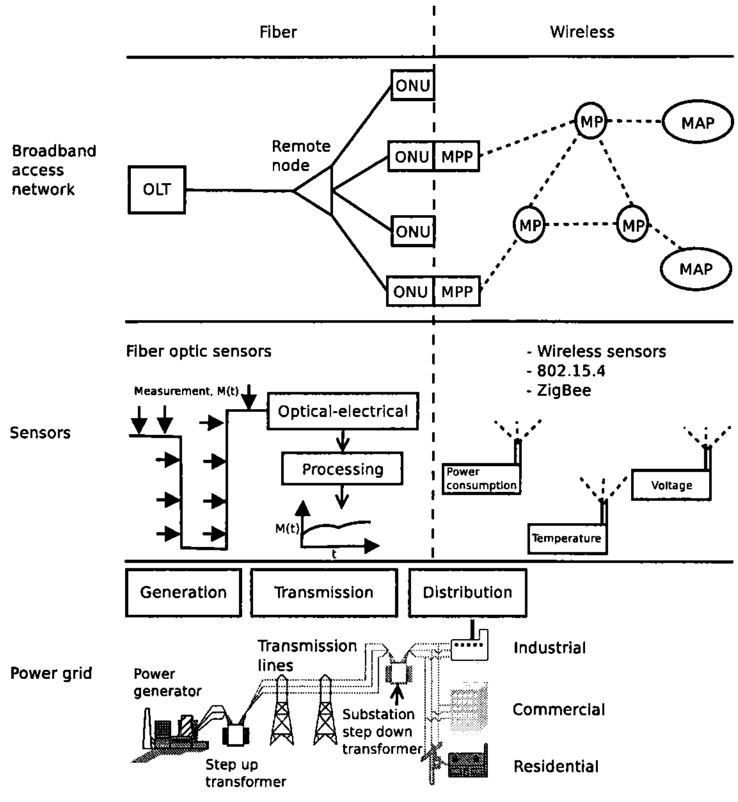

Figure 11.8 – Fiber-wireless sensor networks (Fi-WSNs) enable the monitoring of and interaction with the electrical power grid.

(Fi-WSNs), as shown in Fig. 11.8. Embedding fiber optic and wireless sensors into FiWi access networks enables them to interact with the electrical power grid via monitoring some of the key parameters (temperature, pressure, sound, etc.) of its components, and trigger appropriate actions, if needed.

11.5 FiWi Smart Grid Communications Networks Based on Multi-Tier Business Models

At present, the major roadblocks toward a sustainable low carbon society based on highly dependable critical infrastructures are less technological feasibility and maturity, but more the lack of compelling business cases and regulatory frameworks. In fact, business models, arguably more than technological choices, play a key role in the roll-out of smart grid communications infrastructures. According to [32], utilities along with municipalities are responsible for 22% of households passed with FTTH or FTTB in Europe. These investments enable utilities or municipalities to (*i*) leverage their existing duct, sewer, and other infrastructure; (*ii*) leverage their ability to raise long-term financing at fairly low interest rates; (*iii*) create a new source of revenue in the face of ongoing liberalization of the energy sector, particularly in smart grid solutions; and (*iv*) provide services completely independent from incumbents' infrastructures for the first time. Furthermore, it was recently shown in [33] that cooperation among different utilities in the roll-out phase may drive down the CAPEX of FTTH and FTTB deployments by 17%. Innovative partnerships enable utilities and other players to share smart grid communications infrastructure investments by transitioning from the traditional vertical network integration model towards splitting the value chain into a *three-tier business model* that consists of network infrastructure roll-out, network operation and maintenance, and service provisioning [32]. One of the most promising examples of such a multi-tier business model is the above mentioned Swiss Fibre Net of OPENAXS, where the power utilities are responsible for the installation of the network infrastructure, as well as its operation and maintenance, but leave its access open to all service providers (e.g., triple-play voice, video, and data service providers) on a nondiscriminatory basis.

11.5.1 The Über-FiWi Network

In [34], we have recently introduced our so-called Über-FiWi network, a FiWi network infrastructure shared for both smart grid communications and broadband access. It represents a sustainable FiWi smart grid communications infrastructure that is based on a reduced number of low-cost, simple Ethernet technologies, covers all segments of the power distribution network, and allows for evolutionary pay-as-you-grow fiber build-outs according to a utility's given smart grid roadmap. As shown in Fig. 11.9, homes connect to the smart grid communications infrastructure either via IEEE 802.3ah EPON with optional WDM upgrades or IEEE 802.16 WiMAX. Note that, unlike in 4G cellular networks, WiMAX is expected to succeed with the smart grid [35], as witnessed by Cisco's and GE's recent investments in WiMAX-based smart grid solutions. In suburban and rural areas with

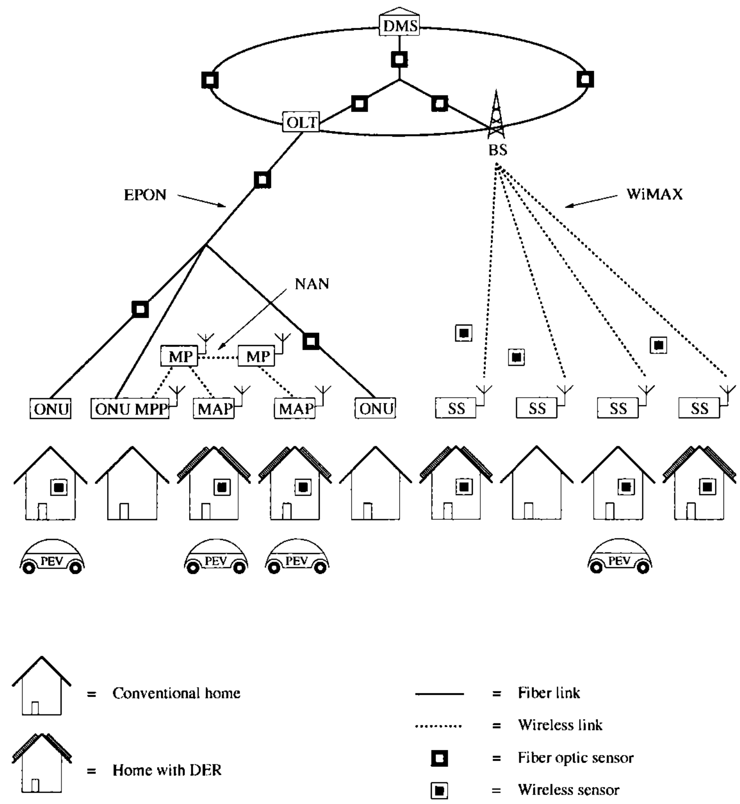

Figure 11.9 – The Über-FiWi network architecture.

a small population density, we use WiMAX due to its lower operational and capital expenditures (OPEX and CAPEX), compared to EPON. For densely populated or fiber-rich settings as well as environments where fiber cuts are less likely (e.g., underground railway tunnels), we use EPON as the preferred medium of choice. For increased reliability and reduced fiber infrastructure costs, the EPON/WDM PON may be replaced with an Ethernet shared protection ring to interconnect ONUs in a more fault-tolerant, fiber-lean manner. EPON and WiMAX networks are interconnected with the distribution management system (DMS) through an optical Gigabit carrier Ethernet augmented ring network, whose star subnetwork provides fault tolerance against multiple ring failures.

In addition, we deploy a WLAN-based mesh neighborhood area network (NAN) based on high-throughput next-generation IEEE 802.11n/ac WLAN, including IEEE 802.11e quality-of-service (QoS), and IEEE 802.11s mesh WLAN technologies. The proposed NAN allows an ONU installed at a given customer's premises to be shared by other nearby homes, thereby significantly reducing the amount of required fiber infrastructure, increasing coverage, and enabling a smooth upgrade path. More interestingly, we exploit the NAN to realize a low-cost communications infrastructure for local *smart microgrids.* To improve scalability and increase capacity, we will also selectively deploy optical fiber links in small-size or greenfield NANs, as envisioned for the Rokkasho Village in Japan, one of the worldwide leading smart microgrid demonstration projects. The use of optical fiber helps enable trust relationships in smart microgrids by capitalizing on the fact that eavesdropping can be more easily detected in optical fiber networks than in their wireless counterparts.

To monitor the status of next-generation power network distribution components, we place fiber optic sensors at the required locations throughout the optical fiber infrastructure, and ZigBee Smart Energy or emerging low-power WLAN based WSNs in the WiMAX and NAN networks. We integrate low-cost passive fiber optic sensors for temperature, voltage, current, and sound into the aforementioned EPON, WDM PON, and Ethernet shared protection ring of our proposed smart grid communications infrastructure. They are remotely controlled in real-time using advanced interrogation subsystems at the DMS of the power distribution network for effectively separating the various measurements (temperature, voltage, current, sound) from the collected data, and to synchronize the fiber optic sensors with the wireless sensors throughout the power distribution network. Note that smart grid wide synchronization is not possible with currently deployed sensors, whose collected information is usually stored in stand-alone servers. Synchronization will be of great benefit to utilities to accurately measure the state of the power grid instead of estimating it, as is the current practice [36].

11.5.2 Coexistence of H2H and M2M Traffic

In this section, we aim at providing deeper insights into the performance of the multi-tier Über-FiWi network that provides not only open-access triple-play service offerings, also known as *human-to-human (H2H)* services, but also enables the support of some of the most important potential smart grid applications, e.g., grid integration of renewable energy resources [37]. The unpredictability of renewable energy sources, in conjunction with other emerging and future smart grid applications that are random in nature (e.g., G2V/V2G), creates challenging problems in the control and reliability of the power grid, which call for a multitude of geographically and temporally

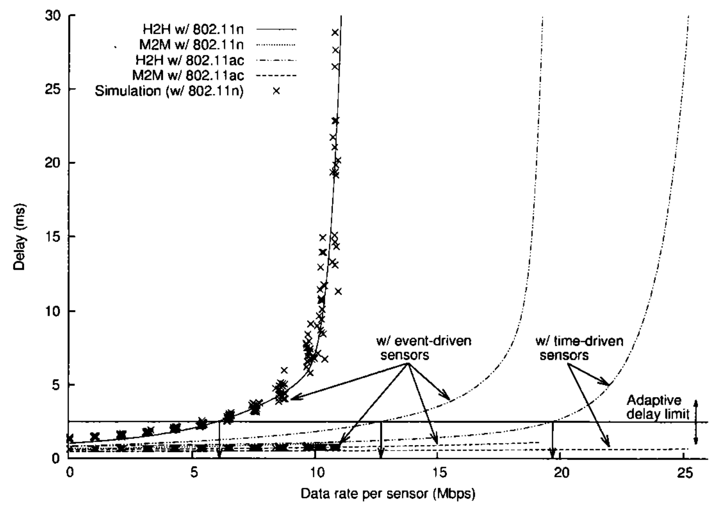

Figure 11.10 – Average end-to-end delay performance vs. data rate per sensor.

coordinated monitoring and control actions over time scales ranging from milliseconds to operational planning horizon [38]. Towards this end, different wireless sensor applications based on ZigBee or low-power WLAN technologies have been considered for the *machine-to-machine (M2M)* interconnection of a wide variety of devices and appliances, giving rise to the so-called Internet of Things (IoT) [39], of which the smart grid represents an important real-world example.

The analysis in [28] can be extended to investigate the coexistence of H2H and M2M traffic over the Über-FiWi network with the objective to quantify the maximum achievable wireless sensor traffic rates without violating the given upper delay limits of conventional H2H traffic. Fig. 11.10 depicts the average end-to-end delay performance of H2H traffic (aggregate load fixed to 144 Mb/s) and M2M sensor traffic vs. the data rate per sensor, including verifying simulations, for a 20 km long TDM EPON with 8 ONUs, each equipped with a QoS-enabled access point (AP) serving 2 STAs and 2 sensors. We observe that the delay of M2M traffic remains low and flat for event- and especially time-driven sensors, whereby event-driven sensors contend for channel access like any other STA after detecting an event of importance such as a power outage. Conversely, time-driven sensors periodically send their measurements to the DMS in dedicated (contention-free) TDM slots without undergoing contention for the wireless channel. However, for increasing sensor data rates, the delay of H2H traffic may cross a given upper delay limit, which is adaptive to meet different H2H traffic requirements. For instance, for an upper delay limit of 2.5 ms, the measured sensor data

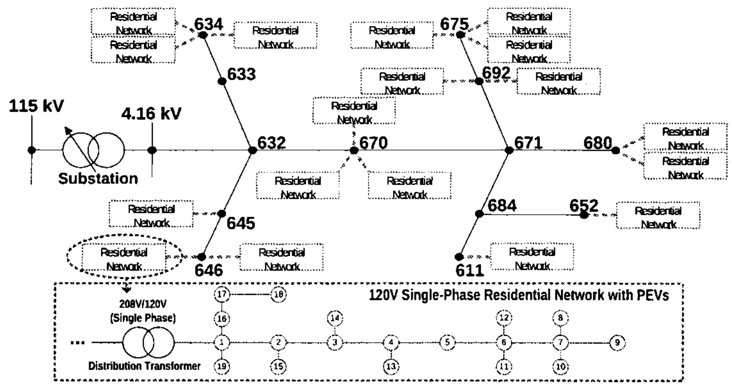

Figure 11.11 – IEEE 13-node distribution power network with grid-connected PEVs.

rates of 6.1, 12.7, and 19.7 Mb/s (vertical arrows in Fig. 11.10) clearly show that higher permissible sensor data rates can be achieved by using VHT WLAN based event- or even better time-driven sensors instead of 802.11n based ones without violating the delay limit. The obtained results can be used as a theoretical upper bound of coexisting M2M traffic for the design and realization of future yet unforeseen smart grid applications.

11.5.3 Co-Simulation

A plethora of simulation tools exist for communications networks and power networks separately. They can be used to study the communications and power system perspectives of IEEE P2030 logically independently from each other. However, very few studies have been carried out on co-simulation by combining both perspectives in a multidisciplinary manner. In [40], we have recently developed a joint communications and power distribution network co-simulator based on OMNeT++ and OpenDSS for enabling multidisciplinary smart grid experimentations and investigating the impact of FiWi smart communications infrastructures, protocols, and algorithms on the performance of the underlying electrical power grid.

For illustration, let us consider the example of PEV charging. Uncontrolled, random PEV charging may cause local grid problems in terms of voltage deviations, increased system losses, and network overloads, resulting in degraded power quality and operation efficiency. Fig. 11.11 shows a modified IEEE 13-node test distribution power network that accommodates 342 residential cus-

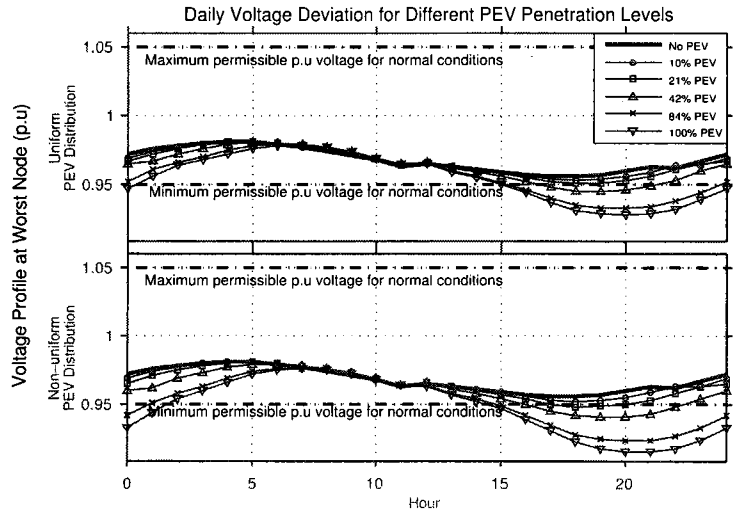

Figure 11.12 – Daily voltage deviations for uniform, and non-uniform PEV distributions at different PEV penetration levels.

tomers with grid-connected PEVs, whose specifications are similar to those of the commercially available electric Nissan LEAF 2012.

Fig. 11.12 shows the daily voltage profile at the node with maximum voltage deviation for different PEV penetration levels without applying any FiWi smart grid communications infrastructure. Expectedly, for both uniform and non-uniform PEV distributions, the daily voltage fluctuation becomes more severe as the penetration level increases. With uniform PEV distribution, as the penetration level goes above 20%, the voltage magnitude at some hours decreases below the minimum permissible level for normal conditions (0.95 per unit (p.u.), defined as the actual voltage magnitude divided by the rated voltage 120V). Below this limit, the quality of power supply is degraded. Compared with uniform PEV distribution, non-uniform PEV distribution leads to a more severe deviation in the local voltage profile. This result is due to the fact that PEVs are more concentrated in some neighborhoods, resulting in more local voltage drops along distribution lines.

Clearly, it is important to avoid such a deviated voltage profile and the resultant deteriorated power quality due to high or non-uniform PEV charging loads or both, which might cause potential overloads that lead to damages in transformers and cables, and thus require reinforcement investment on utility assets. In [41], we have examined several centralized proactive scheduling algorithms to be implemented at the DMS to coordinate PEV charging via our Über-FiWi network. In addi-

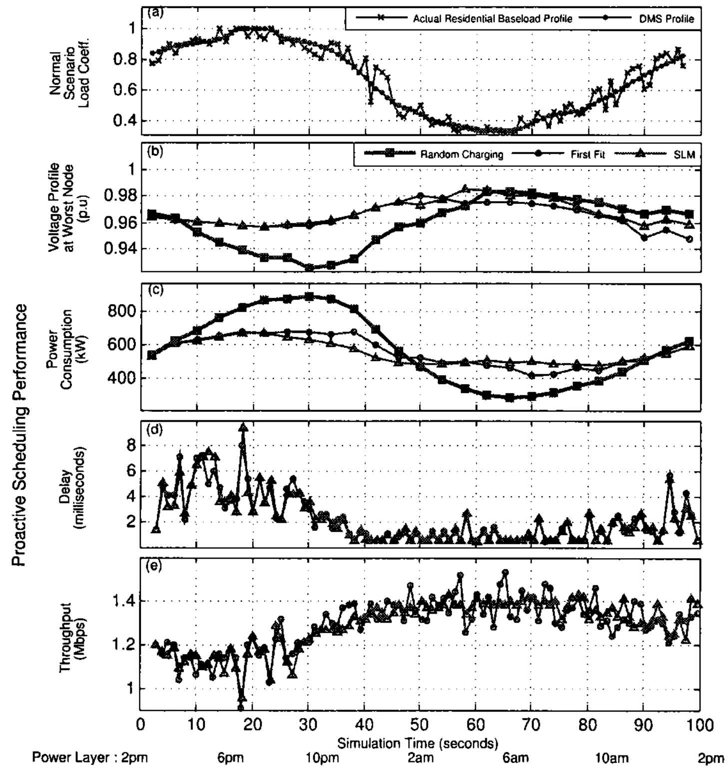

Figure 11.13 – PEV coordination performance of underlying IEEE 13-node distribution power network (in terms of voltage profile and power consumption), and overlaid Über-FiWi network (in terms of delay and throughput).

tion, we proposed a voltage control protocol, which allows the DMS to quickly locate power network nodes with low voltage, and temporarily disconnect PEVs until the voltage constraints are satisfied again for all power distribution network nodes. Fig. 11.13 illustrates the performance of random PEV charging, and our proposed PEV coordination schemes (referred to as first fit and SLM) for a normal scenario, where the daily profile available at the DMS almost matches the actual residential baseload profile (Fig. 11.13(a)). Note that the figure shows the performance of both the underlying IEEE 13-node distribution power network in terms of voltage profile and power consumption (Fig. 11.13(b) and (c)), and the overlaid Über-FiWi network in terms of delay and throughput between PEVs and DMS (Fig. 11.13(d) and (e)). We note that both PEV coordination schemes are able to maintain the voltage always above the acceptable limit, and to flatten the voltage profile and power consumption by shifting PEV loadings to off-peak hours (overnight), and thereby avoiding additional stress on the distribution grid during hours when the baseload demand is already high (6pm-10pm).

IEEE Transactions on Reliability, accepted for publication.

11.5.4 Experimental Smart Grid System

In [42], we have built an IEEE P2030 compliant Über-FiWi network testbed to experimentally investigate the effectiveness of a proposed adaptive admission control algorithm to manage latency and reliability in the event of emulated power blackouts during a distributed security breach via a distributed denial-of-service (DDoS) attack. Fig. 11.14 depicts the experimental set-up of our Über-FiWi network testbed. Two laptops using IEEE 802.11b/g are set up to emulate multiple MAPs: the first laptop emulates a DDoS attack of 9 MAPs, each generating 50 packets per second, and the second laptop (2 in Fig. 11.14) emulates normal MAPs, and an MAP (MAP_9) experiencing successive emulated blackouts. MAP_9 normally consumes between 1 and 9 kWh, whereas in the event of a blackout it consumes 0 kWh. Thus, only the DDoS and blackout events are emulated, while the rest of the testbed uses state-of-the-art wireless and fiber equipment. A Zyxel NWA570n wireless access point (3 in Fig. 11.14), supporting IEEE 802.11b/g/n, represents an MP. The MPP (4 in Fig. 11.14) is emulated by an IEEE 802.11b/g/n laptop. An EPON SUN-GE8100 (1 Gbps) is used (6 in Fig. 11.14) with 5 kilometers of fiber between 4 ONUs (8 in Fig. 11.14) and the optical coupler, and 15 kilometers between the coupler and the OLT (7 in Fig. 11.14). The MPP is connected to an ONU port, and the DMS (5 in Fig. 11.14) is connected to an OLT port. All MAPs send notification packets to its MPP through the MP node and the DMS is reached through the EPON.

We developed an *Experimental Smart Grid System (ESGS)*[2], which comprises several programs written in Java to test our admission control process that dynamically adjusts the data rate of MAP_9 to quickly report on monitored blackouts, and thereby enable the power distribution management system to take swift recovery actions. In our experiment, we implement our admission control algorithm at the MPP. P_1 hosts can send 10 packets per second, and P_2 hosts 1 packet per second. The DMS is responsible for receiving notification packets, feeding the local database, and sending control packets. The DMS sends *change priority request* packets to the MPP based on the following conditions: *(i)* P_1 when the power consumed equals 0 (detected blackout), and *(ii)* P_2 otherwise. We observe from Fig. 11.15 that the throughput of MAP_9 increases in the event of blackouts, even

2. The ESGS source code is freely available at `http://zeitgeistlab.ca/doc/Smart_Grid_Communications_over_UEber-FiWi_Networks.html`.

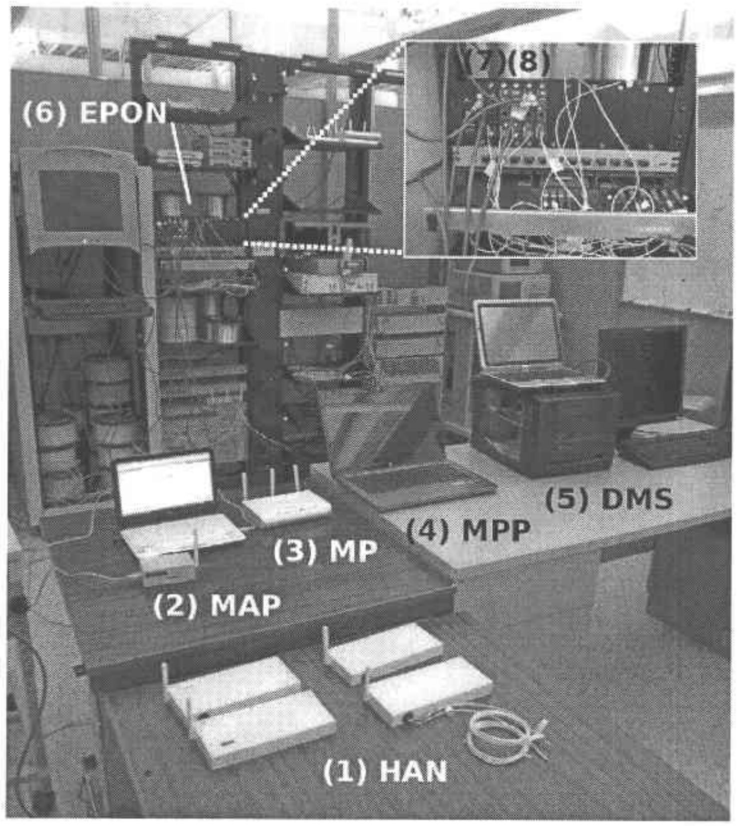

Figure 11.14 – The Über-FiWi network testbed.

during a DDoS attack, which in turn helps decrease the latency between MAP_9 and the DMS, and thus invoke quick fault recovery actions.

11.6 Conclusions

Internet technology and renewable energies are beginning to merge to create the Energy Internet infrastructure for the TIR economy, and a future sustainable low carbon society. We elaborated on the evolution path of current broadband access networks toward integrated bimodal FiWi access networks within the next 10-20 years, whose planning horizon should be aligned with the emergence of the smart grid by 2030 to make investment decisions and technology choices that achieve the long-term smart grid roadmap goals, and meet the requirements of electric utilities. The presented dependability enhancing techniques help improve the reliability, availability, survivability as well as

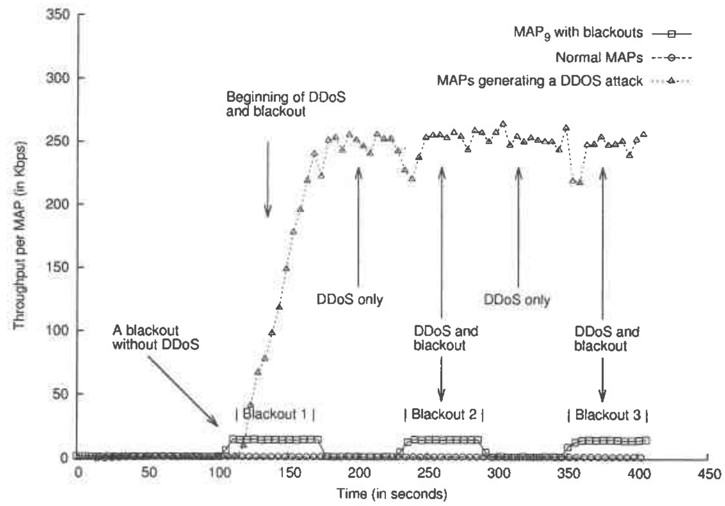

Figure 11.15 – Throughput measurements for MAP$_9$ experiencing a power blackout with malicious MAPs generating a DDoS attack.

(cyber) security and (physical) safety of both the FiWi smart grid communications infrastructures, and underlying power distribution networks. The presented results on the coexistence of conventional H2H triple-play and M2M sensor traffic can be used as a theoretical upper bound for the design and realization of some of the described potential, as well as future yet unforeseen smart grid applications. Furthermore, the presented co-simulation results provide invaluable insights into the interaction of power distribution networks, and overlaid FiWi smart grid communications infrastructures with regard to voltage profile, power consumption, delay, and throughput. The obtained results help better understand the respective performance bottlenecks, and requirements of capacity upgrades as well as design guidelines for more efficient smart grid communications protocols and resource management algorithms.

References

[1] J. Rifkin, "Beyond Austerity A Sustainable Third Industrial Revolution Economic Growth Plan For the European Union," *Mission Growth Summit: Europe at the Lead of the New Industrial Revolution*, The European Commission, May 2012.

[2] V. C. Gungor, D. Sahin, T. Kocak, S. Ergut, C. Buccella, C. Cecati, and G. P. Haneke, "A Survey on Smart Grid Potential Applications and Communication Requirements," *IEEE Transactions on Industrial Informatics*, vol. 9, no. 1, pp. 28-42, Feb. 2013.

[3] X. Fang, S. Misra, G. Xue, and D. Yang, "Smart Grid – The New and Improved Power Grid: A Survey," *IEEE Communications Surveys & Tutorials*, vol. 14, no. 4, pp. 944-980, Fourth Quarter 2012.

[4] V. K. Sood, D. Fischer, J. M. Eklund, and T. Brown, "Developing a Communication Infrastructure for the Smart Grid," in *Proc., IEEE Electrical Power & Energy Conference*, Montréal, QC, Canada, Oct. 2009, pp. 1-7.

[5] F. Rahimi and A. Ipakchi, "Demand Response as a Market Resource Under the Smart Grid Paradigm," *IEEE Transactions on Smart Grid*, vol. 1, no. 1, pp. 82-88, June 2010.

[6] B. Heile, "Smart Grids for Green Communications," *IEEE Wireless Communications*, vol. 17, no. 3, pp. 4-6, June 2010.

[7] V. Oksman and J. Zhang, "G.HNEM: The New ITU-T Standard on Narrowband PLC Technology," *IEEE Communications Magazine*, vol. 49, no. 12, pp. 36-44, Dec. 2011.

IEEE Transactions on Reliability, accepted for publication.

[8] V. C. Gungor, B. Lu, and G. P. Hancke, "Opportunities and Challenges of Wireless Sensor Networks in Smart Grid," *IEEE Transactions on Industrial Electronics*, vol. 57, no. 10, pp. 3557-3564, Oct. 2010.

[9] A. Ghassemi, S. Bavarian, and L. Lampe, "Cognitive Radio for Smart Grid Communications," in *Proc., IEEE SmartGridComm*, Gaithersberg, MD, USA, Oct. 2010, pp. 297-302.

[10] C. Hochgraf, R. Tripathi, and S. Herzberg, "Smart Grid Charger for Electric Vehicles Using Existing Cellular Networks and SMS Text Messages," in *Proc., IEEE SmartGridComm*, Gaithersberg, MD, USA, Oct. 2010, pp. 167-172.

[11] S. Davies, "Grid looks to smart solution," *IET Engineering & Technology*, vol. 5, no. 7, pp. 49-51, May 2010.

[12] "The Power to Live Green: Toronto's Sustainable Energy Strategy," City of Toronto, Oct. 2009.

[13] OECD, "OECD Broadband Portal," `http://www.oecd.org/sti/ict/broadband`.

[14] P. Ödling, T. Magesacher, S. Höst, P. O. Börjesson, M. Berg, and E. Areizaga, "The Fourth Generation Broadband Concept," *IEEE Communications Magazine*, vol. 47, no. 1, pp. 63-69, Jan. 2009.

[15] C. Lange and A. Gladisch, "On Energy Consumption of Telecommunication Networks - A Network Operator's View," in *Proc., OFC/NFOEC, Workshop on Energy Footprint of ICT*, San Diego, CA, USA, March 2009, pp. 1-3.

[16] R. S. Tucker, R. Parthiban, J. Baliga, K. Hinton, R. W. A. Aye, and W. V. Sorin, "Evolution of WDM Optical IP Networks: A Cost and Energy Perspective," *IEEE/OSA Journal of Lightwave Technology*, vol. 27, no. 3, pp. 243-252, Feb. 2009.

[17] J.-I. Kani, F. Bourgart, A. Cui, A. Rafel, M. Campbell, R. Davey, and S. Rodrigues, "Next-Generation PON—Part I: Technology Roadmap and General Requirements," *IEEE Communications Magazine*, vol. 47, no. 11, pp. 43-49, Nov. 2009.

IEEE Transactions on Reliability, accepted for publication.

[18] M. D. Andrade, G. Kramer, L. Wosinska, J. Chen, S. Sallent, and B. Mukherjee, "Evaluating Strategies for Evolution of Passive Optical Networks," *IEEE Communications Magazine*, vol. 49, no. 7, pp. 176-184, July 2011.

[19] G. Kramer, M. D. Andrade, R. Roy, and P. Chowdhury, "Evolution of Optical Access Networks: Architectures and Capacity Upgrades," *Proceedings of the IEEE*, vol. 100, no. 5, pp. 1188-1196, May 2012.

[20] L. Kazovsky, S.-W. Wong, T. Ayhan, K. M. Albeyoglu, M. R. N. Ribeiro, and A. Shastri, "Hybrid Optical-Wireless Access Networks," *Proceedings of the IEEE*, vol. 100, no. 5, pp. 1197-1225, May 2012.

[21] E. H. Ong, J. Kneckt, O. Alanen, Z. Chang, T. Huovinen, and T. Nihtilä, "IEEE 802.11ac: Enhancements for Very High Throughput WLANs," in *Proc., IEEE International Symposium on Personal, Indoor and Mobile Radio Communications (PIMRC)*, Toronto, ON, Canada, Sept. 2011, pp. 849-853.

[22] M. M. Rad, K. Fouli, H. Fathallah, L. Rusch, and M. Maier, "Passive Optical Network (PON) Monitoring: Challenges and Requirements," *IEEE Communications, Special Issue on Advances in Passive Optical Networks*, vol. 49, no. 2, pp. S45-S52, Feb. 2011.

[23] N. Ghazisaidi, M. Scheutzow, and M. Maier, "Survivability Analysis of Next-Generation Passive Optical Networks and Fiber-Wireless Access Networks," *IEEE Transactions on Reliability*, vol. 60, no. 2, pp. 479-492, June 2011.

[24] X. Shao, Y. K. Yeo, L. H. Ngoh, X. Cheng, W. Rong, and L. Zhou, "Availability-Aware Routing for Large-Scale Hybrid Wireless-Optical Broadband Access Networks," in *Proc., OFC/NFOEC*, San Diego, CA, USA, March 2010, pp. 1-3.

[25] M. Kiese, E. Georgieva, D. Schupke, B. Mukherjee, and J. Eberspächer, "Availability Evaluation in Hybrid Wireless-Optical Broadband Access Networks," in *Proc., IEEE International Conference on Communications (ICC)*, Dresden, Germany, June 2009, pp. 1-6.

IEEE Transactions on Reliability, accepted for publication.

[26] Y. Lin and V. W. S. Wong, "Frame Aggregation and Optimal Frame Size Adaptation for IEEE 802.11n WLANs," in *Proc., IEEE GLOBECOM*, San Francisco, CA, USA, Dec. 2006, pp. 1-6

[27] D. Malone, K. Duffy, and D. Leith, "Modeling the 802.11 Distributed Coordination Function in Nonsaturated Heterogeneous Conditions," *IEEE/ACM Transactions on Networking*, vol. 15, no. 1, pp. 159-172, Feb. 2007.

[28] F. Aurzada, M. Lévesque, M. Maier, and M. Reisslein, "FiWi Access Networks Based on Next-Generation PON and Gigabit-Class WLAN Technologies: A Capacity and Delay Analysis," *IEEE/ACM Transactions on Networking*, accepted for publication.

[29] S. Sarkar, H. Yen, S. Dixit, and B. Mukherjee, "A Novel Delay-Aware Routing Algorithm (DARA) for a Hybrid Wireless-Optical Broadband Access Network (WOBAN)," *IEEE Network*, vol. 22, no. 3, pp. 20-28, Jan./Feb. 2008.

[30] Z. Zheng, J. Wang, and X. Wang, "ONU Placement in Fiber-Wireless (FiWi) Networks Considering Peer-to-Peer Communications," in *Proc., IEEE GLOBECOM*, Honolulu, HI, USA, Nov./Dec. 2009, pp. 1-7.

[31] A. R. Metke and R. L. Ekl, "Security Technology for Smart Grid Networks," *IEEE Transactions on Smart Grid*, vol. 1, no. 1, pp. 99-107, June 2010.

[32] "FTTH: Double Squeeze of Incumbents – Forced to Partner?", Arthur D. Little, 2010.

[33] M. Tahon, J. V. Ooteghem, K. Casier, L. Deschuttere, S. Verbrugge, D. Colle, M. Pickavet, and P. Demeester, "Cost allocation model for a synergetic cooperation in the rollout of telecom and utility networks," in *Proc., Conference on Telecommunications Internet and Media Techno-Economics (CTTE)*, Berlin, Germany, May 2011, Paper S3-2.

[34] M. Maier, M. Lévesque, and L. Ivanescu, "NG-PONs 1&2 and Beyond: The Dawn of the Über-FiWi Network," *IEEE Network, Special Issue on Next Generation Optical Access Networks: Dynamic Bandwidth Allocation, Resource Use Optimization and QoS Improvements*, vol. 26, no. 2, pp. 15-21, March/April 2012.

IEEE Transactions on Reliability, accepted for publication.

[35] M. Anderson, "WiMax for Smart Grids," *IEEE Spectrum*, vol. 47, no. 7, p. 14, July 2010.

[36] A. Phillips, "Staying in Shape," *IEEE Power & Energy Magazine*, vol. 8, no. 2, pp. 27-33, March/April 2010.

[37] F. R. Yu, P. Zhang, W. Xiao, and P. Chowdhury, "Communication Systems for Grid Integration of Renewable Energy Resources," *IEEE Network*, vol. 25, no. 5, pp. 22-29, Sept. 2011.

[38] K. Moslehi and R. Kumar, "Smart Grid - A Reliability Perspective," in *Proc., Innovative Smart Grid Technologies*, Washington D.C., USA, Jan. 2010, pp. 1-8.

[39] S. Tozlu, M. Senel, W. Mao, and A. Keshavarzian, "Wi-Fi Enabled Sensors for Internet of Things: A Practical Perspective," *IEEE Communications Magazine*, vol. 50, no. 6, pp. 134-143, June 2012.

[40] M. Lévesque, D. Q. Xu, M. Maier, and G. Joós, "Communications and Power Distribution Network Co-Simulation for Multidisciplinary Smart Grid Experimentations," in *Proc., SCS/ACM Spring Simulation Multiconference (SpringSim), Annual Simulation Symposium*, Orlando, FL, USA, March 2012, pp. 1-7.

[41] M. Lévesque, D. Q. Xu, G. Joós, and M. Maier, "Co-Simulation of PEV Coordination Schemes over a FiWi Smart Grid Communications Infrastructure," in *Proc., IEEE IECON*, Montréal, QC, Canada, Oct. 2012, pp. 1-6.

[42] M. Lévesque, M. Maier, Y. Desai, and G. Joós, "Adaptive Admission Control for a Smart Grid FiWi Communications Network facing Power Blackouts during a DDoS Attack," in *Proc., IEEE Green Technologies Conference*, Tulsa, OK, USA, April 2012, pp. 1-3.